Dizajniranje, sinteza i citostatsko djelovanje sahakina

Beus, Maja

Sveučilište u Zagrebu
FARMACEUTSKO-BIOKEMIJSKI FAKULTET

MAJA BEUS

DIZAJNIRANJE, SINTEZA I CITOSTATSKO DJELOVANJE SAHAKINA

DOKTORSKI RAD

Zagreb, 2020.

University of Zagreb
FACULTY OF PHARMACY AND BIOCHEMISTRY

MAJA BEUS

DESIGN, SYNTHESIS AND CYTOSTATIC ACTIVITY OF SAHAQUINES

DOCTORAL THESIS

Zagreb, 2020

Sveučilište u Zagrebu
FARMACEUTSKO-BIOKEMIJSKI FAKULTET

MAJA BEUS

DIZAJNIRANJE, SINTEZA I CITOSTATSKO DJELOVANJE SAHAKINA

DOKTORSKI RAD

Mentor: prof. dr. sc. Branka Zorc

Zagreb, 2020.

University of Zagreb
FACULTY OF PHARMACY AND BIOCHEMISTRY

MAJA BEUS

DESIGN, SYNTHESIS AND CYTOSTATIC ACTIVITY OF SAHAQUINES

DOCTORAL THESIS

Supervisor: Prof. Branka Zorc, PhD

Zagreb, 2020

Doktorski rad je predan na ocjenu Fakultetskom vijeću Farmaceutsko-biokemijskog fakulteta Sveučilišta u Zagrebu radi stjecanja akademskog stupnja doktora znanosti iz područja biomedicine i zdravstva, polje farmacija, grana farmacija.

Rad je izrađen u Zavodu za farmaceutsku kemiju Farmaceutsko-biokemijskog fakulteta Sveučilišta u Zagrebu i u Department of Pharmacology and Therapeutics Sveučilišta McGill, Montreal (Kanada) u sklopu doktorskog studija „Farmaceutsko-biokemijske znanosti“ Farmaceutsko-biokemijskog fakulteta Sveučilišta u Zagrebu. Rad je financiran iz projekta „Dizajniranje, sinteza i evaluacija derivata primakina, vorinostata i sorafeniba kao potencijalnih citostatika“ (HRZZ-IP-09-2014-1501) Hrvatske zaklade za znanost i „Projekta razvoja karijera mladih istraživača – izobrazba novih doktora znanosti“ Hrvatske zaklade za znanost koji je financirala Europska unija iz Europskog socijalnog fonda.

Zahvale

Puno hvala mojoj mentorici prof. dr. sc. Branki Zorc na nesebičnim savjetima, pomoći i neizmjernoj podršci tijekom izrade ovog doktorskog rada.

Zahvaljujem izv. prof. dr. sc. Zrinki Rajić na uvođenju u farmaceutsku kemiju, na strpljivom učenju mojim prvim koracima u labosu te odabiru teme ovog doktorskog rada.

Many thanks to prof. Dusica Maysinger for showing me the wonderous world of cancer cells and for helping me find my place in the world of science.

Thanks to everyone from Nano family, especially Issan, for teaching me, working with me and for being my home away from home.

Posebno hvala Hrvoju, na svakom ručku i ramenu za plakanje.

Hvala svim članovima Zavoda za farmaceutsku kemiju (mojim antimalaričarima), na svim savjetima, kritikama i na svakoj otpjevanoj pjesmi.

Hvala studentima Barbari Rubinić i Zvonimiru Mlinariću, koji su svojim radom za Rektorovu nagradu doprinijeli izradi ovog doktorata, a svojom osobnošću uljepšali svaku sintezu i olakšali svako pročišćavanje spojeva.

Hvala kolegi i prijatelju s drugog Zavoda – doc. dr. sc. Davoru Šakiću, na svim ispijenim kavama te hvala za sve mentalne i znanstvene podrške tijekom izrade mog doktorskog rada.

Neizmjerno hvala mojim prijateljicama – Antoniji, Kati, Lani i Nini što su uvijek bile uz mene, čak i kad sam bila u drugoj vremenskoj zoni. Antonia, hvala na tvojoj toplini i brizi. Kata, hvala na slušanju i svakom savjetu. Lana, hvala na tvojoj neiscrpnoj energiji i humoru. Nina, hvala što smo se međusobno podržavale i onda kada je bilo najteže.

Hvala mami, tati i Marku što su me uvijek podržavali i trudili se sakriti svoju brigu zbog mog izbivanja.

SAŽETAK

U okviru ovog doktorskog rada dizajnirani su i sintetizirani sahakini, hibridni spojevi u kojima su spojeni dijelovi molekula antimalarika primakina, odnosno klorokina i citostatika SAHA-e (suberoilanilid hidroksamska kiselina). Sahakini sadrže tri ključna dijela: kinolinski prsten (dio molekule primakina ili klorokina), središnji dio (dikarboksilnu kiselinu: jantarnu, fumarnu, glutarnu, adipinsku, tereftalnu) te završni dio s dodatnom funkcionalnom skupinom (esterskom, karboksilnom, amidnom te *O*-benzil-, *O*-metil- ili nesupstituiranom hidroksamskom kiselinom). Sinteza sahakina polazila je od kinolinskog kraja. Primarna amino skupina primakina, odnosno analoga klorokina i monoester odgovarajućih dikarboksilnih kiselina povezani su amidnom vezom pomoću 1-[*bis*(dimetilamino)metilen]-1*H*-1,2,3-triazolo[4,5-*b*]piridinij 3-oksid heksafluorofosfata (HATU) u prisutnosti *N*,*N*-diizopropiletilamina (DIEA) ili preko kiselinskog klorida. Dobiveni su amido-esterski derivati koji su u sljedećem reakcijskom koraku hidrolizirani u amido-karboksilne kiseline te dalje amidirani s *O*-metil- ili *O*-benzilhidroksilaminima, odnosno halogenanilinima (s atomima fluora/klora ili trifluorometilnom skupinom u *meta* ili *para* položaju) uz HATU i DIEA. Sahakini sa slobodnom hidroksamskom skupinom dobiveni su katalitičkom hidrogenolizom *O*-benzilhidroksamskih derivata. Svi sahakini karakterizirani su uobičajenim analitičkim i spektroskopskim metodama (CHN, IR, ^{1}H NMR, ^{13}C NMR, MS). Antiproliferativno djelovanje sahakina ispitano je na humanim tumorskim stanicama: adenokarcinoma gušterače (Capan-1), akutne mijeloične leukemije (Hap1), karcinoma debelog crijeva (HCT-116), karcinoma pluća (NCI-H460), akutne limfoblastičke leukemije (DND-41), akutne promijelocitne leukemije (HL-60), kronične mijeloične leukemije (K-562), multiplog mijeloma (MM.1S), ne-Hodkinovog limfoma (Z-138), osteosarkoma (U2OS), hepatocelularnog karcinoma (HepG2), adenokarcinoma dojke (MCF-7), karcinoma pluća ne-malih stanica (H460) i glioblastoma (U251N). Najaktivniji derivati primakina bili su sahakini iz podskupine hidroksamskih kiselina te *meta*-supstituirani derivati halogenanilina s fumardiamidnom poveznicom. Sahakinu s najjačim citostatskim učinkom, N^{1}-hidroksi-N^{5}-(4-((6-metoksikinolin-8-il)amino)pentil)-glutaramidu, utvrđen je mehanizam djelovanja. Na staničnom modelu glioblastoma dokazano je da selektivno inhibira histon-deacetilazu 6, smanjuje ekspresiju matriks-metaloproteaze-2 i receptora za epidermalni faktor rasta.

Ključne riječi: primakin / klorokin / SAHA / hibridni spoj / hidroksamska kiselina / sinteza / citostatsko djelovanje / karcinom dojke / glioblastom

SUMMARY

Introduction: Despite enormous efforts, cancer is still one of the deadliest diseases. Cancer requires long-term treatment, during which cancer cells develop different mechanisms of resistance. Therefore, novel and more active drugs are needed. One of the current approaches in drug design is repurposing of registered drugs from one indication to another. Drugs that have already been approved can immediately enter phase II of clinical trials. Repurposing of antimalarial drugs as potential anticancer drugs is particularly interesting and extensively explored. Many antimalarials, including primaquine (PQ) and chloroquine (CQ), as well as their derivatives, have shown cytostatic activity in numerous preclinical and clinical trials. On the other hand, several drugs with hydroxamic acid moiety (suberoylanilide hydroxamic acid (SAHA), belinostat, panobinostat) are currently in the use as cytostatic drugs. The hydroxamic acid pharmacophore can inhibit different metalloenzymes overly-expressed in cancer, such as histone deacetylases (HDACs) and matrix metalloproteinases (MMPs). Bearing this in mind, we have designed and prepared a novel series of compounds called sahaquines, hybrid molecules consisting of PQ/CQ and distant functional groups linked by a dicarboxylic acid. Hybrid compounds can have multiple targets, reducing the risk of resistance, lowering effective doses and decreasing side effects, which makes designing of hybrid molecules a popular strategy in drug research and development.

Materials and methods: PQ was prepared from PQ diphosphate prior to use. Primary amine with the CQ core was prepared from 4,7-dichloroquinoline and 1,4-diaminobutane with the microwave-assisted method. Six different subclasses of sahaquines were prepared, with ester, carboxylic acid, *O*-methyl- and *O*-benzylhydroxamic acid, unsubstituted hydroxamic acid or additional amide functionalities. Amido-esters were prepared by the coupling of PQ/CQ and monoester of corresponding dicarboxylic acid in the presence of 1-[bis(dimethylamino) methylene]-1*H*-1,2,3-triazolo[4,5-*b*]pyridinium 3-oxid hexafluorophosphate (HATU) as the coupling reagent, along with Hünig's base (*N*,*N*-diisopropylethylamine, DIEA) or by previously activating carboxylic acid with thionyl chloride. The following dicarboxylic acid monoesters were used: monomethyl succinate, monoethyl fumarate, monomethyl glutarate, monomethyl adipate and monomethyl terephthalate. Obtained amido-esters were hydrolised in the presence of lithium hydroxide to afford the corresponding amido-carboxylic acids, which were transformed into *O*-benzylhydroxamic acids and *O*-methylhydroxamic acids by means of *O*-benzyl- and *O*-methylhydroxylamine, respectively. HATU/DIEA was used again as the

coupling system. Free hydroxamic acids were obtained by catalytic hydrogenation of *O*-benzyl derivatives. Finally, hybrid diamides were prepared by the coupling of amido-carboxylic acids with various halogenanilines in the presence of HATU/DIEA. The following anilines were used: *m*-fluoroaniline, *p*-fluoroaniline, *m*-chloroaniline, *p*-chloroaniline, *m*-trifluoromethylaniline and *p*-trifluoromethylaniline. All new compounds were fully characterized by conventional spectroscopic and analytical methods (IR, ^{1}H and ^{13}C NMR, MS and elemental analyses). To evaluate drug-like properties of sahaquines, a common set of physicochemical parameters was calculated with Chemicalize.org software: topological polar surface area, number of atoms, molecular weight, partition coefficient, number of H-bond donors, number of H-bond acceptors and molar refractivity.

Cytostatic activity of sahaquines was tested on the following cancer cell lines: pancreatic adenocarcinoma (Capan-1), chronic myeloid leukemia (Hap1), colorectal carcinoma (HCT-116), lung carcinoma (NCI-H460), acute lymphoblastic leukemia (DND-41), acute myeloid leukemia (HL-60), chronic myeloid leukemia (K-562), multiple myeloma (MM.1S), non-Hodgkin lymphoma (Z-138), bone osteosarcoma (U2OS), hepatocellular carcinoma (HepG2), breast adenocarcinoma (MCF-7) and glioblastoma (U251N). The potential effect on healthy cells was assessed on human embryonic kidney (Hek293) cells. All tests were performed *in vitro* using (3-(4,5-dimethylthiazol-2-yl)-2,5-diphenyltetrazolium bromide (MTT) or Hoechst dye. The IC_{50} values (concentration required to decrease cell viability by 50 %) were calculated using nonlinear regression on the sigmoidal dose-response plots from at least two independent experiments. Cell migration was measured using the scratch assay and by measuring the area covered by migrating cells. Cell invasion was measured from the radial movement of cells from 3D tumoroids embedded in a collagen matrix and is quantified from the area covered by invading cells. Gelatin zymography was used to study the effect on the expression of matrix metalloproteinases (MMPs) -2 and -9. The effect on histone and α-tubulin acetylation was tested with immunocytochemistry and quantified by measuring the fluorescence. Antibodies against acetyl-histone H3 K9/K14 and acetyl-α-tubulin K40 were used. To test the effect on epidermal growth factor receptor (EGFR) and the activation of downstream kinases, dual ERK1/2 phosphorylation (Thr202/Tyr204) and AKT phosphorylation (Ser473), Western blotting was used. Antibodies against acetyl-α-tubulin K40, α-tubulin, phospho-AKT Ser473, pan-AKT, HDAC6, EGFR, phospho-ERK1/2 Thr202/Tyr204, pan-ERK1/2 and actin were used for Western blotting.

Results:

The first series of sahaquines were PQ derivatives with the ester, carboxylic acid, *O*-methylhydroxamic acid, *O*-benzylhydroxamic acid or unsubstituted hydroxamic acid terminal group linked with a dicarboxylic acid spacer (succinic, fumaric, glutaric, adipic and terephthalic acid). All synthesized compounds were afforded in good to excellent yields. All sahaquines were fully in agreement with Lipinski's and Gelovani's rules for prospective small-molecule drugs (only *O*-benzylhydroxamic acid with the terephthalic linker showed minimal aberration). Synthesized compounds were tested for their anticancer activity on four human cancer cell lines (U2OS, HepG2, MCF-7 and U251N) and Hek293 cells. Sahaquines from the hydroxamic acid subclass were the most potent. The IC_{50} values towards MCF-7 cells were in the low micromolar concentrations (1.6–5.4 μM). Some of the compounds from other subclasses also showed moderate anticancer activity, but significantly lower than hydroxamic acids, whereas amido-carboxylic acid derivatives were practically inactive.

The most potent sahaquine, namely N^1-hydroxy-N^5-(4-((6-methoxyquinolin-8-yl)amino)pentyl)glutaramide, has shown high efficacy in killing glioblastoma cells U251N in both 2D and 3D models with greater potency than temozolomide, the only available drug for the treatment of glioblastoma multiforme (GBM). Glioblastoma multiforme is one of the most aggressive brain tumours. Current treatment involves surgical resection followed by radiotherapy and chemotherapy with temozolomide, however, more than half of GBM patients do not respond to temozolomide due to resistance development. Another problem with the GBM treatment is the presence of brain tumour stem cells, a subset of glioma cells with the abilities of self-renewal and differentiation. Sahaquine abolished the formation of brain tumour stem cells' neurospheres and significantly reduced the size of brain tumour stem cells' aggregates, even more significantly than temozolomide. To determine the possible underlying mechanisms of action, we have tested sahaquine's effects on cell migration and invasion. Sahaquine abolished invasiveness and contributed to the loss of tumoroid viability, but it did not markedly affect the abundance of secreted MMPs. Cell migration wasn't inhibited significantly over 24 h treatment with sahaquine.

Hydroxamic acid pharmacophore of sahaquine is also present in the structure of SAHA, an HDAC inhibitor approved for the treatment of cutaneous T-cell lymphoma that is currently in the clinical trials for the GBM treatment. SAHA is a non-selective HDAC inhibitor and, as such, can cause undesirable side effects in normal cells. We hypothesized that the tested

sahaquine might be selective toward HDAC6, due to the bulky quinoline ring present in its structure. Indeed, it selectively inhibits HDAC6 at nanomolar concentrations, which distinguishes it from SAHA, which is non-selective at equimolar concentrations. Sahaquine can decrease the abundance of EGFR, phosphorylated AKT and phosphorylated ERK1/2 in GBM.

The second series of sahaquines reported in this doctoral thesis were PQ and halogenaniline asymmetric fumardiamides (designed as potential Michael acceptors) and their reduced analogues succindiamides (unable to participate in Michael addition). All compounds were obtained in good to moderate yields. Synthesis of succindiamides gave products in higher yields than the reactions of analogous fumardiamides (49–90 % compared to 31–58 %). Their cytostatic activity was evaluated *in vitro* against a panel of nine different human cancer cell lines, representing various solid tumour types including Capan-1, Hap1, HCT-116, NCI-H460, DND-41, HL-60, K-562, MM.1S and Z-138. The most active sahaquine from this series was fumardiamide with *m*-fluoroaniline moiety, which showed cytostatic activity against all tested cell lines (IC_{50} values varying from 5.7 to 31.2 μM). In general, compounds bearing substituents in *meta*- position were more active than the analogous *para*-substituted fumardiamides. DND-41 cell line was susceptible to all three *meta*-substituted derivatives (IC_{50} values between 6.7 and 8.9 μM). HL-60 and Z-138 cell lines were also susceptible to fumardiamide with *m*-fluoroaniline moiety (IC_{50} values 5.7 and 8.4 μM, respectively). All fumardiamides were more active than the parent drug PQ. In contrast, analogous succindiamides were completely inactive.

The last of the prepared sahaquines were fumardiamides in which PQ was replaced by CQ moiety. The synthesis was carried out in four steps. Yields for the first three reaction steps were high (73–100 %), whereas the yields varied from 25 to 91 % for the last step. Derivatives bearing substituents in *meta*-position were prepared in lower yields than the analogous *para*-substituted derivatives.

Conclusions: In this doctoral thesis, it is shown that the modification of primaquine and chloroquine structures, *e.g.* their incorporation in hybrid molecules named sahaquines can afford more active and/or more selective cytostatic compounds. The overall activity of sahaquines depended on all three sahaquine fragments: quinoline capping group, dicarboxylic acid spacer and terminal functional group. Sahaquines with unsaturated linkers were more active than the analogous compounds with saturated linkers. Too short or too rigid spacer

(succinic or terephthalic acid), has led to weakening or even loss of cytostatic activity. Sahaquines bearing unsubstituted hydroxamic acids or *meta*-substituted halogenanilines with fumaric acid moiety proved to be the most active compounds.

Two cancer cell lines, namely MCF-7 and U251N cells, were particularly susceptible to sahaquine treatment. The results from this doctoral thesis suggest that sahaquines are promising leads for the development of new anticancer agents for breast carcinoma and GBM treatment.

Keywords: primaquine / chloroquine / SAHA / hybrid compound / hydroxamic acid / synthesis / cytostatic activity / breast cancer / glioblastoma

SADRŽAJ

KRATICE

Capan-1	humana stanična linija adenokarcinoma gušterače
CQ	klorokin
DCC	*N*,*N*′-dicikloheksilkarbodiimid
DCIS	duktalni karcinom *in situ*
DIEA	*N*,*N*-diizopropiletilamin
DMEM	Dulbeccov modificirani Eagleov medij
DMF	*N*,*N*-dimetilformamid
DMSO	dimetilsulfoksid
DNA	deoksiribonukleinska kiselina
DND-41	humana stanična linija akutne limfoblastičke leukemije
EGFR	receptor za humani epidermalni faktor rasta (engl. *epidermal growth factor receptor*)
ER	estrogenski receptor
FDA	Agencija za hranu i lijekove (engl. *Food and Drug Administration*)
G6PD	glukoza-6-fosfat-dehidrogenaza
GBM	glioblastom (lat. *glioblastoma multiforme*)
GC/MS	plinska kromatografija/masena spektrometrija
H460	humana stanična linija karcinoma pluća ne-malih stanica
Hap1	humana stanična linija akutne mijeloične leukemije
HATU	1-[*bis*(dimetilamino)metilen]-1*H*-1,2,3- triazolo[4,5-*b*]piridinij 3-oksid heksafluorofosfat
HCT-116	humana stanična linija karcinoma debelog crijeva
HDAC	histon-deacetilaza
Hek293	humana stanična linija embrionalnih bubrežnih stanica
HepG2	humana stanična linija hepatocelularnog karcinoma
HER2	receptor za humani epidermalni faktor rasta 2
HL-60	humana stanična linija akutne promijelocitne leukemije
Hsp90	protein toplinskog šoka 90 (engl. *heat shock protein*)
IC_{50}	koncentracija spoja koja ubija 50 % stanica
INN	međunarodno nezaštićeno ime (engl. *International Nonproprietary Name*)
IR	infracrveno elektromagnetsko zračenje
K-562	humana stanična linija kronične mijeloične leukemije

MCF-7	humana stanična linija adenokarcinoma dojke
MGMT	O^6-metilgvanin-DNA-metiltransferaza
MM.1S	humana stanična linija multiplog mijeloma
MMP	matriks-metaloproteaza
MR	molekularna refraktivnost
MS	masena spektrometrija
MTIC	monometil triazen 5-(3-metiltriazen-1-il)-imidazol-4-karboksamid
MTT	3-(4,5-dimetiltiazol-2-il)-2,5-difeniltetrazolijev bromid
NAD	nikotinamid adenin dinukleotid
NCI-H460	humana stanična linija karcinoma pluća
NF-κB	nuklearni faktor kapa B
NMR	nuklearna magnetska rezonancija
PQ	primakin
PR	progesteronski receptor
SAHA	suberoilanilid hidroksamska kiselina (engl. *suberoylanilide hydroxamic acid*)
SERM	selektivni modulatori estrogenskih receptora *(*engl. *selective modulators of estrogen receptors*)
s.t.	sobna temperatura
TEA	trietilamin
THF	tetrahidrofuran
TLC	tankoslojna kromatografija (engl. *thin-layer chromatography*)
TMS	tetrametilsilan
TPSA	topološka polarna površina molekule (engl. *topological polar surface area*)
t_t	temperatura taljenja
U251N	humana stanična linija glioblastoma
U2OS	humana stanična linija osteosarkoma
VEGF	vaskularni endotelni faktor rasta (engl. *vascular endothelial growth factor)*
Z-138	humana stanična linija ne-Hodkinovog limfoma

1. UVOD

1.1. Karcinom

Karcinom je jedan od vodećih uzroka mortaliteta u svijetu. Prema istraživanju GLOBOCAN 2018, u 2018. godini karcinom je dijagnosticiran u 18,1 milijuna pacijenata, a više od polovice oboljelih (9,6 milijuna) je umrlo (1). Pretpostavlja se da će u iduća dva desetljeća broj novih pacijenata porasti za 70 % (2). Najčešći oblik karcinoma je karcinom pluća i, od svih karcinoma, on najčešće završava smrtnim ishodom. Karcinom pluća je također i najčešće dijagnosticirani karcinom u muškaraca, dok je karcinom dojke najčešći karcinom u žena (1).

Karcinom je vrlo kompleksna bolest koja se može razviti iz bilo koje vrste stanica uslijed genetičkih i epigenetičkih promjena te je do danas poznato više od 280 različitih vrsta karcinoma (3). Jedna od osnovnih karakteristika stanica karcinoma je nekontrolirana proliferacija i izbjegavanje stanične smrti. Nadalje, stanice posjeduju i mogućnost izbjegavanja supresora rasta, mogu se nekontrolirano razmnožavati, aktiviraju invaziju i metastaziranje, reprogramiraju metabolizam usmjerenjem prema glikolizi te izbjegavaju imunosni sustav (4). Tumorske stanice potiču i angiogenezu, koja se pri normalnim fiziološkim uvjetima u odraslih osoba ne događa. Proces stvaranja novih krvnih žila osigurava tumoru dovoljnu količinu kisika i hranjivih tvari (prvenstveno glukoze), koji su nužni za rast i razmnožavanje (5). Jedan od najvažnijih induktora angiogeneze je vaskularni endotelni faktor rasta-A (engl. *vascular endothelial growth factor-A*, VEGF-A). VEGF-A ima ulogu u stvaranju novih krvnih žila u embrionalnom i postnatalom razdoblju, dok u odraslih ima ulogu u fiziološkom i patološkom održavanju krvnih žila (6). Međutim, hipoksija i mnogi onkogeni mogu potaknuti ekspresiju gena za VEGF-A čime se povećava njegova koncentracija. Sintetizirani VEGF, koji se nalazi u izvanstaničnom matriksu u inaktivnom obliku, oslobađa se i aktivira uz matriks--metaloproteaze (MMP) te potiče angiogenezu (7, 8).

Stanice karcinoma usko su povezane s okolnim stanicama koje predstavljaju heterogeni i dinamični sustav, tzv. tumorski mikrookoliš kojeg ispunjava izvanstanični matriks. Izvanstanični matriks oko karcinoma omogućava rast i širenje karcinoma, izbjegavanje imunosnog sustava, ali i utječe na rezistenciju stanica karcinoma na terapiju (9). Pojava rezistencije na terapiju upravo je jedan od najvećih izazova terapije karcinoma.

Neki citostatici djeluju na jednu specifičnu molekularnu metu koja je pretjerano aktivna u karcinomu u odnosu na zdrave stanice (4). Takvi lijekovi uglavnom imaju malo nuspojava i relativno malu nespecifičnu toksičnost. Međutim, takvi lijekovi djeluju samo na jedno od

obilježja karcinoma, pa se preživjele stanice mogu dalje razmnožavati i prenositi rezistenciju na stanice kćeri. Stanice koje su mutirale ili pomoću epigenetičkog reprogramiranja i remodeliranjem stromalnog mikrookoliša postale rezistentne, glavni su razlog ponovne pojavnosti karcinoma. Također, blokiranjem jednog signalnog puta, stanice mogu prijeći na drugi signalni put (10, 11). Zbog toga se danas sve više okreće dizajniranju i razvoju lijekova koji posjeduju mogućnost djelovanja na više različitih meta.

U nastojanju smanjenja ogromnih troškova razvoja novih lijekova, sve se češće pokušava „reciklirati“ već postojeće lijekove (12). Jedan od pristupa je prenamjena registriranih lijekova za druge indikacije. Takvi lijekovi mogu odmah prijeći u drugu fazu kliničkih ispitivanja jer su već prošli prvu fazu kliničkih ispitivanja (13).

1.2. Karcinom dojke

Karcinom dojke najčešći je karcinom u žena i drugi po redu najčešći karcinom u svijetu. Prema podacima GLOBOCAN 2018, u svijetu je 2018. godine dijagnosticirano 2089 milijuna slučajeva karcinoma dojke (14), dok u Hrvatskoj godišnje oboli oko 2500 žena (15). Osim toga, od karcinoma dojke mogu oboljeti i muškarci, koji čine oko 0,8–1 % oboljelih (16). Najvažniji faktori rizika su: genetska predispozicija, izloženost estrogenima (endogenim i egzogenim, uključujući i dugotrajnu nadomjesnu terapiju hormonima), ionizirajuće zračenje, visoka gustoća dojke i atipična hiperplazija. Zapadnjački stil prehrane, pretilost i konzumacija alkohola također pridonose povišenom riziku incidencije karcinoma dojke. Unatoč visokoj učestalosti, izlječenje karcinoma dojke ima pozitivan trend, te oko 90 % pacijenata preživi barem 5 godina nakon dijagnoze (17).

Estrogeni su ključni ženski spolni hormoni i imaju važnu fiziološku ulogu. Međutim, oni mogu promovirati rast i razvoj određenih tipova karcinoma dojke (18), odnosno karcinoma dojke čije stanice eksprimiraju estrogene receptore (ER) (ER+ karcinom dojke, odnosno hormonski ovisan karcinom dojke). Takav karcinom dojke, u pravilu, reagira na endokrinu terapiju (19). Uz ER, važan je i status receptora za progesteron (PR) i receptora za humani epidermalni faktor rasta 2 (HER2). Upravo zbog različitog statusa receptora, karcinom dojke može se podijeliti na tri tipa: trostruko negativni, HER2 pozitivni i estrogen-ovisan karcinom dojke. Karcinomi koji imaju eksprimiran bilo koji od navedena tri receptora imaju bolju prognozu, iako su HER2 pozitivni karcinomi najagresivniji. Trostruko negativni karcinom dojke ima lošiju prognozu jer

se ne može liječiti lijekovima koji utječu na ER i razinu estrogena u organizmu, kao ni inhibitorima HER2, već je potrebna kombinacija operacije, zračenja i nespecifične kemoterapije (20). Oko 80 % karcinoma dojke ima receptore za estrogen (ER+ karcinomi), a 60 % tih karcinoma ima i receptore za progesteron (21).

Osim po statusu receptora, karcinom dojke klasificira se prema TNM sustavu koji uzima u obzir veličinu tumora (T), zahvaćenost limfnih čvorova (engl. *lymph nodes*, N) i prisutnost metastaza (M).

1.2.1. Terapija estrogen-ovisnog karcinoma dojke

Terapijski pristup liječenju karcinoma dojke nije uvijek isti, već ovisi o nekoliko faktora. Prema smjernicama Europskog društva za medicinsku onkologiju, odabir terapije ovisi o veličini i lokaciji tumora (veličina i lokacija primarnog tumora, broj lezija, zahvaćenost limfnih čvorova), biologiji (receptorski status, biomarkeri i ekspresija gena), ali i dobi, menopauzalnom statusu te općem zdravstvenom statusu i preferencijama pacijentica (22, 23). U mlađih predmenopauzalnih pacijentica posebnu pozornost mora se pridodati statusu plodnosti i potencijalnim mjerama očuvanja plodnosti.

Terapija karcinoma dojke uključuje kombinaciju operacije, radioterapije, kemoterapije, endokrine terapije i ciljane terapije.

U terapiji ER+ karcinoma dojke primjenjuju se lijekovi koji utječu na biosintezu estrogena ili njihovo vezanje na estrogenski receptor (24). Lijekove koji utječu na biosintezu estrogena možemo podijeliti na inhibitore aromataze, agoniste faktora oslobađanja gonadotropina, antagoniste faktora oslobađanja gonadotropina i androgene (25). U drugu skupinu lijekova ubrajamo selektivne modulatore estrogenskih receptora (engl. *selective modulators of estrogen receptors,* SERM) i antagoniste estrogenskih receptora. U skupinu SERM-ova spada i tamoksifen, zlatni standard za liječenje ER+ karcinoma dojke (Slika 1) (26). Dokazana je njegova djelotvornost u pacijentica s karcinomom dojke neovisno o njihovoj dobi (27), a najveću učinkovitost ima u prvih pet godina terapije (28, 29).

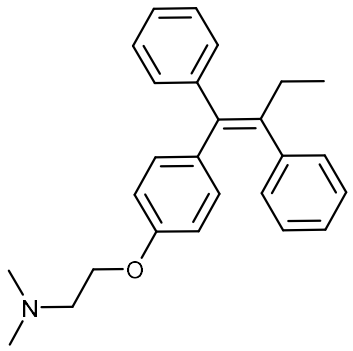

Slika 1. Tamoksifen.

Pacijentice u predmenopauzi terapiju započinju s 20 mg tamoksifena jednom dnevno. Ona obično traje 5 godina, nakon čega se primjenjuje inhibitor aromataze, ali ovisno o menopauzalnom statusu, terapija tamoksifenom može se nastaviti. Pacijentice u postmenopauzi terapiju započinju inhibitorom aromataze, anastrozolom ili letrozolom, međutim, ukoliko je inhibitor aromataze kontraindiciran ili ga pacijentica ne podnosi dobro, može se primijeniti tamoksifen. Terapija inhibitorima aromataze obično traje 5 do maksimalno 10 godina, nakon čega se primjenjuje tamoksifen (29).

Ukoliko dođe do ponovne pojave karcinoma, u pacijentica u predmenopauzi primjenjuje se ili goserelin (agonist faktora oslobađanja gonadotropina), subkutano u dozi od 3,6 mg jednom mjesečno, ili inhibitor aromataze. U pacijentica u postmenopauzi primjenjuje se eksemestan ukoliko su prethodno primale anastrozol ili letrozol. Fulvestrant (antagonist ER) se primjenjuje u pacijentica koje ne toleriraju terapiju ili nisu u mogućnosti pridržavati se oralne terapije jer se primjenjuje jednom mjesečno u obliku intramuskularne injekcije (30).

Iako je najčešće terapija prvog izbora, tamoksifen može uzrokovati ozbiljne nuspojave kao što su pojava krvnih ugrušaka, karcinom endometrija, bol u kostima, promjene raspoloženja i depresivno raspoloženje (31). S druge strane, primjena inhibitora aromataze povećava rizik od pojavnosti osteoporoze. Preporučljivo je da se pacijenticama odredi denzitometrijski status prije početka terapije. Međutim, sam status gustoće kostiju ne bi trebao spriječiti propisivanje inhibitora aromataze, već bi se trebale primijeniti druge mjere opreza kao što je redovito vježbanje, prestanak pušenja i prehrana bogata kalcijem (30).

1.2.2. Kemoterapija karcinoma dojke

Kemoterapija može biti terapijski pristup u liječenju agresivnijih tipova karcinoma dojke, tj. trostruko negativnog ili HER2-pozitivnog karcinoma. Može se primijeniti prije operacije kako bi se smanjilo tumorsko tkivo, nakon operacije za uništavanje stanica karcinoma koje su zaostale ili kod uznapredovalog karcinoma dojke koji se proširio izvan tkiva dojke. Među najčešće korištene lijekove spadaju antraciklini (doksorubicin, epirubicin), taksani (paklitaksel i docetaksel), 5-fluorouracil, ciklofosfamid i karboplatin, a često se primjenjuje i kombinirana terapija dva ili tri lijeka (32).

Za razliku od endokrine terapije koja se uglavnom primjenjuje peroralno, kemoterapija se primjenjuje intravenski i u ciklusima. Ciklusi traju oko 2 ili 3 tjedna. Između ciklusa je razdoblje bez terapije, kako bi se pacijentice oporavile od učinaka lijekova. Adjuvantna ili neoadjuvantna kemoterapija primjenjuje se u razdoblju od 3 do 6 mjeseci, ovisno o učinkovitosti i nuspojavama lijekova (33).

Nuspojave kemoterapije su individualne, te ovise o primijenjenom lijeku, rasporedu doziranja i samoj dozi lijeka. One mogu uključivati umor, povećani rizik od infekcije, mučninu i povraćanje, gubitak kose, gubitak apetita, proljev, zatvor, trnce i gubitak osjeta, uranjenu menopauzu, povećavanje tjelesne mase i blago smanjenje kognitivnih sposobnosti (34). Nuspojave uglavnom nestaju s prestankom primjene lijeka, a katkada se mogu regulirati suportivnom terapijom. U rijetkim slučajevima mogu se dogoditi trajnije nuspojave, kao što je oštećenje srca, trajno oštećenje živaca ili sekundarne zloćudne bolesti kao što su leukemija i limfom (35).

1.3. Glioblastom

Gliomi su primarni tumori mozga nastali iz glija stanica. Prema staničnom podrijetlu, mogu se podijeliti na astrocitne tumore (astrocitom, anaplastični astrocitom i glioblastom), oligodendrogliom, ependiom i miješane gliome (36). Glioblastom (lat. *glioblastoma multiforme*, GBM) je najagresivniji i najčešći oblik tumora mozga u odraslih osoba. Potječe iz astrocita, zvjezdastih glija stanica, i po klasifikaciji spada u gradus IV, čija su obilježja nekrotično tkivo te stanice uopće ne nalikuju na zdrave stanice, a sam tijek bolesti je nagao i progresivan (37, 38).

Simptomi variraju od pacijenta do pacijenta, ovisno o lokaciji glioblastoma, ali i samoj anatomiji mozga pacijenta. Jedan od prvih simptoma glioblastoma je glavobolja koja nastaje uslijed povećanja intrakranijalnog tlaka, zatim fokalne neurološke smetnje, promjene mentalnog statusa, a u 25–50 % pacijenata mogu se pojaviti i konvulzije (39, 40).

Jedna od posebnosti glioblastoma je prisutnost tzv. tumorskih zona koje su jedan od glavnih razloga ponovne pojavnosti tumora (41). Postoje tri tumorske zone. Zonu I čini tumorsko tkivo sačinjeno od stanica karcinoma. Zonu II čine tranzitorne stanice koje su po puno histoloških obilježja slične tumorskim stanicama, ali ipak postoje neke razlike. Tu se nalazi veća koncentracija mikroglija, modificiranih astrocitoma i endotelijskih stanica, a pretpostavlja se da su u ovoj zoni prisutne biološki aktivne stanice tumora. Za razliku od zone I i II, zona III se ne vidi na magnetskim rezonancijskim snimkama i uglavnom se sastoji od zdravog parenhima mozga. Međutim, u tom zdravom tkivu nalaze se i poliklonalne matične stanice tumora koje se mogu, pod određenim uvjetima, razviti u stanice tumora (42).

1.3.1. Terapija glioblastoma

Trenutni pristup u liječenju glioblastoma je kirurško odstranjivanje tumora, nakon čega slijedi zračenje uz kemoterapiju. Ovisno o tome gdje se tumor nalazi, kirurško odstranjivanje tumora može umanjiti simptome glioblastoma i poboljšati kvalitetu života (43). Međutim, odstranjivanje tumora često nije moguće zbog lokacije tumora na mozgu (npr. na moždanom deblu ili bazalnim ganglijima). Također, zbog izostanka oštrih granica tumora u odnosu na zdravo tkivo, kirurško odstranjivanje tumora može biti nepotpuno, što rezultira ponovnom pojavom tumora (44).

Temozolomid je jedini kemoterapeutik odobren za liječenje glioblastoma (37). On je prolijek koji je stabilan pri kiselom pH (što omogućava njegovu oralnu primjenu), a aktivira se pri fiziološkom pH (7,4). U prvom koraku dolazi do otvaranja šesteročlanog prstena koji se dalje razgrađuje na metildiazonijev kation i 5-aminoimidazol-4-karboksamid (Slika 2) (45). Metildiazonijev kation je jako reaktivan te metilira purinske baze (gvanin, adenin) što rezultira krivim sparivanjem baza u DNA i dvostrukim lomom DNA uzvojnice (46).

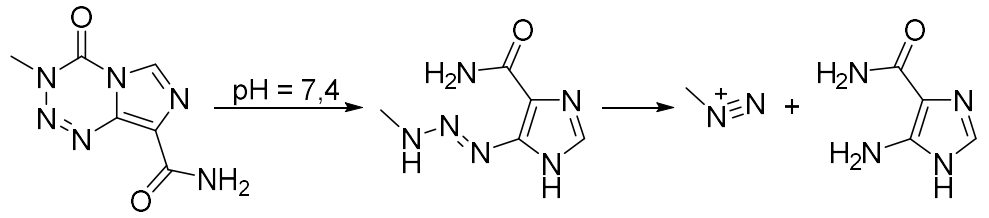

Slika 2. Aktivacija temozolomida.

Međutim, s vremenom tumorske stanice razviju rezistenciju na temozolomid. Povećane koncentracije enzima O^6-metilgvanin-DNA-metiltransferaze (MGMT) pogoduju uklanjanju metilne skupine s metiliranih baza zbog čega temozolomid gubi učinak (47).

Unatoč svemu, preživljavanje pacijenta s glioblastomom je u prosjeku 14–16 mjeseci nakon dijagnoze i početka terapije. Svega 10 % pacijenata preživi 5 godina nakon dijagnoze (48).

1.4. Histon-deacetilaze

Histon-deacetilaze (HDAC) su enzimi koji kataliziraju hidrolizu acetilne skupine s terminalnih amino skupina lizina u histonima. Budući da je DNA negativno nabijena, ona je čvrsto omotana oko pozitivno nabijenih histona i tada je onemogućena transkripcija. Acetilacijom histona, DNA se odmata te je omogućen pristup transkripcijskim faktorima (49). Uklanjanjem acetilne skupine, ponovo jača interakcija između DNA i histona te je transkripcija zaustavljena. Uz acetilaciju, na transkripciju se može utjecati fosforilacijom i metilacijom (50).

Danas je poznato 18 HDAC enzima koji su podijeljene u 4 klase, ovisno o njihovoj funkciji i sličnosti s HDAC iz plijesni (51). Od navedenih klasa humanih HDAC enzima, klase I, II i IV su proteini koji u aktivnom mjestu imaju ion cinka, dok klasa III, tzv. sirtuini, u aktivnom središtu sadrži NAD^+ (52).

U klasu I spadaju HDAC 1, 2, 3 i 8. Rasprostranjeni su u svim ljudskim tkivima, a HDAC1–3 nalaze se isključivo u jezgri stanice, dok se HDAC8 može nalaziti i u citosolu. Glavna meta klase I su histoni, međutim, HDAC1–3 mogu deacetilirati i nehistonske proteine, uključujući i p53, tumor-supresorski protein kojem se acetilacijom povećava stabilnost i potiče povezivanje s drugim proteinima. Acetilacija je potrebna za odgovor p53 na oštećenu DNA i aktivirane onkogene (53, 54). Izuzev histona, ostali supstrati HDAC8 za sada nisu poznati.

Klasa II podijeljena je na IIa u koju pripadaju HDAC 4, 5, 7 i 9, te na IIb u koju spadaju HDAC 6 i 10 (55). Za razliku od klase I, HDAC klase II su tkivno specifični i mogu se nalaziti u citosolu stanice (56, 57). HDAC klase IIa nalaze se uglavnom u srčanim i skeletnim mišićima, mozgu i gušterači te imaju ulogu u razvoju i održavanju kostiju, srca, skeletnih mišića te vaskularnog i živčanog sustava (58). Tako, primjerice, HDAC4 djeluje kao represor hipertrofije hondrocita, HDAC5 je negativni regulator angiogeneze u endotelijskim stanicama, HDAC7 ima funkciju u negativnoj regulaciji i apoptozi T-stanica, a HDAC9 ima ulogu u diferencijaciji kardiomiocita (59–62).

HDAC6 i HDAC10 nalaze se isključivo u citosolu stanice (63). HDAC6 je jedini HDAC enzim koji ima dva katalitička mjesta i mjesto za vezanje ubikvitina (64). Budući da je HDAC6 u citosolu stanice, on ispoljava svoju enzimsku aktivnost isključivo na nehistonskim proteinima. Mete HDAC6 su α-tubulin, kortaktin, protein toplinskog šoka 90 (engl. *heat shock protein* 90, Hsp90) i drugi šaperoni, peroksiredoksini i transmembranski proteini. HDAC6 ima ulogu u kontroli citoskeleta preko koje utječe na migraciju stanice te ima ulogu u angiogenezi (65, 66). Izuzev toga, HDAC6 ima i ulogu u kemotaksiji i poticanju migracije, procesima koji nisu vezani uz enzimsku aktivnost HDAC6 (67). HDAC10 je strukturno sličan HDAC6, ali ima samo jedno katalitičko mjesto. Također može deacetilirati Hsp90 što uzrokuje destabilizaciju kompleksa, smanjenje proteosomalne aktivnosti i kao posljedicu ima povećanje koncentracije faktora koji potiču angiogenezu (68).

U klasu IV spada jedino HDAC11, a nalazi se u mozgu, srcu, skeletnim mišićima i bubrezima. HDAC11 je enzim koji se uglavnom nalazi u jezgri, ali može se naći i u citosolu stanice gdje može stvarati komplekse s HDAC6 (69). Do nedavno je funkcija HDAC11 bila nepoznata, ali 2018. godine otkriveno je da je HDAC11 negativni regulator protuupalnog citokina IL-10 i da smanjuje ekspresiju IL-13 u CD4+T stanicama srca (70, 71).

Iako imaju brojne fiziološke uloge, HDAC su pretjerano eksprimirani u mnogim karcinomima i tako promoviraju nekontrolirani rast stanica, izbjegavanje stanične smrti, potiču migraciju stanica i metastaze (52, 72, 73). Inhibitori HDAC su zato zanimljiva terapijska skupina citostatika, te su danas odobrena od strane američke Agencije za hranu i lijekove (engl. *Food and Drug Administration*, FDA) četiri HDAC inhibitora: suberoilanilid hidroksamska kiselina (SAHA, vorinostat), romidepsin, panobinostat i belinostat (74).

1.4.1. SAHA

SAHA je citostatik, odobren 2006. godine od strane FDA za liječenje kožnog limfoma T-stanica (75) (Slika 3). Indicirana je za progresivni, perzistentni ili ponavljajući oblik bolesti. Dozira se jednom dnevno u dozi od 400 mg, a primjenjuje se peroralno (76). Farmakofor u molekuli je hidroksamska kiselina, funkcionalna skupina koja ima sposobnost kompleksacije metalnih iona, zbog čega može inhibirati enzime koji u aktivnom mjestu sadrže ione metala, primjerice HDAC i MMP (77).

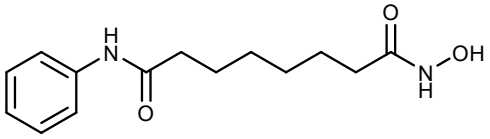

Slika 3. SAHA (vorinostat).

Marks i suradnici sidrili su SAHA-u u aktivno katalitičko mjesto HDAC-sličnog proteina čija je osnova kristalna struktura homologa HDAC enzima izoliranog iz hipertermofilične bakterije, *Aquifex aeolicus* (78). Hidroksamska skupina SAHA-e kompleksira ion cinka iz aktivnog mjesta. Alkilni lanac nalazi se unutar enzimskog džepa i povezuje hidroksamsku kiselinu s fenilnim prstenom koji se nalazi unutar katalitičke domene, a usmjeren je prema površini HDAC enzima (Slika 4).

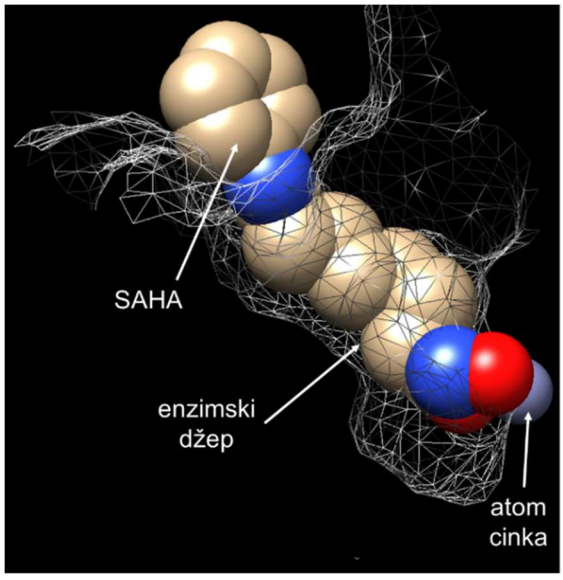

Slika 4. SAHA (vorinostat) usidren u aktivno mjesto HDAC-sličnog proteina.

Kompleksiranje cinka u aktivnom središtu HDAC dovodi do inhibicije enzima i smanjenja interakcija između DNA i histona te može doći do reaktivacije gena odgovornih za sintezu proapoptotičkih proteina (79). Također dolazi i do nakupljanja acetiliranih histona i acetiliranih proteina, kao što su transkripcijski faktori, strukturni proteini, šaperoni, kromatin-remodelirajući kompleksi, medijatori signalnog puta i nuklearni transportni proteini, što dovodi do smrti stanica karcinoma (80). Osim histona, primjenom SAHA-e povećava se koncentracija acetiliranih receptora za androgene, E2F-1, YY1, Smad7, EKLF, p53, BCL-6, HIF-1, NF-Y, NF-κB i GATA-1. Acetilacija tih transkripcijskih faktora također može utjecati na ekspresiju određenih gena (78).

Kao i ostali citostatici, SAHA može uzrokovati nuspojave. Većina nuspojava SAHA-e ne zahtjeva intervencije, ali ukoliko je potrebno, doza se može smanjiti na 300 mg dnevno. U oko 30 % pacijenata, mogu se pojaviti umor, proljev, mučnina i povraćanje. Te nuspojave nisu po život opasne, ali dugotrajni proljev i povraćanje mogu dovesti do dehidracije i gubitka elektrolita te je u tom slučaju potrebno primijeniti lijekove koji umanjuju nuspojave ili nadoknađuju elektrolite, a ukoliko ni to ne pomogne, potrebno je promijeniti terapiju (81). Primjena SAHA-e utječe na koncentraciju hematopoetskih stanica koštane srži te se može smanjiti broj eritrocita, leukocita i trombocita. Dugotrajnom primjenom može doći do anemije, sklonosti infekcijama i stvaranju podljeva (82). Jedna od najopasnijih nuspojava SAHA-e je kardiotoksičnost. Budući da SAHA nije selektivan HDAC inhibitor, njegova primjena može utjecati na funkciju i drugih proteina, uključujući (hERG)K^+ kanal. (hERG)K^+ kanal je ionski kanal koji se nalazi u živčanom sustavu i srcu gdje utječe na repolarizaciju akcijskog potencijala u ventrikularnim miocitima. Iako mehanizam kardiotoksičnosti SAHA-e još uvijek nije u potpunosti razjašnjen, pretpostavlja se da SAHA izravno stupa u interakciju s (hERG)K^+ kanalom te tako utječe na njegovu funkciju (83).

SAHA spada u D kategoriju rizika primjene u trudnoći, te se smije primijeniti samo ako je korist veća od rizika. U animalnim studijama dokazano je da utječe na proces organogeneze i uzrokuje fetalnu toksičnost (84). Još uvijek nije odobren za primjenu u djece, ali se trenutno nalazi u kliničkim ispitivanjima za pedijatrijsku primjenu (85, 86).

1.4.1.1. Sinteza SAHA-e

Breslow i suradnici prvi su opisali sintezu SAHA-e (87). Temeljem prijašnjih istraživanja primijetili su da *N*,*N*'-heksametilen bisacetamid i njemu srodni spojevi posjeduju citostatsko djelovanje (Slika 5). Međutim, kao simetrični dimeri, ti spojevi nemaju selektivno djelovanje, već djeluju i na zdrave stanice (88). Daljnjom modifikacijom spojeva, otkrili su da najaktivnije molekule sadrže dvije različite polarne skupine koje su međusobno povezane fleksibilnim ugljikovodičnim lancem. Polarne skupine trebale su se nalaziti na suprotnim krajevima lanca od kojih je jedna velika hidrofobna skupina (87).

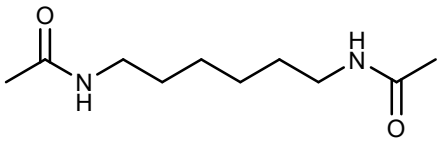

Slika 5. *N*,*N*'-heksametilen bisacetamid.

U svom radu, Breslow i sur. opisali su 4 različita sintetska puta dobivanja SAHA-e (87). U Shemi 1. opisana je sinteza SAHA-e u jednom koraku. Kiselinski diklorid suberinske kiseline reagira s anilinom i slobodnim hidroksilamin-hidrokloridom pri sobnoj temperaturi u prisutnosti kalijevog hidroksida kao baze. Međutim, iskorištenje reakcije je vrlo nisko (15–30 %).

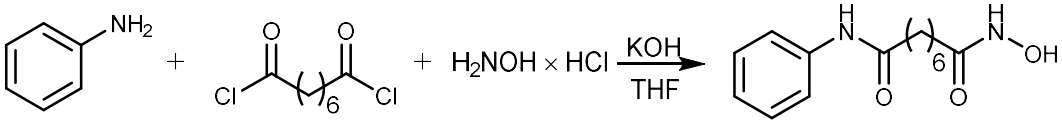

Shema 1. Sinteza SAHA-e u jednom koraku prema Breslow i sur. (87).

Razdvajanjem sinteze na pet koraka, uspjeli su dobiti više iskorištenje (35–65 %). Kiselinski klorid monoestera suberinske kiseline reagira s anilinom pri čemu nastaje amidoester. Hidrolizom esterske skupine u bazičnim uvjetima nastaje slobodna karboksilna skupina, koja može reagirati s *O*-benzilhidroksilaminom u prisutnost *N*,*N*'-dicikloheksilkarbodiimida (DCC) kao *coupling* reagensa. SAHA je dobivena katalitičkom hidrogenolizom nastale zaštićene hidroksamske kiseline (Shema 2). Iako je iskorištenje bolje, reakcija se sastoji od 5 koraka i u

reakciji je korišten skupi monometilni ester, što nije prihvatljivo za sintezu u industrijskim razmjerima (87).

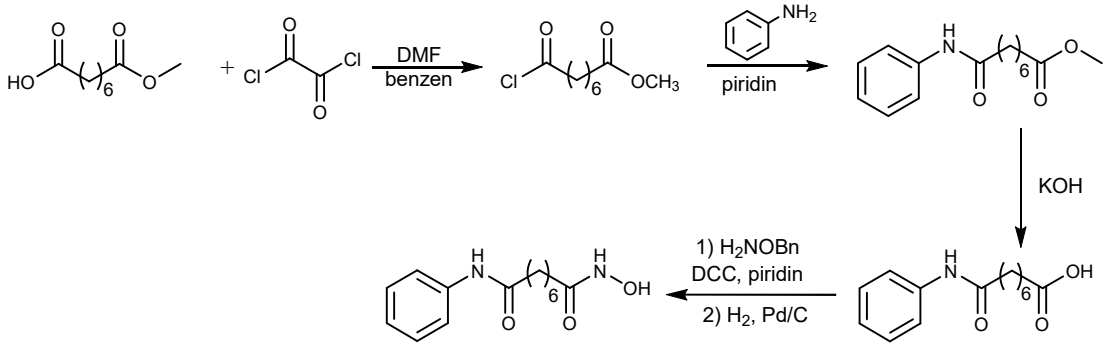

Shema 2. Sinteza SAHA-e u pet koraka prema Breslow i sur. (87).

Daljnjom optimizacijom sinteze, skratili su sintezu na dva koraka. U prvom koraku kiselinski diklorid suberinske kiseline reagira s anilinom i *O*-benzilhidroksilaminom nakon čega slijedi deprotekcija katalitičkom hidrogenolizom (Shema 3). Međutim, ukupno iskorištenje je slabije od prethodne sinteze (20–35 %). Također, zamjena *O*-benzilhidroksilamina *O*-trimetilsilil-hidroksilaminom nije značajno utjecala na ukupno iskorištenje reakcije (20–33 %).

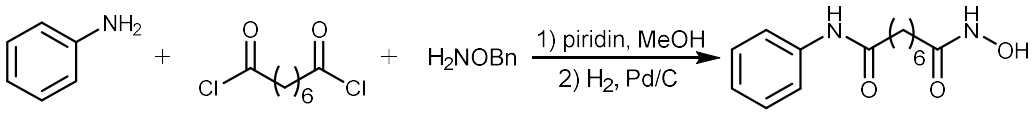

Shema 3. Sinteza SAHA-e u dva koraka prema Breslow i sur. (87).

Mai i suradnici opisali su sintezu SAHA-e prethodnim prevođenjem suberinske kiseline u anhidrid (Shema 4). Anhidrid zatim reagira s anilinom pri čemu nastaje amid sa slobodnom karboksilnom skupinom koji prvo reagira s etil-klorformijatom, a zatim s hidroksilaminom. Međutim, reakcijom mogu nastati različiti nusprodukti. Tako, primjerice, u prvom koraku može nastati linearni anhidrid, u drugom koraku dianilinski produkt, a u trećem koraku miješani anhidrid suberinske kiseline s etil-kloroformijatom koji je nestabilan i raspada se u suberinsku kiselinu. Svi navedeni nusprodukti otežavaju pročišćavanje produkta i utječu na ukupno iskorištenje koje može varirati između 38 i 58 % (89).

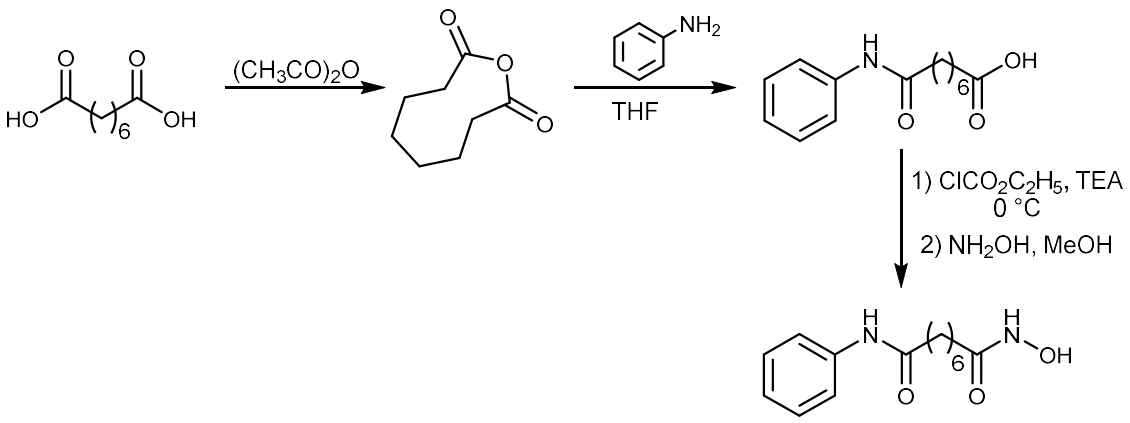

Shema 4. Sinteza SAHA-e prema Mai i sur. (89).

Gediya i suradnici opisali su sintezu SAHA-e u samo dva koraka s ukupnim iskorištenjem reakcije od 80 % (Shema 5). U prvom koraku reakcije monometilni ester suberinske kiseline reagira s anilinom u prisutnosti hidroksibenzotriazola (HOBt) i DCC-a. U drugom koraku dobiveni se ester hidrolizira u prisutnosti kalijevog hidroksida, a nastala karboksilna kiselina bez prethodnog pročišćavanja reagira s hidroksilamin-hidrokloridom. Tim sintetskim putem postignuto je najviše iskorištenje i reakcija se zbiva u samo dva koraka, iako i dalje nije izbjegnuto korištenje skupog monometilnog estera suberinske kiseline (90).

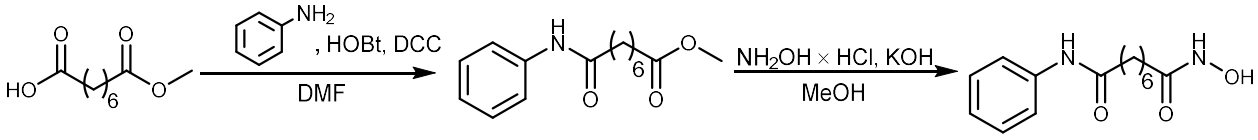

Shema 5. Sinteza SAHA-e prema Gediya i sur. (90).

1.4.2. Belinostat

Belinostat je odobren 2014. godine od strane FDA za liječenje perifernog limfoma T-stanica (91). Kao i SAHA, inhibira HDAC enzime te sadrži isti farmakofor – hidroksamsku kiselinu (Slika 6) (92). Belinostat je derivat cimetne kiseline i u svojoj strukturi sadrži nezasićenu dvostruku vezu. Upravo je uvođenje nezasićene dvostruke veze bio ključan korak u njegovom dizajniranju jer je povećana rigidnost molekule (93) te je aktivnost belinostata bila višestruko veća u odnosu na strukturnog analoga sa zasićenom vezom (94). U strukturi belinostata također

je prisutna i sulfonamidska skupina. Belinostat je testiran *in vitro* na 60 različitih staničnih linija karcinoma te je, prema podacima Nacionalnog instituta za istraživanje raka (engl. *National Cancer Institute*), inhibirao rast stanica u prosječnoj IC_{50} vrijednosti od 0,18 μM što ga čini pet puta aktivnijim od SAHA-e (94).

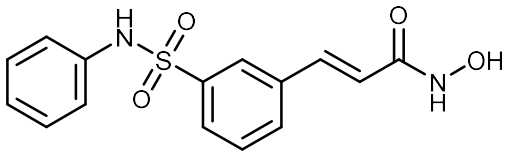

Slika 6. Belinostat.

Belinostat se primjenjuje intravenski u dozi od 1000 mg/m^2 kroz 30 minuta jednom dnevno prvih pet dana ciklusa koji traje 21 dana. Infuzija se može primjenjivati i kroz 45 minuta ukoliko se javlja bol na mjestu uboda. Ciklusi od 21 dan mogu se ponavljati ukoliko nema napredovanja bolesti ili se ne pojavi nepodošljiva tokičnost lijeka (95).

Najčešće nuspojave belinostata su mučnina, umor, vrućica i povraćanje, ali moguće su i ozbiljnije nuspojave kao što su anemija, trombocitopenija, dispneja, povišenje kreatinina i produljenje QTc signala (96). U jednoj od prvih kliničkih studija, 9 od 129 pacijenata umrlo je unutar 30 dana od zadnje primijenjene doze belinostata. Razlozi su bili zatajenje više organa (srce, jetra), infekcija pluća, gastrointestinalna hemoragija i šok. Međutim, jedino se zatajenje jetre povezuje s primjenom belinostata (95).

Dokazano je da belinostat uzrokuje genotoksičnost na psećim i mišjim animalnim modelima. Daljnja ispitivanja na trudnim životinjama nisu provedena jer se smatra da zbog genotoksičnosti djeluje teratogeno i može uzrokovati smrt embrija/fetusa (95). Primjena belinostata u trudnica spada u D kategoriju rizika, a još uvijek nema dovoljno podataka o izlučivanju belinostata u majčino mlijeko (97).

1.4.2.1. Sinteza belinostata

Reisch i sur. opisali su sintezu belinostata u 6 koraka (98). U prvom koraku iz benzaldehida u prisutnosti oleuma (dimeće sumporne kiseline) i taloženjem natrijevim karbonatom nastaje

natrijeva sol 3-formilbenzensulfonske kiseline. Dobivena sol Wittigovom reakcijom daje metilni ester koji u reakciji s tionil-kloridom daje kiselinski klorid koji može reagirati s anilinom. Dobiveni produkt je podvrgnut hidrolizi natrijevim hidroksidom pri čemu nastaje slobodna karboksilna kiselina koja u reakciji s hidroksilaminom daje belinostat (Shema 6). Sama reakcija nije prihvatljiva za sintezu u industrijskim razmjerima zbog niskog iskorištenja i upotrebe oleuma.

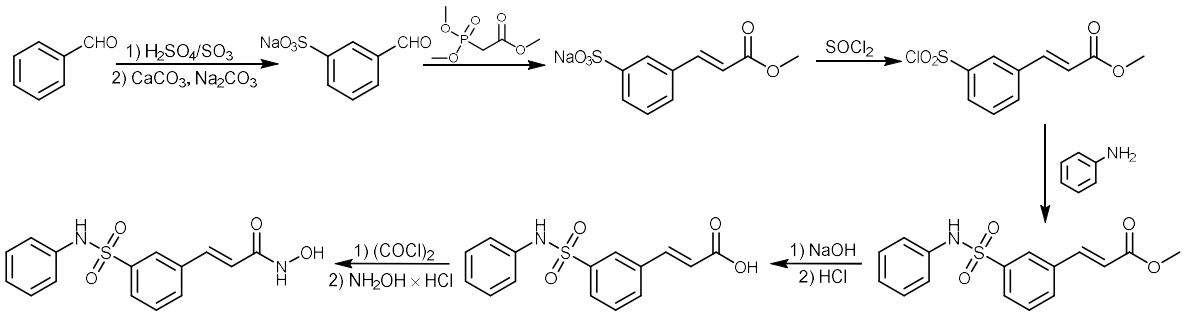

Shema 6. Sinteza belinostata prema Reisch i sur. (98).

Kako bi izbjegli navedene nedostatke, Yang i sur. opisali su sintezu bez upotrebe oleuma i tionil-klorida (99). Početni reaktant je 3-nitrobenzaldehid koji u prvom koraku Wittig-Hornerovom reakcijom s metil-dimetilfosfoacetatom daje ester, a u drugom koraku je njegova nitro skupina reducirana do amina uz kositrov(II) klorid. U idućem koraku je amino skupina uz natriev nitrit prevedena u diazonijevu sol koja je supstituirana sa sumporovim dioksidom u klorovodičnoj kiselini. Dobiveni spoj s klorosulfonilnom skupinom reagira s anilinom pri čemu nastaje sulfonamid koji u reakciji s hidroksilaminom daje belinostat. Osim što je reakcija pojednostavljena, ukupno iskorištenje reakcije je više i iznosi 41 %.

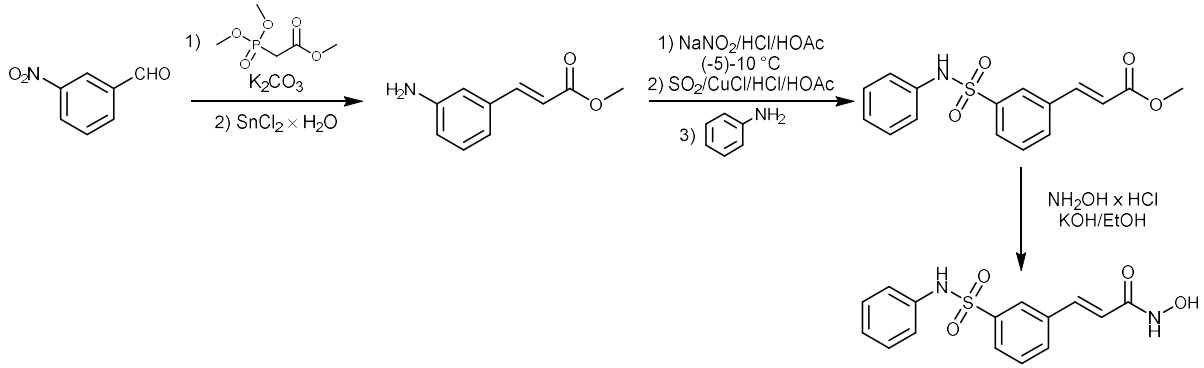

Shema 7. Sinteza belinostata prema Yang i sur. (99).

Jedna od zadnje opisanih sinteza belinostata objavljena je 2016. godine (100). Sinteza se zbiva u 5 koraka, a počinje reakcijom benzaldehida s natrijevim bisulfitom kako bi se zaštitila aldehidna skupina. Zatim slijedi sulfokloriranje, reakcija s anilinom kako bi se dobio sulfonamid, Doebnerova modifikacija Knoevenagelove kondenzacije s malonskom kiselinom uz koju se odvija dekarboksilacija pri čemu se dobiva mono-karboksilna kiselina koja u zadnjem koraku reagira s hidroksilaminom (Shema 8). Iako ukupno iskorištenje reakcije nije pretjerano visoko (33 %), u sintezi su korišteni jeftini reaktanti te je reakcija prihvatljiva za potrebe industrijske sinteze.

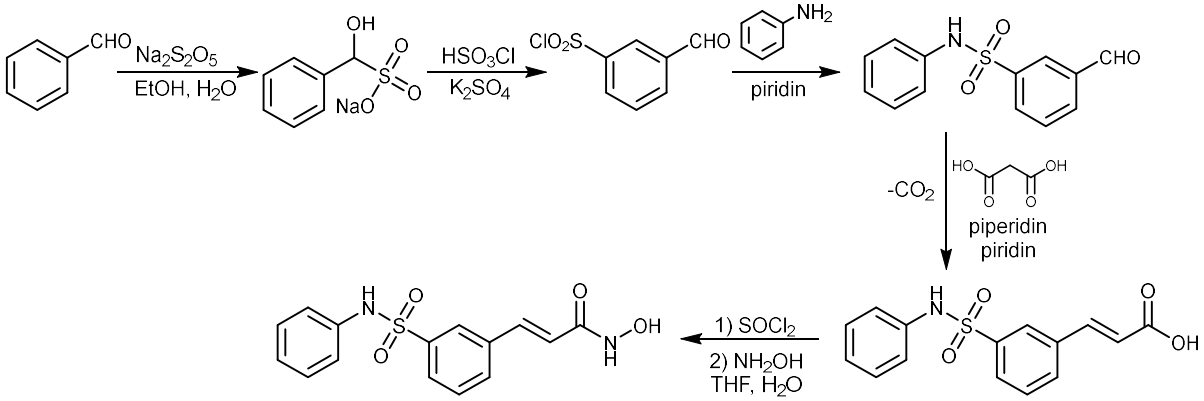

Shema 8. Sinteza belinostata prema Bao i sur. (100).

1.4.3. Panobinostat

Panobinostat je zadnji iz skupine HDAC inhibitora koji je odobren od strane FDA 2015. godine. Derivat je cimetne kiseline, a farmakofor također sadrži hidroksamsku kiselinu (Slika 7). Koristi se u terapiji multiplog mijeloma u kombinaciji s bortezomibom i deksametazonom u pacijenata koji su već prije primali bortezomib i neki drugi imunomodulatorni lijek (101). Za razliku od SAHA-e i belinostata, panobinostat se primjenjuje peroralno svaki drugi dan prva dva tjedna ciklusa koji traje 21 dan (102).

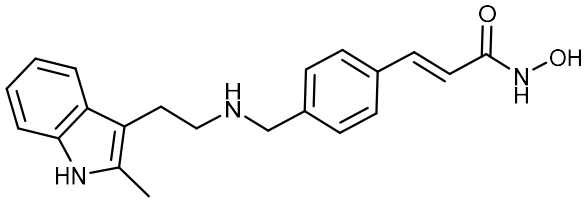

Slika 7. Panobinostat.

Panobinostat inhibira sve HDAC enzime koji u svom aktivnom središtu sadrže atom cinka i na taj način regulira transkripciju gena, diferencijaciju stanica, stanični ciklus i potiče stanice karcinoma na apoptozu (103). Izrazito je aktivan inhibitor HDAC enzima te djeluje već u niskim nanomolarnim koncentracijama i deset puta je jači inhibitor od SAHA-e (104).

Najčešće nuspojave primjene panobinostata su trombocitopenija, neutropenija, anemija, dijarea, mučnina, povraćanje, edemi udova, smanjen apetit, slabost i umor. Nuspojave vezane uz poremećaje krvne slike mogu se ublažiti smanjenjem doze panobinostata, a puno veći problem predstavlja umor koji može utjecati na kvalitetu života pacijenta i koji se pojačava s napredovanjem bolesti (105). Zbog smanjenog broja trombocita, može doći do unutarnjeg krvarenja te se preporuča redovito praćenje krvne slike kako bi se pacijentu po potrebi dala transfuzija. Ukoliko primjena panobinostata uzrokuje teške dijareje, potrebno je primijeniti antidijaroike, smanjiti dozu panobinostata ili prekinuti terapiju (102).

Kao i SAHA, zbog svoje neselektivnosti, panobinostat je kardiotoksičan te može utjecati na produljenje QT intervala, uzrokovati teške aritmije ili neke druge promjene elektrokardiograma. Budući da panobinostat može utjecati na ravnotežu elektrolita koja posljedično pojačava kardiološku toksičnost, potrebno je redovito praćenje elektrolita. Također, vjerojatnost za produljenje QT intervala je smanjena ukoliko se panobinostat primjenjuje peroralno, a ne intravenski (103, 105, 106).

Oko 40 % panobinostata metabolizira se putem CYP3A4 enzima, a manji dio putem CYP2D6 i CYP2C19 te je potrebna korekcija doze ukoliko se primjenjuje istovremeno s lijekovima koji utječu na aktivnost tih enzima (107).

Animalne studije pokazale su da je panobinostat teratogen i može uzrokovati smrt majke. Također je dokazano da smanjuje plodnost pacijenta neovisno o spolu. Još uvijek nema dovoljno podataka o izlučivanju panobinostata u majčino mlijeko te se preporuča prestanak dojenja ili uzimanja lijeka tijekom dojenja kako bi se izbjegli potencijalni štetni učinci (108).

1.4.3.1. Sinteza panobinostata

Bair i sur. objavili su 2002. jednu od prvih sinteza panobinostata u patentu WO 02/22577 A2 (Shema 9) (109). Prvi korak je esterifikacija 4-formil cinamata, nakon čega 2-metiltriptamin

reagira s esterom u prisutnosti natrijeva triacetoksiborhidrida kao reducensa. Dobiveni spoj reagira s hidroksilaminom u prisutnosti kalijevog hidroksida i daje konačan produkt, tj. panobinostat.

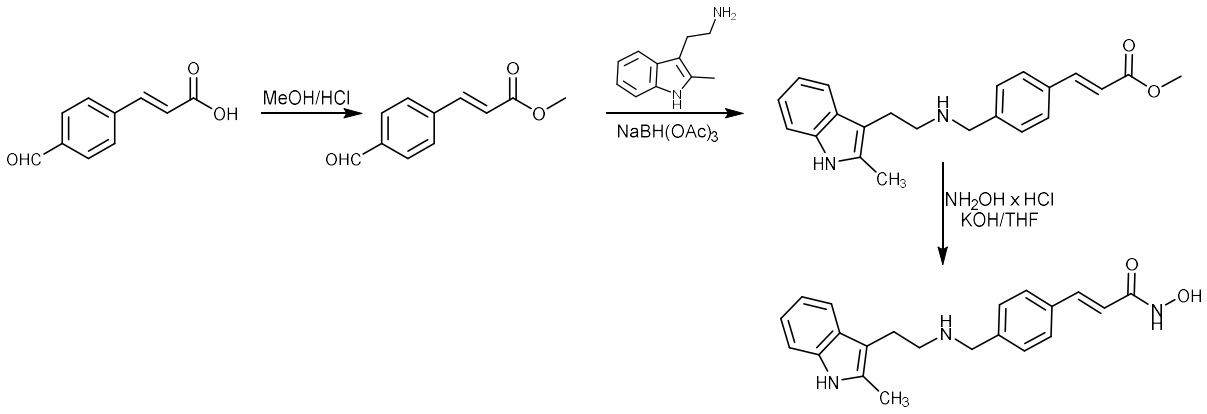

Shema 9. Sinteza panobinostata prema Bair i sur. (109).

Chen i sur. opisali su sintezu panobinostata u dva koraka (110). 4-Klormetilbenzaldehid Wittig-Hornerovom reakcijom s metil-dietilfosfoacetatom daje produkt koji reagira s 2-metiltriptaminom. Dobiveni ester nukleofilnom supstitucijom s hidroksilaminom daje panobinostat (Shema 10). Prednost ove sinteze je jednostavno pročišćavanje bez upotrebe kromatografije na koloni, a ukupno iskorištenje reakcije je 40 %.

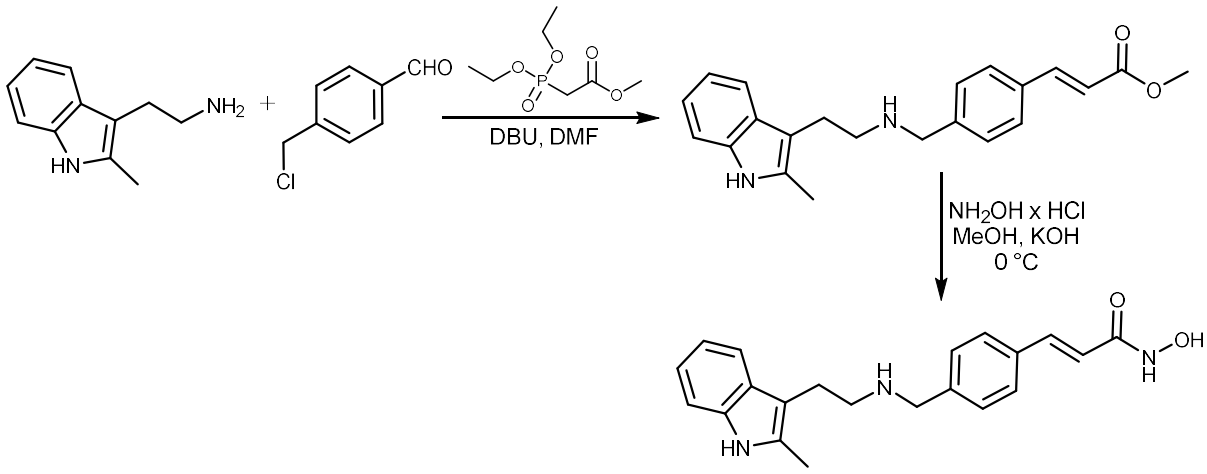

Shema 10. Sinteza panobinostata prema Chen i sur. (110).

1.5. Malarija

Malarija je zarazna bolest koju uzrokuju paraziti iz roda *Plasmodium* (*P. vivax, P. falciparum, P. knowlesi, P. malariae*, *P. ovale*), a prenosi se ubodom ženke komarca iz porodice *Anopheles*. Prema podacima Svjetske zdravstvene organizacije, u 2018. godini malarija je dijagnosticirana kod 228 milijuna pacijenata, od kojih je 405 000 umrlo (111). Kao što je spomenuto, malarija započinje ubodom zaražene ženke komarca pri čemu sporozoit ulazi u krvotok i putuje do jetre, gdje se događa prva faza malarije koja je asimptomatska. Kroz dva tjedna, razvija se na tisuće merozoita koji se ispuštaju u krvotok nakon pucanja hepatocita. Kada merozoiti uđu u eritrocite javljaju se simptomi malarije: vrućica, bolovi u mišićima, tresavica, glavobolja, mučnina, povraćanje, abdominalni bolovi, proljev, anemija i konvulzije (Slika 8) (112).

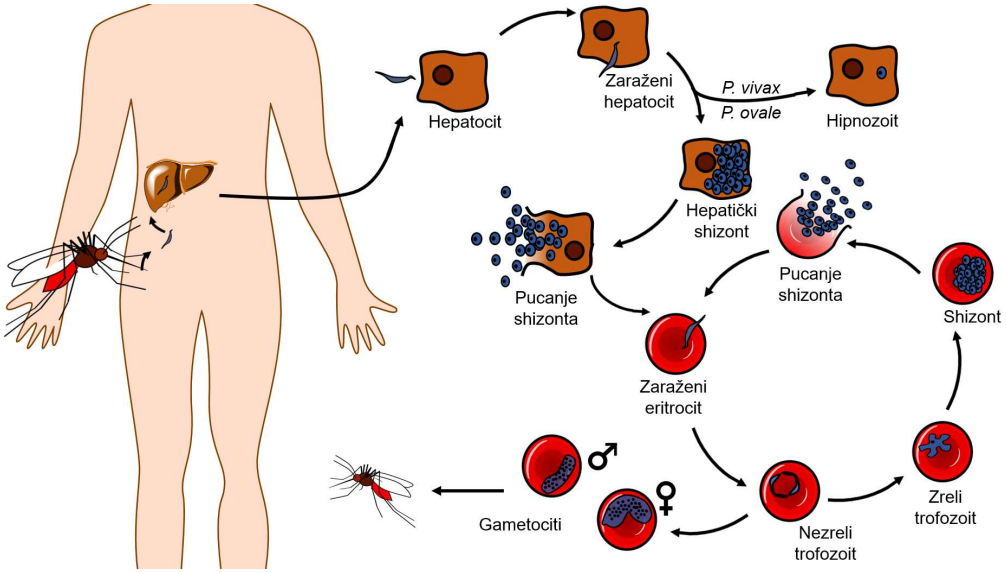

Slika 8. Ciklus malarije u čovjeku.

Ukoliko se terapija primjeni na vrijeme, simptomi se obično povuku kroz nekoliko dana. Posebna pozornost treba se pridodati u slučaju infekcije *P. falciparum*, jer svaka ponovna pojavnost simptoma nakon završene terapije upućuje na nepotpunu terapiju, prisutnost rezistencije na lijek ili novu infekciju (113).

Trenutna terapija uključuje artemizinin-kombiniranu terapiju ili klorokin, a oni se najčešće kombiniraju s primakinom (114).

1.5.1. Primakin

Primakin je antimalarik koji je u upotrebi od 1940-ih te se danas nalazi na listi esencijalnih lijekova Svjetske zdravstvene organizacije (Slika 9) (115). On djeluje na gametocite i egzoeritrocitne oblike svih vrsta parazita koji uzrokuju malariju, uključujući i *Plasmodium* vrste koje su otporne na klorokin (116). Sve do 2018., kada je registriran tafenokin, primakin je bio jedini lijek koji je djelovao na hipnozoite, odnosno latentne oblike *P. vivax* i *P. ovale*, koji uzrokuju relaps malarije.

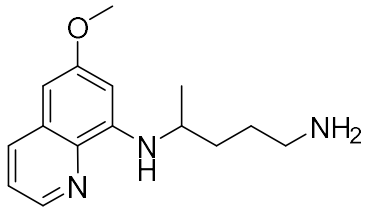

Slika 9. Primakin.

Primakin se primjenjuje peroralno u dozi od 15 mg/kg u odraslih, odnosno u dozi od 0,5 mg/kg u djece. Primjenjuje se jednom dnevno, a terapija traje 14 dana. Kontraindiciran je u trudnica, ali se smije primjenjivati u dojilja unatoč tome što se u niskim koncentracijama izlučuje u majčinom mlijeku (117).

Nuspojave primakina su rijetke, međutim, kontraindiciran je u osoba s nedostatkom glukoza--6-fosfat-dehidrogenaze (G6PD) zbog pojave hemolitičke anemije. Od ostalih nuspojava mogu se pojaviti mučnina, povraćanje i bol u trbuhu (118). Ostali nedostaci primakina su brza metabolička razgradnja do inaktivnog karboksiprimakina i smanjenje koncentracije aktivnog oblika ukoliko se primjenjuje s lijekovima koji inhibiraju CYP2D6 (119, 120).

1.5.2. Klorokin

Klorokin je antimalarik koji je otkriven 1934. godine te se nalazi na listi esencijalnih lijekova Svjetske zdravstvene organizacije (Slika 10) (115). U upotrebu je ušao 40-ih godina prošlog stoljeća, međutim, već 1950-ih su zabilježeni prvi slučajevi rezistencije (121). Danas se, zbog toga, klorokin koristi za prevenciju i liječenje malarije uzrokovane *P. vivax*, *P. malariae* i *P. ovale*, te malarije uzrokovane *P. falciparum* u područjima gdje nije zabilježena rezistencija na klorokin (122).

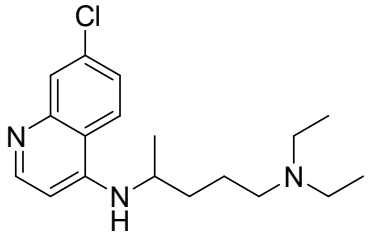

Slika 10. Klorokin.

Za razliku od primakina, klorokin djeluje na eritrocitnu fazu malarije tako što sprječava polimerizaciju toksičnog hema u netoksični hemozoin što dovodi do nagomilavanja slobodnog hema i smrti parazita (123). Primjenjuje se preoralno u dozi od 300 mg tjedno za profilaksu i u dozi od 300 mg dnevno kroz tri dana za liječenje malarije. Primjena u djece smatra se sigurnom te se primjenjuje u dozi od 5 mg/kg tjedno za profilaksu i 5 mg/kg dnevno za liječenje malarije (124). Klorokin se smije primjenjivati u trudnica i, budući da se samo u malim količinama izlučuje u majčinom mlijeku, smiju ga koristiti i dojilje.

Nuspojave klorokina su rijetke, a najčešće uključuju zamućenje vida, mučninu, povraćanje, bolove i grčeve u trbuhu, glavobolju, proljev, prolazan gubitak kose, promjene u boji kose i slabost mišića (125). Jedna od najopasnijih nuspojava je ireverzibilno oštećenje retine (Slika 11) (126). S obzirom da pojavnost oštećenja ovisi o dozi i duljini terapije, manja je vjerojatnost da će se pojaviti ukoliko se klorokin primjenjuje u terapiji malarije, a veća ako se koristi u terapiji reumatskih bolesti i sistemskog eritemskog lupusa (127). Kontraindiciran je u osoba s manjkom enzima G6PD ili u osoba koje su osjetljive na 4-aminokinoline. Zbog mogućnosti interakcija, potrebna je kontrola doza u slučaju primjene s antacidima, cimetidinom, ampicilinom, ciklosporinom i meflokinom (128).

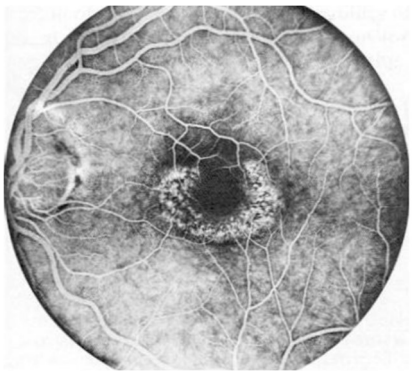

Slika 11. Fluoresceinski angiogram oka pacijenta s retinopatijom uzrokovanom klorokinom: jača fluorescencija obrubljuje crno oštećenje oka. Preuzeto iz ref. (129) uz dozvolu izdavača.

1.5.3. Antimalarici u terapiji karcinoma

Iako na prvi pogled malarija i karcinom nisu povezani, mnogo antimalarika, kao što su artemizinin, artemeter, klorokin, hidroksiklorokin i kinin, nalazi se u kliničkim ispitivanjima za liječenje karcinoma (130). Trenutno je u tijeku oko 80 studija o učinkovitosti antimalarika u terapiji karcinoma, a 58 kliničkih ispitivanja je već završeno (131). Iako mehanizam citostatskog djelovanja antimalarika nije u potpunosti razjašnjen, uočeno je da antimalarici povećavaju osjetljivost i inhibiraju razvoj rezistencije stanica karcinoma, te da pojačavaju djelovanje citostatika. Jedan od mogućih razloga je inhibicija autofagije, nepoželjnog oblika preživljavanja stanica karcinoma, u kojem stanica proždire vlastite stanične komponente kako bi se održala razina stanične energije. Klorokin se, zbog bazičnih svojstava, akumulira u lizosomima, mijenja pH lizosoma te ometa fuziju lizosoma s autofagosomima, proces ključan u procesu autofagije (132). Drugi predloženi mehanizmi djelovanja su indukcija apoptoze ili ometanje angiogeneze (133, 134).

Efferth i sur. ispitali su djelovanje artemizinina na 55 staničnih linija karcinoma, uključujući stanice karcinoma kolona, dojke, jajnika, prostate, mozga, bubrega, te leukemije i melanoma. Iako je pokazao citostatsko djelovanje na sve ispitane stanične linije, IC_{50} vrijednosti kretale su se između 246 nM i >100 μM. Općenito su stanice koje se brzo razmnožavaju podložnije djelovanju artemizinina od onih koje se sporije umnožavaju (135). Druga ispitivanja pokazala su da artemizinin potiče apoptozu stanica karcinoma povećavajući koncentraciju proapoptotičkih gena u staničnim linijama karcinoma (136), a slična djelovanja imaju i derivati artemizinina (137-140). Osim što ubija stanice karcinoma, artemizinin ometa matastaziranje povećanjem aktivnosti E-kadherina (141), te inhibira neovaskularizaciju utišavanjem ekspresije gena za VEGF, MMP-9, MMP-11 i druge gene koji potiču angiogenezu, a potiče ekspresiju gena za inhibitore angiogeneze (142, 143).

Choi i sur. testirali su primakin i klorokin u kombinaciji s vinorelbinom, paklitakselom, docetakselom, vinkristinom ili halavenom na stanicama karcinoma koje su otporne na djelovanje navedenih citostatika. U svom ispitivanju dokazali su da primakin i klorokin inhibiraju P-glikoprotein te na taj način čine stanice karcinoma osjetljivijima na djelovanje citostatika (144).

Klorokin i njegov hidroksilirani derivat, hidroksiklorokin, su antimalarici čije je citostatsko djelovanje najviše ispitano. Često se kombiniraju s ostalim citostaticima jer povećavaju

osjetljivost stanica karcinoma na djelovanje citostatika (145). Dokazano je da primjena klorokina smanjuje ukupan volumen karcinoma ili ometa rast karcinoma u animalnim modelima glioblastoma (146, 147), hepatocelularnog karcinoma (148–150), karcinoma kolona (151), melanoma (152) te karcinoma dojke (153).

1.5.3.1. Klorokin u kliničkim ispitivanjima za terapiju karcinoma

Klorokin je trenutno uključen u 11 kliničkih ispitivanja, a nekoliko kliničkih studija je već završeno (131).

Liječnici *National Institute of Neurology and Neurosurgery* u Meksiku pokrenuli su početkom 2005. godine kliničko ispitivanje djelotvornosti terapije klorokinom u kombinaciji s operacijom, kemoterapijom i zračenjem kod oboljelih od glioblastoma. Tri tjedna nakon kirurškog odstranjenja tumora, pacijenti su započeli terapiju zračenjem u ukupnoj dozi od 60 Gy, a terapiju karmustinom (200 mg/m^2 svakih pet tjedana) započeli su osmi tjedan nakon operacije u ukupnom trajanju od 20 tjedana. Terapija klorokinom (150 mg dnevno) započela je peti dan nakon operacije, a trajala je 12 mjeseci. Pacijenti su praćeni 24 mjeseca po završetku terapije. Pokazano je da su pacijenti koji su uzimali klorokin preživjeli 24 mjeseca nakon operacije, u usporedbi s pacijentima koji nisu uzimali klorokin (11 mjeseci). Međutim, ispitivanje je povedeno na relativno malom broju pacijenata, te bi se trebalo ponoviti na većem broju ispitanika (154).

Znanstvenici *Inova Health Care Services* pokrenuli su ispitivanje djelotvornosti terapije klorokinom kod oboljelih od duktalnog karcinoma *in situ* (DCIS). Mjesec dana prije kirurškog odstranjenja tumora, pacijentice su peroralno primale klorokin u standardnoj (500 mg tjedno) ili niskoj (250 mg tjedno) dozi. Od 12 pacijentica koje su sudjelovale u ispitivanju, u 7 se smanjio promjer lezije, u 3 pacijentice nije bilo promjene, a u 2 se blago povećao promjer. Također, utvrđena je povećana prisutnost makrofaga u duktovima DCIS-a nakon primjene klorokina. Zaključeno je da klorokin smanjuje proliferaciju DCIS lezija i potiče migraciju stanica imunosnog sustava u dukt (155).

Iduća četiri ispitivanja su provedena i završena, a obrada rezultata je u tijeku.

Albert DeNittis u suradnji s *Main Line Health* ispitivao je utjecaj terapije klorokinom u kombinaciji sa zračenjem na preživljavanje i pojavnost metastaza u pacijenata s karcinomom mozga. Pacijenti su primali 250 mg klorokina dnevno počevši tjedan dana prije zračenja u ukupnom trajanju od pet tjedana (156).

Liječnici s *University of Zurich* određivali su sigurnost primjene i optimalnu dozu klorokina u kombinaciji s gemcitabinom u pacijenata s karcinomom gušterače. Pacijenti su primali klorokin u dozi od 100, 200 ili 300 mg na dane 2, 9 i 16, a gemcitabin (u dozi od 1000 mg/m^2) na dane 1, 8 i 15 ciklusa od 18 dana. Ispitivanje je trajalo osam tjedana (157).

Liječnici s *University of Cincinnati* istraživali su učinke istovremene primjene klorokina s karboplatinom i gemcitabinom u pacijenta sa solidnim tumorima. Pacijenti su primali klorokin u dozi od 50, 100, 150 ili 200 mg dnevno, postupno povećavajući dozu. Ciklusi su trajali 21 dan, a pacijenti su ukupno primali lijekove 4–6 ciklusa (158).

Jenny C. Chang u suradnji s *The Methodist Hospital System* pokrenula je ispitivanja terapije klorokinom u kombinaciji s paklitakselom, docetakselom ili iksabepilonom. Pratila se podnošljivost terapije, vrijeme odgovora na terapiju, te vrijeme bez daljnje progresije bolesti. Sve pacijentice uzimale su klorokin u dozi od 250 mg dnevno u kombinaciji s intravenskom primjenom kemoterapije svaka tri tjedna. Paklitaksel se primjenjivao u dozi od 175 mg/m^2, docetaksel u dozi od 75 mg/m^2, a iksabeplion u dozi od 40 mg/m^2. Terapija klorokinom je trajala godinu dana, a pacijentice su praćene tri godine po završetku terapije klorokinom (159).

2. Sahakini, novi hibridi temeljeni na motivima SAHA-e i primakina kao potencijalni citostatici i antiplazmodijski agensi

ChemPubSoc Europe

DOI: 10.1002/open.201800117

Open Access ChemistryOPEN Full Papers

SAHAquines, Novel Hybrids Based on SAHA and Primaquine Motifs, as Potential Cytostatic and Antiplasmodial Agents

Maja Beus,[a] Zrinka Rajić,*[a] Dusica Maysinger,[b] Zvonimir Mlinarić,[a] Maja Antunović,[c] Inga Marijanović,[c] Diana Fontinha,[d] Miguel Prudêncio,[d] Jana Held,[e] Sureyya Olgen,[f] and Branka Zorc*[a]

We report the synthesis of SAHAquines and related primaquine (PQ) derivatives. SAHAquines are novel hybrid compounds that combine moieties of suberoylanilide hydroxamic acid (SAHA), an anticancer agent with weak antiplasmodial activity, and PQ, an antimalarial drug with low antiproliferative activity. The preparation of SAHAquines is simple, cheap, and high yielding. It includes the following steps: coupling reaction between primaquine and a dicarboxylic acid monoester, hydrolysis, a new coupling reaction with *O*-protected hydroxylamine, and deprotection. SAHAquines **5a**–**d** showed significant reduction in cell viability. Among the three human cancer cell lines (U2OS, HepG2, and MCF-7), the most responsive were the MCF-7 cells. The antibodies against acetylated histone H3K9/H3K14 in MCF-7 cells revealed a significant enhancement following treatment with *N*-hydroxy-*N*′-{4-[(6-methoxyquinolin-8-yl)amino]pentyl}-pentanediamide (**5b**). Ethyl (2*E*)-3-({4-[(6-methoxyquinolin-8-yl)amino]pentyl}carbamoyl)prop-2-enoate (**2b**) and SAHAquines were the most active compounds against both the hepatic and erythrocytic stages of *Plasmodium* parasites, some of them at sub-micromolar concentrations. The results of our research suggest that SAHAquines are promising leads for new anticancer and antimalarial agents.

1. Introduction

Despite extensive efforts and significant progress in cancer treatment, therapeutic interventions are not yet satisfactory. Almost all available cytostatic drugs cause undesirable side effects, whereas drug resistance presents an additional problem.[1–3] In another field of medicine, an ongoing battle is being fought against malaria, a parasitic disease caused by *Plasmodium* species.[4,5] Malaria still poses a great health and economic burden to the highly populated countries in the tropical and subtropical parts of the world. The need for new, effective antimalarials arises from several factors, including the absence of an effective vaccine, insufficient vector control, and the emergence of multidrug-resistant *Plasmodium* strains.[6–8] The currently adopted approaches to the design of antiplasmodial compounds include the development of analogues of existing drugs, resistance reversers, and novel compounds with new mechanisms of action.[6,9]

A number of studies have shown a relationship between cancer and malaria in regard to diagnostics, drug research, treatment, prevention, and epidemiology.[10–13] Different classes of antimalarial drugs display direct or adjuvant activity against cancer cell lines, are known as sensitivity reversers of resistant tumor cell lines or inhibitors of drug resistance development, or have synergistic action with known anticancer drugs.[14–20] Although their exact mode of action against cancer is still not completely understood, various mechanisms have been proposed.[21–23]

[a] *M. Beus, Prof. Z. Rajić, Z. Mlinarić, Prof. B. Zorc*
Faculty of Pharmacy and Biochemistry, University of Zagreb
A. Kovačića 1, 10 000 Zagreb (Croatia)
E-mail: zrajic@pharma.hr
bzorc@pharma.hr

[b] *Prof. D. Maysinger*
Department of Pharmacology and Therapeutics, McGill University
23655 Promenade Sir-William-Osler, McIntyre Medical Sciences Building
Montreal, Quebec H3G 1Y6 (Canada)

[c] *Dr. M. Antunović, Prof. I. Marijanović*
Faculty of Science, University of Zagreb
Horvatovac 102A, 10 000 Zagreb (Croatia)

[d] *Dr. D. Fontinha, Dr. M. Prudêncio*
Instituto de Medicina Molecular, Faculdade de Medicina
Universidade de Lisboa
Av. Prof. Egas Moniz, 1649-028 Lisboa (Portugal)

[e] *Dr. J. Held*
Institute of Tropical Medicine, University of Tübingen
Wilhelmstraße 27, 72074 Tübingen (Germany)

[f] *Prof. S. Olgen*
Faculty of Pharmacy, Biruni University
10th street No: 45, 34010 Topkapi Istanbul (Turkey)

Supporting Information and the ORCID identification number(s) for the author(s) of this article can be found under: https://doi.org/10.1002/open.201800117.

Such observations prompted us, and others, to design and prepare novel derivatives of known antimalarial drugs and evaluate their cytostatic potential.[24–34] Our efforts have been focused on primaquine (PQ), which is an old drug with many flaws (e.g., induction of hemolytic anemia in individuals lacking glucose-6-phosphate dehydrogenase, quick metabolism, degradation to inactive carboxyprimaquine, altering the treatment outcome in dependence of CYP 2D6 enzyme activity)[35] but is currently the only available *Plasmodium* hypnozoitocide.[36] We previously showed that various PQ derivatives of amides, ureas, bis-ureas, semicarbazides, and acylsemicarbazide-type derivatives possessed significant cytostatic activity against a panel of cancer cell lines or high selectivity towards the breast adenocarcinoma cell line (MCF-7).[24–30] On the other hand, cytostatic agents of different classes, including histone deacetylase (HDAC) inhibitors, have been shown to exert antiplasmodial activity.[6,37–42] Suberoylanilide hydroxamic acid (SAHA, vorinostat) was the first marketed pan-HDAC inhibitor, and it was followed by other drugs from the same class (e.g., romidepsin, belinostat, and panobinostat.[43,44] Their hydroxamic group chelates zinc ion found in the active site of Zn-dependent HDACs (classes I, II, and IV), and this leads to the accumulation of acetylated histones and other proteins.[45] HDACs were also identified as transcription regulators in *P. falciparum*.[46,47] Out of five *P. falciparum* HDACs, three are Zn-dependent enzymes, prone to inhibition by SAHA, and thus represent viable targets for drug development.[48] Several studies have shown the antimalarial activity of SAHA and related HDAC inhibitors.[49,50]

In this study, we employed one of the classical medicinal chemists' tools—the combination of two pharmacophores in one molecule.[7,51–54] The concept of hybrid drugs is also a valuable strategy to overcome the limitations of a combined therapy, as the resulting molecules could exhibit inhibitory activities on multiple targets.[55] The hybrid compounds described here, SAHAquines, combine motifs of SAHA, an anticancer agent with weak antiplasmodial activity, and PQ, an antimalarial drug with low antiproliferative activity. Other here-reported PQ derivatives differ in the linker length/type and/or functional groups: compounds **2** are esters, compounds **3** are carboxylic acids, and compounds **4** and **6** are *O*-benzyl- and *O*-methyl-substituted hydroxamic acids. Similar to the known HDAC inhibitors, hydroxamic acids **5** consist of a capping group (quinoline ring), a linker, and a Zn-binding group (hydroxamic acid) (Figure 1). Given that hydroxamic acid is a strong binding group for metal ions that might lead to poor selectivity and confer undesired properties, such as poor pharmacokinetics,[56,57] we introduced other functional groups instead: an ester, carboxylic acid, or *O*-protected hydroxamic group.

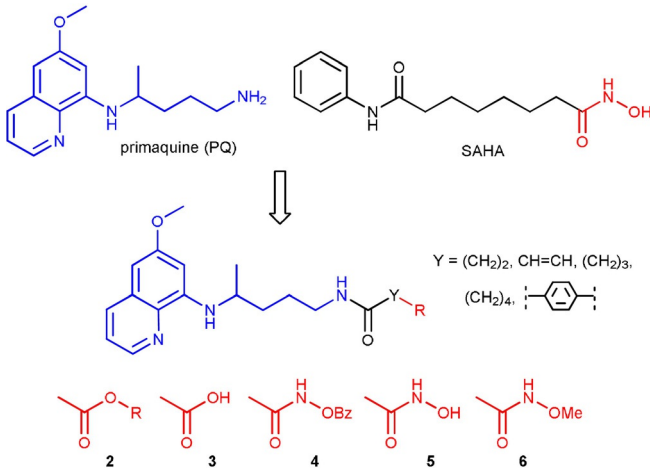

Figure 1. Design of SAHAquines **5** and other PQ derivatives.

Herein, we report the synthesis of SAHAquines **5a–d** as well as 20 novel PQ derivatives, their chemical characterization, the assessment of their cytostatic activity, and the evaluation of their activity against the erythrocytic and hepatic stages of *Plasmodium*.

2. Results and Discussion

2.1. Chemistry

The objective of our research was to prepare SAHAquines **5** and related PQ derivatives, which differ in the type/length of the spacer and/or functional groups: compounds **2** are esters and compounds **3** are carboxylic acids, whereas compounds **4** and **6** are *O*-protected hydroxamic acids. Scheme 1 shows the synthetic pathway leading to derivatives **2–6**. In the first reaction step, dicarboxylic acid monoesters **1a–e** were coupled with PQ to give derivatives **2a–e** by using 1-[bis(dimethylamino)methylene]-1*H*-1,2,3-triazolo[4,5-*b*]pyridinium 3-oxid hexafluorophosphate (HATU) as the coupling reagent, along with Hünig's base (*N*,*N*-diisopropylethylamine, DIEA). The following dicarboxylic acid monoesters were used: 4-methoxy-4-oxobutanoic acid (monomethyl hydrogen succinate) (**1a**), (*E*)-4-ethoxy-4-oxobut-2-enoic acid (monoethyl fumarate) (**1b**), 5-methoxy-5-oxopentanoic acid (monomethyl glutarate) (**1c**), 6-methoxy-6-oxohexanoic acid (monomethyl adipate) (**1d**), and 4-(methoxycarbonyl)benzoic acid (monomethyl terephtalate) (**1e**). Notably, an analogous coupling reaction between PQ and monomethyl malonate failed in our hands. Amide formation between these two compounds by using thionyl chloride or benzotriazolide[58] was also unsuccessful and gave a mixture of products. Classical activation of the carboxylic group with thionyl chloride worked well with other dicarboxylic acid monoesters. Hydrolysis of **2a–e** with lithium hydroxide afforded corresponding acids **3a–e**, which were transformed into *O*-benzylhydroxamic acids **4a–e** and *O*-methylhydroxamic acids **6a–e** by means of *O*-benzyl- and *O*-methylhydroxylamine, respectively. Again, HATU/DIEA was used as the coupling system. Free hydroxamic acids **5a–d** were obtained by catalytic hydrogenation of *O*-benzyl derivatives **4a–e**. Selective deprotection of the benzyl group in fumaric derivative **4b** failed. As a result of double-bond hydrogenation, succinylhydroxamic acid **5a** was obtained instead of fumarylhydroxamic acid.

All new compounds were fully characterized by conventional spectroscopy and analytical methods (IR, ^{1}H NMR, and ^{13}C NMR spectroscopy; MS; and elemental analyses). The data were consistent with the proposed structures and are given in short in

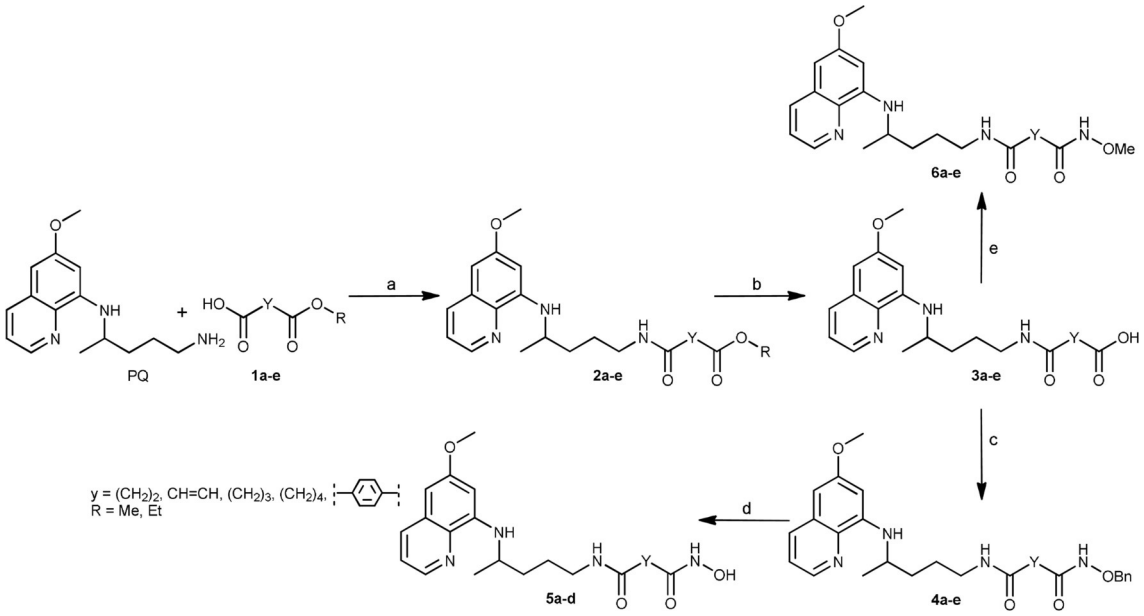

Scheme 1. Synthesis of PQ derivatives **2**–**6**. *Reagents and conditions:* a) HATU, DIEA, CH_2Cl_2, RT, 1 h; b) LiOH, MeOH, H_2O, RT, 1 h; c) H_2NOBn, HATU, DIEA, CH_2Cl_2, RT, 2 h; d) H_2, Pd/C, MeOH, RT, 2–4 h; NH_2OMe, HATU, DIEA, CH_2Cl_2, RT, 2 h.

the Experimental Section and in detail in the Supporting Information.

To evaluate the drug-like properties of our novel compounds, a common set of physicochemical parameters were calculated: topological polar surface area (TPSA), number of atoms, molecular weight (MW), partition coefficient (log *P*), number of H-bond donors (HBDs), number of H-bond acceptors (HBAs), and molar refractivity (MR). The parameters were calculated with Chemicalize.org software and are presented in Table 1.[59] All compounds **2**–**6** (except **4e**, which showed minimal aberration) are fully in agreement with Lipinski's and Gelovani's rules for prospective small-molecule drugs (MW $\leq$ 500, log $P \leq 5$, number of H-bond donors ≤ 5, number of H-bond acceptors ≤ 10, TPSA < 140 Å^2, MR within the range of 40 and 130 cm^3 mol^{-1}, number of atoms 20–70).[60]

Table 1. Properties of compounds **2**–**6** calculated with the Chemicalize.org program.[59] The Lipinski's and Gelovani's parameters.

Compd	Molecular formula	Number of atoms	MW	log *P*	HBD[a]	HBA[b]	Lipinski score[c]	MR[d] [cm^3 mol^{-1}]	TPSA[e] [Å^2]
2a	$C_{20}H_{27}N_3O_4$	54	373.453	1.43	2	5	4	103.62	89.55
2b	$C_{21}H_{27}N_3O_4$	55	385.464	2.38	2	5	4	109.44	89.55
2c	$C_{21}H_{29}N_3O_4$	57	387.480	1.88	2	5	4	108.22	89.55
2d	$C_{22}H_{31}N_3O_4$	60	401.507	2.32	2	5	4	112.82	89.55
2e	$C_{24}H_{27}N_3O_4$	58	421.497	3.32	2	5	4	120.65	89.55
3a	$C_{19}H_{25}N_3O_4$	51	359.426	0.80	3	6	4	98.85	100.55
3b	$C_{19}H_{23}N_3O_4$	49	357.410	0.90	3	6	4	99.92	100.55
3c	$C_{20}H_{27}N_3O_4$	54	373.453	1.29	3	6	4	103.45	100.55
3d	$C_{21}H_{29}N_3O_4$	57	387.480	1.74	3	6	4	108.05	100.55
3e	$C_{23}H_{25}N_3O_4$	55	407.470	2.23	3	6	4	115.89	100.55
4a	$C_{26}H_{32}N_4O_4$	66	464.566	2.58	3	6	4	131.53	101.58
4b	$C_{26}H_{30}N_4O_4$	64	462.515	2.94	3	6	4	132.60	101.58
4c	$C_{27}H_{34}N_4O_4$	69	478.580	3.02	3	6	4	136.13	101.58
4d	$C_{28}H_{36}N_4O_4$	72	492.620	3.47	3	6	4	140.74	101.58
4e	$C_{30}H_{32}N_4O_4$	70	512.600[b]	4.27	3	6	3[f]	148.57	101.58
5a	$C_{19}H_{26}N_4O_4$	53	374.441	0.48	4	6	4	102.44	112.58
5b	$C_{20}H_{28}N_4O_4$	56	388.468	0.92	4	6	4	107.04	112.58
5c	$C_{21}H_{30}N_4O_4$	59	402.495	1.37	4	6	4	111.64	112.58
5d	$C_{23}H_{26}N_4O_4$	57	422.485	2.16	4	6	4	119.47	112.58
6a	$C_{20}H_{28}N_4O_4$	56	388.468	0.85	3	6	4	106.92	101.58
6b	$C_{20}H_{26}N_4O_4$	54	386.452	1.21	3	6	4	107.99	101.58
6c	$C_{21}H_{30}N_4O_4$	59	402.495	1.30	3	6	4	111.52	101.58
6d	$C_{22}H_{32}N_4O_4$	62	416.522	1.74	3	6	4	116.12	101.58
6e	$C_{24}H_{28}N_4O_4$	60	436.512	2.54	3	6	4	123.95	101.58

[a] H-bond donor. [b] H-bond acceptor. [c] Out of four. [d] Molar refractivity. [e] Topological polar surface area. [f] Minimal aberrations of the rules.

2.2. Biological Evaluation

Synthesized compounds **2**–**6** were tested for their anticancer activity on three human cancer cell lines (bone osteosarcoma U2OS, hepatocellular carcinoma HepG2, and breast adenocarcinoma MCF-7) and human embryonic kidney (Hek293) cells. The cells were treated with the different compounds at different concentrations, and the median inhibitory concentration (IC_{50}) values were determined (Table 2).

The data from Table 2 clearly indicate that the SAHAquines were the most potent in the selected cancer cell lines. The IC_{50} values towards MCF-7 cells were in the low micromolar concentrations (1.6–5.4 μM). Compounds from the other subclasses were, in general, less active than compounds **5**. Compounds **4d** and **4e** were the most effective *O*-benzylhydroxamic acids. In contrast, *O*-methylhydroxamic acids **6** exhibited weak activity, except for succinic acid derivative **6a**. All compounds from the ester series, except **2c**, showed moderate activity, whereas carboxylic acid derivatives **3a**–**e** were practically inactive.

MCF-7 cells were sensitive to 15 of the 24 tested compounds, namely, **5a**–**d**, **2d**, **2e**, **4a**, **4c**–**e**, and **6a**–**d**. Similar results were obtained in our previous studies with various PQ

Table 2. Antiproliferative screening of novel compounds **2**–**6** towards human cancer cell lines (U2OS, HepG2, MCF-7) and human embryonic kidney cell line (Hek293) in vitro.

Compd	Structure	IC_{50}[a] [μM] U2OS	HepG2	MCF-7	Hek293
2a	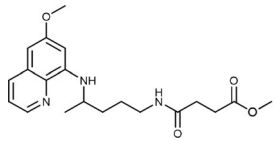	6.7 ± 3.1	> 50	> 50	> 50
2b	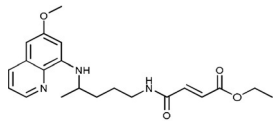	14.9 ± 2.2	> 50	> 50	17.0 ± 1.7
2c	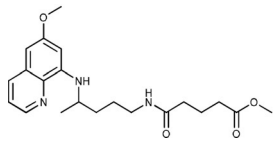	> 50	> 50	> 50	> 50
2d	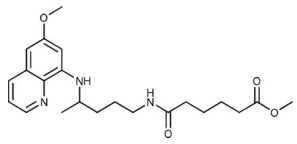	24.3 ± 1.5	> 50	5.3 ± 3.2	> 50
2e	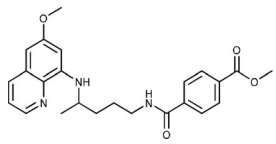	> 50	> 50	7.1 ± 3.0	> 50
3a	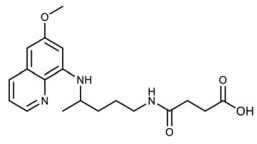	> 50	> 50	> 50	> 50
3b	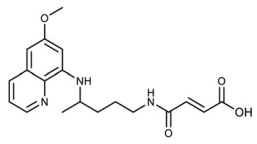	> 50	> 50	> 50	> 50
3c	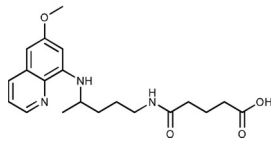	33.8 ± 2.9	> 50	> 50	> 50
3d	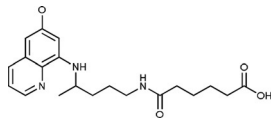	> 50	> 50	> 50	> 50

Table 2. (Continued)

Compd	Structure	IC_{50}[a] [μM] U2OS	HepG2	MCF-7	Hek293
3e	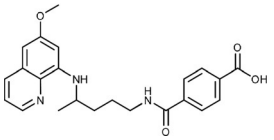	>50	>50	15.2±0.5	>50
4a	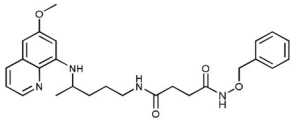	>50	>50	12.0±1.4	>50
4b	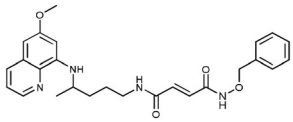	>50	>50	>50	>50
4c	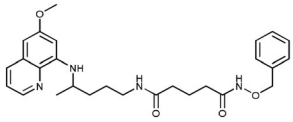	>50	>50	16.6±0.8	>50
4d	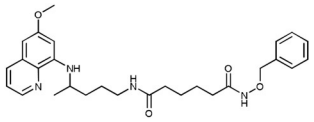	32.8±3.0	9.9±1.1	13.9±1.5	>50
4e	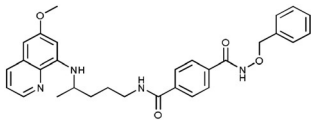	7.1±1.2	>50	11.5±0.1	13.2±2.6
5a	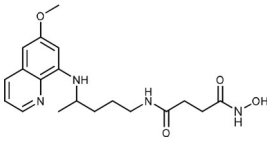	16.9±2.2	18.0±3.3	5.4±0.1	25.5±0.8
5b	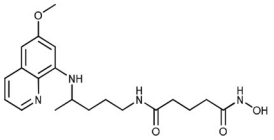	3.3±0.05	20.0±0.2	1.6±0.8	8.5±0.5
5c	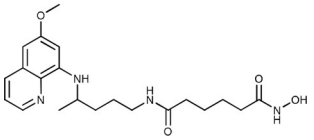	11.6±2.0	28.4±2.1	5.0±0.4	13.7±3.4
5d	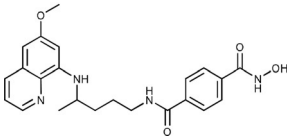	11.6±2.1	21.7±0.2	4.7±0.1	6.1±1.9
6a	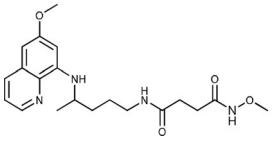	6.6±1.2	>50	5.9±0.6	8.6±2.0
6b	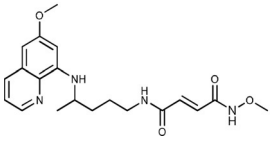	>50	>50	10.0±2.8	>50

Table 2. (Continued)

Compd	Structure	IC_{50}[a] [μM] U2OS	HepG2	MCF-7	Hek293
6c	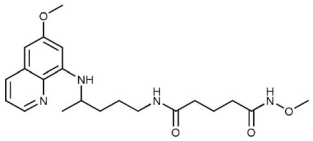	>50	>50	7.1±0.4	>50
6d	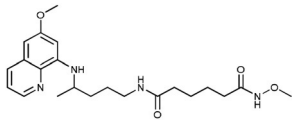	>50	>50	9.8±0.4	>50
6e	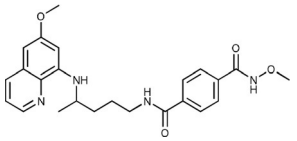	>50	>50	>50	>50
PQ[b]		12.0±0.7	37.7±5.8	13.8±1.4	8.1±1.3
SAHA[c]		5.7±0.8	4.0±0.1	2.8±0.7	7.4±0.9
Cis[d]		2.5±0.7	–	3.2±1.0	2.0±0.6

[a] The concentration required to decrease viability by 50%. [b] Primaquine. [c] Suberoylanilide hydroxamic acid. [d] Cisplatin.

derivatives.[24–30] On the other hand, HepG2 cells were very robust and only responded towards **4d** and compounds from subclass **5**. The non-cancer human cell line Hek293 was sensitive to **2b**, **4e**, **5a–d**, and **6a** but to a lesser extent than the cancer cell lines. Selectivity indices ranged from 2 to 12, depending on the tested compound and the cancer cell line employed.

To show the loss of MCF-7 cells following their exposure to the most potent compounds from subclasses **4** and **5**, that is, **4e** and **5b**, we labeled the cell nuclei with Hoechst 33342 and assessed the number of cells (Figure 2). The results from these studies complement the data from the MTT [3-(4,5-dimethylthiazol-2-yl)-2,5-diphenyltetrazolium bromide] assay (Table 2), showing a correlation between significant loss of mitochondrial metabolic activity and a concentration-dependent decrease in the number of cells. A reduction in the number of MCF-7 cells was found for treatment over periods of 24 and 72 h. The IC_{50} values for **5b** and **4e** obtained from these assays were

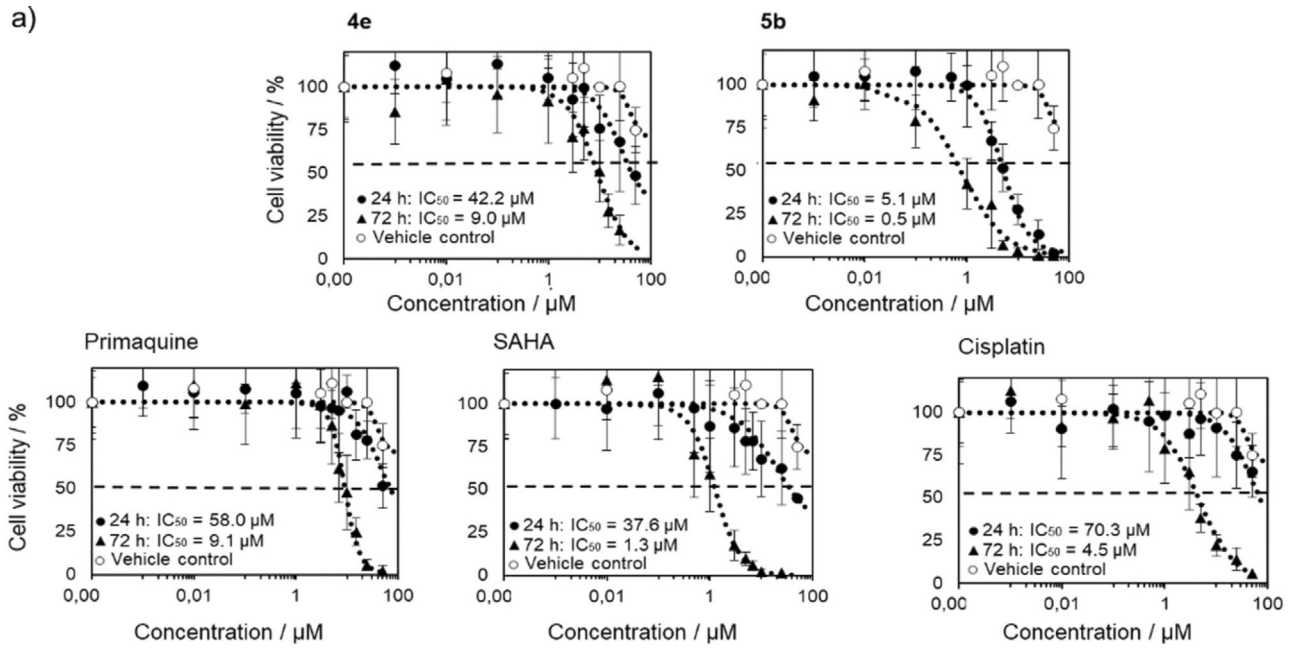

Figure 2. MCF-7 cell viability following treatment with **4e**, **5b**, primaquine, SAHA, and cisplatin for 24 or 72 h at various concentrations ranging from 50 to 0.001 μM. Cell viability was measured by counting Hoechst 33342 labeled nuclei imaged by using a fluorescence microscope. Shown are average percentage cell viability compared to the untreated controls ± SD from two independent experiments.

within a comparable micromolar concentration range (**5b**: 0.5 and 1.6 μM; **4e**: 9.0 and 11.5 μM). Determination of the number of cells is a more direct way of showing cell loss.

As SAHAquines **5** with a free hydroxamic acid have the potential to chelate metal ions in Zn-dependent HDACs and to increase the content of acetylated histones, we performed a immunocytochemical assay for histone acetylation. MCF-7 cells were treated with **5b** and acetylated H3K9/H3K14 was measured. SAHA, PQ, and **4e** were used as controls in the histone acetylation experiments. Indeed, the results show that **5b** caused a significant accumulation of acetylated H3 histone (Figure 3), which suggested that HDAC inhibition was a possible contributing mechanism for SAHAquines **5** but not for the other PQ derivatives. Given that HDAC inhibition correlated with cellular histone acetylation but not with cell loss, we did not extensively study the kinetics of HDAC inhibition.[61] An in-depth mechanistic study should be performed to explain the mode of cell death caused by the SAHAquines.

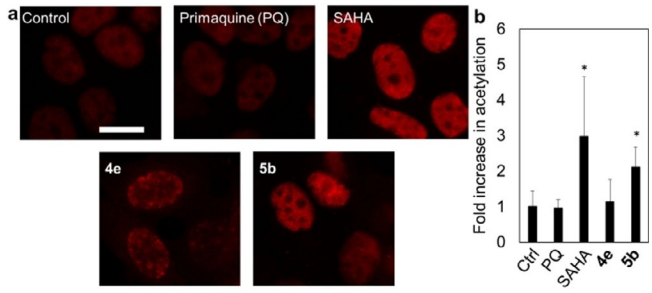

Figure 3. MCF-7 cells were treated with PQ, SAHA, **4e**, or **5b** (1 μM) for 24 h. a) Representative fluorescence micrographs of MCF-7 histone H3 acetylation (red) at lysine 9/lysine 14 in response to treatments. Cells were incubated with primary antibody (rabbit anti-acetyl-Histone-H3 polyclonal antibody, 500× dilution) for 24 h and then with secondary antibody (Alexa Fluor 647 goat anti-rabbit IgG −2 mg mL^{-1}; 500× dilution) for 1 h in the dark. Cells were imaged by using a fluorescence microscope with a CY5 filter. Fluorescence was analyzed in ImageJ. Scale bar represents 20 μM. b) Averages of fluorescence per cell ± SD (as fold increase in untreated control = 1) from at least two independent experiments. * $p < 0.05$, *t*-test.

Literature data on the antimalarial activity of SAHA and related HDAC inhibitors[49,50] prompted us to evaluate SAHAquines and their synthetic precursors for their in vitro activity against *P. falciparum* erythrocytic stages. The IC_{50} values of SAHAquines **2**–**6** against the erythrocytic stage of two *P. falciparum* strains, 3D7 and Dd2, were determined (Table 3). In general, the 3D7 strain was more sensitive than the Dd2 strain. Again, the most active compounds were SAHAquines **5**, the hydroxamic acid subclass. Compound **5b** had the lowest IC_{50} value (0.4 μM for the *Pf*3D7 strain and 1.9 μM for the *Pf*Dd2 strain), followed by **5d** (IC_{50} = 0.6 and 1.2 μM, respectively), **5c** (IC_{50} = 3.7 and 13.6 μM, respectively), and finally **5a** (IC_{50} = 15.8 and 27.1 μM, respectively). Derivatives **2b** and **2d** were the most active compounds from the ester subclass, and **4e** was the most active from the *O*-benzylhydroxamic acids. Carboxylic acids **3a**–**e** were inactive.

We further evaluated the in vitro activity of compounds **2**–**6** against the hepatic stages of *P. berghei*. Two concentrations of SAHAquines were tested: 1 and 10 μM. For comparison, the same concentrations of PQ were included in the assay as a positive control (IC_{50} = 8.4 ± 3.4 μM), and DMSO was used as a negative control (Figure 4).

As shown in Figure 4, only ester **2b** and SAHAquines **5a**–**d** were active against the *P. berghei* hepatic stages, whereas the other tested compounds were completely inactive. All compounds from hydroxamic acid subclass **5** exhibited strong antiplasmodial activity at both concentrations tested, with IC_{50} values ranging from 0.3 to 1.25 μM and without any noticeable effects on host-cell confluency (Figure 5). Our results show that the free hydroxamic acid moiety was crucial for antiplasmodial activity, as activity was lost if this group was protected or replaced by a carboxylic acid. The activity of compound **2b** from the ester subclass was probably due to the α,β-unsaturated carbonyl group (Michael acceptor moiety), which is capable of conjugate addition.

The relationship between antimalarial and anticancer activity is complex and is discussed in detail in a review by Duffy, Wade, and Chang.[62] Both main groups of existing antimalarial

Table 3. IC_{50} values for compounds **2**–**6** against erythrocytic stage of two *P. falciparum* strains.

Compd	IC_{50} [μM] *Pf*3D7	*Pf*3Dd2	Compd	IC_{50} [μM] *Pf*3D7	*Pf*3Dd2
2a	100.0 ± 11.0	74.1 ± 5.3	**4d**	> 27.7	> 27.7
2b	2.9 ± 0.2	7.2 ± 1.9	**4e**	6.1 ± 0.1	> 27.7
2c	81.1 ± 3.4	80.1 ± 31.0	**5a**	15.8 ± 1.7	27.1 ± 0.8
2d	6.6 ± 0.2	50.4 ± 4.6	**5b**	0.4 ± 0.1	1.9 ± 0.8
2e	27.1 ± 0.6	25.0 ± 2.8	**5c**	3.7 ± 1.3	13.6 ± 0.2
3a	> 111	> 111	**5d**	0.6 ± 0.2	1.2 ± 0.04
3b	> 111	> 111	**6a**	> 111	94.4 ± 8.6
3c	> 111	> 111	**6b**	8.3 ± 0.9	14.8 ± 0.1
3d	> 111	> 111	**6c**	> 111	> 111
3e	> 111	> 111	**6d**	> 111	> 111
4a	> 55	50.0 ± 5.0	**6e**	> 25	> 27.7
4b	> 27.7	> 27.7	PQ[a]	1.5 ± 0.02	4.3 ± 1.5
4c	39.5 ± 15.5	35.5 ± 1.2	CQ[b]	1.6×10^{-3}	0.265 ± 0.003

[a] Primaquine. [b] Chloroquine.

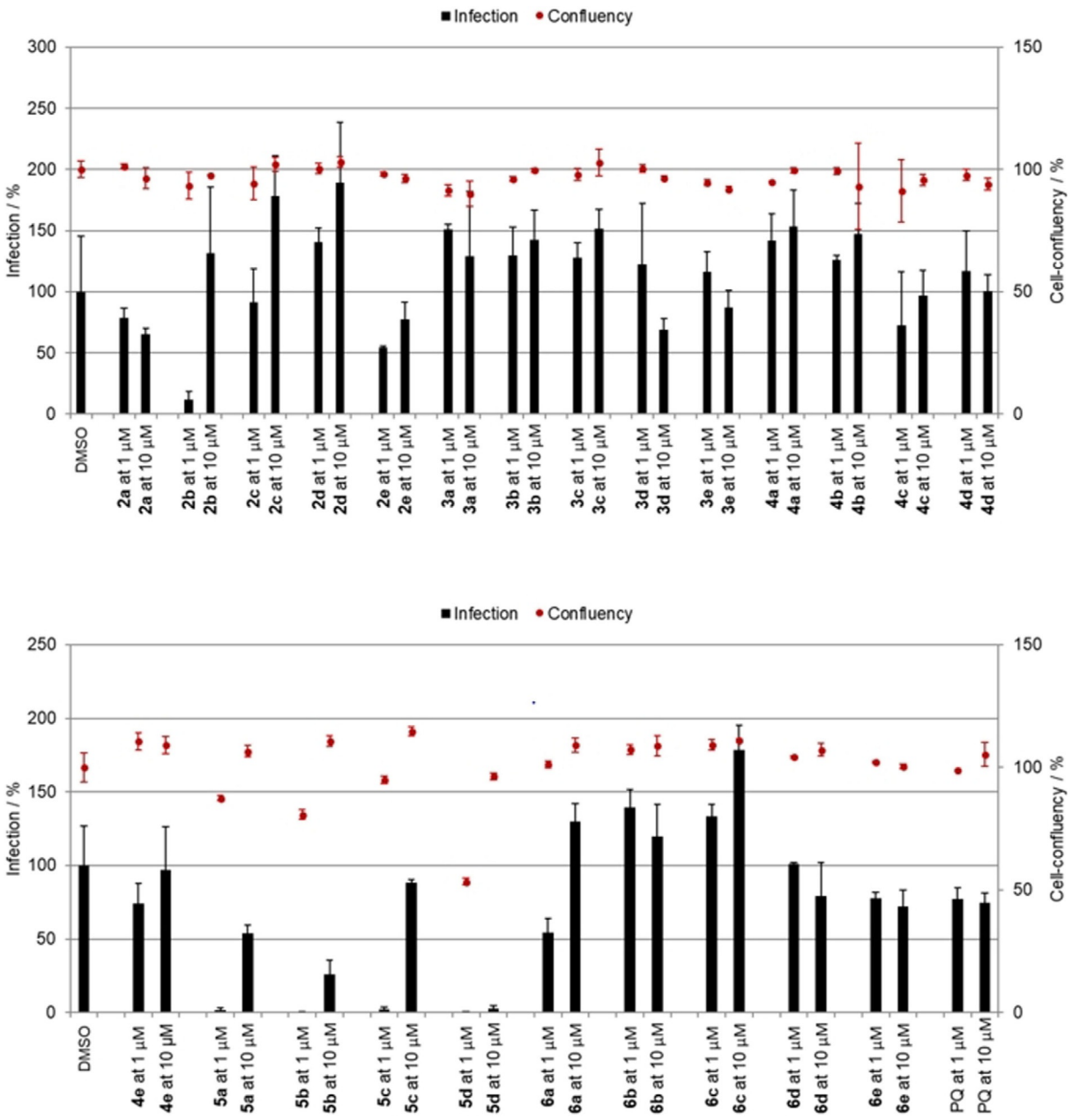

Figure 4. Activity of compounds **2**–**6** against *P. berghei* hepatic stages at concentrations of 1 and 10 µM. Anti-infective activity (infections scale, bars) are shown.

agents, the quinolines and the sesquiterpene lactones, have a range of known anticancer properties that could either be distinct from or overlap with their antimalarial properties. Although our results show a similar pattern of activity, it should be noted that the activities of **5b** and **5d** are an order of magnitude higher towards the *P. falciparum* erythrocytic stage than towards the tested cancer cell lines and the human embryonic kidney cells (Hek293).

Having in mind that very good safety profiles are needed for antimalarial drugs, as they should be delivered, amongst others, to two particularly vulnerable populations, small children and pregnant women,[63] we are aware that our finding can only be a starting point for the development of a clinically applicable antimalarial drug. As the antiplasmodial activities of compounds **2b** and **5a**–**d** were comparable to the activity of PQ, they might potentially replace PQ against PQ-resistant *Plasmodium* strains or in the treatment of glucose-6-phosphate dehydrogenase deficient patients and poor metabolizers, but this hypothesis still remains to be evaluated. Notably, the synthesis of SAHAquines is cheap and short (1–4 h) with good to excellent yields (43–97%), which is beneficial for the development of antimalarial agents.[64]

3. Conclusions

Four SAHAquines based on SAHA and PQ motifs and 20 other PQ derivatives were synthesized and evaluated in vitro against three human cancer cell lines and a human embryonic kidney

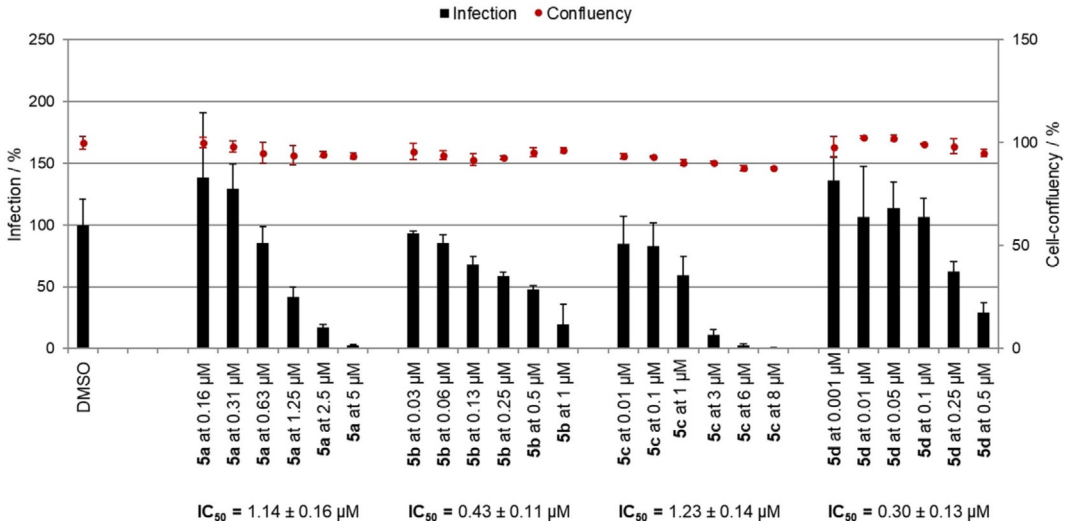

Figure 5. IC_{50} of SAHAquines **5a–d** against *P. berghei* hepatic stages.

cell line. SAHAquines **5a–d** displayed cytostatic activity at low micromolar concentrations. A few compounds from other subclasses were also effective, but less so than **5a–d**. We showed that the most active hydroxamic acid, that is, **5b**, caused a significant accumulation of acetylated histone H3K9/H3K14, a downstream target of class I HDACs. The results from the antiplasmodial activity of SAHAquines against the erythrocytic stages of the 3D7 and Dd2 *P. falciparum* strains and against *P. berghei* hepatic stages correlated with their cytostatic activity. The in vitro cytostatic and dual-stage antiplasmodial activity of SAHAquines suggest that these novel compounds could constitute a basis for the development of effective anticancer or malaria prophylactic/curative agents with improved potency and selectivity.

Experimental Section

General Methods

Melting points were measured with a Stuart Melting Point (SMP3) apparatus (Barloworld Scientific, UK) in open capillaries. IR spectra were recorded with a FTIR PerkinElmer Spectrum One, and UV/Vis spectra were recorded with a Lambda 20 double-beam spectrophotometer (PerkinElmer, UK). All NMR (^1H and ^{13}C) spectra were obtained at 25 °C by using an NMR Avance 600 spectrometer (Bruker, Germany) at 300 and 150 MHz for ^1H and ^{13}C nuclei, respectively. Chemical shifts (δ) are reported in parts per million (ppm) relative to tetramethylsilane in the ^1H spectra and relative to [D_6]DMSO in the ^{13}C spectra ($\delta = 39.51$ ppm). Coupling constants (J) are reported in hertz. Mass spectra were collected with a HPLC-MS/MS instrument (HPLC, Agilent Technologies 1200 Series; MS, Agilent Technologies 6410 Triple Quad). Mass determination was realized by using electrospray ionization (ESI) in the positive mode. Elemental analyses were performed with a CHNS LECO analyzer (LECO Corporation, USA). All compounds were routinely checked by TLC with Merck silica gel 60F-254 glass plates by using the following solvent systems: dichloromethane/methanol 9:1, 9.5:0.5, and 9.6:0.4; cyclohexane/ethyl acetate 1:1; and cyclohexane/ethyl acetate/methanol 3:1:0.5. Spots were visualized by short-wave UV light and iodine vapor. Column chromatography was performed on silica gel 0.063–0.200 mm. All chemicals and solvents were of analytical grade and were purchased from commercial sources. PQ diphosphate, 4-methoxy-4-oxobutanoic acid (monomethyl succinate), (*E*)-4-ethoxy-4-oxobut-2-enoic acid (monoethyl fumarate), 5-methoxy-5-oxopentanoic acid (monomethyl glutarate), 6-methoxy-6-oxohexanoic acid (monomethyl adipate), 4-(methoxycarbonyl)-benzoic acid (monomethyl terephtalate), DIEA, HATU, *O*-benzylhydroxylamine, *O*-methylhydroxylamine, triethylamine, MTT, cisplatin (Cis), and Hoechst 33342 were purchased from Sigma–Aldrich; rabbit anti-acetyl-Histone-H3 polyclonal antibody was purchased from Millipore, Alexa Fluor 647 goat anti-rabbit IgG was purchased from Life Technologies, and SAHA was acquired from Cayman Chemicals. PQ was prepared from PQ diphosphate prior to use. All reactions with PQ were performed under light-protected conditions.

Synthesis

General Procedure for the Preparation of Esters 2a–e

Method A: A solution of dicarboxylic acid monoester **1a–e** (1.4 mmol), HATU (0.532 g, 1.4 mmol), and DIEA (0.362 g, 2.8 mmol) in dichloromethane (8 mL) was stirred at room temperature. After 10 min, a solution of PQ (0.401 g, 1.5 mmol) in dichloromethane (7 mL) was added. The mixture was stirred at room temperature for 1 h and was then concentrated under reduced pressure. The residue was dissolved in ethyl acetate and extracted with brine (3×). The organic layer was dried with sodium sulfate, filtered, and concentrated under reduced pressure.

Method B: A solution of dicarboxylic acid monoester **1a–e** (1.8 mmol) in thionyl chloride (7 mL) was kept overnight and concentrated under reduced pressure. The residue was triturated with dichloromethane (2×), and the solvent was evaporated again. A solution of PQ (0.401 g, 1.5 mmol) and Et_3N (0.152 g, 1.5 mmol) in dichloromethane (8 mL) was added dropwise to the carboxylic acid chloride dissolved in dichloromethane (10 mL). The mixture was stirred at room temperature for 1 h and extracted with brine (3×). The organic layer was dried with sodium sulfate, filtered, and concentrated under reduced pressure.

Methyl 3-({4-[(6-methoxyquinolin-8-yl)amino]pentyl}carbamoyl)propanoate (**2a**): Method A, from the reaction of monomethyl succinate (**1a**, 0.185 g) and after purification by column chromatography (dichloromethane/methanol 9.5:0.5) and crystallization (ether), **2a** was obtained as a pale-yellow solid (0.460 g, 88%): m.p. 71–73 °C; ^{1}H NMR ([D$_6$]DMSO): δ = 8.55–8.53 (dd, J = 1.6, 4.2 Hz, 1H, 10), 8.09–8.06 (dd, J = 1.5, 8.3 Hz, 1H, 12), 7.86 (t, J = 5.3 Hz, 1H, 1), 7.45–7.40 (m, 1H, 11), 6.47 (d, J = 2.4 Hz, 1H, 16), 6.26 (d, J = 2.4 Hz, 1H, 14), 6.12 (d, J = 8.7 Hz, 1H, 7), 3.82 (s, 3H, 17), 3.66–3.57 (m, 1H, 5), 3.56 (s, 1H, 5′), 3.08–3.02 (m, 2H, 2), 2.48 (t, J = 6.6 Hz, 2H, 2′), 2.33 (t, J = 6.8 Hz, 2H, 3′), 1.70–1.58, 1.58–1.42 (2m, 4H, 3,4), 1.20 ppm (d, J = 6.3 Hz, 3H, 6); ^{13}C NMR ([D$_6$]DMSO): δ = 173.30, 170.87, 159.00, 144.62, 144.23, 134.79, 134.52, 129.57, 122.09, 96.09, 91.58, 54.97, 51.21, 46.97, 38.46, 33.37, 29.82, 28.82, 25.95, 20.19 ppm; IR (ATR): $\tilde{\nu}$ = 2278, 3306, 3060, 2959, 2927, 2857, 1732, 1636, 1619, 1552, 1518, 1454, 1387, 1224, 1200, 1170, 1052, 1031, 825, 793, 679 cm^{-1}; MS (ESI): *m/z*: 374.2 $[M+1]^+$; elemental analysis calcd (%) for $C_{20}H_{27}N_3O_4$ (373.45): C 64.32, H 7.21, N 11.25; found: C 64.02, H 7.47, N 11.00.

Ethyl (2*E*)-3-({4-[(6-methoxyquinolin-8-yl)amino]pentyl}carbamoyl)-prop-2-enoate (**2b**): Method B, from the reaction of monoethyl fumarate (**1b**, 0.202 g) and after purification by column chromatography (dichloromethane/methanol 9.6:0.4) and crystallization (ether), **2b** was obtained as a pale-yellow solid (0.378 g, 70%): m.p. 71–73 °C; ^{1}H NMR ([D$_6$]DMSO): δ = 8.54–8.53 (dd, J = 1.6, 4.2 Hz, 1H, 10), 8.51 (t, J = 5.5 Hz, 1H, 1), 8.08–8.06 (dd, J = 1.5, 8.3 Hz, 1H, 12), 7.43–7.41 (m, 1H, 11), 6.98 (d, J = 15.5 Hz, 1H, 2′), 6.55 (d, J = 15.5 Hz, 1H, 3′), 6.47 (d, J = 2.4 Hz, 1H, 16), 6.27 (d, J = 2.4 Hz, 1H, 14), 6.13 (d, J = 8.8 Hz, 1H, 7), 4.20–4.16 (q, J = 7.1 Hz, 2H, 5′), 3.82 (s, 3H, 17), 3.66–3.61 (m, 1H, 5), 3.20–3.17 (dd, J = 6.4, 12.3 Hz, 2H, 2), 1.71–1.65, 1.62–1.51 (2m, 4H, 3,4), 1.23 (t, J = 7.1 Hz, 3H, 6′), 1.22 ppm (d, J = 6.3 Hz, 3H, 6); ^{13}C NMR ([D$_6$]DMSO): δ = 165.05, 162.63, 158.98, 144.60, 144.20, 137.60, 134.76, 134.51, 129.55, 128.08, 122.06, 96.11, 91.51, 60.60, 54.94, 46.93, 38.81, 33.36, 25.63, 20.18, 13.97 ppm; IR (ATR): $\tilde{\nu}$ = 3391, 3325, 3079, 2969, 2939, 1716, 1645, 1616, 1554, 1520, 1457, 1424, 1388, 1365, 1334, 1302, 1224, 1205, 1163, 1159, 1038, 999, 831, 819, 790, 681, 660 cm^{-1}; MS (ESI): *m/z*: 386.2 $[M+1]^+$; elemental analysis calcd (%) for $C_{21}H_{27}N_3O_4$ (385.46): C 65.44, H 7.06, N 10.90; found: C 65.25, H 7.09, N 10.70.

Methyl 4-({4-[(6-methoxyquinolin-8-yl)amino]pentyl}carbamoyl)butanoate (**2c**): Method A, from the reaction of monomethyl glutarate (**1c**, 0.206 g) and after purification by column chromatography (dichloromethane/methanol 9.5:0.5), **2c** was obtained as an oil (0.439 g, 81%): ^{1}H NMR ([D$_6$]DMSO): δ = 8.53 (d, J = 2.6 Hz, 1H, 10), 8.07 (d, J = 8.2 Hz, 1H, 12), 7.78 (t, J = 3 Hz, 1H, 1), 7.43–7.41 (m, 1H, 11), 6.47 (d, J = 2.2 Hz, 1H, 16), 6.26 (d, J = 2.2 Hz, 1H, 14), 6.11 (d, J = 8.8 Hz, 1H, 7), 3.82 (s, 3H, 17), 3.64–3.60 (m, 1H, 5), 3.57 (s, 3H, 6′), 3.05 (t, J = 6.0 Hz, 2H, 2), 2.27 (t, J = 3.0 Hz, 2H, 2′), 2.07 (t, J = 7.3 Hz, 2H, 4′), 1.74–1.69 (m, 2H, 3′), 1.67–1.62, 1.54–1.44 (2m, 4H, 3, 4), 1.21 ppm (d, J = 6.2 Hz, 3H, 6); ^{13}C NMR ([D$_6$]DMSO): δ = 173.00, 171.18, 158.98, 144.60, 144.20, 134.76, 134.50, 129.55, 122.05, 96.08, 91.59, 54.95, 51.14, 46.97, 38.36, 34.28, 33.40, 32.64, 25.93, 20.62, 20.17 ppm; IR (ATR): $\tilde{\nu}$ = 3376, 3246, 3086, 2993, 2961, 2927, 1736, 1632, 1612, 1574, 1520, 1458, 1423, 1386, 1219, 1203, 1172, 1161, 1052, 992, 817, 788, 751, 720, 676 cm^{-1}; MS (ESI): *m/z*: 388.3 $[M+1]^+$; elemental analysis calcd (%) for $C_{21}H_{29}N_3O_4$ (387.47): C 65.09, H 7.54, N 10.84; found: C 65.35, H 7.33, N 10.99.

Methyl 5-({4-[(6-methoxyquinolin-8-yl)amino]pentyl}carbamoyl)-pentanoate (**2d**): Method A, from the reaction of monomethyl adipate (**1d**, 0.224 g) and after purification by column chromatography (dichloromethane/methanol 9.5:0.5) and crystallization (ether/petroleum ether), **2d** was obtained as a pale-yellow solid (0.483 g, 86%): m.p. 56–58 °C; ^{1}H NMR ([D$_6$]DMSO): δ = 8.54–8.52 (dd, J = 4.2, 1.6 Hz, 1H, 10), 8.09–8.06 (dd, J = 8.3, 1.5 Hz, 1H, 12), 7.78 (t, J = 5.4 Hz, 1H, 1), 7.45–7.40 (m, 1H, 11), 6.48 (d, J = 2.4 Hz, 1H, 16), 6.26 (d, J = 2.4 Hz, 1H, 14), 6.12 (d, J = 8.8 Hz, 1H, 7), 3.82 (s, 3H, 17), 3.66–3.59 (m, 1H, 5), 3.57 (s, 3H, 7′), 3.08–3.04 (m, 2H, 2), 2.28 (t, J = 6.9 Hz, 2H, 2′), 2.04 (t, J = 6.9 Hz, 2H, 5′), 1.68–1.57, 1.57–1.42 (2m, 8H, 3, 4, 3′, 4′), 1.20 ppm (d, J = 6.3 Hz, 3H, 6); ^{13}C NMR ([D$_6$]DMSO): δ = 173.22, 171.60, 159.00, 144.63, 144.23, 134.79, 134.53, 129.57, 122.09, 96.09, 91.58, 54.97, 51.15, 46.98, 38.36, 35.00, 33.43, 32.98, 25.99, 24.73, 24.03, 20.18 ppm; IR (ATR): $\tilde{\nu}$ = 3373, 3311, 2943, 2876, 1730, 1640, 1618, 1518, 1508, 1461, 1425, 1389, 1265, 1222, 1169, 1055, 821, 680, 625 cm^{-1}; MS (ESI): *m/z*: 402.3 $[M+1]^+$; elemental analysis calcd (%) for $C_{22}H_{31}N_3O_4$ (401.50): C 65.81, H 7.78, N 10.47; found: C 65.66, H, 7.66, N 10.31.

Methyl 4-({4-[(6-methoxyquinolin-8-yl)amino]pentyl}carbamoyl)benzoate (**2e**): Method A, from the reaction of monomethyl terephtalate (**1e**, 0.252 g) and after purification by column chromatography (dichloromethane/methanol 9.5:0.5) and crystallization (ether), **2e** was obtained as a pale-yellow solid (0.489 g, 83%): m.p. 112–113 °C; ^{1}H NMR ([D$_6$]DMSO): δ = 8.65 (t, J = 5.5 Hz, 1H, 1), 8.54–8.52 (dd, J = 4.2, 1.6 Hz, 1H, 10), 8.08–8.06 (dd, J = 8.2, 1.1 Hz, 1H, 12), 8.01 (d, J = 8.3 Hz, 2H, 3′, 7′), 7.94 (d, J = 8.3 Hz, 2H, 4′, 6′), 7.43–7.41 (m, 1H, 11), 6.47 (d, J = 2.2 Hz, 1H, 16), 6.28 (d, J = 2.1 Hz, 1H, 14), 6.15 (d, J = 8.7 Hz, 1H, 7), 3.88 (s, 3H, 9′), 3.81 (s, 3H, 17), 3.69–3.65 (m, 1H, 5), 3.32–3.29 (m, 2H, 2), 1.76–1.65, 1.65–1.57 (2m, 4H, 3, 4), 1.23 ppm (d, J = 6.3 Hz, 3H, 6); ^{13}C NMR ([D$_6$]DMSO): δ = 165.69, 165.24, 158.97, 144.59, 144.18, 138.76, 134.73. 134.51, 131.54, 129.53, 128.99, 127.47, 122.03, 96.09, 91.59, 54.91, 52.26, 47.00, 39.27, 33.39, 25.79, 20.15 ppm; IR (ATR): $\tilde{\nu}$ = 3403, 3318, 3060, 2936, 1714, 1634, 1615, 1519, 1425, 1386, 1278, 1225, 1169, 1111, 820, 791, 736, 703 cm^{-1}; MS (ESI): *m/z*: 422.2 $[M+1]^+$; elemental analysis calcd (%) for $C_{24}H_{27}N_3O_4$ (421.49): C 68.39, H 6.46, N 9.97; found: C 68.25, H 6.76, N 10.08.

General procedure for the preparation of carboxylic acids **3a–e**: A solution of lithium hydroxide monohydrate (0.126 g, 3 mmol) in water (10 mL) was added to a solution of ester **2** (6 mmol) in methanol (10 mL). The mixture was stirred at room temperature for 1 h. Methanol was evaporated under reduced pressure, and the aqueous residue was neutralized with 10% HCl and extracted with dichloromethane (3×). The organic layer was dried with sodium sulfate, filtered, and concentrated under reduced pressure.

3-({4-[(6-Methoxyquinolin-8-yl)amino]pentyl}carbamoyl)propanoic acid (**3a**): From the reaction of ester **2a** (0.224 g) and after crystallization (ether), **3a** was obtained as a pale-yellow solid (0.209 g, 97%): m.p. 146–148 °C; ^{1}H NMR ([D$_6$]DMSO): δ = 12.06 (s, 1H, 5′), 8.55–8.53 (dd, J = 4.2, 1.6 Hz, 1H, 10), 8.09–8.06 (dd, J = 8.3, 1.6 Hz, 1H, 12), 7.85–7.82 (t, J = 5.4 Hz, 1H, 1), 7.45–7.41(m, 1H, 11), 6.48 (d, J = 2.4 Hz, 1H, 16), 6.26 (d, J = 2.4 Hz, 1H, 14), 6.12 (d, J = 8.7 Hz, 1H, 7), 3.82 (s, 3H, 17), 3.66–3.57 (m, 1H, 5), 3.08–3.03 (m, 2H, 2), 2.41 (t, J = 6.5 Hz, 2H, 2′), 2.29 (t, J = 6.7 Hz, 2H, 3′), 1.70–1.58, 1.58–1.38 (2m, 4H, 3, 4), 1.2 ppm (d, J = 6.3 Hz, 3H, 6); ^{13}C NMR ([D$_6$]DMSO): δ = 173.87, 170.73, 159.00, 144.63, 144.24, 134.80, 134.52, 129.58, 122.10, 96.10, 91.59, 54.97, 46.99, 38.48, 33.38, 30.04, 29.21, 25.96, 20.19 ppm; IR (ATR): $\tilde{\nu}$ = 3454, 3268, 3094, 3009, 2962, 2928, 2863, 1713, 1649, 1615,1584, 1562, 1524, 1452, 1386, 1346, 1227, 1203, 1156, 1161, 824, 785, 746, 674 cm^{-1}; MS (ESI): *m/z*: 360.2 $[M+1]^+$; elemental analysis calcd (%) for $C_{19}H_{25}N_3O_4$ (359.42): C 63.49, H 7.01, N 11.69; found: C 63.22, H 7.30, N 11.45.

(2*E*)-3-({4-[(6-Methoxyquinolin-8-yl)amino]pentyl}carbamoyl) prop-2-enoic acid (**3b**): From the reaction of ester **2b** (0.231 g) and after

crystallization (ether), **3b** was obtained as a pale-yellow solid (0.178 g, 83%): m.p. 147–149 °C; ^{1}H NMR ([D$_6$]DMSO): δ = 12.83 (s, 1H, 5′), 8.55–8.53 (dd, J = 1.6, 4.2 Hz, 1H, 10), 8.49 (t, J = 5.5 Hz, 1H, 1), 8.09–8.06 (dd, J = 1.5, 8.3 Hz, 1H, 12), 7.45–7.40 (m, 1H, 11), 6.91 (d, J = 15.5 Hz, 1H, 2′), 6.50 (d, J = 15.5 Hz, 1H, 3′), 6.47 (d, J = 2.4 Hz, 1H, 16), 6.27 (d, J = 2.4 Hz, 1H, 14), 6.14 (d, J = 8.7 Hz, 1H, 7), 3.82 (s, 3H, 17), 3.68–3.58 (m, 1H, 5), 3.22–3.16 (m, 2H, 2), 1.71–1.49 (m, 4H, 3, 4), 1.21 ppm (d, J = 6.3 Hz, 3H, 6); ^{13}C NMR ([D$_6$]DMSO): δ = 166.49, 162.95, 159.00, 144.62, 144.22, 137.11, 134.79, 134.52, 129.57, 129.33, 122.09, 96.13, 91.62, 54.96, 46.96, 38.80, 33.40, 25.71, 20.19 ppm; IR (ATR): $\tilde{\nu}$ = 3453, 3271, 3087, 2937, 1716, 1654, 1613, 1564, 1527, 1380, 1337, 1269, 1236, 1213, 1198, 1171, 981, 909, 820, 785, 767, 673 cm^{-1}; MS (ESI): *m/z*: 358.2 $[M+1]^+$; elemental analysis calcd (%) for $C_{19}H_{23}N_3O_4$ (357.40): C 63.85, H 6.49, N 11.76; found: C 63.77, H 6.72, N 11.99.

4-({4-[(6-Methoxyquinolin-8-yl)amino]pentyl}carbamoyl)butanoic acid (**3c**): From the reaction of ester **2c** (0.232 g) and after crystallization (ether), **3c** was obtained as a pale-yellow solid (0.186 g, 88%): m.p. 95–96 °C; ^{1}H NMR ([D$_6$]DMSO): δ = 12.00 (s, 1H, 6′), 8.55–8.53 (dd, J = 4.2, 1.6 Hz, 1H, 10), 8.10–8.07 (dd, J = 8.3, 1.5 Hz, 1H, 12), 7.80 (t, J = 5.4 Hz, 1H, 1), 7.45–7.41 (m, 1H, 11), 6.48 (d, J = 2.4 Hz, 1H, 16), 6.27 (d, J = 2.4 Hz, 1H, 14), 6.13 (d, J = 8.7 Hz, 1H, 7), 3.83 (s, 3H, 17), 3.69–3.55 (m, 1H, 5), 3.09–3.05 (m, 2H, 2), 2.20 (t, J = 7.4 Hz, 2H, 2′), 2.08 (t, J = 7.4 Hz, 2H, 4′), 1.75–1.43 (m, 6H, 3′, 3, 4), 1.21 ppm (d, J = 6.3 Hz, 3H, 6); ^{13}C NMR ([D$_6$]DMSO): δ = 147.15, 171.36, 159.00, 144.63, 144.23, 134.79, 134.53, 129.57, 122.09, 96.11, 91.60, 54.97, 46.98, 38.38, 34.46, 33.41, 33.04, 25.97, 20.71, 20.19 ppm; IR (ATR): $\tilde{\nu}$ = 3453, 3324, 2933, 1720, 1643, 1613, 1580, 1524, 1386, 1227, 1204, 1161, 1139, 1058, 822, 786, 675 cm^{-1}; MS (ESI): *m/z*: 374.2 $[M+1]^+$; elemental analysis calcd (%) for $C_{20}H_{27}N_3O_4$ (373.45): C 64.32, H 7.29, N 11.25; found: C 64.21, H 7.15, N 11.48.

5-({4-[(6-Methoxyquinolin-8-yl)amino]pentyl}carbamoyl)pentanoic acid (**3d**): From the reaction of ester **2d** (0.241 g) and after crystallization (ether), **3d** was obtained as a pale-yellow solid (0.198 g, 85%): m.p. 68–69 °C; ^{1}H NMR ([D$_6$]DMSO): δ = 11.99 (s, 1H, 7′), 8.54 (d, J = 2.9 Hz, 1H, 10), 8.08 (d, J = 8.1 Hz, 1H, 12), 7.78 (t, J = 6.0 Hz, 2H, 1), 7.45–7.40 (m, 1H, 11), 6.48 (d, J = 3.0 Hz, 1H, 16), 6.26 (d, J = 3.0 Hz, 1H, 14), 6.12 (d, J = 8.6 Hz, 1H, 7), 3.82 (s, 3H, 17), 3.69–3.56 (m, 1H, 5), 3.09–3.0 (m, 2H, 2), 2.18 (t, J = 6.0 Hz, 2H, 5′), 2.04 (t, J = 6.0 Hz, 2H, 2′), 1.70–1.57, 1.57–1.42 (2m, 8H, 3, 4, 3′, 4′), 1.20 ppm (d, J = 6.2 Hz, 3H, 6); ^{13}C NMR ([D$_6$]DMSO): δ = 174.37, 171.67, 159.00, 144.63, 144.23, 134.79, 134.52, 129.57, 122.09, 96.10, 91.59, 54.97, 46.98, 38.36, 35.11, 33.38, 25.99, 24.84, 24.13, 20.19 ppm; IR (ATR): $\tilde{\nu}$ = 3453, 3370, 3294, 2943, 2863, 1731, 1609, 1562, 1519, 1455, 1424, 1385, 1224, 1203, 1166, 1156, 1133, 1053, 819, 790, 765, 677 cm^{-1}; MS (ESI): *m/z*: 388.2 $[M+1]^+$; elemental analysis calcd (%) for $C_{21}H_{29}N_3O_4$ (387.47): C 65.10, H 7.54, N 10.84; found: C 65.44, H 7.79, N 10.63.

4-({4-[(6-Methoxyquinolin-8-yl)amino]pentyl}carbamoyl)benzoic acid (**3e**): From the reaction of ester **2e** (0.253 g) and after crystallization (ether), **3e** was obtained as a pale-yellow solid (0.210 g, 86%): m.p. 142–144 °C; ^{1}H NMR ([D$_6$]DMSO): δ = 13.12 (s, 1H, 9′), 8.64 (t, J = 5.5 Hz, 1H, 1), 8.54–8.53 (dd, J = 4.2, 1.6 Hz, 1H, 10), 8.09–8.06 (dd, J = 8.3, 1.5 Hz, 1H, 12), 8.00 (d, J = 8.4 Hz, 2H, 3′, 7′), 7.92 (d, J = 8.4 Hz, 2H, 4′, 6′), 7.45–7.41 (m, 1H, 11), 6.47 (d, J = 2.4 Hz, 1H, 16), 6.28 (d, J = 2.4 Hz, 1H, 14), 6.16 (d, J = 8.4 Hz, 1H, 7), 3.81 (s, 3H, 17), 3.71–3.63 (m, 1H, 5), 3.34–3.28 (m, 2H, 2), 1.76–1.57 (m, 4H, 3, 4), 1.22 ppm (d, J = 7.3 Hz, 3H, 6); ^{13}C NMR ([D$_6$]DMSO): δ = 166.80, 165.42, 159.00, 144.61, 144.22, 138.45, 134.80, 134.52, 132.79, 129.58, 129.16, 127.36, 122.09, 96.14, 91.59, 54.96, 47.02, 39.28, 33.40, 25.86, 20.19 ppm; IR (ATR): $\tilde{\nu}$ = 3413, 3308, 2941, 2864 1727, 1691, 1636, 1613, 1575, 1519, 1454, 1422, 1385, 1276, 1220, 1201, 1156, 818, 786, 674 cm^{-1}; MS (ESI): *m/z*: 408.2 $[M+1]^+$; elemental analysis calcd (%) for $C_{23}H_{25}N_3O_4$ (407.46): C 67.80, H 6.18, N 10.31; found: C 67.93, H 6.02, N 10.68.

General procedure for the preparation of *O*-benzylhydroxamic acids **4a–e**: A solution of acid **3** (0.6 mmol), DIEA (0.155 g, 1.2 mol), and HATU (0.228 g, 0.6 mmol) in dichloromethane (6 mL) was stirred at room temperature. After 10 min, *O*-benzylhydroxylamine hydrochloride (0.112 g, 0.7 mmol) and Et$_3$N (0.071 g, 0.7 mmol) were added. The mixture was stirred at room temperature for 2 h and concentrated under reduced pressure. The residue was dissolved in ethyl acetate (20 mL) and extracted with brine (3×). The organic layer was dried with sodium sulfate, filtered, and concentrated under reduced pressure.

N-(Benzyloxy)-*N*′-{4-[(6-methoxyquinolin-8-yl)amino]pentyl}butanediamide (**4a**): From the reaction of **3a** (0.216 g) and after purification by column chromatography (dichloromethane/methanol 9.5:0.5) and crystallization (ether), **4a** was obtained as a pale-yellow solid (0.111 g, 40%): m.p. 121–123 °C; ^{1}H NMR ([D$_6$]DMSO): δ = 10.99 (s, 1H, 5′), 8.54 (d, J = 2.7 Hz, 1H, 10), 8.08 (d, J = 7.2 Hz, 1H, 12), 7.85 (s, 1H, 1), 7.44-7-35 (m, 6H, 11, 8′-12′), 6.47 (d, J = 2.2 Hz, 1H, 16), 6.26 (d, J = 2.0 Hz, 1H, 14), 6.12 (d, J = 8.6 Hz, 1H, 7), 4.76 (s, 2H, 6′), 3.82 (s, 3H, 17), 3.66–3.57 (m, 1H, 5), 3.08–3.02 (m, 2H, 2), 2.30 (t, J = 6.9 Hz, 2H, 3′), 2.18 (t, J = 6.8 Hz, 2H, 2′), 1.70–1.57, 1.57–1.43 (2m, 4H, 3, 4), 1.20 ppm (d, J = 6.2 Hz, 3H, 6); ^{13}C NMR ([D$_6$]DMSO): δ = 170.71, 168.80, 159.00, 144.62, 144.23, 136.06, 134.79, 134.52, 129.57, 128.72, 128.26, 128.16, 122.09, 96.09, 91.59, 76.75, 54.97, 46.99, 38.49, 33.39, 30.37, 27.91, 25.97, 20.19 ppm; IR (ATR): $\tilde{\nu}$ = 3367, 3311, 3060, 2936, 2862, 1728, 1636, 1615, 1546, 1519, 1457, 1424, 1387, 1223, 1200, 1159, 1052, 820, 790, 679 cm^{-1}; MS (ESI): *m/z*: 465.3 $[M+1]^+$; elemental analysis calcd (%) for $C_{26}H_{32}N_4O_4$ (464.56): C 67.22, H 6.94, N 12.06; found: C 67.46, H 6.69, N, 12.31.

(2*E*)-*N*-(Benzyloxy)-*N*′-{4-[(6-methoxyquinolin-8-yl)amino]pentyl}-but-2-ene-diamide (**4b**): From the reaction of **3b** (0.215 g) and after purification by column chromatography (dichloromethane/methanol/ethyl acetate/cyclohexane 9.5:0.5:10:10) and crystallization (ether), **4b** was obtained as a pale-yellow solid (0.119 g, 43%): m.p. 157–158 °C; ^{1}H NMR ([D$_6$]DMSO): δ = 11.52 (s, 1H, 5′), 8.55–8.53 (dd, J = 1.5, 4.2 Hz, 1H, 10), 8.45 (t, J = 5.5 Hz, 1H, 1), 8.09–8.06 (dd, J = 1.4, 8.3 Hz, 1H, 12), 7.45–7.37 (m, 1H, 11, 8′-12′), 6.90 (d, J = 15.1 Hz, 1H, 2′), 6.62 (d, J = 15.2 Hz, 1H, 3′), 6.47 (d, J = 2.4 Hz, 1H, 16), 6.27 (d, J = 2.3 Hz, 1H, 14), 6.15 (d, J = 8.7 Hz, 1H, 7), 4.86 (s, 2H, 6′), 3.82 (s, 3H, 17), 3.68–3.58 (m, 2H, 5), 3.20–3.15 (m, 2H, 2), 1.70–1.49 (m, 4H, 3,4), 1.21 ppm (d, J = 6.2 Hz, 3H, 6); ^{13}C NMR ([D$_6$]DMSO): δ = 163.17, 161.22, 158.99, 144.60, 144.22, 134.82, 134.49, 133.58, 129.58, 129.07, 122.09, 96.16, 91.64, 63.35, 54.97, 46.97, 38.95, 33.42, 25.76, 20.19 ppm; IR (ATR): $\tilde{\nu}$ = 3383, 3283, 3213, 3008, 2936, 2865, 1738, 1626, 1575, 1556, 1518, 1454, 1386, 1337, 1219, 1203, 1157,1051, 974, 818, 790, 738, 695, 675 cm^{-1}; MS (ESI): *m/z*: 463.1 $[M+1]^+$; elemental analysis calcd (%) for $C_{26}H_{30}N_4O_4$ (462.54): C 67.51, H 6.54, N 12.11; found: C 67.79, H 6.81, N 11.95.

N-(Benzyloxy)-*N*′-{4-[(6-methoxyquinolin-8-yl)amino]pentyl}pentanediamide (**4c**): From the reaction of **3c** (0.224 g) and after purification by column chromatography (dichloromethane/methanol 9.5:0.5) and crystallization (ether/petroleum ether), **4c** was obtained as a pale-yellow solid (0.144 g, 50%): m.p. 84–85 °C; ^{1}H NMR ([D$_6$]DMSO): δ = 10.95 (s, 1H, 6′), 8.54–8.53 (dd, J = 4.1, 1.5 Hz, 1H, 10), 8.09–8.06 (dd, J = 8.3, 1.4 Hz, 1H, 12), 7.78 (t, J = 5.4 Hz, 1H, 1), 7.44–7.33 (m, 6H, 11, 9′-13′), 6.47 (d, J = 2.4 Hz, 1H, 16), 6.26 (d, J =

2.3 Hz, 1H, 14), 6.13 (d, J=8.8 Hz, 1H, 7), 4.77 (s, 2H, 7′), 3.82 (s, 3H, 17), 3.62–3.56 (m, 1H, 5), 3.08–3.04 (m, 2H, 2), 2.04 (t, J=7.4 Hz, 2H, 4′), 1.95 (t, J=7.3 Hz, 2H, 2′), 1.74–1.43 (m, 6H, 3′, 3, 4), 1.20 ppm (d, J=6.2 Hz, 3H, 6); ^{13}C NMR ([D$_6$]DMSO): δ=171.32, 169.03, 159.00, 144.62, 144.23, 136.09, 134.79, 134.52, 129.57, 128.72, 128.26, 128.16, 122.09, 96.10, 91.59, 76.77, 54.97, 46.98, 38.41, 34.57, 33.43, 31.70, 25.99, 21.21, 20.19 ppm; IR (ATR): $\tilde{\nu}$= 3367, 3325, 3187, 2960, 2931, 2857, 1738, 1677, 1634, 1614, 1518, 1455, 1387, 1219, 1203, 1170, 1157, 1052, 1033, 821, 790, 740, 696, 676 cm^{-1}; MS (ESI): m/z: 479.3 $[M+1]^+$; elemental analysis calcd (%) for $C_{27}H_{34}N_4O_4$ (478.58): C 67.76, H 7.16, N 11.71; found: C 67.59, H 6.98, N, 12.04.

N-(Benzyloxy)-*N*′-{4-[(6-methoxyquinolin-8-yl)amino]pentyl}hexanediamide (**4d**): From the reaction of **3d** (0.232 g) and after purification by column chromatography (dichloromethane/methanol 9.5:0.5) and crystallization (ether), **4d** was obtained as a pale-yellow solid (0.151 g, 51%): m.p. 102–105 °C; ^{1}H NMR ([D$_6$]DMSO): δ=10.91 (s, 1H, 7′), 8.53 (dd, J=4.0, 1.4 Hz, 1H, 10), 8.06 (dd, J=8.2 Hz, 1H, 12), 7.74 (s, 1H, 1), 7.43–7.41 (m, 1H, 11), 7.37–7.34 (m, 5H, 10′-14′), 6.47 (d, J=2.3 Hz, 1H, 16), 6.26 (d, J=2.2 Hz, 1H, 14), 6.11 (d, J=8.7 Hz, 1H, 7), 4.77 (s, 2H, 8′), 3.82 (s, 3H, 17), 3.65–3.59 (m, 1H, 5), 3.08–3.02 (m, 2H, 2), 2.02 (s, 2H, 2′), 1.93 (s, 2H, 5′), 1.68–1.62, 1.56–1.41 (2m, 8H, 3, 4, 3′, 4′), 1.20 ppm (d, J=6.3 Hz, 3H, 6); ^{13}C NMR ([D$_6$]DMSO): δ=171.61, 169.19, 158.96, 144.59, 144.17, 136.03, 134.72, 134.48, 129.52, 128.66, 128.19, 129.09, 122.02, 96.06, 91.60, 76.70, 54.93, 53.57, 46.97, 38.34, 35.13, 33.42, 32.04, 25.94, 24.83, 24.62, 20.15 ppm; IR (ATR): $\tilde{\nu}$=3383, 3287, 2934, 2865, 1737, 1635, 1578, 1519, 1457, 1423, 1387, 1224, 1202, 1168, 1052, 820, 791, 743, 696 cm^{-1}; MS (ESI): m/z: 493.3 $[M+1]^+$; elemental analysis calcd (%) for $C_{28}H_{36}N_4O_4$ (492.61): C 68.27, H 7.37, N 11.37; found: C 68.47, H 7.25, N, 11.49.

N^1-(Benzyloxy)-N^4-{4-[(6-methoxyquinolin-8-yl)amino]pentyl}-benzene-1,4-dicarboxamide (**4e**): From the reaction of **3e** (0.245 g) and after purification by column chromatography (dichloromethane/methanol 9.5:0.5) and crystallization (ether), **4e** was obtained as a pale-yellow solid (0.188 g, 61%): m.p. 183–184 °C; ^{1}H NMR ([D$_6$]DMSO): δ=11.88 (s, 1H, 9′), 8.59 (t, J=5.5 Hz, 1H, 1), 8.54–8.52 (dd, J=4.2, 1.6 Hz, 1H, 10), 8.09–8.06 (dd, J=8.3, 1.6 Hz, 1H, 12), 7.89 (d, J=8.4 Hz, 2H, 3′, 7′), 7.80 (d, J=8.4 Hz, 2H, 4′, 6′), 7.45–7.34 (m, 6H, 11, 12′-16′), 6.47 (d, J=2.5 Hz, 1H, 16), 6.28 (d, J=2.4 Hz, 1H, 14), 6.15 (d, J=8.6 Hz, 1H, 7), 4.94 (s, 2H, 10′), 3.81 (s, 3H, 17), 3.71–3.63 (m, 1H, 5), 3.33–3.27 (m, 2H, 2), 1.75–1.58 (m, 4H, 3, 4), 1.23 ppm (d, J=6.3 Hz, 3H, 6); ^{13}C NMR ([D$_6$]DMSO): δ= 165.35, 163.70, 158.99, 144.61, 144.22, 137.30, 135.82, 134.80, 134.52, 134.38, 129.57, 128.93, 128.32, 127.32, 127.02, 122.09, 96.13, 91.59, 77.03, 54.96, 47.02, 39.23, 33.39, 25.88, 20.19 ppm; IR (ATR): $\tilde{\nu}$=3384, 3287, 2969, 2935, 1738, 1630, 1577, 1519, 1492, 1387, 1320, 1224, 1159, 1053, 863, 820, 790, 747, 718, 69 cm^{-1}; MS (ESI): 513.3 $[M+1]^+$; elemental analysis calcd (%) for $C_{30}H_{32}N_4O_4$ (512.60): C 70.29, H 6.29, N 10.93; found: C 70.55, H 6.03, N, 11.21.

General procedure for the preparation of SAHAquines **5a–d**: A suspension of *O*-benzylhydroxamic acid **4** (0.27 mmol) and 10% Pd/C (20 mg) in methanol (7 mL) was stirred at room temperature for 2–4 h under a hydrogen atmosphere. The catalyst was filtered off, and the mother liquor was concentrated under reduced pressure.

N-Hydroxy-*N*′-{4-[(6-methoxyquinolin-8-yl)amino]pentyl}butanediamide (**5a**): From the reaction of **4a** (0.125 g) and after crystallization (ether), **5a** was obtained as a pale-yellow solid (0.077 g, 76%): m.p. 109–110 °C; ^{1}H NMR ([D$_6$]DMSO): δ=10.37 (s, 1H, 5′), 8.67 (s, 1H, 6′), 8.54–8.53 (dd, J=4.2, 1.6 Hz, 1H, 10), 8.09–8.06 (dd, J=8.3, 1.5 Hz, 1H, 12), 7.85 (t, J=5.3 Hz, 1H, 1), 7.45–7.41 (m, 1H, 11), 6.47 (d, J=2.4 Hz, 1H, 16), 6.26 (d, J=2.4 Hz, 1H, 14), 6.12 (d, J=8.7 Hz, 1H, 7), 3.82 (s, 3H, 17), 3.67–3.56 (m, 1H, 5), 3.09–3.00 (m, 2H, 2), 2.29 (t, J=6.5 Hz, 2H, 2′), 2.17 (t, J=6.5 Hz, 2H, 3′), 1.72–1.56, 1.56–1.39 (2m, 4H, 3, 4), 1.20 ppm (d, J=6.3 Hz, 3H, 6); ^{13}C NMR ([D$_6$]DMSO): δ=170.84, 168.46, 159.00, 144.63, 144.24, 134.80, 134.52, 129.58, 122.11, 96.10, 91.60, 54.98, 47.00, 38.49, 33.42, 30.64, 27.92, 25.97, 20.20 ppm; IR (ATR): $\tilde{\nu}$=3471, 3375, 3283, 3204, 3008, 2964, 2934, 1744, 1647, 1612, 1556, 1521, 1455, 1385, 1366, 1226, 1205, 1172, 1157, 1056, 821, 789, 677 cm^{-1}; MS (ESI): m/z: 375.2 $[M+1]^+$; elemental analysis calcd (%) for $C_{19}H_{26}N_4O_4$ (374.43): C 60.95, H 7.00, N 14.96; found: C 60.84, H 6.81, N, 15.17.

N-Hydroxy-*N*′-{4-[(6-methoxyquinolin-8-yl)amino]pentyl}pentanediamide (**5b**): From the reaction of **4c** (0.129 g) and after crystallization (ether), **5b** was obtained as a pale-yellow solid (0.077 g, 73%): m.p. 99–102 °C; ^{1}H NMR ([D$_6$]DMSO): δ=10.32 (s, 1H, 6′), 8.63 (s, 1H, 7′), 8.55–8.52 (dd, J=4.2, 1.6 Hz, 1H, 12), 8.09–8.05 (dd, J=8.3, 1.6 Hz, 1H, 12), 7.76 (t, J=5.3 Hz, 1H, 1), 7.45–7.39 (m, 1H, 11), 6.47 (d, J=2.4 Hz, 1H, 16), 6.26 (d, J=2.4 Hz, 1H, 14), 6.11 (d, J=8.7 Hz, 1H, 7), 3.82 (s, 3H, 17), 3.68–3.56 (m, 1H, 5), 3.05 (d, J=5.6 Hz, 2H, 2), 2.04 (t, J=7.4 Hz, 2H, 2′), 1.94 (t, J=7.4 Hz, 2H, 4′), 1.76–1.57, 1.57–1.40 (2m, 6H, 3, 4, 3′), 1.21 ppm (d, J=6.3 Hz, 3H, 6); ^{13}C NMR ([D$_6$]DMSO): δ=171.37, 168.74, 158.98, 144.60, 144.20, 134.75, 134.50, 129.54, 122.05, 96.08, 91.61, 54.95, 46.98, 38.39, 34.73, 33.43, 31.75, 25.95, 21.42, 20.17 ppm; IR (ATR): $\tilde{\nu}$=3468, 3375, 3283, 3210, 3008, 2963, 2933, 1744, 1645, 1613, 1520, 1455, 1386, 1204, 1171, 1158, 1056, 821, 789, 677 cm^{-1}; MS (ESI): m/z: 389.2 $[M+1]^+$; elemental analysis calcd (%) for $C_{20}H_{28}N_4O_4$ (388.46): C 61.84, H 7.27, N 14.42; found: C 61.69, H 7.03, N, 14.77.

N-Hydroxy-*N*′-{4-[(6-methoxyquinolin-8-yl)amino]pentyl}hexanediamide (**5c**): From the reaction of **4d** (0.133 g) and after crystallization (ether), **5c** was obtained as a pale-yellow solid (0.082 g, 75%): m.p. 109–111 °C; ^{1}H NMR ([D$_6$]DMSO): δ=10.34 (s, 1H, 7′), 8.66 (s, 1H, 8′), 8.55–8.52 (dd, J=4.2, 1.5 Hz, 1H, 10), 8.10–8.05 (dd, J=8.3, 1.4 Hz, 1H, 12), 7.77 (t, J=5.3 Hz, 1H, 1), 7.45–7.40 (m, 1H, 11), 6.47 (d, J=2.4 Hz, 1H, 16), 6.26 (d, J=2.4 Hz, 1H, 14), 6.12 (d, J=8.8 Hz, 1H, 7), 3.82 (s, 3H, 17), 3.67–3.57 (m, 1H, 5), 3.04 (d, J=5.5 Hz, 2H, 2), 2.03 (s, 2H, 2′), 1.92 (s, 2H, 5′), 1.72–1.58, 1.58–1.41 (2m, 8H, 3, 4, 3′, 4′), 1.20 ppm (d, J=6.3 Hz, 3H, 6); ^{13}C NMR ([D$_6$]DMSO): δ= 171.70, 168.95, 159.00, 144.62, 144.24, 134.80, 134.52, 129.57, 122.10, 96.10, 91.60, 54.98, 46.98, 38.38, 35.20, 33.44, 32.11, 26.01, 24.97, 24.87, 20.20 ppm; IR (ATR): $\tilde{\nu}$=3428, 3283, 3191, 3088, 3044, 2943, 2923, 2856, 1738, 1621, 1578,1556, 1523, 1385, 1367, 1204, 1170, 1160, 954, 822, 788, 676 cm^{-1}; MS (ESI): m/z: 403.3 $[M+1]^+$; elemental analysis calcd (%) for $C_{21}H_{30}N_4O_4$ (402.49): C 62.67, H 7.51, N 13.92; found: C 62.98, H 7.36, N, 14.09.

N^1-Hydroxy-N^4-{4-[(6-methoxyquinolin-8-yl)amino]pentyl}benzene-1,4-dicarboxamide (**5d**): From the reaction of **4e** (0.138 g) and after purification by column chromatography (dichloromethane/methanol 9:1) and crystallization (ether), **5d** was obtained as a pale-yellow solid (0.048 g, 42%): m.p. 156–158 °C; ^{1}H NMR ([D$_6$]DMSO): δ=11.32 (s, 1H, 9′), 9.12 (s, 1H, 10′), 8.57 (t, J=5.5 Hz, 1H, 1), 8.54–8.53 (dd, J=4.2, 1.6 Hz, 1H, 10), 8.09–8.06 (d, J=8.3, 1.6 Hz, 1H, 12), 7.88 (d, J=8.3 Hz, 2H, 3′, 7′), 7.80 (d, J=8.3 Hz, 2H, 4′, 6′), 7.44–7.40 (m, 1H, 11), 6.47 (d, J=2.2 Hz, 1H, 16), 6.28 (d, J=2.1 Hz, 1H, 14), 6.15 (d, J=8.7 Hz, 1H, 7), 3.81 (s, 3H, 17), 3.71–3.62 (m, 1H, 5), 3.33–3.27 (m, 2H, 2), 1.75–1.58 (m, 4H, 3, 4), 1.23 ppm (d, J=6.2 Hz, 3H, 6); ^{13}C NMR ([D$_6$]DMSO): δ=165.44, 163.49, 159.00, 144.62, 144.20, 136.91, 134.86, 134.79, 134.53, 129.57, 127.17, 126.78, 122.09, 96.12, 91.60, 54.96, 47.02, 39.23, 33.41, 25.89, 20.19 ppm; IR (ATR): $\tilde{\nu}$=3427, 3303, 3199, 2969, 2938, 1738, 1672, 1636, 1616, 1521, 1458, 1388, 1223, 1203, 1172, 1015, 898,

858, 821, 789, 677 cm^{-1}; MS (ESI): *m/z*: 423.1 $[M+1]^+$; elemental analysis calcd (%) for $C_{23}H_{26}N_4O_4$ (422.48): C 65.39, H 6.20, N 13.26; found: C 65.47, H 6.12, N, 12.99.

General procedure for the preparation of *O*-methylhydroxamic acids **6a–e**: A solution of corresponding acid **3** (0.2 mmol), DIEA (0.052 g, 0.4 mmol), and HATU (0.076 g, 0.2 mmol) in dichloromethane (5 mL) was stirred at room temperature. After 10 min, *O*-methylhydroxylamine hydrochloride (0.020 g, 0.24 mmol) and Et_3N (0.024 g, 0.24 mmol) were added. The mixture was stirred at room temperature for 2 h and was then concentrated under reduced pressure. The residue was dissolved in ethyl acetate (8 mL) and extracted with water (3×). The organic layer was dried with sodium sulfate, filtered, and concentrated under reduced pressure.

N-Methoxy-*N*′-{4-[(6-methoxyquinolin-8-yl)amino]pentyl}butanediamide (**6a**): From the reaction of **3a** (0.072 g) and after purification by column chromatography (dichloromethane/methanol 9.5:0.5) and crystallization (ether/petroleum ether), **6a** was obtained as a pale-yellow solid (0.055 g, 71%): m.p. 121–122 °C; ^{1}H NMR ([D$_6$]DMSO): δ = 10.93 (s, 1H, 5′), 8.54–8.53 (dd, *J* = 3.0 Hz, 1H, 10), 8.06 (d, *J* = 8.2 Hz, 1H, 12), 7.82 (s, 1H, 1), 7.43–7.41 (m, 1H, 11), 6.47 (d, *J* = 2.2 Hz, 1H, 16), 6.26 (d, *J* = 2.1 Hz, 1H, 14), 6.11 (d, *J* = 8.7 Hz, 1H, 7), 3.83 (s, 3H, 17), 3.63–3.58 (m, 1H, 5), 3.54 (s, 3H, 6′), 3.08–3.02 (m, 2H, 2), 2.29 (t, *J* = 7.4 Hz, 2H, 2′), 2.16 (t, *J* = 7.0 Hz, 2H, 3′), 1.67–1.63, 1.55–1.45 (2m, 4H, 3, 4), 1.21 ppm (d, *J* = 6.3 Hz, 3H, 6); ^{13}C NMR ([D$_6$]DMSO): δ = 170.64, 168.44, 158.96, 144.59, 144.17, 134.71, 134.48, 129.52, 122.01, 96.04, 91.60, 62.97, 54.92, 46.97, 38.44, 33.37, 30.27, 27.84, 25.90, 20.14 ppm; IR (ATR): $\tilde{\nu}$ = 3302, 3234, 3001, 2969, 2933, 1739, 1658, 1634, 1556, 1519, 1457, 1424, 1388, 1336, 1224, 1204, 1168, 1053, 820, 791, 679 cm^{-1}; MS (ESI): *m/z*: 389.2 $[M+1]^+$; elemental analysis calcd (%) for $C_{20}H_{28}N_4O_4$ (388.46): C 61.84, H 7.27, N 14.42; found: C 62.05, H 7.01, N 14.65.

(2*E*)-*N*-Methoxy-*N*′-{4-[(6-methoxyquinolin-8-yl)amino]pent-yl}but-2-enediamide (**6b**): From the reaction of **3b** (0.072 g) and after purification by column chromatography (cyclohexane/ethyl acetate/methanol 3:1:0.5) and crystallization (ether), **6b** was obtained as a pale-yellow solid (0.038 g, 49%): m.p. 177–179 °C; ^{1}H NMR ([D$_6$]DMSO): δ = 11.53 (s, 1H, 5′), 8.55–8.53 (dd, *J* = 1.6, 4.2 Hz, 1H, 10), 8.44 (t, *J* = 5.5 Hz, 1H, 1), 8.09–8.06 (dd, *J* = 1.5, 8.3 Hz, 1H, 12), 7.45–7.41 (m, 6H, 11), 6.89 (d, *J* = 15.1 Hz, 1H, 2′), 6.60 (d, *J* = 15.1 Hz, 1H, 3′), 6.47 (d, *J* = 2.2 Hz, 1H, 16), 6.27 (d, *J* = 2.2 Hz, 1H, 14), 6.14 (d, *J* = 8.7 Hz, 1H, 7), 3.82 (s, 3H, 17), 3.65 (s, 4H, 5, 6′), 3.20–3.14 (m, 2H, 2), 1.70–1.49 (m, 4H, 3, 4), 1.21 ppm (d, *J* = 6.2 Hz, 3H, 6); ^{13}C NMR ([D$_6$]DMSO): δ = 163.16, 160.97, 159.00, 144.60, 144.22, 135.72, 134.82, 134.49, 133.58, 129.58, 129.12, 128.85, 129.34, 122.09, 96.16, 91.63, 76.97, 54.97, 46.97, 38.77, 33.42, 25.77, 20.19 ppm; IR (ATR): $\tilde{\nu}$ = 3285, 3223, 3097, 3007, 2969,2935, 1738, 1630, 1570, 1519, 1457, 1388, 1338, 1224, 1168, 1066, 1053, 991, 821, 792, 659 cm^{-1}; MS (ESI): *m/z*: 387.1 $[M+1]^+$; elemental analysis calcd (%) for $C_{20}H_{26}N_4O_4$ (386.44): C 62.16, H 6.78, N 14.50; found: C 61.94, H 6.55, N 14.87.

N-Methoxy-*N*′-{4-[(6-methoxyquinolin-8-yl)amino]pentyl}pentanediamide (**6c**): From the reaction of **3c** (0.075 g) and after crystallization (ether), **6c** was obtained as a pale-yellow solid (0.045 g, 56%): m.p. 112–113 °C; ^{1}H NMR ([D$_6$]DMSO): δ = 10.94 (s, 1H, 6′), 8.55–8.53 (dd, *J* = 4.2, 1.5 Hz, 1H, 10), 8.09–8.06 (dd, *J* = 8.3, 1.4 Hz, 1H, 12), 7.89 (t, *J* = 5.3 Hz, 1H, 1), 7.45–7.41 (m, 1H, 11), 6.48 (d, *J* = 2.4 Hz, 1H, 16), 6.26 (d, *J* = 2.3 Hz, 1H, 14), 6.12 (d, *J* = 8.7 Hz, 1H, 7), 3.82 (s, 3H, 17), 3.62 (m, 1H, 5), 3.56 (s, 3H, 7′), 3.06–3.04 (m, 2H, 2), 2.04 (t, *J* = 7.3 Hz, 2H, 2′), 1.93 (t, *J* = 7.3 Hz, 2H, 4′), 1.74–1.40 (m, 6H, 3′, 3,4′), 1.20 ppm (d, *J* = 6.3 Hz, 3H, 6); ^{13}C NMR ([D$_6$]DMSO): δ = 171.31, 168.72, 159.00, 144.62, 144.23, 134.79, 134.52, 129.57, 122.10, 96.10, 91.59, 63.10, 54.98, 46.98, 38.41, 34.54, 33.43, 31.68, 25.98, 21.12, 20.19 ppm; IR (ATR): $\tilde{\nu}$ = 3396, 3285, 3162, 3097, 2969, 2936, 1737, 1670, 1630, 1564, 1521, 1456, 1424, 1388, 1227, 1206, 1170,1161, 1030, 820, 790, 679 cm^{-1}; MS (ESI): *m/z*: 403.3 $[M+1]^+$; elemental analysis calcd (%) for $C_{21}H_{30}N_4O_4$ (402.49): C 62.67, H 7.51, N 13.92; found: C 62.46, H 7.31, N 13.95.

N-Methoxy-*N*′-{4-[(6-methoxyquinolin-8-yl)amino]pentyl}hexanediamide (**6d**): From the reaction of **3d** (0.075 g) and after purification by column chromatography (dichloromethane/methanol 9.5:0.5) and crystallization (ether), **6d** was obtained as a pale-yellow solid (0.042 g, 51%): m.p. 108–109 °C; ^{1}H NMR ([D$_6$]DMSO): δ = 10.91 (s, 1H, 7′), 8.55–8.52 (dd, *J* = 4.1, 1.6 Hz, 1H, 10), 8.09–8.06 (dd, *J* = 8.3, 1.5 Hz, 1H, 12), 7.75 (t, *J* = 5.4 Hz, 1H, 1), 7.44–7.41 (m, 1H, 11), 6.47 (d, *J* = 2.4 Hz, 1H, 16), 6.26 (d, *J* = 2.4 Hz, 1H, 14), 6.11 (d, *J* = 8.7 Hz, 1H, 7), 3.82 (s, 3H, 17), 3.65–3.55 (m, 4H, 5, 8′), 3.08–3.00 (m, 2H, 2), 2.03 (s, 2H, 2′), 1.92 (s, 2H, 5′), 1.55–1.49, 1.49–1.40 (m, 8H, 3, 4, 3′, 4′), 1.20 ppm (d, *J* = 6.3 Hz, 3H, 6); ^{13}C NMR ([D$_6$]DMSO): δ = 171.64, 168.91, 158.98, 144.61, 144.20, 134.76, 134.50, 129.55, 122.06, 96.08, 91.60, 63.05, 54.95, 46.97, 38.36, 35.15, 33.43, 32.07, 25.97, 24.86, 24.60, 20.17 ppm; IR (ATR): $\tilde{\nu}$ = 3395, 3287, 3166, 3090, 2927, 2861, 1739, 1674, 1631, 1577, 1563, 1521, 1457, 1423, 1388, 1227, 1206, 1170, 1161, 1053, 821, 790, 679 cm^{-1}; MS (ESI): *m/z*: 417.3 $[M+1]^+$; elemental analysis calcd (%) for $C_{22}H_{32}N_4O_4$ (416.51): C 63.44, H 7.74, N 13.45; found: C 63.26, H 7.53, N 13.71.

N^1-Methoxy-N^4-{4-[(6-methoxyquinolin-8-yl)amino]pentyl}benzene-1,4-dicarboxamide (**6e**): From the reaction of **3e** (0.082 g) and after crystallization (ether), **6e** was obtained as a pale-yellow solid (0.040 g, 45%): m.p. 142–145 °C; ^{1}H NMR ([D$_6$]DMSO): δ = 11.84 (s, 1H, 9′), 8.58 (t, *J* = 5.56 Hz, 1H, 1), 8.54–8.53 (dd, *J* = 1.6, 4.2 Hz, 1H, 10), 8.08–8.06 (dd, *J* = 1.6, 8.3 Hz, 1H, 12), 7.89 (d, *J* = 8.4 Hz, 2H, 3′, 7′), 7.80 (d, *J* = 8.4 Hz, 2H, 4′, 6′), 7.43–7.41 (m, 1H, 11), 6.47 (d, *J* = 2.5 Hz, 1H, 16), 6.28 (d, *J* = 2.4 Hz, 1H, 14), 6.15 (d, *J* = 8.8 Hz, 1H, 7), 3.82 (s, 3H, 17), 3.72 (s, 2H, 10′), 3.69–3.65 (m, 1H, 5), 3.31–3.28 (m, 2H, 2), 1.76–1.66, 1.65–1.56 (m, 4H, 3, 4), 1.23 ppm (d, *J* = 6.3 Hz, 3H, 6); ^{13}C NMR ([D$_6$]DMSO): δ = 165.32, 163.36, 158.98, 144.61, 144.20, 137.28, 134.76, 134.52, 134.31, 129.55, 127.21, 126.93), 122.06, 96.10, 91.60, 63.26, 54.94, 47.01, 39.23, 33.41, 25.85, 20.17 ppm; IR (ATR): $\tilde{\nu}$ = 3394, 3309, 3176, 3060, 2970, 2937, 1738, 1670, 1624, 1557, 1520, 1456, 1389, 1221, 1205, 1161, 1039, 867, 821, 791, 678 cm^{-1}; MS (ESI): *m/z*: 437.3 $[M+1]^+$; elemental analysis calcd (%) for $C_{24}H_{28}N_4O_4$ (436.50): C 66.04, H 6.47, N 12.84; found: C 66.33, H 6.31, N 13.04.

Biological Evaluation

Cell viability: All synthesized compounds were first screened for their inhibition of mitochondrial metabolic activity by using the MTT assay.[65] Mitochondrial metabolic activity correlates with cell viability. The following cell lines were tested: U2OS, HepG2, MCF-7, and Hek293 cells. The compounds were dissolved in DMSO (3×10^{-3} M) and stored at −20 °C. The cells were seeded at a density of 3000 cells per 200 µL in a 96-well plate (Sarsted) in triplicate and grown in Dulbecco's modified Eagle medium with 4500 mg L^{-1} glucose (DMEM-high glucose) (Lonza) containing 10% fetal bovine serum (FBS) (Gibco), 100 U mL^{-1} penicillin, and 100 µg mL^{-1} streptomycin (Sigma–Aldrich). The next day, the medium was aspirated and cells were treated for 72 h. Only the compounds that led to more than a 40% reduction in mitochondrial metabolic activity at a concentration of 5×10^{-5} M were selected for further analysis. The following concentrations of selected compounds were used: 5×

10^{-5}, 1×10^{-5}, 1×10^{-6}, 1×10^{-7}, and 1×10^{-8} M. All working concentrations were freshly prepared in DMEM on the day of the testing. A fresh growth medium was added to untreated control cells, which were defined as 100% viable. DMSO (1.67, 0.33, 0.03, 0.3×10^{-2}, and 0.3×10^{-3}%) in DMEM was considered as a negative control. Cisplatin, PQ, and SAHA were used as positive controls. After 72 h of incubation in the presence of selected compounds, media were aspirated and MTT (0.5 mg mL^{-1}; 40 μL per well) was added, and the cells were incubated for 4 h 37 °C. Media were aspirated and formazan crystals were dissolved in DMSO (170 μL per well). The absorbance was measured on a microplate reader (Promega) at $\lambda = 560$ nm. The IC_{50} values (concentration required to decrease viability by 50%) were calculated by using nonlinear regression on the sigmoidal dose–response plots and are expressed as mean ± SD of two independent experiments.

MCF-7 cell labeling with Hoechst 33342: Fluorescent dye Hoechst 33342 was used to determine the total number of cells. MCF-7 cells were seeded at a density of 3000 cells per 100 μL (72 h treatment) or 6000 cells per 100 μL (24 h treatment) in a 96-well plate (Corning Inc.). Cells were grown in triplicate in DMEM containing 10% FBS (Wisent), 100 U mL^{-1} penicillin, and 100 μg mL^{-1} streptomycin (Thermo Fischer). The next day, cells were treated with SAHAquines **4e** and **5b**, SAHA, PQ, and cisplatin in ten different concentrations ranging from 5×10^{-5} to 1×10^{-9} M. After 72 h, cells were stained with Hoechst 33342 (10 μM, 10 min). Cells were then imaged by using a fluorescence microscope (Leica, DMI4000B). Results were calculated by using nonlinear regression on the sigmoidal dose–response plot and are expressed as mean ± SD of two independent experiments.

In vitro drug sensitivity assay against erythrocytic stages of *P. falciparum*: The antiplasmodial activity of compounds **2**–**6** was tested in a drug-sensitivity assay against two laboratory *P. falciparum* strains (3D7—chloroquine sensitive, Dd2—chloroquine-resistant) as described before by using the histidine-rich protein 2 (HRP2) assay.[66,67] In brief, 96-well plates were precoated with the tested compounds in a threefold dilution before ring-stage parasites were added in complete culture medium at a hematocrit of 1.5% and a parasitaemia of 0.05%. After 3 days of incubation at 37 °C, 5% CO_2 and 5% oxygen, plates were frozen until analyzed by HRP2-ELISA. All compounds were evaluated in duplicate in at least two independent experiments. The IC_{50} was determined by analyzing the nonlinear regression of log concentration–response curves using the drc-package v0.9.0 of R v2.6.1.[68]

In vitro activity against *P. berghei* hepatic stages: Compound activity on *P. berghei* infection of a human hepatoma cell line (HuH7) was assessed employing the luminescence-based method, as previously described.[69] Briefly, hepatic infection was determined by measuring the luminescence intensity of lysates of HuH7 cells infected with a firefly luciferase-expressing *P. berghei* line. HuH7 cells (1.0×10^4 per well) were seeded in 96-well plates the day before infection. One hour prior to infection, the medium was replaced by medium containing the appropriate drug concentrations. The addition of 1.0×10^4 sporozoites was followed by centrifugation at $1800\times g$ for 5 min and parasite infection load was measured 48 h after parasite addition by a bioluminescence assay (Biotium, USA) using a multiplate reader Infinite M200 (Tecan, Switzerland). The effect of the different treatments on the viability of HuH7 cells was assessed by the CellTiter-Blue assay (Promega, USA) according to the manufacturer's protocol. Nonlinear regression analysis was employed to fit the normalized results of the dose–response curves, and IC_{50} values were determined using GraphPad Prism V5.0.

Immunocytochemistry for histone acetylation: MCF-7 cells were seeded at a density of 5000 cells per coverslip in DMEM containing 10% FBS, 100 U mL^{-1} penicillin, and 100 μg mL^{-1} streptomycin and were left for 24 h to adhere. Cells were treated with **4e**, **5b**, SAHA, or PQ (at 1 μM concentration) for 24 h. Following treatment, cells were fixed with 4% paraformaldehyde (10 min), then permeabilized using 0.1% Triton X-100 (10 min). Blocking was performed using 10% goat serum in phosphate buffer saline (PBS) (1 h), followed by incubation with primary antibody (rabbit anti-acetyl-Histone-H3 polyclonal antibody 1/500; Millipore 06–559) for 24 h in a humidified chamber at 4 °C. Samples were washed with PBS (3× 5 min). Samples were then incubated with secondary antibody (Alexa Fluor 647 goat anti-rabbit IgG −2 mg mL^{-1} 1/500; Life Technologies A21244) for 1 h in the dark, after which they were washed with PBS (3×5 min). Nuclei were labeled with Hoechst 33342 (10 μM, 10 min). Samples were mounted on microscope slides using Poly Aqua Mount (PolySciences) and were dried overnight before imaging with a fluorescence microscope (Leica). Fluorescence intensity was quantified using ImageJ software, and the results are presented as means of fluorescence per cell ± SD (as fold increase in the untreated control = 1).

Acknowledgements

Support for this study by Croatian Science Foundation (project number IP-09–2014-1501), Canadian Institute of Health Research (CIHR; project number MOP-119425), and National Sciences and Engineering Research Council of Canada (NSERC; project number RGPIN 04994-15) is acknowledged.

Conflict of Interest

The authors declare no conflict of interest.

Keywords: acetylation · anticancer agents · antiplasmodial activity · cytostatic activity · drug design

[1] A. Remesh, *Int. J. Basic Clin. Pharmacol.* **2012**, *1*, 2–12.
[2] D. B. Longley, P. G. Johnston, *J. Pathol.* **2005**, *205*, 275–292.
[3] N. J. Curtin, *Nat. Rev.* **2012**, *12*, 801–817.
[4] C. Azad, M. Saxena, A. J. Siddiqui, J. Bhardwaj, S. K. Puri, G. P. Dutta, N. Anand, A. K. Saxena, *Chem. Biol. Drug Des.* **2017**, *90*, 254–261.
[5] C. Teixeira, N. Vale, B. Pérez, A. Gomes, J. R. Gomes, P. Gomes, *Chem. Rev.* **2014**, *114*, 11164–11220.
[6] D. Shahinas, A. Folefoc, D. R. Pillai, *Pathogens* **2013**, *2*, 33–54.
[7] D. Agarwal, R. D. Gupta, S. K. Awasthi, *Antimicrob. Agents Chemother.* **2017**, *61*, e00249-17.
[8] K. Takasu, T. Shomogama, C. Saiin, H.-S. Kim, Y. Wataya, R. Brun, M. Ihara, *Chem. Pharm. Bull.* **2005**, *53*, 653–661.
[9] A. Gomes, M. Machado, L. Lobo, F. Nogueira, M. Prudencio, C. Teixeira, P. Gomes, *ChemMedChem* **2015**, *10*, 1344–1349.
[10] S. Higginbotham, W. R. Wong, R. G. Linington, C. Spadafora, L. Iturrado, A. E. Arnold, *PLoS One* **2014**, *9*, e84549.
[11] W. T. Johnston, N. Mutalima, D. Sun, B. Emmanuel, K. Bhatia, P. Aka, X. Wu, E. Borgstein, G. N. Liomba, S. Kamiza, N. Mkandawire, M. Batumba, L. M. Carpenter, H. Jaffe, E. M. Molyneux, J. J. Goedert, D. Soppet, R. Newton, S. M. Mbulaiteye, *Sci. Rep.* **2014**, *4*, 3741.
[12] K. H. Khan, *Germs* **2013**, *3*, 26–35.
[13] D. A. Fedosov, M. Dao, G. E. Karniadakis, S. Suresh, *Ann. Biomed. Eng.* **2014**, *42*, 368–387.
[14] R. Hooft van Huijsduijnen, R. K. Guy, K. Chibale, R. K. Haynes, I. Peitz, G. Kelter, M. A. Phillips, J. L. Vennerstrom, Y. Yuthavong, T. N. Wells, *PLoS One* **2013**, *8*, e82962.

[15] K.-C. Keum, N.-C. Yoo, W.-M. Yoo, K. K. Chang, Y. N. Choon, Y. W. Min, WO 2002013826 A1, **2002**.
[16] F. Liu, Y. Shang, S-Z. Chen, *Acta Pharmacol. Sin.* **2014**, *35*, 645 – 652.
[17] A. Kamal, A. Aziz, S. Shouman, E. El-Demerdash, M. Elgendy, A. B. Abdel-Naim, *Sci. Proc.* **2014**, *1*, e384.
[18] A. Ganguli, D. Choudhury, S. Datta, S. Bhattacharya, G. Chakrabarti, *Biochimie* **2014**, *107*, 338 – 349.
[19] G. W. Soo, J. H. Law, E. Kan, S. Y. Tan, W. Y. Lim, G. Chay, N. I. Bukhari, I. Segarra, *Anticancer Drugs* **2010**, *21*, 695 – 703.
[20] Y. K. Wong, C. Xu, K. A. Kalesh, Y. He, Q. Lin, W. S. F. Wong, H. M. Shen, J. Wang, *Med. Res. Rev.* **2017**, *37*, 1492 – 1517.
[21] I. Nakase, H. Lai, N. P. Singh, T. Sasaki, *Int. J. Pharm.* **2008**, *354*, 28 – 33.
[22] C. Cheng, T. Wang, Z. Song, L. Peng, M. Gao, O. Hermine, S. Rousseaux, S. Khochbin, J. Q. Mi, J. Wang, *Cancer Med.* **2018**, *7*, 380 – 396.
[23] T. Shi, X. X. Yu, L. J. Yan, H. T. Xiao, *Cancer Chemother. Pharmacol.* **2017**, *79*, 287 – 294.
[24] G. Džimbeg, B. Zorc, M. Kralj, K. Ester, K. Pavelić, J. Balzarini, E. De Clercq, M. Mintas, *Eur. J. Med. Chem.* **2008**, *43*, 1180 – 1187.
[25] M. Šimunović, I. Perković, B. Zorc, K. Ester, M. Kralj, D. Hadjipavlou-Litina, E. Pontiki, *Bioorg. Med. Chem.* **2009**, *17*, 5605 – 5613.
[26] I. Perković, S. Tršinar, J. Žanetić, M. Kralj, I. Martin-Kleiner, J. Balzarini, D. Hadjipavlou-Litina, A. M. Katsori, B. Zorc, *J. Enzyme Inhib. Med. Chem.* **2013**, *28*, 601 – 610.
[27] K. Pavić, I. Perković, M. Cindrić, M. Pranjić, I. Martin-Kleiner, M. Kralj, D. Schols, D. Hadjipavlou-Litina, A.-M. Katsori, B. Zorc, *Eur. J. Med. Chem.* **2014**, *86*, 502 – 514.
[28] I. Perković, M. Antunović, I. Marijanović, K. Pavić, K. Ester, M. Kralj, J. Vlainić, I. Kosalec, D. Schols, D. Hadjipavlou-Litina, E. Pontiki, B. Zorc, *Eur. J. Med. Chem.* **2016**, *124*, 622 – 636.
[29] K. Pavić, I. Perković, P. Gilja, F. Kozlina, K. Ester, M. Kralj, D. Schols, D. Hadjipavlou-Litina, E. Pontiki, B. Zorc, *Molecules* **2016**, *21*, 1629 – 1653.
[30] K. Pavić, I. Perković, Š. Pospíšilová, M. Machado, D. Fontinha, M. Prudêncio, J. Jampilek, A. Coffey, L. Endersen, H. Rimac, B. Zorc, *Eur. J. Med. Chem.* **2018**, *143*, 769 – 779.
[31] A. Gomes, I. Fernandes, C. Teixeira, N. Mateus, M. J. Sottomayor, P. Gomes, *ChemMedChem* **2016**, *11*, 2703 – 2712.
[32] C. Pérez, I. Fernandes, N. Mateus, C. Teixeira, P. Gomes, *Bioorg. Med. Chem. Lett.* **2013**, *23*, 6769 – 6772.
[33] S. Slezakova, J. Ruda-Kucerova, *Anticancer Res.* **2017**, *37*, 5995 – 6003.
[34] Q. Sun, J. Wang, Y. Li, J. Zhuang, Q. Zhang, X. Sun, D. Sun, *Chem. Biol. Drug Des.* **2017**, *90*, 1019 – 1028.
[35] B. S. Pybus, S. R. Marcsisin, X. Jin, G. Deye, J. C. Sousa, Q. Li, D. Caridha, Q. Zeng, G. A. Reichard, C. Ockenhouse, J. Bennett, L. A. Walker, C. Ohrt, V. Melendez, *Malar. J.* **2013**, *12*, e212.
[36] N. Vale, R. Moreira, P. Gomes, *Eur. J. Med. Chem.* **2009**, *44*, 937 – 953.
[37] S. O. Tcherniuk, O. Chesnokova, I. V. Oleinikov, A. I. Potopalsky, A. V. Oleinikov, *Malar. J.* **2015**, *14*, 425.
[38] A. Wildbolz, *Ther. Umsch.* **1973**, *30*, 218 – 222.
[39] B. Pouvelle, P. J. Farley, C. A. Long, T. F. Taraschi, *J. Clin. Invest.* **1994**, *94*, 413 – 417.
[40] E. A. Usanga, *FEBS Lett.* **1986**, *209*, 23 – 27.
[41] L. Nair, V. K. Bhasin, *Jpn. J. Med. Sci. Biol.* **1994**, *47*, 241 – 252.
[42] A. Kreidenweiss, P. G. Kremsner, B. Mordmüller, *Malar. J.* **2008**, *7*, 187.
[43] S. Grant, C. Easley, P. Kirkpatrick, *Nat. Rev. Drug. Discov.* **2007**, *6*, 21 – 22.
[44] M. J. Chua, M. S. J. Arnold, W. Xu, J. Lancelot, S. Lamotte, G. F. Späth, E. Prina, R. J. Pierce, D. P. Fairlie, T. S. Skinner-Adams, K. T. Andrews, *Int. J. Parasitol.* **2017**, *7*, 42 – 50.
[45] K. T. Andrews, A. Haque, M. K. Jones, *Immunol. Cell Biol.* **2012**, *90*, 66 – 77.
[46] B. K. Chaal, A. P. Gupta, B. D. Wastuwidyaningtyas, Y. H. Luah, Z. Bozdech, *PLoS Pathog.* **2010**, *6*, e1000737.
[47] H. Hu, A. Cabrera, M. Kono, S. Mok, B. K. Chaal, S. Haase, K. Engelberg, S. Cheemadan, T. Spielmann, P. R. Preiser, T.-W. Gillberger, Z. Bozdech, *Nat. Biotechnol.* **2010**, *28*, 91 – 98.
[48] K. T. Andrews, T. N. Tran, N. C. Wheatley, D. P. Fairlie, *Curr. Top. Med. Chem.* **2009**, *9*, 292 – 308.
[49] J. A. Engel, A. J. Jones, V. M. Avery, S. D. Sumanadasa, S. S. Ng, D. P. Fairlie, T. Skinner-Adams, K. T. Andrews, *Int. J. Parasitol.* **2015**, *5*, 117 – 126.
[50] K. Trenholme, L. Marek, S. Duffy, G. Pradel, G. Fisher, F. K. Hansen, T. S. Skinner-Adams, A. Butterworth, C. J. Ngwa, J. Moecking, C. D. Goodman, G. I. McFadden, S. D. M. Sumanadasa, D. P. Fairlie, V. M. Avery, T. Kurz, K. T. Andrews, *Antimicrob. Agents Chemother.* **2014**, *58*, 3666 – 3678.
[51] F. W. Muregi, A. Ishih, *Drug Dev. Res.* **2010**, *71*, 20 – 32.
[52] R. Oliveira, D. Miranda, J. Magalhaes, R. Capela, M. J. Perry, P. M. O'Neill, R. Moreira, F. Lopes, *Bioorg. Med. Chem.* **2015**, *23*, 5120 – 5130.
[53] S. Shaveta, S. Mishra, P. Singh, *Eur. J. Med. Chem.* **2016**, *124*, 500 – 536.
[54] M. Mishra, V. K. Mishra, V. Kashaw, A. K. Iyer, S. K. Kashaw, *Eur. J. Med. Chem.* **2017**, *125*, 1300 – 1320.
[55] X. Zhang, J. Zhang, L. Tong, Y. Luo, S. Mingbo, Y. Zang, J. Li, W. Lu, Y. Chen, *Bioorg. Med. Chem.* **2013**, *21*, 3240 – 3244.
[56] J. E. Payne, C. Bonnefous, C. A. Hassig, K. T. Symons, X. Guo, P. M. Nguyen, T. Annable, P. L. Wash, T. Z. Hoffman, T. S. Rao, A. K. Shiau, J. W. Malecha, S. A. Noble, J. F. Hager, N. D. Smith, *Bioorg. Med. Chem. Lett.* **2008**, *18*, 6093 – 6096.
[57] A. S. Madsen, H. M. Kristensen, G. Lanz, C. A. Olsen, *ChemMedChem* **2014**, *9*, 614 – 626.
[58] B. Zorc, Z. Rajić Džolić, I. Butula, *Croat. Chem. Acta* **2012**, *85*, 595 – 602.
[59] Chemicalize, 2017, ChemAxon Ltd. Available from: http://www.chemicalize.org.
[60] E. L. Luzina, A. V. Popov, *Eur. J. Med. Chem.* **2012**, *53*, 364 – 373.
[61] B. E. Lauffer, R. Mintzer, R. Fong, S. Mukund, C. Tam, I. Zilberleyb, B. Flicke, A. Ritscher, G. Fedorowicz, R. Vallero, D. F. Ortwine, J. Gunzner, Z. Modrusan, L. Neumann, C. M. Koth, P. J. Lupardus, J. S. Kaminker, C. E. Heise, P. Steiner, *J. Biol. Chem.* **2013**, *288*, 26926 – 26943.
[62] R. Duffy, C. Wade, R. Chang, *Drug Discovery Today* **2012**, *17*, 942 – 953.
[63] J. Held, A. Kreidenweiss, B. Mordmüller, *Expert Opin. Drug Discovery* **2013**, *8*, 1325 – 1337.
[64] D. Barbaras, M. Kaiser, R. Brun, K. Gademann, *Bioorg. Med. Chem. Lett.* **2008**, *18*, 4413 – 4415.
[65] M. R. Boyd, K. D. Paull, *Drug Dev. Res.* **1995**, *34*, 91 – 109.
[66] J. Held, T. Gebru, M. Kalesse, R. Jansen, K. Gerth, R. Müller, B. Mordmüller, *Antimicrob. Agents Chemother.* **2014**, *58*, 6378 – 6384.
[67] H. Noedl, J. Bronnert, K. Yingyuen, B. Attlmayr, H. Kollaritsch, M. Fukuda, *Antimicrob. Agents Chemother.* **2005**, *49*, 3575 – 3577.
[68] R Core Team (2015). R: A Language and Environment for Statistical Computing. R Foundation for Statistical Computing, Vienna, Austria. https://www.R-project.org/.
[69] A. M. Mendes, I. S. Albuquerque, M. Machado, J. Pissarra, P. Meireles, M. Prudêncio, *Antimicrob. Agents Chemother.* **2017**, *61*, e02005-16.

Received: June 21, 2018

3. Asimetrični fumardiamidi primakina i halogenanilina kao novi biološki aktivni Michaelovi akceptori

molecules

MDPI

Article

Asymmetric Primaquine and Halogenaniline Fumardiamides as Novel Biologically Active Michael Acceptors

Zrinka Rajić [1,*], Maja Beus [1], Hana Michnová [2], Josipa Vlainić [3], Leentje Persoons [4], Ivan Kosalec [1], Josef Jampílek [2], Dominique Schols [4], Toma Keser [1] and Branka Zorc [1,*]

1 Faculty of Pharmacy and Biochemistry, University of Zagreb, A. Kovačića 1, 10000 Zagreb, Croatia; mbeus@pharma.hr (M.B.); ikosalec@pharma.hr (I.K.); tkeser@pharma.hr (T.K.)
2 Department of Pharmaceutical Chemistry, Faculty of Pharmacy, Comenius University, Odbojárov 10, 83232 Bratislava, Slovakia; michnova.hana@gmail.com (H.M.), josef.jampilek@gmail.com (J.J.)
3 Laboratory for Advanced Genomics, Division of Molecular Medicine, Rudjer Bošković Institute, Bijenička cesta 54, 10000 Zagreb, Croatia; josipa.vlainic@irb.hr
4 Laboratory of Virology and Chemotherapy, Rega Institute for Medical Research, KU Leuven, Herestraat 49, 3000 Leuven, Belgium; leentje.persoons@rega.kuleuven.be (L.P.); dominique.schols@rega.kuleuven.be (D.S.)
* Correspondence: zrajic@pharma.hr (Z.R.); bzorc@pharma.hr (B.Z.); Tel.: +385-1-48-56-202 (Z.R. & B.Z.)

Academic Editor: Michal Szostak

Received: 3 July 2018; Accepted: 11 July 2018; Published: 14 July 2018

Abstract: Novel primaquine (PQ) and halogenaniline asymmetric fumardiamides **4a–f**, potential Michael acceptors, and their reduced analogues succindiamides **5a–f** were prepared by simple three-step reactions: coupling reaction between PQ and mono-ethyl fumarate (**1a**) or mono-methyl succinate (**1b**), hydrolysis of PQ-dicarboxylic acid mono-ester conjugates **2a**,**b** to corresponding acids **3a**,**b**, and a coupling reaction with halogenanilines. 1-[bis(Dimethylamino)methylene]-1*H*-1,2,3-triazolo[4,5-*b*]pyridinium 3-oxide hexafluorophosphate (HATU) was used as a coupling reagent along with Hünig's base. Compounds **4** and **5** were evaluated against a panel of bacteria, several *Mycobacterium* strains, fungi, a set of viruses, and nine different human tumor cell lines. *p*-Chlorofumardiamide **4d** showed significant activity against *Staphylococcus aureus*, *Streptococcus pneumoniae* and *Acinetobacter baumannii*, but also against *Candida albicans* (minimum inhibitory concentration (MIC) 6.1–12.5 μg/mL). Together with *p*-fluoro and *p*-CF_3 fumardiamides **4b**,**f**, compound **4d** showed activity against *Mycobacterium marinum* and **4b**,**f** against *M. tuberculosis*. In biofilm eradication assay, most of the bacteria, particularly *S. aureus*, showed susceptibility to fumardiamides. *m*-CF_3 and *m*-chloroaniline fumardiamides **4e** and **4c** showed significant antiviral activity against reovirus-1, sindbis virus and Punta Toro virus (EC_{50} = 3.1–5.5 μM), while **4e** was active against coxsackie virus B4 (EC_{50} = 3.1 μM). *m*-Fluoro derivative **4a** exerted significant cytostatic activity (IC_{50} = 5.7–31.2 μM). Acute lymphoblastic leukemia cells were highly susceptible towards *m*-substituted derivatives **4a**,**c**,**e** (IC_{50} = 6.7–8.9 μM). Biological evaluations revealed that fumardiamides **4** were more active than succindiamides **5** indicating importance of Michael conjugated system.

Keywords: fumardiamide; primaquine; succindiamide; Michael acceptor; biofilm eradication; antibacterial screening; antiviral activity; cytostatic activity

1. Introduction

Compounds bearing α,β-unsaturated carbonyl groups are Michael acceptors capable of conjugate addition, also known as Michael addition. The simplest and the best Michael acceptors

are α,β-unsaturated carbonyl compounds with exposed unsaturated β-carbon atoms, such as exomethylene ketones and lactones or vinyl ketones [1]. These fragments are often used in the design of new anticancer drugs, together with others (6-methylhept-5-ene-1,4-dione, propiolamide, 4-(dimethylamino)but-2-enamide) (Figure 1). They assure the irreversible covalent binding to a cysteine residue of a specific protein and may modulate selectivity and potency of the drug candidate. The targeted covalent modification has emerged as a validated approach to drug discovery with the drug candidate canertinib [2], approved drugs afatinib, neratinib and osimertinib (inhibitors of human epidermal growth factor receptors) and ibrutinib (Bruton's tyrosine kinase inhibitor) [3,4]. A comprehensive review published by Jackson et al. gives an overview of biological activity and applicability of various Michael acceptors [5].

Michael acceptors have been explored in a prodrug strategy for cancer cell-specific targeting. In the review published by Zhang et al., two doxorubicin prodrugs with maleimide moieties have been described [6]. The maleimide component is responsible for the binding to human serum albumin. Once the drug carrier arrives at the targeted cancer tissue, doxorubicin is released from the carrier by the cleavage of hydrazone or glycosidic bond in the acidic environment of cancer cells. The prodrugs demonstrate superior anticancer efficacy than the parent drug.

Michael acceptors are present in other classes of drugs. Examples of such drugs are entacapone (antiparkinsonic) [7], dimethyl fumarate (antipsoriatic; since 2013 used in treatment of multiple sclerosis) [5], rupintivir (experimental antiviral drug against human rhinoviruses) [8], exemestane (cytostatic) [9], and ethacrynic acid (diuretic) [10].

α,β-Unsaturated carbonyl group is also a motif found in plant and microbial metabolites and their semisynthetic/synthetic derivatives. Many of them are used in clinical practice or are still under the evaluation in clinical trials (vernolepin, helenalin, curcumin, pyrrocidine, fumaric and angelic acid derivatives), but some are classified as toxins [11]. Vernolepin and helenalin are sesquiterpenes with exomethylene lactones responsible for irreversible DNA polymerase inhibition. Pyrrocidine A is a 13-membered macrocyclic alkaloid produced by endophytic fungi, which directly binds to *N*-acetyl-L-cysteine methyl ester through the Michael-type addition and exerts both antimicrobial and cytostatic effect on leukemia HL60 cells [12]. Angelic acid ester ingenol mebutate has been identified as the most active component of *Euphorbia peplus* L. latex sap, effective against human nonmelanoma skin cancer [13] and actinic keratosis [14]. A gel formulation of ingenol mebutate has been recently approved for the treatment of actinic keratosis [15] and fumaric acid esters are used for the management of psoriasis [16,17]. Curcumin is a symmetric α,β-unsaturated β-diketone extracted from *Curcuma longa* L., a tropical Southeast Asian plant used as a spice and in traditional Indian medicine [18]. Currently, there are 17 open clinical trials involving curcumin, of which mainly evaluate the combination of curcumin with other substances used in anticancer therapy [19].

In this paper, we report design and preparation of novel Michael acceptors, fumaric acid diamides **4a**–**f**. We have chosen α,β-unsaturated amides because they are less electrophilic than analogous esters and better Michael acceptors [1]. Based on our previous findings [20,21], one of the amide bonds was achieved with a terminal amino group of primaquine (PQ), while the other with halogenanilines (Figure 1). Sharing the same conjugated C=C-CO system and a benzene ring, our compounds are similar to cinnamic acid (*trans*-3-phenyl-2-propenoic acid) derivatives as well. Taking literature data into account [22–24] and our previous experience with PQ derivatives [20,21,25–28], we have assumed that the designed compounds have a high pharmacological potential. Here we report their synthesis, evaluation of antimicrobial activity on a wide spectrum of bacteria, fungi and viruses, their biofilm eradication ability, and finally, cytostatic activity against several human tumor cell lines.

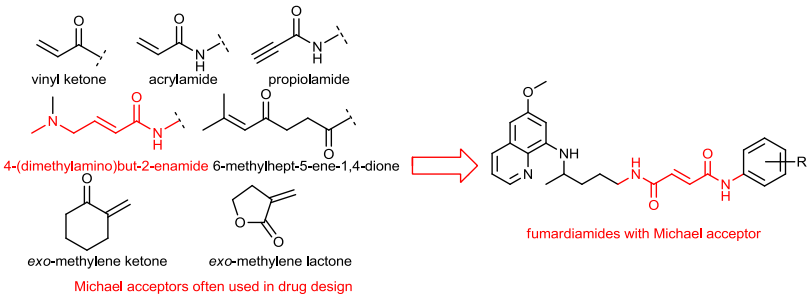

Figure 1. Design of novel fumardiamides.

2. Results and Discussion

2.1. Chemistry

In this paper, we aimed to prepare and biologically evaluate new Michael acceptors **4a–f**, asymmetric diamides of fumaric acid. To prove the significance of the conjugated Michael system for activity, we have also prepared a series of analogous compounds without a double bond, e.g., a series of succindiamides **5a–f** (compound **5a** is a reduced derivative of **4a**, **5b** of **4b** etc.). In both series of compounds, one of the amide bonds was achieved with the primary amino group of PQ and the other one with a selected halogenaniline. In the first reaction step, mono-ethyl fumarate (**1a**) and mono-methyl succinate (**1b**) were coupled with PQ to give derivatives **2a**,**b** using 1-[bis(dimethylamino)methylene]-1*H*-1,2,3-triazolo[4,5-*b*]pyridinium 3-oxide hexafluorophosphate (HATU) as a coupling reagent, along with *N*,*N*-diisopropylethylamine (DIEA) [29]. However, the transformation of **1a** to carboxylic acid chloride and amidation with PQ gave better yields of product **2a**. Hydrolysis of **2a**,**b** by lithium hydroxide afforded the corresponding acids **3a**,**b**, which were again coupled with halogenanilines in the presence of HATU/DIEA. The following anilines were used: 3-fluoroaniline, 4-fluoroaniline, 3-chloroaniline, 4-chloroaniline, 3-trifluoromethylaniline and 4-trifluoromethylaniline. Scheme 1 shows the synthetic pathway leading to compounds **4** and **5**.

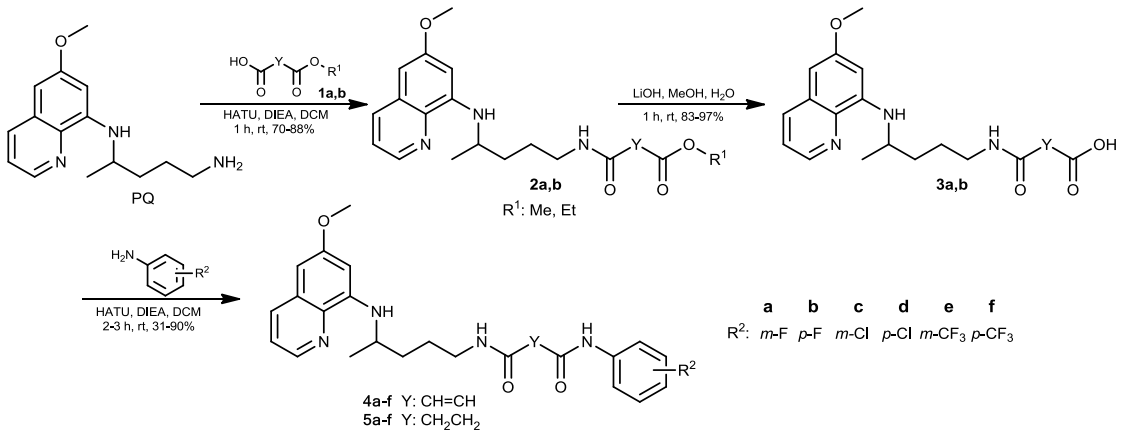

Scheme 1. Synthesis of fumardiamides **4a–f** and succindiamides **5a–f**.

New compounds are fully characterized by MS, IR, ^{1}H and ^{13}C NMR spectroscopic methods and elemental analyses. Spectral data are consistent with the proposed structures and are given in short in the Materials and Methods and in detail in the Supplementary Material. The presence of carbonyl functional groups in compounds **4** and **5** was indicated by the appearance of strong stretching vibration bands in IR spectra between ν 1677 and 1628 (amide I) and 1555 and 1515 cm^{-1} (amide II). PQ residue showed characteristic signals in ^{1}H NMR spectra: hydrogen atom CH-15 occurred between δ 8.52 and 8.55, methoxy group at δ 3.82, the hydrogen attached to chiral carbon

(CH-10) as a multiplet at δ 3.57–3.65, a methyl group at δ 1.19–1.22. NH-1 appeared as a singlet between δ 9.98 and 10.75 ppm, NH-6 as a triplet at δ 7.86–8.55, while NH-12 as a doublet at δ 6.11–6.15 ppm. ^{13}C spectra showed characteristic PQ signals at δ 54.92–54.98 (methoxy group), 46.19–47.02 (C-10), 38.46–39.23 (C-7), 33.37–33.45 (C-9), 25.70–25.99 (C-8), 20.14–20.21 (C-11) ppm and corresponding signals in aromatic region. Two signals of carbonyl groups in fumardiamides **4a**–**f** appeared between 161.17 and 163.34 ppm, while in succindiamides **5a**–**f** between 170.35 and 171.18 ppm. The other two succinic acid carbons (C-3 and C-4) appeared in the aliphatic region between 30.10 and 31.75, and fumaric acid carbons connected by double bond were located very high between 132.11 and 134.66 ppm. CF_3 groups in compounds **4e**, **4f**, **5e** and **5f** showed characteristic quartets at 121.32–127.05 with average J = 272 Hz, and the closest C-atom to trifluoromethyl quartets at 124–129 ppm with J = 31 Hz. *m*-Fluorophenyl derivatives **4a** and **5a** showed doublets at 162 ppm and *p*-fluorophenyl derivatives **4b** and **5b** doublets at 158 ppm (C-atom bearing fluorine) with a similar J-coupling constant of 240 Hz, while two neighbouring C-atoms appeared at 105–110 ppm (average J = 21 Hz). C-atom substituted with chloro atom appeared at 133 ppm (*m*-Cl) and 127 ppm (*p*-Cl). Chemical structures of new compounds were also supported by mass spectroscopy. Molecular ion peaks corresponding to expected relative molecular masses were obtained for all compounds.

Diamides **4** and **5** were subjected to in silico analysis to evaluate the diversity of the set of compounds against topological polar surface area (TPSA) calculations and relevant drug-like properties: number of atoms, molecular weight (MW), partition coefficient (log P), H-bond donor (HBD), H-bond acceptor (HBA) and molecular refractivity (MR). The parameters are calculated with the Chemicalize.org program [30] and presented in Table S1. All compounds are fully in agreement with the Lipinski and Gelovani rules for prospective small molecular drugs (MW $\leq$ 500, log $P \leq 5$, number of H-bond donors $\leq$ 5, number of H-bond acceptors $\leq$ 10, TPSA < 140 Å^2, MR within the range of 40 and 130 cm^3/mol, the number of atoms 20–70), although **4e**,**f** and **5e**,**f** have the highest permitted relative molecular masses.

2.2. Biological Evaluation

2.2.1. Antibacterial and Antifungal Activity

The antimicrobial screening was assessed against a panel of Gram-positive bacteria (*S. pneumoniae* MFBF 10373, *S. aureus* ATCC 6538, methicillin-resistant *S. aureus* MRSA 63718, SA 630 and SA 3202, *E. faecalis* ATCC 29212 and three vancomycin-resistant *Enterococci* VRE 342 B, 365 and 725 B, *B. cereus* ATCC 11778, and *B. subtilis* ATCC 6633), Gram-negative species (*P. aeruginosa* ATCC 27853, *E. coli* ATCC 10536, *S. marcescens* ATCC 10905, *P. mirabilis* MFBF 10430, *A. baumannii* MFBF 10913, and *S. enteritidis* MFBF 11945), four *Mycobacterium* strains (*M. tuberculosis* H37Ra, *M. smegmatis* ATCC 700084, *M. kansasii* DSM 44162, and *M. marinum* CAMP 5644) and fungi (two strains of *C. albicans* ATCC 90028 and CCM 8361, *C. krusei* CCM 8271, *C. parapsilosis* CCM 8260 and *A. brasiliensis* ATCC 16404). The results of the antimicrobial screening of fumardiamides **4a**–**f** are presented in Table 1 (the results for inactive fumardiamides and succindiamides **5a**–**f** are not shown). In general, Gram-positive bacteria, especially *S. pneumoniae* and *S. aureus* ATCC 6538 were susceptible to **4b**–**f**. Compounds **4a**,**b** were active against *B. cereus* as well. However, Gram-negative bacterium *A. baumannii* was the most susceptible among all tested microorganisms: all compounds, except *m*-fluoro derivative **4a**, showed selective antimicrobial activity against this bacterium strain. Comparison of *meta* and *para* derivatives, e.g., **a** vs. **b**, **c** vs. **d**, **e** vs. **f** revealed that in the most cases *p*-substituted derivatives were more active than the analogous *m*-derivatives. *p*-Chlorofumardiamide **4d** showed significant activity against three bacterial strains (*S. aureus*, *S. pneumoniae* and *A. baumannii*), but also against *C. albicans* ATCC 90028, with minimum inhibitory concentration (MIC) values ranging from 6.1 to 12.5 µg/mL. This compound, together with *p*-fluoro and *p*-CF_3 fumardiamides **4b**,**f** showed antitubercular activity against *M. marinum*, while **4b**,**f** were active against *M. tuberculosis* as well.

2.2.2. Biofilm Eradication Assay

We tested the susceptibility of different bacterial and yeast strains to fumardiamides **4a–f** and succindiamides **5a–f** by determining minimum biofilm eradication concentrations (MBECs). The results are presented in Table 2. Again, fumardiamides **4** were much more active than the analogous succindiamides **5**. The most active compounds were **4a** and **4b**. Two microorganisms, namely *E. faecalis* and *S. aureus* showed high susceptibility to all fumardiamides, while *E. coli*, *S. pneumoniae* and *P. aeruginosa* were susceptible to five out of six fumardiamides. A high biofilm eradication potential of fumardiamides might be explained by the reaction of Michael acceptors with cysteine thiol, which could prevent disulfide bond formation. It is a well-known fact that cysteine homeostasis impacts biofilm formation and production of extracellular matrix components, as well as folding and stability of extracytoplasmic proteins [31]. They are also crucial for dental plaque formation, autolysis, extracellular DNA release, genetic competence, bacteriocin production and stabilization of outer membrane porin proteins [32].

2.2.3. Antiviral Evaluation

Compounds **4a–f** and **5a–f** were evaluated against a broad variety of viral infections including herpes simplex viruses, vaccinia virus, adenovirus-2, human coronavirus (229E), vesicular stomatitis virus, coxsackie virus B4, respiratory syncytial virus, para-influenza-3 virus, reovirus-1, sindbis virus, coxsackie virus B4, Punta Toro virus and yellow fever virus. Only fumardiamides with *m*-chloro and *m*-trifluoromethyl aniline residues, namely **4c** and **4e**, showed significant antiviral activity against reovirus-1, sindbis virus and Punta Toro virus with EC_{50} = 3.1–5.5 μM (EC_{50} = concentration required to reduce virus-induced cytopathogenicity by 50%). Compound **4e** was also active against coxsackie virus B4 (EC_{50} = 3.1 μM). However, their selectivity index (SI), e.g., minimum cytotoxicity concentration (MCC) and EC_{50} ratio, was quite low (1.8–3.7). Cytotoxicity and antiviral activity of fumardiamides **4a–f** in Vero cell cultures are displayed in Table 3 (data for HEL (human erythroleukemia cell line), Hela (cervical carcinoma cell line) and Madin-Darby Canine Kidney cells (MDCK) cultures are not shown, as well as data for inactive succindiamides **5a–f**).

Table 1. Antimicrobial susceptibility assay in vitro (minimum inhibitory concentration (MIC) determination) for compounds **4a**–**f**.

Compd.	MIC (μg/mL)								
	Staphylococcus aureus ATCC 6538	*Streptococcus pneumoniae* MFBF 10373	*Enterococcus faecalis* ATCC 29212	*Bacillus cereus* ATCC 11778	*Bacillus subtilis* ATCC 6633	*Acinetobacter baumannii* MFBF 10913	*Mycobacterium tuberculosis* H37Ra	*Mycobacterium marinum* CAMP 5644	*Candida albicans* ATCC 90028
4a	>100	>100	128	>100	50	>100	128	>256	>100
4b	12.5	12.5	64	25	25	25	32	64	>100
4c	12.5	25	256	25	50	25	128	128	>100
4d	6.1	12.5	64	>100	>100	12.5	128	64	12.5
4e	50	50	128	>100	>100	25	128	256	>100
4f	50	50	64	>100	>100	25	64	64	>100
PQ [1]	50	50	128	70	80	50	256	256	>100
TC [2]	0.3	0.3	–	0.3	0.3	3	–	–	–
CIP [3]	–	–	–	–	–	–	16.0	0.3	–
INH [4]	–	–	–	–	–	–	5.0	64.0	–
RIF [5]	–	–	–	–	–	–	8.7	2.2	–
Amph [6]	–	–	–	–	–	–	–	–	0.5

[1] PQ—primaquine; [2] TC—tetracycline; [3] CIP—ciprofloxacin; [4] INH—isoniazid; [5] RIF—rifampicin; [6] Amph—amphotericin B.

Table 2. Sensitivity of microbial strains to fumardiamides **4a**–**f** expressed as minimum biofilm eradication concentrations (MBEC).

Compd.	MBEC (μg/mL)										
	Staphylococcus aureus ATCC 6538	*Streptococcus pneumonia* MFBF 10373	*Enterococcus faecalis* ATCC 29212	*Bacillus cereus* ATCC 11778	*Bacillus subtilis* ATCC 6633	*Escherichia coli* ATCC 10536	*Pseudomonas aeruginosa* ATCC 27853	*Serratia marcescens* ATCC 10905	*Proteus mirabilis* MFBF 10430	*Salmonella enteritidis* MFBF 11945	*Acinetobacter baumannii* MFBF 10913
4a	12.5	12.5	25	>100	50	100	25	25	>100	>100	6.3
4b	12.5	25	25	25	25	50	12.5	>100	25	>100	25
4c	12.5	100	25	25	50	50	50	>100	>100	>100	100
4d	25	50	50	>100	>100	50	>100	>100	>100	>100	100
4e	50	50	50	>100	>100	50	50	>100	>100	>100	100
4f	25	50	50	>100	>100	50	25	>100	>100	>100	100
PQ [1]	50	70	>100	70	80	65	65	>100	>100	70	50
Gen [2]	12.5	25	50	50	50	25	50	50	50	50	25

[1] PQ—primaquine; [2] Gen—gentamycin.

Table 3. Cytotoxicity and antiviral activity of fumardiamides **4a–f** evaluated in Vero cell cultures.

Compd.	Cytotoxicity		EC_{50} [1] (μM)											
	CC_{50} [2]	MCC [3]	Para-Influenza-3 Virus		Reovirus-1		Sindbis Virus		Coxsackie Virus B4		Punta Toro Virus		Yellow Fever Virus	
			MTS	Visual CPE Score	MTS	Visual CPE Score	MTS	Visual CPE Score	MTS	Visual CPE Score	MTS	Visual CPE Score	MTS	Visual CPE Score
4a	46.9	–	>50	–	>50	–	>50	–	>50	–	>50	–	>50	–
4b	>50	–	>50	–	>50	–	>50	–	>50	–	>50	–	>50	–
4c	>50	10	>50	>50	3.8	>50	3.0	>50	>50	>50	5.5	>50	>50	>50
4d	>50	–	>50	–	>50	–	>50	–	>50	–	>50	–	>50	–
4e	>50	10	>50	>50	3.1	>50	5.3	4.2	3.1	2.7	5.4	>50	>50	>50
4f	>50	–	>50	–	>50	–	>50	–	>50	–	>50	–	>50	–
PQ	>50	–	>50	–	>50	–	>50	–	>50	–	>50	–	>50	–
DS-10.000 [4]	>100	>100	>100	>100	>100	>100	4.0	10	>100	34	16	8.9	1.6	>100
RIB [5]	>250	>250	73	111	107	126	>250	11	>250	>250	85	111	119	>250
MPA [6]	>100	>100	1.0	0.8	0.6	0.8	12	1.7	>100	>100	11	8.9	0.5	0.8

[1] Concentration required to reduce virus-induced cytopathicity by 50%, as determined by visual scoring of the cytopathic effect (CPE), or by measuring the cell viability with the colorimetric formazan-based 3-(4,5-dimethylthiazol-2-yl)-5-(3-carboxymethoxyphenyl)-2-(4-sulfophenyl)-2*H*-tetrazolium (MTS) assay; [2] Concentration that causes 50% cytotoxic effect, as determined by measuring the cell viability with the colorimetric formazan-based MTS assay; [3] Minimum cytotoxic concentration, i.e., the minimum concentration that causes a microscopically detectable alteration of normal cell morphology; [4] Concentration in μg/mL; [5] RIB—ribavirin; [6] MPA—mycophenolic acid. All experiments were performed in duplicate.

2.2.4. Cytostatic Activity

To gain insight into cytotoxicity of newly synthesized compounds **4a**–**f** and **5a**–**f**, their cytostatic activity was evaluated in vitro against a panel of nine different human cancer cell lines, representing various solid tumor types including pancreatic adenocarcinoma (Capan-1), chronic myeloid leukemia (Hap1), colorectal carcinoma (HCT-116), lung carcinoma (NCI-H460), acute lymphoblastic leukemia (DND-41), acute myeloid leukemia (HL-60), chronic myeloid leukemia (K-562), multiple myeloma (MM.1S) and non-Hodgkin lymphoma (Z-138). Succindiamides **5a**–**f** were completely inactive, while free fumardiamides showed activity towards the selected tumor cell lines (Table 4). Fumardiamide **4a** with *m*-fluoroaniline moiety showed cytostatic activity against all tested cell lines, with IC_{50} values from 5.7 to 31.2 μM (IC_{50} = the lowest concentration resulting in 50% growth inhibition). DND-41 cell line was susceptible to all three *m*-substituted derivatives, e.g., **4a**, **4c** and **4f** (IC_{50} values between 6.7 and 8.9 μM). HL-60 and Z-138 cell lines were also susceptible to compound **4a** (IC_{50} values 5.7 and 8.4 μM, respectively).

Table 4. Antiproliferative screening of fumardiamides **4a**–**f** in diverse human tumor cell lines.

Compd.	IC_{50} (μM)								
	Capan-1	**Hap1**	**HCT-116**	**NCI-H460**	**DND-41**	**HL-60**	**K-562**	**MM.1S**	**Z-138**
4a	16.9	19.3	22.3	15.5	6.7	5.7	31.2	13.0	8.4
4b	50.5	66.4	>100	29.1	>100	>100	70.5	>100	>100
4c	69.9	>100	73.0	43.7	8.4	>100	>100	>100	46.5
4d	91.8	>100	>100	>100	>100	>100	>100	>100	>100
4e	56.5	>100	>100	34.2	8.9	>100	71.2	>100	68.4
4f	79.4	>100	>100	>100	>100	>100	>100	>100	>100
PQ [1]	18.7	42.7	30.9	52.6	11.4	2.2	35.2	28.3	7.1
DXT [2]	0.75	1.17	7.66	1.30	0.94	1.24	1.22	3.38	5.42
EPEG [3]	0.15	0.04	1.35	0.09	0.03	0.03	0.01	0.97	0.02
STS [4]	0.66	3.56	0.78	1.66	6.96	13.10	0.23	1.61	0.40

[1] PQ—primaquine; [2] DXT—docetaxel (nM); [3] EPEG—etoposide; [4] STS—staunoporin (nM). All compounds were tested with duplicate data points and averaged.

2.2.5. Interaction with Glutathione (GSH)

Glutathione (GSH) is an important compound present in most mammalian cells, a tripeptide, with the central amino acid cysteine bearing thiol group, which scavenges carcinogenic compounds by conjugate addition and protects from oxidative damage [1]. In the drug development process, it is usual to evaluate the Michael acceptor–GSH interaction [33]. That is why the final step in our research was to study the interaction of fumarmides with GSH. Fumardiamide **4b** (1.25 μM) was incubated with GSH (125 μM) in ammonium formate buffer (pH = 7.4) containing 10% acetonitrile at 37 °C for 216 h. The MS analysis confirmed the consumption of **4b** with GSH. However, the rate of GSH addition was slow and incomplete, as only 18.3% of **4b** reacted in the monitored period (See Supporting Material).

3. Materials and Methods

3.1. Chemistry

3.1.1. Materials and General Methods

Melting points were determined on an SMP3 apparatus (Barloworld Scientific, UK) in open capillaries and were uncorrected. IR spectra were recorded on Spectrum One FT-IR (Perkin-Elmer, UK) and UV-Vis spectra on Lambda 20 double-beam spectrophotometers (Perkin-Elmer, UK). NMR ^{1}H and ^{13}C spectra were recorded at 25 °C on an NMR Avance 600 spectrometer (Bruker, Germany) at 300.13 or 600.13 and 75.47 or 150.9 MHz for ^{1}H and ^{13}C nuclei, respectively. Chemical shifts (δ) were reported in parts per million (ppm) relative to tetramethylsilane in the ^{1}H and the

dimethyl sulfoxide residual peak as a reference in the ^{13}C NMR spectra (39.51 ppm). Coupling constants (*J*) were reported in hertz (Hz). Mass spectra were collected on an HPLC-MS/MS instrument (HPLC, Agilent Technologies 1200 Series; MS, Agilent Technologies 6410 Triple Quad) using electrospray ionization in positive mode. Elemental analyses were performed on a CHNS LECO analyzer (LECO Corporation, USA). All compounds were routinely checked by thin-layer chromatography (TLC) with Merck silica gel 60F-254 glass plates using appropriate solvent systems. Spots were visualized by short-wave UV light and iodine vapour. Column chromatography was performed on silica gel 0.063–0.200 mm. All chemicals and solvents were of analytical grade and purchased from commercial sources. PQ diphosphate, 4-methoxy-4-oxobutanoic acid (mono-methyl succinate), (*E*)-4-ethoxy-4-oxobut-2-enoic acid (mono-ethyl fumarate), 3-fluoroaniline, 4-fluoroaniline, 3-chloroaniline, 4-chloroaniline, 3-trifluoromethylaniline, 4-trifluoromethylaniline, DIEA, and HATU were purchased from Sigma-Aldrich. PQ was prepared from PQ diphosphate prior to use. All reactions with PQ were run light protected.

3.1.2. General Procedure for the Synthesis of Esters **2a**,**b**

PQ-succinamide and fumaramide monoesters **2a**,**b** were prepared by condensation of PQ base with mono-methyl succinate (**1a**) or mono-ethyl fumarate (**1b**), following the previously described procedure [29].

3.1.3. General Procedure for the Synthesis of Carboxylic Acids **3a**,**b**

Carboxylic acids **3a**,**b** were prepared by hydrolysis of esters **2a**,**b** with lithium hydroxide following the previously described procedure [29].

3.1.4. General Procedure for the Synthesis of Fumardiamides **4a**–**f** and Succindiamides **5a**–**f**

A solution of 0.27 mmol of **3a** or **3b**, 0.068 g (0.54 mmol) DIEA and 0.103 g (0.27 mmol) HATU in 6 mL of dichloromethane was stirred at room temperature. After 10 min, 0.297 mmol of the corresponding halogenaniline was added. The reaction mixture was stirred for 2–3 h at room temperature, evaporated under reduced pressure, dissolved in 8 mL ethyl acetate and extracted 3 times with water. The organic layer was dried over sodium sulfate, filtered and evaporated under reduced pressure.

*(2E)-N-(3-Fluorophenyl)-N′-{4-[(6-methoxyquinolin-8-yl)amino]pentyl}but-2-enediamide (**4a**).* From the reaction of 0.096 g acid **3a** and 0.033 g (0.297 mmol) 3-fluoroaniline and after purification by column chromatography (mobile phase dichloromethane/methanol 9.5:0.5) and crystallization from ether, 0.041 g (34%) of **4a** was obtained; mp 203–204 °C; IR (ATR): ν_{max} 3388, 3319, 3269, 3080, 2961, 2935, 2866, 1630, 1554, 1520, 1452, 1387, 1334, 1201, 1158, 782, 680 cm^{-1}; ^{1}H NMR (DMSO-d_6) δ 10.63 (s, 1H), 8.55–8.53 (dd, 1H, *J* = 1.6, 4.2), 8.52 (t, 1H, *J* = 5.4), 8.09–8.06 (dd, 1H, *J* = 1.5, 8.3), 7.69 (d, 2H, *J* = 11.7), 7.45–7.41 (m, 1H), 7.39–7.36 (m, 2H), 7.06–7.96 (m, 2H), 6.96–6.92 (m, 1H), 6.47 (d, 1H, *J* = 2.4), 6.28 (d, 1H, *J* = 2.4), 6.15 (d, 1H, *J* = 8.8), 3.82 (s, 3H), 3.70–3.61 (m, 1H), 3.24–3.18 (m, 2H), 1.74–1.64, 1.63–1.52 (2m, 4H), 1.22 (d, 3H, *J* = 6.3); ^{13}C NMR (DMSO-d_6) δ 163.25, 162.62, 162.09 (d, *J* = 242.0), 159.00, 144.63, 144.23, 140.50 (d, *J* = 11.5), 134.79, 134.52, 134.40, 132.28, 130.50 (d, *J* = 9.5), 129.57, 122.09, 115.14, 110.28, 106.13 (d, *J* = 27.2), 96.14, 91.62, 54.96, 46.97, 38.95, 33.45, 25.77, 20.21; MS/MS *m/z* 451.1 (M + 1)$^+$; Anal. Calcd. for $C_{25}H_{27}FN_4O_3$: C, 66.65; H, 6.04; N, 12.44. Found: C, 66.32; H, 6.30; N, 12.49.

*(2E)-N-(4-Fluorophenyl)-N′-{4-[(6-methoxyquinolin-8-yl)amino]pentyl}but-2-enediamide (**4b**).* From the reaction of 0.096 g acid **3a** and 0.033 g (0.297 mmol) 4-fluoroaniline and after purification by column chromatography (mobile phase dichloromethane/methanol 9.5:0.5) and crystallization from ether, 0.071 g (58%) of **4b** was obtained; mp 226–227 °C; IR (ATR): ν_{max} 3386, 3294, 3072, 2963, 2928, 2863, 1635, 1548, 1513, 1452, 1391, 1330, 1212, 1160, 1051, 973, 829, 673 cm^{-1}; ^{1}H NMR (DMSO-d_6) δ 10.49 (s, 1H), 8.55–8.53 (dd, 1H, *J* = 1.6, 4.2), 8.52 (t, 1H, *J* = 5.4), 8.09–8.06 (dd, 1H, *J* = 1.5, 8.3), 7.72–7.68 (dd, 2H, *J* = 5.0, *J* = 8.9), 7.45–7.41 (m, 1H), 7.18 (t, 2H, *J* = 8.8), 7.05–6.93 (m, 2H), 6.47 (d, 1H, *J* = 2.1), 6.28 (d,

1H, *J* = 2.1), 6.15 (d, 1H, *J* = 8.8), 3.82 (s, 3H), 3.69–3.61 (m, 1H), 3.24–3.18 (m, 2H), 1.74–1.64, 1.63–1.52 (2m, 4H), 1.22 (d, 3H, *J* = 6.3); ^{13}C NMR (DMSO-d_6) δ 163.34, 162.21, 159.00, 158.26 (d, *J* = 240.0), 144.63, 144.23, 135.22, 134.79, 134.53, 133.98, 132.52, 129.58, 122.09, 121.05 (d, *J* = 7.6), 115.44 (d, *J* = 21.9), 96.14, 91.62, 54.96, 46.97, 38.95, 33.45, 25.79, 20.21; MS/MS *m/z* 451.1 (M + 1)$^+$; Anal. Calcd. for $C_{25}H_{27}FN_4O_3$: C, 66.65; H, 6.04; N, 12.44. Found: C, 66.47; H, 6.38; N, 12.35.

*(2E)-N-(3-Chlorophenyl)-N′-{4-[(6-methoxyquinolin-8-yl)amino]pentyl}but-2-enediamide (**4c**).* From the reaction of 0.096 g acid **3a** and 0.038 g (0.297 mmol) 3-chloroaniline and after purification by column chromatography (mobile phase dichloromethane/methanol 9.5:0.5) and crystallization from ether, 0.053 g (42%) of **4c** was obtained; mp 187–188 °C; IR (ATR): ν_{max} 3381, 3298, 3068, 2959, 2928, 2863, 1635, 1591, 1521, 1465, 1419, 1386, 1331, 1210, 1163, 976, 821, 783, 670 cm^{-1}; ^{1}H NMR (DMSO-d_6) δ 10.59 (s, 1H), 8.54–8.53 (dd, 1H, *J* = 1.5, 4.1), 8.50 (t, 1H, *J* = 5.5), 8.08–8.06 (dd, 1H, *J* = 1.4, 8.2), 7.90 (s, 1H), 7.51 (d, 1H, *J* = 8.1), 7.43–7.41 (m, 1H), 7.37 (t, H, *J* = 8.1), 7.16–7.14 (dd, 1H, *J* = 1.2, *J* = 8.0), 7.00 (q, 2H, *J* = 15.1), 6.47 (d, 1H, *J* = 2.4), 6.28 (d, 1H, *J* = 2.3), 6.14 (d, 1H, *J* = 8.8), 3.82 (s, 3H), 3.67–3.63 (m, 1H), 3.23–3.20 (m, 2H), 1.73–1.67, 1.63–1.53 (2m, 4H), 1.22 (d, 3H, *J* = 6.3); ^{13}C NMR (DMSO-d_6) δ 163.21, 162.60, 158.97, 144.60, 144.19, 140.19, 134.74, 134.50, 134.41, 133.10, 132.19, 130.48, 129.54, 123.45, 122.03, 118.74, 117.72, 96.11, 91.63, 54.93, 46.98, 39.23, 33.44, 25.72, 20.18; MS/MS *m/z* 467.0 (M+1)$^+$; Anal. tCalcd. for $C_{25}H_{27}ClN_4O_3$: C, 64.30; H, 5.83; N, 12.00. Found: C, 64.21; H, 6.05; N, 11.78.

*(2E)-N-(4-Chlorophenyl)-N′-{4-[(6-methoxyquinolin-8-yl)amino]pentyl}but-2-enediamide (**4d**).* From the reaction of 0.096 g acid **3a** and 0.038 g (0.297 mmol) 4-chloroaniline and after purification by column chromatography (mobile phase cyclohexane/ethyl acetate/methanol 3:1:0.5) and crystallization from ether, 0.062 g (49%) of **4d** was obtained; mp 223–226 °C; IR (ATR): ν_{max} 3381, 3289, 3071, 2959, 2931, 2864, 1640, 1526, 1452, 1388, 1331, 1210, 1163, 1094, 1049, 973, 822, 787, 686, 631, 507 cm^{-1}; ^{1}H NMR (DMSO-d_6) δ 10.56 (s, 1H), 8.55–8.53 (dd, 1H, *J* = 1.7, 4.2), 8.50 (t, 1H, *J* = 5.6), 8.09–8.06 (dd, 1H, *J* = 1.6, 8.3), 7.72–7.68 (m, 2H), 7.45–7.37 (m, 3H), 7.06–6.94 (m, 2H), 6.47 (d, 1H, *J* = 2.5), 6.27 (d, 1H, *J* = 2.4), 6.14 (d, 1H, *J* = 8.8), 3.82 (s, 3H), 3.69–3.60 (m, 1H), 3.24–3.18 (m, 2H), 1.74–1.64, 1.63–1.51 (2m, 4H), 1.22 (d, 3H, *J* = 6.3); ^{13}C NMR (DMSO-d_6) δ 163.29, 162.43, 159.00, 144.63, 144.23, 137.76, 134.79, 134.52, 134.21, 132.38, 129.57, 128.75, 127.36, 122.09, 120.84, 96.14, 91.61, 54.96, 46.97, 38.82, 33.44, 25.77, 20.21; MS/MS *m/z* 467.0 (M+1)$^+$; Anal. Calcd. for $C_{25}H_{27}ClN_4O_3$: C, 64.30; H, 5.83; N, 12.00. Found: C, 64.21; H, 5.56; N, 11.83.

*(2E)-N′-{4-[(6-Methoxyquinolin-8-yl)amino]pentyl}-N-[3-(trifluoromethyl)phenyl]but-2-enediamide (**4e**).* From the reaction of 0.096 g acid **3a** and 0.048 g (0.297 mmol) 3-trifluoroaniline and after purification by column chromatography (mobile phase dichloromethane/methanol 9.5:0.5) after crystallization from acetone/water, 0.042 g (31%) of **4e** was obtained; mp 149–150 °C; IR (ATR): ν_{max} 3399, 3357, 3282, 3094, 2960, 2935, 2867, 1651, 1621, 1563, 1526, 1452, 1388, 1331, 1168, 1122, 973, 893, 788, 694 cm^{-1}; ^{1}H NMR (DMSO-d_6) δ 10.75 (s, 1H), 8.55–8.52 (m, 2H), 8.18 (s, 1H), 8.08–8.06 (dd, 1H, *J* = 1.1, 8.2), 7.83 (d, 1H), 7.59 (t, 1H, *J* = 7.9), 7.45–7.42 (m, 2H), 7.00–6.98 (q, 2H, *J* = 15.1), 6.47 (d, 1H, *J* = 2.4), 6.28 (d, 1H, *J* = 2.0), 6.15 (d, 1H, *J* = 8.7), 3.82 (s, 3H), 3.67–3.63 (m, 1H), 3.23–3.20 (m, 2H), 1.73–1.67, 1.63–1.53 (2m, 4H), 1.22 (d, 3H, *J* = 6.3); ^{13}C NMR (DMSO-d_6) δ 163.19, 162.81, 158.99, 144.62, 144.21, 139.54, 134.77, 134.55, 134.52, 132.15, 130.09, 129.56, 129.82–129.19 (q, *J* = 31.7), 126.73–121.32 (q, *J* = 273.3), 122.88, 122.07, 120.09, 115.33, 96.13, 91.62, 54.95, 46.19, 39.23, 33.45, 25.76, 20.20; MS/MS *m/z* 501.1 (M+1)$^+$; Anal. Calcd. for $C_{26}H_{27}F_3N_4O_3$: C, 62.39; H, 5.44; N, 11.19. Found: C, 62.25; H, 5.76; N, 11.08.

*(2E)-N′-{4-[(6-Methoxyquinolin-8-yl)amino]pentyl}-N-[4-(trifluoromethyl)phenyl]but-2-enediamide (**4f**).* From the reaction of 0.096 g acid **3a** and 0.048 g (0.297 mmol) 4-trifluoroaniline and after crystallization from ether, 0.046 g (34%) of **4f** was obtained; mp 189–191 °C; IR (ATR): ν_{max} 3387, 3309, 3071, 2963, 2932, 1636, 1527, 1457, 1417, 1390, 1328, 1213, 1166, 1122, 1065, 970, 832, 681 cm^{-1}; ^{1}H NMR (DMSO-d_6) δ 10.75 (s, 1H), 8.54–8.53 (m, 1H), 8.51 (t, 1H, *J* = 5.3), 8.07 (d, 1H, *J* = 8.2), 7.88 (d, 2H, *J* = 8.5), 7.71 (d, 2H, *J* = 8.5), 7.43–7.41 (m, 1H), 7.07–6.99 (q, 2H, *J* = 15.1), 6.47 (d, 1H, *J* = 2.2), 6.28 (d, 1H,

J = 2.2), 6.14 (d, 1H, *J* = 8.7), 3.82 (s, 3H), 3.67–3.63 (m, 1H), 3.23–3.20 (dd, 2H, *J* = 6.1, 12.1), 2.59 (t, 2H, *J* = 7.0), 1.73–1.67, 1.61–1.53 (2m, 4H), 1.22 (d, 3H, *J* = 6.3); ^{13}C NMR (DMSO-d_6) δ 161.17, 162.83, 158.97, 144.60, 144.17, 142.28, 134.72, 134.66, 134.50, 132.11, 129.53, 126.95–121.55 (q, *J* = 271.6), 126.11–126.04 (q, *J* = 3.0), 124.02–123.39 (q, *J* = 31.7), 122.02, 119.26, 96.10, 91.63, 54.92, 46.96, 38.80, 33.43, 25.70, 20.17; MS/MS *m/z* 501.1 $(M+1)^+$; Anal. Calcd. for $C_{26}H_{27}F_3N_4O_3$: C, 62.39; H, 5.44; N, 11.19. Found: C, 62.17; H, 5.61; N, 11.40.

*N-(3-Fluorophenyl)-N′-{4-[(6-methoxyquinolin-8-yl)amino]pentyl}butanediamide (**5a**).* From the reaction of 0.097 g acid **3b** and 0.033 g (0.297 mmol) 3-fluoroaniline and after purification by column chromatography (mobile phase dichloromethane/methanol 9.5:0.5), 0.077 g (63%) of **5a** was obtained; mp 140–142 °C; IR (ATR): ν_{max} 3391, 3283, 3145, 3080, 2959, 2926, 1744, 1646, 1615, 1555, 1507, 1387, 1224, 1202, 1167, 1157, 838, 815, 786, 681 cm^{-1}; ^{1}H NMR (DMSO-d_6) δ 10.13 (s, 1H), 8.54–8.53 (dd, 1H, *J* = 1.7, 4.2), 8.08–8.06 (dd, 1H, *J* = 1.6, 8.3), 7.86 (t, 1H, *J* = 5.6), 7.60–7.58 (m, 1H), 7.43–7.41 (m, 1H), 7.31–7.27 (m, 2H), 6.85–6.81 (m, 1H), 6.47 (d, 1H, *J* = 2.5), 6.26 (d, 1H, *J* = 2.5), 6.11 (d, 1H, *J* = 8.7), 3.82 (s, 3H), 3.64–3.59 (m, 1H), 3.10–3.03 (m, 2H), 2.55 (t, 2H, *J* = 7.2), 2.37 (t, 2H, *J* = 7.2), 1.67–1.63, 1.55–1.45 (2m, 4H), 1.19 (d, 3H, *J* = 6.3); ^{13}C NMR (DMSO-d_6) δ 170.86, 162.10 (d, *J* = 240.1), 158.98, 144.61, 144.19, 141.03 (d, *J* = 13.1), 134.75, 134.51, 130.19 (d, *J* = 9.0), 129.55, 122.05, 114.55, 109.22 (d, *J* = 20.1), 105.61, 96.07, 91.59, 54.94, 46.99, 38.46, 33.38, 31.75, 30.16, 25.95, 20.15; MS/MS *m/z* 453.3 $(M+1)^+$; Anal. Calcd. for $C_{25}H_{29}FN_4O_3$: C, 66.35; H, 6.46; N, 12.38. Found: C, 66.25; H, 6.50; N, 12.20.

*N-(4-Fluorophenyl)-N′-{4-[(6-methoxyquinolin-8-yl)amino]pentyl}butanediamide (**5b**).* From the reaction of 0.097 g acid **3b** and 0.033 g (0.297 mmol) 4-fluoroaniline and after purification by column chromatography (mobile phase dichloromethane/methanol 9.5:0.5) and crystallization from ether, 0.098 g (80%) of **5b** was obtained; mp 118–120 °C; IR (ATR): ν_{max} 3391, 3283, 3145, 3080, 2959, 2926, 1744, 1646, 1615, 1555, 1507, 1387, 1224, 1202, 1167, 1157, 838, 815, 786, 681 cm^{-1}; ^{1}H NMR (DMSO-d_6) δ 9.98 (s, 1H), 8.55–8.53 (dd, 1H, *J* = 1.6, 4.2), 8.09–8.06 (dd, 1H, *J* = 1.5, 8.3), 7.87 (t, 1H, *J* = 5.5), 7.62–7.57 (m, 2H), 7.45–7.40 (m, 1H), 7.14–7.08 (m, 2H), 6.47 (d, 1H, *J* = 2.4), 6.26 (d, 1H, *J* = 2.4), 6.12 (d, 1H, *J* = 8.8), 3.82 (s, 3H), 3.65–3.57 (m, 1H), 3.10–3.04 (m, 2H), 2.54 (t, 2H, *J* = 7.1), 2.37 (t, 2H, *J* = 7.0), 1.69–1.59, 1.58–1.43 (2m, 4H), 1.19 (d, 3H, *J* = 6.3); ^{13}C NMR (DMSO-d_6) δ 170.96, 170.35, 159.00, 157.72 (d, *J* = 246.3), 144.63, 144.22, 135.76, 134.79, 134.52, 129.57, 122.09, 120.53 (d, *J* = 7.8), 115.14 (d, *J* = 22.1), 96.09, 91.58, 54.97, 47.00, 38.48, 33.39, 31.66, 30.34, 25.99, 20.17; MS/MS *m/z* 453.4 $(M+1)^+$; Anal. Calcd. for $C_{25}H_{29}FN_4O_3$: C, 66.35; H, 6.46; N, 12.38. Found: C, 66.53, H, 6.29; N, 12.55.

*N-(3-Chlorophenyl)-N′-{4-[(6-methoxyquinolin-8-yl)amino]pentyl}butanediamide (**5c**).* From the reaction of 0.097 g acid **3b** and 0.038 g (0.297 mmol) 3-chloroaniline and after purification by column chromatography (mobile phase cyclohexane/ethyl acetate/methanol 3:1:0.5) and crystallization from ether, 0.062 g (49%) of **5c** was obtained; mp 156–158 °C; IR (ATR): ν_{max} 3390, 3287, 3242, 3180, 3102, 3074, 2962, 2922, 2856, 1738, 1650, 1612, 1591, 1572, 1539, 1516, 1422, 1388, 1202, 1066, 816, 787, 698, 682 cm^{-1}; ^{1}H NMR (DMSO-d_6) δ 10.11 (s, 1H), 8.54–8.53 (dd, 1H, *J* = 1.6, 4.2), 8.08–8.06 (dd, 1H, *J* = 1.6, 8.3), 7.86 (t, 1H, *J* = 5.5), 7.81 (t, 1H, *J* = 2.0), 7.43–7.41 (m, 2H), 7.31–7.28 (m, 1H), 7.07–7.05 (m, 1H), 6.47 (d, 1H, *J* = 2.5), 6.25 (d, 1H, *J* = 2.5), 6.11 (d, 1H, *J* = 8.2), 3.82 (s, 3H), 3.63–3.59 (m, 1H), 3.10–3.03 (m, 2H), 2.55 (t, 2H, *J* = 7.1), 2.37 (t, 2H, *J* = 7.2), 1.67–1.63, 1.56–1.44 (2m, 4H), 1.19 (d, 3H, *J* = 6.3); ^{13}C NMR (DMSO-d_6) δ 170.89, 170.85, 158.98, 144.60, 144.19, 140.73, 134.77, 134.49, 132.97, 130.29, 129.55, 122.51, 122.06, 118.31, 117.19, 96.08, 91.59, 54.95, 46.99, 38.46, 33.38, 31.74, 30.16, 25.96, 20.16; MS/MS *m/z* 469.2 $(M+1)^+$; Anal. Calcd. for $C_{25}H_{29}ClN_4O_3$: C, 64.03; H, 6.23; N, 11.95. Found: C, 63.91; H, 6.33; N, 11.70.

*N-(4-Chlorophenyl)-N′-{4-[(6-methoxyquinolin-8-yl)amino]pentyl}butanediamide (**5d**).* From the reaction of 0.097 g acid **3b** and 0.038 g (0.297 mmol) 3-chloroaniline and after purification by column chromatography (mobile phase dichloromethane/methanol 9.5:0.5) and crystallization from ether, 0.076 g (60%) of **5d** was obtained; mp 152–153 °C; IR (ATR): ν_{max} 3390, 3287, 3242, 3180, 3102, 3074, 2962, 2922, 2856, 1738, 1650, 1612, 1591, 1572, 1539, 1516, 1422, 1388, 1202, 1066, 816, 787, 698, 682 cm^{-1}; ^{1}H NMR (DMSO-d_6) δ 10.07 (s, 1H), 8.55–8.53 (dd, 1H, *J* = 1.5, 4.2), 8.10–8.07 (dd, 1H, *J* = 1.4,

8.3), 7.88 (t, 1H, *J* = 5.4), 7.61 (d, 2H, *J* = 8.9), 7.45–7.41 (m, 1H), 7.32 (d, 2H, *J* = 8.9), 6.48 (d, 1H, *J* = 2.3), 6.26 (d, 1H, *J* = 2.3), 6.13 (bs, 1H), 3.81 (s, 3H), 3.63–3.57 (m, 1H), 3.09–3.03 (m, 2H), 2.55 (t, 2H, *J* = 7.4), 2.39 (t, 2H, *J* = 7.0), 1.70–1.59, 1.58–1.43 (2m, 4H), 1.19 (d, 3H, *J* = 6.3); ^{13}C NMR (DMSO-d_6) δ 170.92, 170.64, 159.01, 144.55, 144.18, 138.28, 134.89, 134.42, 129.59, 128.51, 126.33, 122.09, 120.37, 96.19, 91.63, 54.98, 47.02, 38.47, 33.37, 31.73, 30.23, 25.98, 20.15 (11); MS/MS *m/z* 469.3 $(M+1)^+$; Anal. Calcd. for $C_{25}H_{29}ClN_4O_3$: C, 64.03; H, 6.23; N, 11.95. Found: C, 64.35; H, 6.57; N, 12.13.

*N′-{4-[(6-Methoxyquinolin-8-yl)amino]pentyl}-N-[3-(trifluoromethyl)phenyl]butanediamide (**5e**).* From the reaction of 0.097 g acid **3b** and 0.048 g (0.297 mmol) 3-trifluoromethylaniline and after purification by column chromatography (mobile phase dichloromethane/methanol 9.5:0.5) and crystallization from ether, 0.122 g (90%) of **5e** was obtained; mp 146–149 °C; IR (ATR): ν_{max} 3394, 3302, 3263, 3216, 3164, 3097, 2963, 2928, 2859, 1651, 1617, 1562, 1518, 1450, 1389, 1331, 1265, 1173, 1127, 1064, 894, 816 cm^{-1}; ^{1}H NMR (DMSO-d_6) δ 10.26 (s, 1H), 8.54–8.53 (dd, 1H, *J* = 1.6, 4.2), 8.11 (s, 1H), 8.08–8.06 (dd, 1H, *J* = 1.6, 8.3), 7.88 (t, 1H, *J* = 5.5), 7.74 (d, 1H, *J* = 8.1), 7.52 (t, 1H, *J* = 8.0), 7.43–7.41 (m, 1H), 7.36 (d, 1H, *J* = 7.8), 6.47 (d, 1H, *J* = 2.5), 6.25 (d, 1H, *J* = 2.5), 6.11 (d, 1H, *J* = 8.7), 3.82 (s, 3H), 3.63–3.58 (m, 1H), 3.10–3.04 (m, 2H), 2.57 (t, 2H, *J* = 7.2), 2.41 (t, 2H, *J* = 7.2), 1.67–1.63, 1.56–1.44 (2m, 4H), 1.19 (d, 3H, *J* = 6.3); ^{13}C NMR (DMSO-d_6) δ 171.11, 170.84, 158.98, 144.61, 144.19, 140.03, 134.75, 134.50, 129.83, 129.55, 129.67–129.04 (q, *J* = 31.9), 126.81–121.40 (q, *J* = 269.8), 122.33, 122.05, 119.14, 114.88, 96.06, 91.58, 54.94, 46.98, 38.46, 33.38, 31.72, 30.11, 25.96, 20.14; MS/MS *m/z* 503.3 $(M+1)^+$; Anal. Calcd. for $C_{26}H_{29}F_3N_4O_3$: C, 62.14; H, 5.82; N, 11.15. Found: C, 62.25; H, 5.99; N, 11.08.

*N′-{4-[(6-Methoxyquinolin-8-yl)amino]pentyl}-N-[4-(trifluoromethyl)phenyl]butanediamide (**5f**).* From the reaction of 0.097 g acid **3b** and 0.048 g (0.297 mmol) 4-trifluoromethylaniline and after purification by column chromatography (mobile phase dichloromethane/methanol 9.5:0.5), 0.068 g (50%) of **5f** was obtained; mp 163–165 °C; IR (ATR): ν_{max} 3387, 3287, 3256, 3198, 3123, 3071, 2963, 2925, 2859, 1652, 1614, 1547, 1515, 1452, 1419, 1389, 1327, 1264, 1169, 1124, 1064, 846, 784 cm^{-1}; ^{1}H NMR (DMSO-d_6) δ 10.31 (s, 1H), 8.54–8.52 (dd, 1H, *J* = 1.5, 4.2), 8.09–8.06 (dd, 1H, *J* = 1.5, 8.3), 7.89 (t, 1H, *J* = 5.3), 7.79 (d, 2H, *J* = 8.5), 7.63 (d, 2H, *J* = 8.7), 7.44–7.40 (m, 1H), 6.47 (d, 1H, *J* = 2.4), 6.25 (d, 1H, *J* = 2.4), 6.11 (d, 1H, *J* = 8.7), 3.82 (s, 3H), 3.65–3.57 (m, 1H), 3.09–3.04 (m, 2H), 2.59 (t, 2H, *J* = 7.0), 2.40 (t, 2H, *J* = 7.0), 1.71–1.58, 1.57–1.43 (2m, 4H), 1.19 (d, 3H, *J* = 6.2); ^{13}C NMR (DMSO-d_6) δ 171.18, 170.86, 158.99, 144.61, 144.20, 142.83, 134.77, 134.51, 129.55, 125.95, 127.05–121.68 (q, *J* = 274.2), 123.15-122.52 (q, *J* = 28.2), 122.06, 118.69, 96.08, 91.59, 54.95, 46.99, 38.47, 33.38, 31.79, 30.10, 25.96, 20.14; MS/MS *m/z* 503.3 $(M+1)^+$; Anal. Calcd. for $C_{26}H_{29}F_3N_4O_3$: C, 62.14; H, 5.82; N, 11.15. Found: C, 62.39; H, 5.76; N, 11.41.

3.2. Biological Evaluation

3.2.1. In Vitro Antibacterial Susceptibility Assay (MIC Determination)

(a) *Staphylococci* and *Enterococci*: The synthesized compounds were evaluated for in vitro antibacterial activity against representatives of multidrug-resistant bacteria and clinical isolates of methicillin-resistant *Staphylococcus aureus* (MRSA) 63718, SA 630 and SA 3202, that were obtained from the National Institute of Public Health (Prague, Czech Republic). *S. aureus* ATCC 29213 was used as a reference and quality control strain. In addition, all the compounds were tested for their activity against vancomycin-susceptible *Enterococcus faecalis* ATCC 29212 as a reference strain and three isolates from American crows of vanA-carrying vancomycin-resistant *E. faecalis* (VRE) 342B, 368 and 725B [34]. Ampicillin (Amp) and ciprofloxacin (CIP) (Sigma-Aldrich, St. Louis, MO, USA) were used as standards. Prior to testing, each strain was passaged onto nutrient agar (Oxoid, Basingstoke, UK) with 5% of bovine blood, and bacterial inocula were prepared by suspending a small portion of the bacterial colony in sterile phosphate-buffered saline (pH 7.2–7.3). The cell density was adjusted to 0.5 McFarland units using a densitometer (Densi-La-Meter, LIAP, Riga, Latvia). This inoculum was diluted to reach the final concentration of bacterial cells 5×10^5 CFU/mL in the wells. The compounds were dissolved in DMSO (Sigma-Aldrich, St. Louis, MO, USA), and the final concentration of DMSO in the Cation Adjusted

Mueller-Hinton (CaMH) broth (Oxoid) for *Staphylococci* or brain-heart infusion for *Enterococci* did not exceed 2.5% of the total solution composition. The final concentrations of the evaluated compounds ranged from 256 to 0.008 μg/mL. The broth dilution micro-method, modified according to NCCLS (National Committee for Clinical Laboratory Standards) guidelines [35] in MH broth for *Staphylococcus* strains and CaMH for *Enterococcus* strains, was used to determine MIC. Drug-free controls, sterility controls, and controls consisting of MH and CaMH broths and DMSO alone were included. The determination of results was performed visually after 24 h of static incubation in darkness at 37 °C in an aerobic atmosphere.

(b) Other Gram-positive (*Streptococcus pneumoniae* MFBF 10373, *Bacillus cereus* ATCC 11778, and *Bacillus subtilis* ATCC 6633) and Gram-negative bacteria species (*Pseudomonas aeruginosa* ATCC 27853, *Escherichia coli* ATCC 10536, *Serratia marcescens* ATCC 10905, *Proteus mirabilis* MFBF 10430, *Acinetobacter baumannii* MFBF 10913, and *Salmonella enteritidis* MFBF 11945): Serial microdilution broth assay was used to determine MIC of compounds **4a**–**f** and **5a**–**f** [36]. Cell suspensions were prepared from stock cultures using phosphate-buffered saline (PBS) (Gibco Laboratories, USA) pH 7.4 and adjusted to 0.5 McFarland units using a nephelometer (ATB 1550, BioMérieux, France). Stock solutions of the tested compounds were prepared in DMSO (10 mg/mL). Testing was performed using serial dilution in microtiter flat-bottom 96-well plates with compounds ranging from 100 to 0.78125 μg/mL. After inoculation (10^7 CFU/mL) and incubation (18 h, 35 °C, aerobically in darkness), MICs for bacterial species were determined by addition of 0.5 mg/mL TTC (2,3,5-triphenyl-2*H*-tetrazolium chloride). The absorbance was recorded at 540 nm. As a positive quality control (susceptibility of strains) tetracycline hydrochloride (TC) (Sigma-Aldrich) was added into wells. MICs were determined as non-linear regression using GraphPad Prism as the lowest concentrations resulting in 50% growth inhibition of growth in comparison to control.

(c) *Mycobacteria: Mycobacterium tuberculosis* H37Ra ATCC 25177 was grown in Middlebrook broth (MB), supplemented with Oleic-Albumin-Dextrose-Catalase (OADC) supplement (Difco, Lawrence, KS, USA) and mycobactin J (2 μg/mL). At log phase growth, a culture sample (10 mL) was centrifuged at 15,000 rpm/20 min using a bench-top centrifuge (MPW-65R, MPW Med Instruments, Poland). Following removal of the supernatant, the pellet was washed in fresh Middlebrook 7H9GC broth and re-suspended in fresh, ODAC-supplemented MB (10 mL). The turbidity was adjusted to match McFarland standard No. 1 (3×10^8 CFU) with MB broth. A further 1:20 dilution of the culture was then performed in MB broth. The antimicrobial susceptibility of *M. tuberculosis* was investigated in a 96-well plate format. In these experiments, sterile deionised water (300 μl) was added to all outer-perimeter wells of the plates to minimize evaporation of the medium in the test wells during incubation. Each evaluated compound (100 μL) was incubated with *M. tuberculosis* (100 μl). Dilutions of each compound were prepared in duplicate. For all synthesized compounds, final concentrations ranged from 1000 μg/mL to 8 μg/mL. All compounds were dissolved in DMSO, and subsequent dilutions were made in supplemented MB. The plates were sealed with parafilm and incubated at 37 °C for 7 days. Following incubation, 10% of alamarBlue (Difco, Lawrence, KS, USA) was mixed into each well, and readings at 570 nm and 600 nm were taken, initially for background subtraction and subsequently after 24 h reincubation. The background subtraction is necessary for strongly coloured compounds, where the colour may interfere with the interpretation of any colour change. For non-interfering compounds, a blue colour in the well was interpreted as the absence of growth, and a pink colour was scored as growth.

The evaluation of the in vitro antimycobacterial activity of the compounds was additionally performed against *M. smegmatis* ATCC 700084, *M. marinum* CAMP 5644 and *M. kansasii* DSM 44162. The broth dilution micro-method in Middlebrook 7H9 medium (Difco, Lawrence, KS, USA) supplemented with ADC Enrichment (Becton, Dickinson and Comp.) was used to determine MIC as previously described [37]. The compounds were dissolved in DMSO (Sigma-Aldrich), and the final concentration of DMSO did not exceed 2.5% of the total solution composition. Final concentrations of the evaluated compounds ranging from 256 μg/mL to 0.125 μg/mL were obtained by twofold

serial dilution of the stock solution in a microtiter plate with sterile medium. Bacterial inocula were prepared by transferring colonies from culture to sterile water. The cell density was adjusted to 0.5 McFarland units using a densitometer (Densi-La-Meter, LIAP, Riga, Latvia). The final inoculum was made by 1:1000 dilution of the suspension with sterile water. Drug-free controls, sterility controls and controls consisted of medium and DMSO (Sigma-Aldrich, St. Louis, MO, USA) alone were included. The determination of results was performed visually after 3 days of static incubation in darkness at 37 °C in an aerobic atmosphere for *M. smegmatis*, after 7 days of static incubation in darkness at 37 °C in an aerobic atmosphere for *M. kansasii* and after 21 days of static incubation in darkness at 28 °C in an aerobic atmosphere for *M. marinum*. Ciprofloxacin (CIP), rifampicin (RIF) and isoniazid (INH) (Sigma-Aldrich, St. Louis, MO, USA) were used as the standards.

3.2.2. In Vitro Antifungal Susceptibility Testing

Microdilution method was used for testing the antifungal activities of newly synthesized compounds against *Candida albicans* CCM 8261 and ATCC 90028, *C. krusei* CCM 8271, *C. parapsilosis* CCM 8260 (Czech Collection of Microorganisms, Brno, Czech Republic) [38]. Tested compounds were diluted in RPMI-1640 (Sigma) broth to concentrations 128–0.016 μg/mL. Flucytosine (FLU) (Sigma) and amphotericin B (Amph) were used as positive controls. The plates were inoculated by an inoculum prepared in RPMI-1640 broth. The final concentration of fungal cells was 5×10^2–2.5×10^3 CFU/mL in each well. The plates were incubated at 37 °C for 24 (*C. albicans*, *C. krusei*) or 48 (*C. parapsilosis*) hours. Drug-free controls were included. MIC was defined as 80% or greater (IC_{80}) reduction of growth in comparison with the control [35].

MIC determination for *Aspergillus brasiliensis* was performed in RPMI 1640 broth with glutamine supplemented with 2% glucose, following the same scheme as for bacteria, procedure b). After incubation period (48 h, 35 °C, aerobically in dark), XTT (2*H*-tetrazolium, 2,3-bis(2-methoxy-4-nitro-5-sulfophenyl)-5-[(phenylamino)carbonyl]-hydroxide) (10 mg/mL) in combination with menadione (1 mg/mL in acetone) (7:1, *v*/*v*) was added [36]. Absorbance was read at 540 nm. Amph was used as a positive control and solvent and media (no microorganisms added) as negative controls.

3.2.3. Minimum Biofilm Eradication Assay

Biofilm eradication screening was performed on the following microorganisms: *S. aureus* ATCC 6538, *S. pneumoniae* MFBF 10373, *E. faecalis* ATCC 29212, *B. cereus* ATCC 11778, *B. subtilis* ATCC 6633, *E. coli* ATCC 10536, *P. aeruginosa* ATCC 27853, *S. marcescens* ATCC 10905, *P. mirabilis* MFBF 10430, *S. enteritidis* MFBF 11945, *A. baumannii* MFBF 10913, and *C. albicans* ATCC 90028. MBECs of fumardiamides **4a**–**f** and succindiamides **5a**–**f** were determined as follows [39]. Each well (96-well plate) was filled with 100 μl of bacterial (10^7 CFU/mL) or yeast (5×10^6 CFU/mL) suspension. When the inhibition of yeast biofilm formation was tested, the wells were pre-treated with fetal bovine serum (FBS) (250 μl per well). Negative controls contained broth only. Positive controls were performed using standard antimicrobial drugs gentamycin (Gen) and Amph, respectively. The plates were covered and incubated aerobically for 24 h (bacteria) or 48 h (yeast) at 37 °C. Following incubation period, each well was aspirated, washed three times and vigorously shaken to remove all non-adherent bacteria/yeast. The remaining attached cells were fixed with methanol (15 min) and the plates were left to dry overnight. Formed biofilm was stained with crystal violet (1%, 5 min). Excess stain was rinsed by placing the plate under running tap water and the plates were left to dry. Adherent cells were solubilized using ethanol. The absorbance was read at 570 nm. The MBEC value represents the lowest dilution of a compound at which bacteria fail to grow.

3.2.4. Antiviral Evaluation

Antiviral activity of compounds **4a**–**f** and **5a**–**f** was determined as described previously [40]. Cytotoxicity and antiviral activity assay towards herpes simplex virus (HSV) strains HSV-1 KOS, HSV-2 G, HSV-1 TK-KOS ACVr, vaccinia virus, adenovirus-2, human coronavirus (229E) in HEL

cell cultures, vesicular stomatitis virus, coxsackie virus B4, respiratory syncytial virus in Hela cell cultures, para-influenza-3 virus, reovirus-1, sindbis, coxsackie virus B4, Punta Toro virus, yellow fever virus in Vero cell cultures, while influenza A/H1N1 A/Ned/378/05, influenza A/H3N2 A/HK/7/87 and influenza B B/Ned/537/05 viruses in Madin-Darby Canine Kidney (MDCK) cell cultures were performed. On the day of the infection, growth medium was aspirated and replaced by serial dilutions of the test compounds. Virus was then added to each well, diluted to obtain a viral input of 100 $CCID_{50}$ ($CCID_{50}$ being the virus dose that is able to infect 50% of the cell cultures). Mock-treated cell cultures receiving solely the test compounds were included, to determine their cellular cytotoxicity. After 3 to 10 days of incubation the virus-induced cytopathicity was determined by visual scoring of the cytopathic effect (CPE) (light microscopic evaluation of the virus-induced CPE and inhibition of evaluated compounds), as well as by measuring the cell viability with the colorimetric formazan-based MTS assay (3-(4,5-dimethylthiazol-2-yl)-5-(3-carboxymethoxyphenyl)-2-(4-sulfophenyl)-2*H*-tetrazolium). All experiments were performed in duplicate. Antiviral activity was expressed as EC_{50}. The activities were compared with the activities of the parent drug PQ, DS-10.000 (dextran sulfate, approx. MW = 10.000) and standard antiviral drugs: ribavirin (Rib), mycophenolic acid (MPA), brivudin, cidofovir, acyclovir, gancyclovir, zalcitabine, alovudine, UDA, zanamivir, amantadine and rimantadine.

3.2.5. Cytostatic Activity

Cytostatic activity was evaluated in vitro on nine different types of human tumor cell lines: Capan-1, Hap1, HCT-116, and NCI-H460, as well as hematological tumors such as DND-41, HL-60, K-562, MM.1S and Z-138 as described previously [41]. All human tumor cell lines were acquired from the American Type Culture Collection (ATCC, Manassas, VA, USA), except for the DND-41 cell line which was purchased from the Deutsche Sammlung von Mikroorganismen und Zellkulturen (DSMZ Leibniz-Institut, Braunschweig, Germany) and the Hap1 cell line which was purchased from Horizon Discovery (Waterbeach, UK). Capan-1, Hap1, HL-60, K-562, Z-138, MM.1S and DND-41 were cultured in Iscove′s Modified Dulbecco′s Medium (IMDM, Gibco Life Technologies, Gaithersburg, MD, USA), HCT-116 were grown in McCoy′s 5A Medium (Gibco Life Technologies) and NCI-H460 were cultured in RPMI (Gibco Life Technologies). All media were supplemented with 10% FBS (HyClone, GE Healthcare Life Sciences, USA). Adherent cell lines HCT-116, Hap1, NCI-H460, and Capan-1 cells were seeded at a density between 400 and 1250 cells per well, in 384-well, black-walled, clear-bottomed tissue culture plates (Greiner Bio-One, Kremsmünster, Germany). After overnight incubation, cells were treated with test compounds at four different concentrations ranging from 100 to 0.8 μM. Suspension cell lines HL-60, K-562, Z-138, MM.1S, and DND-41 were seeded at densities ranging from 3000 to 10,000 cells per well in 384-well, black-walled, clear-bottomed tissue culture plates containing test compounds at the same four concentrations. The plates were incubated and monitored at 37 °C for 72 h in an IncuCyte (Essen BioScience Inc., Ann Arbor, MI, USA) for real-time imaging. Images were taken every 3 h, with one field image per well under 10× magnification. All compounds were tested with duplicate data points and averaged. The activities were compared with the activities of the parent drug PQ and standard anticancer drugs docetaxel (DXT), etoposide (EPEG) and staurosporine (STS).

3.2.6. Interaction with Glutathione (GSH)

Fumardiamide **4b** (1.25 μM) was incubated with GSH (125 μM) in ammonium formate buffer (pH = 7.4) containing 10% acetonitrile at 37 °C for 216 h [33]. The progress of the reactions was monitored with the percent of remaining fumardiamide determined by MS using an internal standard (*N*-(benzyloxy)-*N*′-{4-[(6-methoxyquinolin-8-yl)amino]pentyl}butanediamide). Aliquots of the reaction mixture (taken after 0, 4.5, 26, 52, 124 and 216 h) were analysed with Synapt G2-Si ESI-QTOF-MS system (Waters, Milford, USA). The aliquots were diluted 10 times with acetonitrile and sprayed at a flow rate of 50 μL/min using the fluidics system of the instrument. MS conditions were set as follows: positive ion mode, capillary voltage 3 kV, sampling cone voltage 10 V, source temperature

120 °C, desolvation temperature 350 °C, desolvation gas flow 800 L/h. Mass spectra were recorded from 100–1000 *m/z* at a frequency of 1 Hz. Data were acquired and analysed with Waters MassLynx v4.1 software.

4. Conclusions

Twelve novel PQ-derivatives of diamide type were designed and synthesized. These compounds differ in the type of spacer and/or halogen atom in aniline region. Compounds **4a–f** are fumardiamides and **5a–f** succindiamides. Compounds **4a**,**b**, **5a**,**b** are fluoro, **4c**,**d**, **5c**,**d** chloro and **4e**,**f**, **5e**,**f** are trifluoroderivatives. All new compounds were screened for antibacterial, antitubercular, antiviral and cytostatic activity as well as biofilm eradication ability. In all biological assays, fumardiamides **4** were superior to succindiamides **5**, which indicates that the double bond conjugated to the carbonyl was important for the activity. With their high bioactivity, low cytotoxicity and convenient drug-like properties, *p*-substituted derivatives **4b**,**d**,**f** provide a strong basis for further research and optimization of novel agents useful in the treatment of bacterial and biofilm-associated infections, while *m*-substituted derivatives **4a**,**c**,**e** could be potential leads for the development of antitumor agents.

Supplementary Materials: The following are available online: Table S1. Properties of novel compounds calculated with Chemicalize.org program. The Lipinski and Gelovani parameters; Table S2. Analytical and spectral data of compounds **4a–f** and **5a–f**; Table S3. ^{1}H and ^{13}C NMR spectra of amides **4a–f** and **5a–f**; Table S4. Interaction of fumardiamide **4b** with GSH; Figure S1. Interaction of fumardiamide **4b** with GSH (⧫). Control: (*N*-(benzyloxy)-*N*′-{4-[(6-methoxyquinolin-8-yl)amino]pentyl}butanediamide) (•). Spectra of all compounds.

Author Contributions: Conceptualization, Z.R. and B.Z.; Synthesis and characterization of compounds M.B., Z.R.; Antibacterial, antifungal and biofilm eradication assay, H.M., J.V., I.K., J.J.; Antiviral and cytostatic evaluaton, L.P., D.S.; Interaction with GSH T.K.; Writing of Manuscript, Z.R. and B.Z.

Funding: This work has been fully supported by the Croatian Science Foundation (project IP-09-2014-1501), University of Zagreb (support for 2017), Comenius University in Bratislava (grant UK/229/2018), Faculty of Pharmacy of Comenius University in Bratislava (grant FaFUK/9/2018) and SANOFI-AVENTIS Pharma Slovakia, s.r.o.

Conflicts of Interest: The authors declare no conflicts of interest.

References

1. Clayden, J.; Greeves, N.; Warren, S. *Organic Chemistry*, 2nd ed.; Oxford University Press: New York, NY, USA, 2012.
2. Smaill, J.B.; Rewcastle, G.W.; Loo, J.A.; Greis, K.D.; Chan, O.H.; Reyner, E.L.; Lipka, E.; Showalter, H.D.; Vincent, P.W.; Elliott, W.L.; et al. Tyrosine kinase inhibitors. 17. Irreversible inhibitors of the epidermal growth factor receptor: 4-(phenylamino)quinazoline- and 4-(phenylamino)pyrido[3,2-*d*]pyrimidine-6-acrylamides bearing additional solubilizing functions. *J. Med. Chem.* **2000**, *43*, 1380–1397. [CrossRef] [PubMed]
3. Minami, Y.; Shimamura, T.; Shah, K.; LaFramboise, T.; Glatt, K.A.; Liniker, E.; Borgman, C.L.; Haringsma, H.J.; Feng, W.; Weir, B.A.; et al. The major lung cancer-derived mutants of ERBB2 are oncogenic and are associated with sensitivity to the irreversible EGFR/ERBB2 inhibitor HKI-272. *Oncogene* **2007**, *26*, 5023–5027. [CrossRef] [PubMed]
4. Baselga, J.; Coleman, R.E.; Cortés, J.; Janni, W. Advances in the management of HER2-positive early breast cancer. *Crit. Rev. Oncol. Hematol.* **2017**, *119*, 113–122. [CrossRef] [PubMed]
5. Jackson, P.A.; Widen, J.C.; Harki, D.A.; Brummond, K.M. Covalent modifiers: A chemical perspective on the reactivity of α,β-unsaturated carbonyls with thiols via hetero-Michael addition reactions. *J. Med. Chem.* **2017**, *60*, 839–885. [CrossRef] [PubMed]
6. Zhang, X.; Li, X.; You, Q.; Zhang, X. Prodrug strategy for cancer cell-specific targeting: A recent overview. *Eur. J. Med. Chem.* **2017**, *139*, 542–563. [CrossRef] [PubMed]
7. Compound Summary for CID 5281081. Available online: https://pubchem.ncbi.nlm.nih.gov/compound/entacapone#section=Top (accessed on 25 May 2018).

8. Matthews, D.A.; Dragovich, P.S.; Webber, S.E.; Fuhrman, S.A.; Patick, A.K.; Zalman, L.S.; Hendrickson, T.F.; Love, R.A.; Prins, T.J.; Marakovits, J.T.; et al. Structure-assisted design of mechanism-based irreversible inhibitors of human rhinovirus 3C protease with potent antiviral activity against multiple rhinovirus serotypes. *Proc. Natl. Acad. Sci. USA* **1999**, *96*, 11000–11007. [CrossRef] [PubMed]
9. Buzdar, A.U.; Robertson, J.F.; Eiermann, W.; Nabholtz, J.M. An overview of the pharmacology and pharmacokinetics of the newer generation aromatase inhibitors anastrozole, letrozole, and exemestane. *Cancer* **2002**, *95*, 2006–2016. [CrossRef] [PubMed]
10. Somberg, J.C.; Molnar, J. The pleiotropic effects of ethacrynic acid. *Am. J. Ther.* **2009**, *16*, 102–104. [CrossRef] [PubMed]
11. Dawson, R.M. The toxicology of microcystins. *Toxicon* **1998**, *36*, 953–962. [CrossRef]
12. Eusugi, S.; Fujisawa, N.; Yoshida, J.; Watanabe, M.; Dan, S.; Yamori, T.; Shiono, Y.; Kimura, K.; Pyrrocidine, A. A metabolite of endophytic fungi, has a potent apoptosis-inducing activity against HL60 cells through caspase activation via the Michael addition. *J. Antibiot.* **2016**, *69*, 133–140. [CrossRef]
13. Ramsay, J.R.; Suhrbier, A.; Aylward, J.H.; Ogbourne, S.; Cozzi, S.J.; Poulsen, M.G.; Baumann, K.C.; Welburn, P.; Redlich, G.L.; Parsons, P.G. The sap from *Euphorbia peplus* is effective against human nonmelanoma skin cancers. *Br. J. Dermatol.* **2011**, *164*, 633–636. [CrossRef] [PubMed]
14. Lebwohl, M.; Swanson, N.; Anderson, L.L.; Melgaard, A.; Xu, Z.; Berman, B. Ingenol mebutate gel for actinic keratosis. *N. Engl. J. Med.* **2012**, *366*, 1010–1019. [CrossRef] [PubMed]
15. Picato®gel–FDA. Available online: https://www.accessdata.fda.gov/drugsatfda_docs/label/2012/202833lbl.pdf. (accessed on 9 June 2018).
16. Sebök, B.; Bonnekoh, B.; Geisel, J.; Mahrle, G. Antiproliferative and cytotoxic profiles of antipsoriatic fumaric acid derivatives in keratinocyte cultures. *Eur. J. Pharmacol.* **1994**, *270*, 79–87. [CrossRef]
17. Smith, D. Fumaric acid esters for psoriasis: A systematic review. *Ir. J. Med. Sci.* **2017**, *186*, 161–177. [CrossRef] [PubMed]
18. Kocaadam, B.; Şanlier, N. Curcumin, an active component of turmeric (*Curcuma longa*), and its effects on health. *Crit. Ver. Food Sci. Nutr.* **2017**, *57*, 2889–2895. [CrossRef] [PubMed]
19. Seca, A.M.L.; Pinto, D.C.G.A. Plant secondary metabolites as anticancer agents: Successes in clinical trials and therapeutic application. *Int. J. Mol. Sci.* **2018**, *19*, 263. [CrossRef] [PubMed]
20. Pavić, K.; Perković, I.; Cindrić, M.; Pranjić, M.; Martin-Kleiner, I.; Kralj, M.; Schols, D.; Hadjipavlou-Litina, D.; Katsori, A.-M.; Zorc, B. Novel semicarbazides and ureas of primaquine with bulky aryl or hydroxyalkyl substituents: Synthesis, cytostatic and antioxidative activity. *Eur. J. Med. Chem.* **2014**, *86*, 502–514. [CrossRef] [PubMed]
21. Perković, I.; Antunović, M.; Marijanović, I.; Pavić, K.; Ester, K.; Kralj, M.; Vlainić, J.; Kosalec, I.; Schols, D.; Hadjipavlou-Litina, D.; et al. Novel urea and bis-urea primaquine derivatives with hydroxyphenyl and halogenphenyl substituents: Synthesis and biological evaluation. *Eur. J. Med. Chem.* **2016**, *124*, 622–636. [CrossRef] [PubMed]
22. Guzman, J.D. Natural cinnamic acids, synthetic derivatives and hybrids with antimicrobial activity. *Molecules* **2014**, *19*, 292–349. [CrossRef] [PubMed]
23. Kakwani, M.D.; Suryavanshi, P.; Ray, M.; Rajan, M.G.R.; Majee, S.; Samad, A.; Devarajan, P.; Degani, M.S. Design, synthesis and antimycobacterial activity of cinnamide derivatives: A molecular hybridization approach. *Bioorg. Med. Chem. Lett.* **2011**, *21*, 1997–1999. [CrossRef] [PubMed]
24. De, P.; Baltas, M.; Bedos-Belval, F. Cinnamic acid derivatives as anticancer agents-a review. *Curr. Med. Chem.* **2011**, *18*, 1672–1703. [CrossRef] [PubMed]
25. Pavić, K.; Perković, I.; Gilja, P.; Kozlina, F.; Ester, K.; Kralj, M.; Schols, D.; Hadjipavlou-Litina, D.; Pontiki, E.; Zorc, B. Design, synthesis and biological evaluation of novel primaquine-cinnamic acid conjugates of amide and acylsemicarbazide type. *Molecules* **2016**, *21*, 1629. [CrossRef] [PubMed]
26. Pavić, K.; Perković, I.; Pospíšilová, Š.; Machado, M.; Fontinha, D.; Prudêncio, M.; Jampilek, J.; Coffey, A.; Endersen, L.; Rimac, H.; et al. Primaquine hybrids as promising antimycobacterial and antimalarial agents. *Eur. J. Med. Chem.* **2018**, *143*, 769–779. [CrossRef] [PubMed]
27. Vlainić, J.; Kosalec, I.; Pavić, K.; Hadjipavlou-Litina, D.; Pontiki, E.; Zorc, B. Insights into biological activity of ureidoamides with primaquine and amino acid moieties. *J. Enzyme Inhib. Med. Chem.* **2018**, *33*, 376–382. [CrossRef] [PubMed]

28. Levatić, J.; Pavić, K.; Perković, I.; Uzelac, L.; Ester, K.; Kralj, M.; Kaiser, M.; Rottmann, M.; Supek, F.; Zorc, B. Machine learning prioritizes synthesis of primaquine ureidoamides with high antimalarial activity and attenuated cytotoxicity. *Eur. J. Med. Chem.* **2018**, *146*, 651–667. [CrossRef] [PubMed]
29. Beus, M.; Rajić, Z.; Maysinger, D.; Mlinarić, Z.; Antunović, M.; Marijanović, I.; Fontinha, D.; Prudêncio, M.; Held, J. SAHA-primaquine hybrids (sahaquines) as potential anticancer and antimalarial compounds. *Chem. Open*, submitted.
30. Chemicalize, 2017, ChemAxon Ltd. Available online: http://www.chemicalize.org (accessed on 5 April 2018).
31. Hufnagel, D.A.; Price, J.E.; Stephenson, R.E.; Kelley, J.; Benoit, M.F.; Chapman, M.R. Thiol starvation induces redox-mediated dysregulation of *Escherichia coli* biofilm components. *J. Bacteriol.* **2018**, *200*, e00389-17. [CrossRef] [PubMed]
32. Lee, S.F.; Davey, L. Disulfide bonds: A key modification in bacterial extracytoplasmic proteins. *J. Dent. Res.* **2017**, *96*, 1465–1473. [CrossRef] [PubMed]
33. Flanagan, M.E.; Abramite, J.A.; Anderson, D.P.; Aulabaugh, A.; Dahal, U.P.; Gilbert, A.M.; Li, C.; Montgomery, J.; Oppenheimer, S.R.; Ryder, T.; et al. Chemical and computational methods for the characterization of covalent reactive groups for the prospective design of irreversible inhibitors. *J. Med. Chem.* **2014**, *57*, 10072–10079. [CrossRef] [PubMed]
34. Oravcova, V.; Zurek, L.; Townsend, A.; Clark, A.B.; Ellis, J.C.; Cizek, A. American crows as carriers of vancomycin-resistant enterococci with vanA gene. *Environ. Microbiol.* **2014**, *16*, 939–949. [CrossRef] [PubMed]
35. Clinical and Laboratory Standards Institute. *Performance Standards for Antimicrobial Susceptibility Testing*; The 8th informational supplement document; CLSI: Wayne, PA, USA, 2012; M100-S22.
36. EUCAST, European Committee on Antimicrobial Susceptibility Testing. Determination of minimum inhibitory concentrations (MICs) of antibacterial agents by broth micro dilution. EUCAST Discussion Document. *Clin. Microbiol. Infect.* **2013**, *9*, 1–10.
37. Schwalbe, R.; Steele-Moore, L.; Goodwin, A.C. (Eds.) *Antimicrobial Susceptibility Testing Protocols*; CRC Press: Boca Raton, FL, USA, 2007.
38. Sheehan, D.J.; Espinel-Ingroff, A.; Steele, M.; Webb, C.D. Antifungal susceptibility testing of yeasts: A brief overview. *Clin. Infect. Dis.* **1993**, *17*, 494–500. [CrossRef]
39. Stepanović, S.; Vuković, D.; Hola, V.; Di Bonaventura, G.; Djukić, S.; Cirković, I.; Ruzicka, F. Quantification of biofilm in microtiter plates: Overview of testing conditions and practical recommendations for assessment of biofilm production by *Staphylococci*. *APMIS* **2007**, *115*, 891–899. [CrossRef] [PubMed]
40. Tzioumaki, N.; Manta, S.; Tsoukala, E.; Vande Voorde, J.; Liekens, S.; Komiotis, D.; Balzarini, J. Synthesis and biological evaluation of unsaturated keto and exomethylene D-arabinopyranonucleoside analogs: Novel 5-fluorouracil analogs that target thymidylate synthase. *Eur. J. Med. Chem.* **2011**, *46*, 993–1005. [CrossRef] [PubMed]
41. Li, Q.; Lescrinier, E.; Groaz, E.; Persoons, L.; Daelemans, D.; Herdewijn, P.; De Jonghe, S. Synthesis and biological evaluation of pyrrolo[2,1-f][1,2,4]triazine C-nucleosides with a ribose, 2′-deoxyribose, and 2′,3′-dideoxyribose sugar moiety. *ChemMedChem.* **2018**, *13*, 97–104. [CrossRef] [PubMed]

Sample Availability: Samples of all compounds are available from the authors.

4. Inhibicija proliferacije i invazije stanica glioblastoma, te mehanizam djelovanja sahakina 17

Zhang et al. *Cell Death Discovery* (2019)5:41
DOI 10.1038/s41420-018-0103-0

Cell Death Discovery

ARTICLE Open Access

Inhibition of glioblastoma cell proliferation, invasion, and mechanism of action of a novel hydroxamic acid hybrid molecule

Issan Zhang[1], Maja Beus[1,2], Ursula Stochaj[3], Phuong Uyen Le[4], Branka Zorc[2], Zrinka Rajić[2], Kevin Petrecca[4] and Dusica Maysinger[1]

Abstract

Glioblastoma multiforme is one of the most aggressive brain tumors and current therapies with temozolomide or suberoylanilide hydroxamic acid (SAHA, vorinostat) show considerable limitations. SAHA is a histone deacetylase (HDAC) inhibitor that can cause undesirable side effects due to the lack of selectivity. We show here properties of a novel hybrid molecule, sahaquine, which selectively inhibits cytoplasmic HDAC6 at nanomolar concentrations without markedly suppressing class I HDACs. Inhibition of HDAC6 leads to significant α-tubulin acetylation, thereby impairing cytoskeletal organization in glioblastoma cells. The primaquine moiety of sahaquine reduced the activity of P-glycoprotein, which contributes to glioblastoma multiforme drug resistance. We propose the mechanism of action of sahaquine to implicate HDAC6 inhibition together with suppression of epidermal growth factor receptor and downstream kinase activity, which are prominent therapeutic targets in glioblastoma multiforme. Sahaquine significantly reduces the viability and invasiveness of glioblastoma tumoroids, as well as brain tumor stem cells, which are key to tumor survival and recurrence. These effects are augmented with the combination of sahaquine with temozolomide, the natural compound quercetin or buthionine sulfoximine, an inhibitor of glutathione biosynthesis. Thus, a combination of agents disrupting glioblastoma and brain tumor stem cell homeostasis provides an effective anti–cancer intervention.

Introduction

Glioblastoma multiforme (GBM) is the most common and aggressive form of brain cancer, with limited treatment options and dismal survival rates. Current treatment involves surgical resection followed by radiotherapy and chemotherapy with temozolomide (TMZ)[1]. However, more than half of GBM patients do not respond to TMZ due to the overexpression of DNA repair enzymes, notably O^6-methylguanine transferase[2–4].

Histone deacetylase (HDAC) inhibitors exert anticancer effects by inducing cell differentiation, cell cycle arrest, and apoptotic cell death through the upregulation of tumor suppressor and cell cycle-regulatory genes[5]. Suberoylanilide hydroxamic acid (SAHA, vorinostat) is a Food and Drug Administration-approved drug for the treatment of cutaneous T cell lymphoma. It is currently in clinical trials for GBM as monotherapy and combined with radiotherapy[6–9]. Despite advancements in treatments, the median survival rate for GBM remains low (14–16 months) and new therapeutic options are urgently needed[3,10].

In this study, we combined hydroxamic acid—the active moiety of SAHA exerting biological effects in cancer cells—with primaquine to generate a new class of hybrid anticancer agents: sahaquines. Hydroxamic acid inhibits HDACs;

Correspondence: Dusica Maysinger (dusica.maysinger@mcgill.ca)
[1]Department of Pharmacology and Therapeutics, McGill University, Montreal, QC, Canada
[2]Faculty of Pharmacy and Biochemistry, University of Zagreb, Zagreb, Croatia
Full list of author information is available at the end of the article.
These authors contributed equally: Issan Zhang, Maja Beus
Edited by M.V. Niklison Chirou

SPRINGER NATURE CDDpress

these enzymes are overexpressed in many cancers, including GBM[11,12]. The hydroxamic acid pharmacophore of SAHA chelates metal ions, thereby inhibiting metalloenzymes such as HDACs and matrix metalloproteinases (MMPs), which promote cancer growth and invasiveness[13–15]. Hydroxamic acid is a weak acid, which is favorable in the acidic tumor microenvironment as weak bases become protonated, resulting in ion trapping, lysosomal accumulation, elimination by lysosomal exocytosis, and overall decreased biological activity[16–18]. Primaquine can directly interfere with endosomal trafficking to the plasma membrane[19], inhibit the multidrug resistance transporter P-glycoprotein, and autophagy, thereby sensitizing cancer cells to anti-mitotic drugs[20,21]. Considering that monotherapies have limited effectiveness in GBM, we tested sahaquine in combination with TMZ, the standard of care for GBM, quercetin, and buthionine sulfoxamine. Quercetin is an abundant flavonoid found in fruits and vegetables, such as apples and onions. Its estimated daily intake ranges from 3–40 mg, but supplements up to 1000 mg per day are considered safe[22]. Although it shows no toxicity in normal cells, several studies have shown that quercetin has anticancer effects. Its mechanism of action involves the upregulation of pro-apoptotic and downregulation of anti-apoptotic factors, cell cycle arrest, and DNA intercalation, resulting in DNA damage, activation of apoptosis, and cell death[23]. In animal studies, quercetin inhibited tumor growth and improved the lifespan of tumor-bearing mice[23,24]. Furthermore, the anticancer effects of quercetin are enhanced in combination with chemotherapeutic agents or other drugs[25–27].

We investigated the loss of cell viability and invasiveness in GBM as functional read-outs of the effects of sahaquine alone or in combination with TMZ and quercetin. Sahaquine was tested in both differentiated GBM cells and brain tumor stem cells (BTSCs), which are key to tumor survival and recurrence[28–31]. Our study supports the model that sahaquine-induced cell death of GBM is mediated through multiple pathways, including inhibition of HDAC6, reduction of epidermal growth factor receptor (EGFR) protein abundance, and decreased activation of downstream kinases AKT and ERK1/2. The primaquine moiety of sahaquine contributes to the inhibition of P-glycoprotein. Considering that sahaquine significantly reduced BTSC viability and markedly inhibited GBM invasion by disruption of GBM homeostasis, further systematic studies are warranted in patient-derived organoids.

Results

Sahaquine synthesis and physicochemical properties of the selected anticancer agents

Sahaquine is a primaquine and hydroxamic acid derivative linked with glutaric acid. It is synthesized in four steps (Fig. 1). The pharmacophore, hydroxamic acid, was introduced in the last step. Yields were good to excellent (50–88%). Sahaquine was fully characterized by conventional spectroscopic and analytical methods (melting point, IR, MS, ^{1}H-NMR, ^{13}C-NMR), and the data were consistent with the proposed structure (Supplementary Fig. S1). The quinoline ring of sahaquine acts as the capping group and the hydroxamic acid binds zinc. Calculations of physicochemical properties showed that TMZ is a hydrophilic compound ($\log P = -0.28$), whereas sahaquine and particularly quercetin are more lipophilic ($\log P = 0.92$ and 2.16, respectively) (Table 1). The isoelectric point (pI) values of these compounds vary from 2.9 (quercetin) to 9.2 (SAHA)[32].

Sahaquine is more potent than TMZ for killing human glioblastoma and BTSCs

The half maximal inhibitory concentration (IC_{50}) value of sahaquine (10 μM) was about threefold lower than that

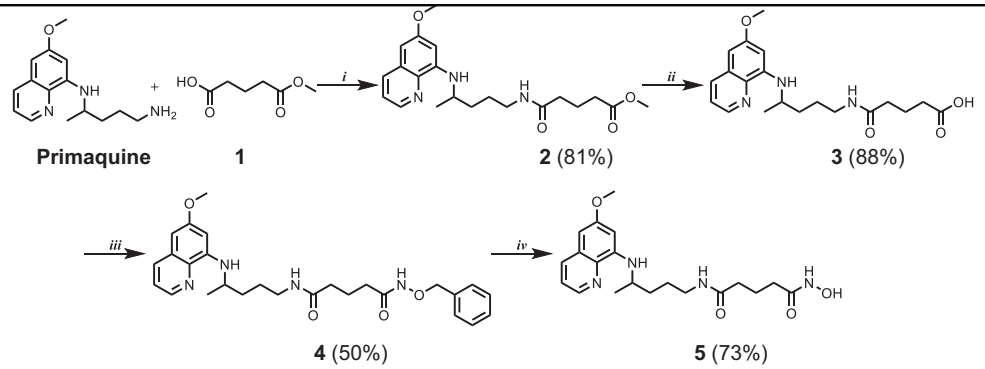

Figure 1 Synthesis of sahaquine and its precursors. Reagents and conditions: (i) HATU, DIEA, dichloromethane, 1 h, (ii) LiOH, methanol, H_2O, 1 h, (iii) *O*-benzylhydroxylamine, HATU, DIEA, dichloromethane, 2 h, (iv) H_2, 10% Pd/C, methanol, 4 h. All reactions were performed at room temperature. Yields are shown in brackets. HATU 1-[*bis*(dimethylamino)methylene]-1*H*-1,2,3-triazolo[4,5-*b*]pyridinium 3-oxid hexafluorophosphate, DIEA *N*,*N*-diisopropylethylamine, LiOH lithium hydroxide)

Table 1 Structures of sahaquine, temozolomide, quercetin, and SAHA with basic physicochemical properties

Structure	IUPAC name	Molecular mass	log*P*	pI
Sahaquine 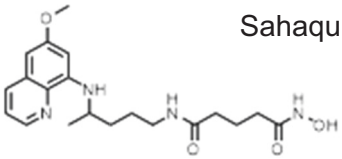	*N*-hydroxy-*N*'-{4-[(6-methoxyquinolin-8-yl)amino]pentyl}pentanediamide	388.47	0.92	6.48
Temozolomide 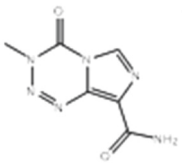	3-methyl-4-oxo-3*H*,4*H*-imidazo[4,3-*d*][1,2,3,5]tetrazine-8-carboxamide	194.15	-0.28	7.1
Quercetin 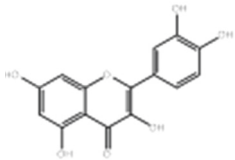	2-(3,4-dihydroxyphenyl)-3,5,7-trihydroxy-4*H*-chromen-4-one	302.24	2.16	2.9
SAHA 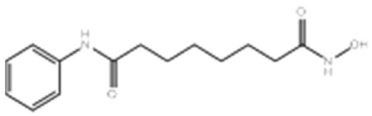	*N*'-hydroxy-*N*-phenyloctanediamide	264.33	1.0	9.2

The physicochemical properties are calculated with the Chemicalize.org program (Instant Cheminformatics Solutions. Available online at http://www.chemicalize.org/ (accessed on 10 October 2017))

of TMZ (31 μM), whereas it was less potent than its parent compound SAHA after 72 h incubation (Fig. 2). Sahaquine precursors were also tested, but because of the relatively high IC_{50} values (>50 μM), further experiments were not pursued (Supplementary Table S1). Enhanced cell killing was achieved by combining quercetin with sahaquine in a dose-dependent manner, although quercetin alone showed limited cytotoxicity ($IC_{50} = 140$ μM after 72 h) (Fig. 2e). Combination of TMZ with sahaquine, quercetin, or SAHA at IC_{50} concentrations was more effective than any of the compounds alone (Supplementary Fig. S2). Similar results were obtained by measurements of mitochondrial metabolic activity using the MTT (3-[4,5-dimethylthiazol-2-yl]-2,5-diphenyl tetrazolium bromide) assay (Supplementary Fig. S3).

We further tested the selected compounds on GBM tumoroids, which are more drug-resistant and representative models of brain tumors in vivo. Sahaquine and TMZ reduced tumoroid sizes by 37 and 40%, respectively, while quercetin did not have a significant effect after 7 days (Supplementary Fig. S4).

Based on the results shown in Fig. 2, we investigated the cytotoxic effects of the selected compounds on BTSCs. BTSCs are a key subpopulation of GBM tumors implicated in tumor initiation, propagation and recurrence[28,30]. In vitro BTSC cultures spontaneously formed neurospheres of approximately 100 μm in diameter within 7 days. Sahaquine and quercetin were most effective at reducing the size of BTSC aggregates and abolishing the formation of neurospheres (Fig. 3).

Sahaquine inhibits GBM invasion and P-glycoprotein activity

GBM is characterized by a diffuse brain tissue distribution[33]. Tumors commonly reoccur within a few centimeters of the original lesion, making surgical resection difficult[33]. We tested the effect of sahaquine and quercetin on GBM migration using a scratch assay, and invasion using a three-dimensional (3D) collagen matrix. Sahaquine did not significantly inhibit cell migration over 24 h, while quercetin reduced cell migration by 20% (Fig. 4a). The combination of sahaquine with quercetin

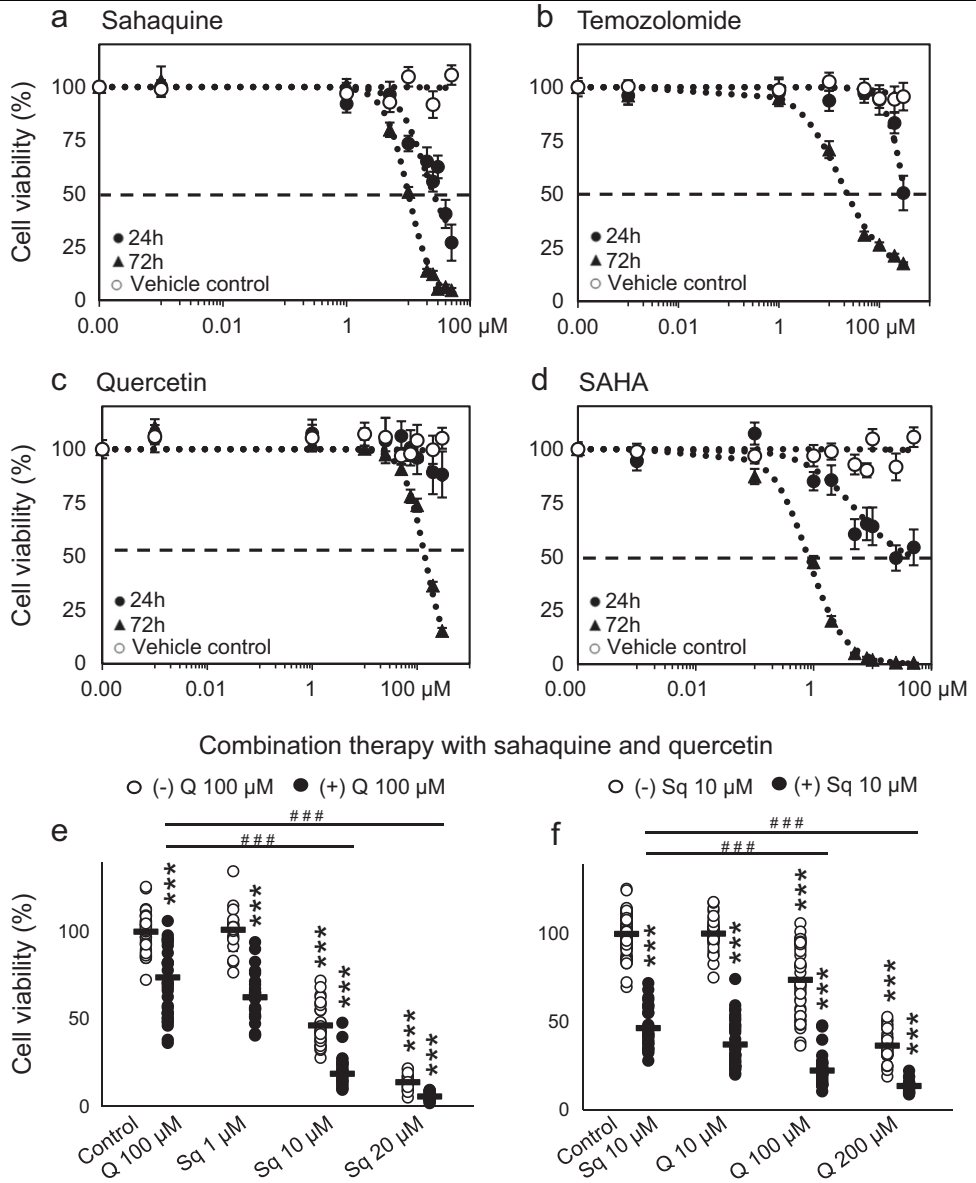

Figure 2 Sahaquine kills human glioblastoma cells in a dose-dependent and time-dependent manner. GBM cell viability ($n = 9$) following treatment with **a** sahaquine (Sq, 0.001–50 μM), **b** temozolomide (TMZ, 0.001–500 μM), **c** quercetin (Q, 0.001–300 μM), and **d** SAHA (0.001–50 μM) for 24 or 72 h. Shown is the mean (SEM) percentage cell viability compared to untreated controls from three independent experiments. **e**, **f** Dose-dependent decrease in cell viability (72 h) with the combination of either a fixed concentration of quercetin (100 μM, n = 41) and increasing concentrations of sahaquine (Sq 1 μM, $n = 21$, Sq 10 μM, $n = 30$, Sq 20 μM, $n = 21$, Sq 1 μM + Q, $n = 25$, Sq 10 μM + Q, $n = 29$, Sq 20 μM + Q, $n = 27$), or a fixed concentration of sahaquine (10 μM $n = 30$) and increasing concentrations of quercetin (Q 10 μM, $n = 37$, Q 100 μM, $n = 41$, Q 200 μM, $n = 28$, Q 10 μM + Sq, $n = 34$, Q 100 μM + Sq, $n = 35$, Q 200 μM + Sq, $n = 21$). Each point represents a percentage value normalized to the untreated control (**e** $n = 47$, **f** $n = 125$). Horizontal bars represent the mean (SD) from at least three independent experiments (***$p < 0.001$ compared to the untreated control; $^{###}p < 0.001$ compared to **e** Q 100 μM alone or **f** Sq 10 μM alone; Welch's ANOVA with Games–Howell post hoc test). Cell viability was measured by counting Hoechst 33342-labeled nuclei imaged using a fluorescence microscope

was most effective, reducing migration by 42%. This effect was not observed when combining sahaquine with TMZ. In contrast, sahaquine significantly inhibited GBM invasiveness, whereas quercetin and TMZ reduced cell invasion by 35 and 45% after 4 days, respectively (Fig. 4c). GBM invasiveness is enabled by MMP degradation of the extracellular matrix and basement membranes[34,35]. We investigated the effect of the selected compounds on the abundance of secreted MMPs using gelatin zymography and showed that quercetin decreases MMP abundance in a dose-dependent manner (Supplementary Fig. S5). Neither sahaquine nor TMZ reduced MMP concentrations,

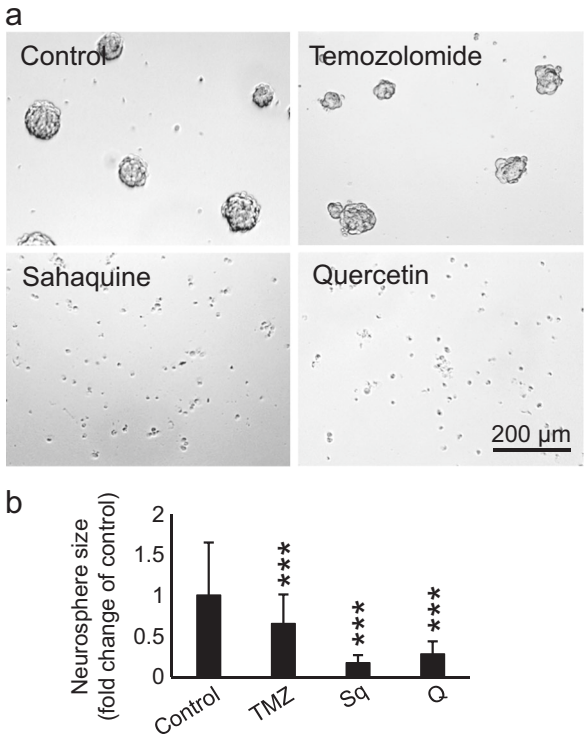

Figure 3 Sahaquine and quercetin are most effective in killing human brain cancer stem cells. a Representative micrographs of BTSCs treated with temozolomide (100 µM, $n = 99$), sahaquine (10 µM, $n = 183$) or quercetin (100 µM, $n = 264$) for 7 days. **b** The surface area of neurospheres was measured based on 2D micrographs from three independent experiments. Shown are average values (SD) normalized to the untreated controls (set to 1, $n = 334$) (***$p < 0.001$, Welch's ANOVA with Games–Howell post hoc test)

although the hydroxamic acid moiety in sahaquine can bind zinc within the MMP structure[36]. The primaquine moiety of sahaquine contributed to the inhibition of P-glycoprotein, as assessed by intracellular retention of calcein-AM (Supplementary Fig. S6). The primaquine concentration within sahaquine (10 µM) effectively inhibited P-glycoprotein activity, whereas 60 µM of unincorporated primaquine was required to achieve a comparable effect. A smaller extent of P-glycoprotein inhibition by SAHA was obtained with equimolar sahaquine concentrations (10 µM) (Supplementary Fig. S6).

Sahaquine selectively inhibits HDAC6

We further examined the HDAC inhibitory activity of sahaquine compared to its parent compound SAHA. SAHA is a pan-HDAC inhibitor that caused an increase in both acetylated α-tubulin (K40) and acetylated histone H3 (K9/K14) (Fig. 5). We hypothesized sahaquine to be selective toward HDAC6, because its bulky capping group would fit better into the wide binding site of the enzyme[37,38]. Nanomolar concentrations (100 nM) of sahaquine resulted in a 1.5-fold increase in acetylated α-tubulin compared to the untreated control, but did not affect histone acetylation (Fig. 5a). Similar results were obtained with the HDAC6-selective inhibitor ACY-1215 (Supplementary Fig. S7). TMZ and quercetin did not inhibit HDAC6. These results were supported by Western blot analyses (Fig. 5c). HDAC6 abundance was comparable following all treatments, suggesting that sahaquine inhibited the enzyme activity without affecting its protein levels (Fig. 5d).

Sahaquine reduces EGFR abundance, ERK1/2, and AKT phosphorylation

EGFR overexpression and downstream hyperactivity of ERK1/2 and AKT are associated with worse prognosis in GBM[39,40]. We assessed the abundance of these markers and HDAC6 in GBM by immunohistochemistry, and showed an increase in EGFR, dually phosphorylated (active) ERK1/2, phosphorylated (active) AKT, and HDAC6 compared to control brains (Fig. 6a). To test whether sahaquine impinges on EGFR and the activation of downstream kinases, we measured EGFR abundance, dual ERK1/2 phosphorylation (Thr202/Tyr204), and AKT phosphorylation (Ser473) by Western blotting (Fig. 6b). Sahaquine reduced EGFR concentrations in GBM. Interestingly, combining sahaquine and TMZ abrogated this inhibitory effect. Sahaquine also reduced levels of phosphorylated ERK1/2 and phosphorylated AKT, alone and in combination with quercetin or TMZ. Total ERK1/2 and AKT protein levels remained unchanged (Supplementary Fig. S8).

Discussion

Results from this study show that sahaquine is more effective than TMZ in killing glioblastoma and BTSCs, as well as inhibiting glioblastoma invasiveness. The mode of action of sahaquine implicates in part excessive α-tubulin acetylation due to the selective inhibition of HDAC6, resulting in cytoskeletal reorganization (Supplementary Fig. S9) and reduced invasiveness. Additional modes of action involve decreased EGFR abundance and downstream activity of AKT and ERK1/2. These results are particularly striking in combination with TMZ or quercetin.

TMZ is one of few clinically approved drugs for the treatment of GBM, but a substantial portion of newly diagnosed tumors and recurrent tumors are resistant to this drug[3,41]. HDAC inhibitors are of particular interest for GBM treatment, as their effectiveness is unaltered by mechanisms of resistance upregulated in GBM, such as mismatch-repair, O^6-methylguanine methyltransferase and base-excision repair[3,4,42]. The pan-HDAC inhibitor SAHA is currently in clinical trials for GBM, but results so far showed marginal improvement in overall survival (5.7 months compared to

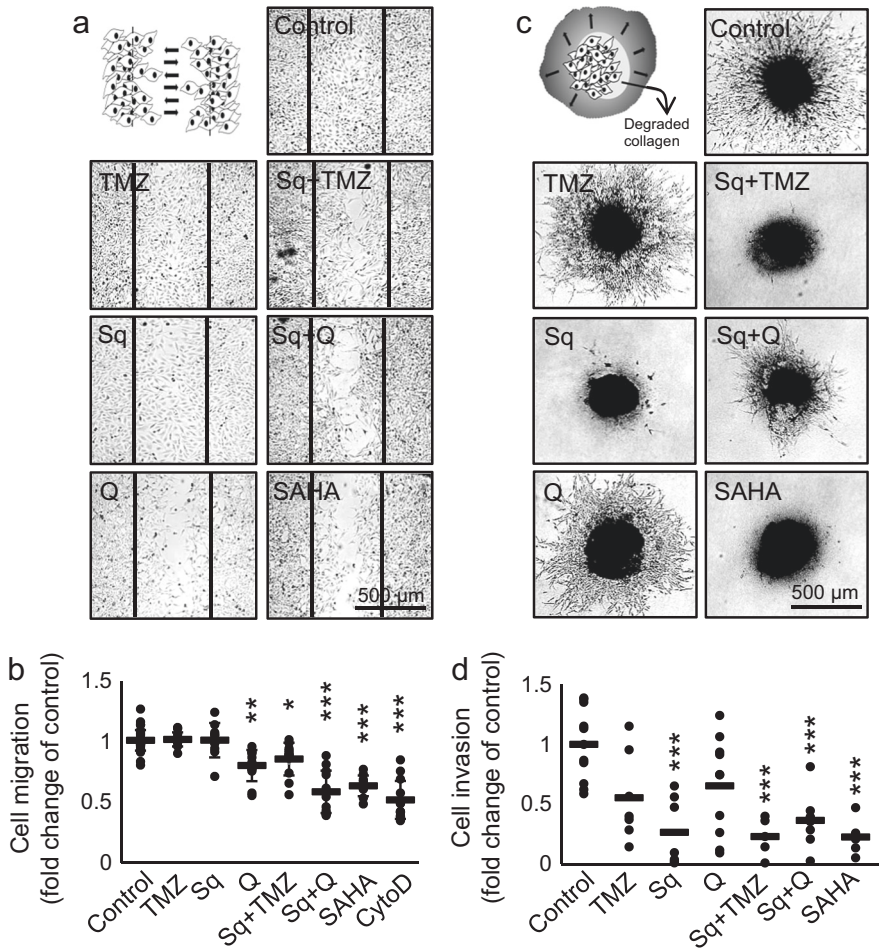

Figure 4 Sahaquine inhibits human glioblastoma cell migration and invasion. Cell migration was measured using the scratch assay, as schematically represented in **a**. Representative micrographs show migration of cells into the scratch (delineated by vertical black bars) after treatment with temozolomide (100 µM, $n = 12$), sahaquine (Sq, 10 µM, $n = 10$), quercetin (Q, 100 µM, $n = 12$) or SAHA (10 µM, $n = 10$), alone or in combination (Sq + TMZ, $n = 12$; Sq + Q, n = 12) for 24 h. Cytochalasin D (40 nM, $n = 13$) served as a positive control. **b** Cell migration was quantified as the area covered by migrating cells. Each point represents a value normalized to the untreated control (set to 1, $n = 35$). Horizontal bars represent the mean (SD) from at least three independent experiments (*$p < 0.05$, **$p < 0.01$, ***$p < 0.001$, Welch's ANOVA with Games–Howell post hoc test). **c** Cell invasion was measured from the radial movement of cells from 3D tumoroids embedded in a collagen matrix, as schematically represented in the first panel. Representative micrographs show cell movement from 3D tumoroids treated with temozolomide (100 µM, $n = 7$), sahaquine (Sq, 10 µM, $n = 7$), quercetin (Q, 100 µM, $n = 10$), or SAHA (10 µM, $n = 5$), alone or in combination (Sq + TMZ, $n = 5$; Sq + Q, $n = 8$) after 4 days. **d** Cell invasion was quantified from the area covered by invading cells. Each point represents a value normalized to the untreated control (set to 1, $n = 11$). Horizontal bars represent the mean from at least three independent experiments (***$p < 0.001$, two-tailed one-way ANOVA with Tukey–Kramer's post hoc test)

4.4 months) and several serious side effects[6–9,43,44]. This and other current therapeutic interventions for GBM are ineffective[28,29,31].

Thus, our goal was to test a new hybrid compound. The development of hybrid molecules is one of the most active areas in therapeutics. Hybrid compounds can have multiple targets, reducing the risk of resistance, lowering effective doses, and decreasing side effects[45,46]. Sahaquine is a hybrid molecule consisting of hydroxamic acid and primaquine linked by a dicarboxylic acid. Primaquine is a strong base (pI = 13.7), but addition of the hydroxamic acid group lowers its pI to 6.48, making sahaquine a weak acid. Weak acids are more advantageous than weak bases as anticancer therapeutics, because they will not be protonated in the acidic tumor environment or trigger lysosomal exocytosis[16–18]. Similarly to primaquine, sahaquine can also inhibit P-glycoprotein activity (Supplementary Fig. S6), thereby preventing multidrug resistance.

One of the great challenges in GBM treatment is heterogeneity, both within and between tumors[47–50]. Interpatient heterogeneity has been shown through genomic and transcriptomic analyses by the Cancer Genome Atlas research network[51,52]. Intratumoral heterogeneity can be attributed to the different cellular lineages and subtypes

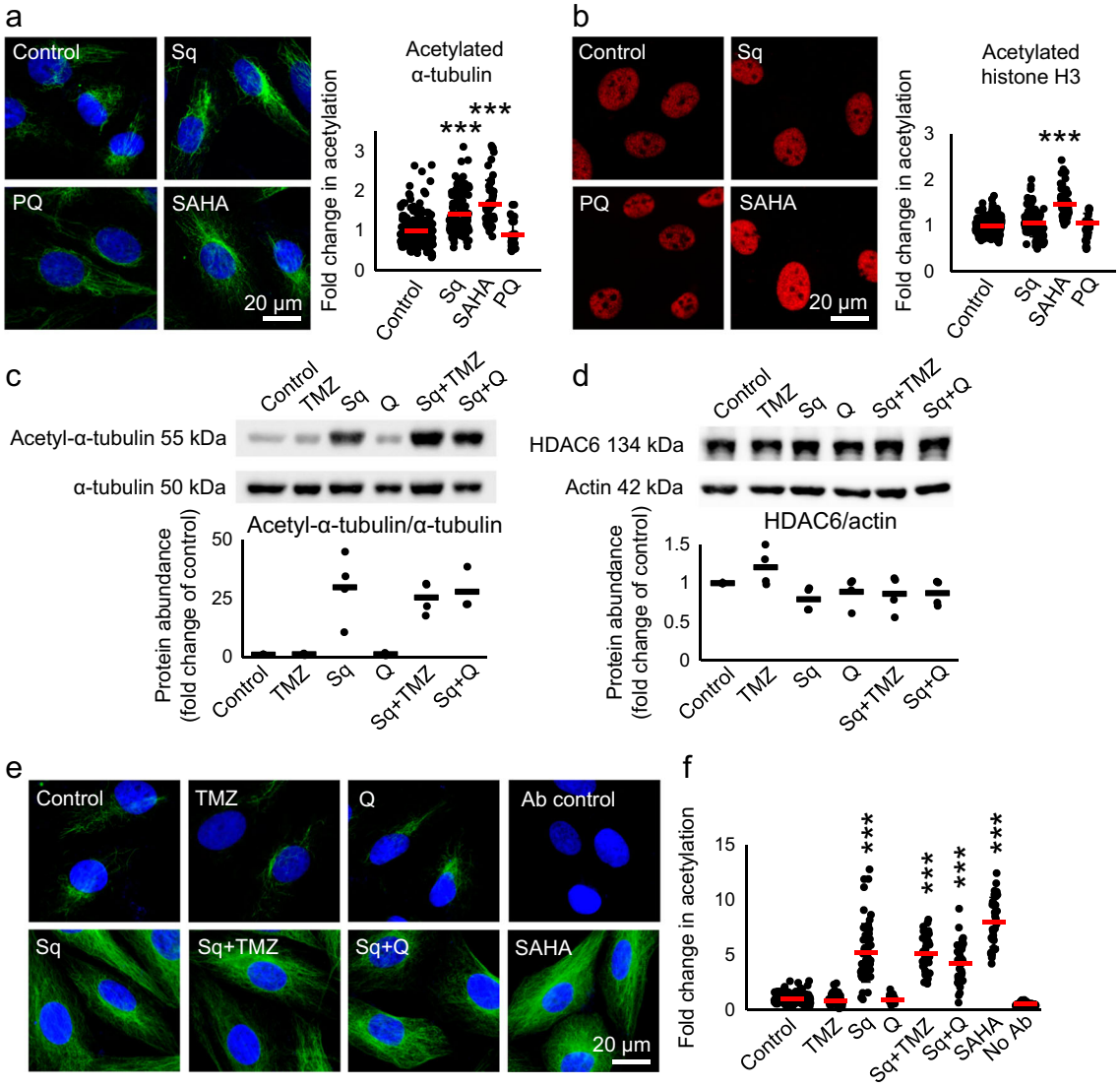

Figure 5 Sahaquine-mediated HDAC6 inhibition results in selective α-tubulin hyperacetylation at nanomolar concentrations. a Representative fluorescence micrographs of GBM α-tubulin acetylation (green) at lysine 40 in response to sahaquine (Sq, 100 nM, $n = 121$ cells), SAHA (100 nM, $n = 54$ cells) or primaquine (PQ, 10 μM, $n = 30$ cells) treatment for 24 h. **b** Representative fluorescence micrographs of GBM histone H3 acetylation (red) at lysine 9/lysine 14 in response to sahaquine (Sq, 100 nM, $n = 120$ cells), SAHA (100 nM, $n = 90$ cells) or primaquine (PQ, 10 μM, $n = 83$ cells) for 24 h. Nuclei (blue) were labeled with Hoechst 33342. Cells were imaged using a fluorescence microscope and fluorescence was analyzed in ImageJ. Shown are averages of fluorescence per cell (SD) normalized to the untreated controls (set to 1) from at least three independent experiments (***$p < 0.001$, Welch's ANOVA with Games–Howell post hoc test). **c** Acetylated α-tubulin ($n = 3$) and **d** HDAC6 protein abundance ($n = 4$) in GBM cells treated with temozolomide (TMZ, 100 μM), sahaquine (Sq, 10 μM) or quercetin (Q, 100 μM) alone or in combination for 24 h, measured by Western blotting. Acetylated α-tubulin and HDAC6 were normalized to total α-tubulin and actin, respectively. Each point represents a value normalized to the untreated control (set to 1). Horizontal bars represent the mean from at least three independent experiments. **e** Representative fluorescence micrographs of GBM α-tubulin acetylation (green) at lysine 40 in response to temozolomide (TMZ, 100 μM, $n = 76$ cells), sahaquine (Sq, 10 μM, $n = 56$ cells), quercetin (Q, 100 μM, $n = 32$ cells) or SAHA (10 μM, $n = 36$ cells) alone or in combination for 24 h. Nuclei (blue) were labeled with Hoechst 33342. **f** Shown are averages (SD) of fluorescence per cell normalized to the untreated control (set to 1, $n = 197$ cells) from at least three independent experiments (***$p < 0.001$, Welch's ANOVA with Games–Howell post hoc test)

present in different parts of the same tumor[53,54], or even in individual cells within a tumor[52,55]. Another cause of GBM heterogeneity is the presence of BTSCs, a subset of glioma cells with the abilities of self-renewal, differentiation, and recapitulation of the original tumor upon xenotransplantation[56–58]. They are resistant to radiation[28] and chemotherapy[59–61], and are thought to promote tumor recurrence[30,31]. Therefore, effective GBM treatment demands a better understanding of tumor origin and heterogeneity to identify new therapeutic targets[3,62].

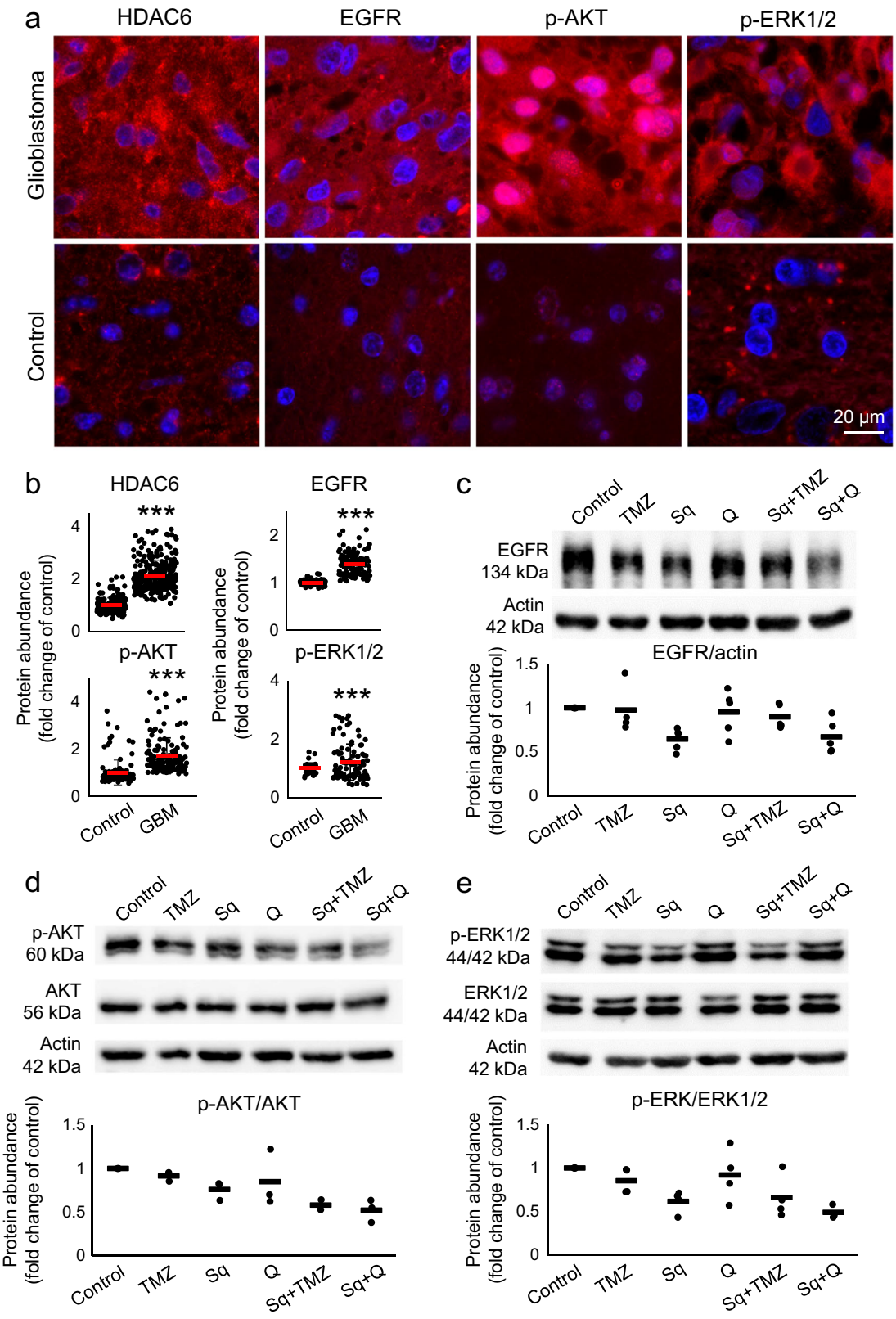

Figure 6 (See legend on next page.)

(see figure on previous page)

Figure 6 Sahaquine reduces EGFR abundance and AKT/ERK1/2 phosphorylation in human glioblastoma. a Representative fluorescence micrographs of human brain sections (GBM or healthy control) labeled for HDAC6, EGFR, phosphorylated AKT (p-AKT), or dually phosphorylated ERK1/2 (p-ERK1/2). Nuclei (blue) were labeled with Hoechst 33342. Cells were imaged using a fluorescence microscope and fluorescence was analyzed in ImageJ. **b** Horizontal bars represent averages of fluorescence per cell (SD) for HDAC6 (control, $n = 181$ cells, GBM, $n = 272$ cells), EGFR (control, $n = 94$ cells, GBM, $n = 116$ cells), p-AKT (control, $n = 115$ cells, GBM, $n = 147$ cells) and p-ERK1/2 (control, $n = 35$ cells, GBM, $n = 104$ cells). Each point represents a value normalized to the healthy control (set to 1) (***$p < 0.001$, Welch's ANOVA with Games–Howell post hoc test). **c** EGFR (TMZ, $n = 4$, Sq, $n = 5$, Q, $n = 5$, Sq + TMZ, $n = 5$, Sq + Q, $n = 5$), **d** phosphorylated AKT ($n = 3$), and **e** phosphorylated ERK1/2 (TMZ, $n = 4$, Sq, $n = 4$, Q, $n = 4$, Sq + TMZ, $n = 4$, Sq + Q, $n = 3$) protein abundances were measured in GBM cells treated with temozolomide (TMZ, 100 μM), sahaquine (Sq, 10 μM), or quercetin (Q, 100 μM) alone or in combination for 24 h, by Western blotting. EGFR protein abundance was normalized to the actin loading control. Phosphorylated AKT and ERK1/2 were normalized to total AKT and total ERK1/2, respectively. Each point represents a value normalized to the untreated control (set to 1). Horizontal bars represent means from at least three independent experiments

Sahaquine (10 μM) abolished the formation of BTSC neurospheres and significantly reduced the size of BTSC aggregates. TMZ was less effective, even at a tenfold higher concentration (100 μM). Quercetin was as effective as sahaquine in killing BTSCs, but showed limited cytotoxicity toward differentiated GBM cells. Sahaquine eliminated both BTSCs and differentiated cancer cells.

Another factor contributing considerably to GBM recurrence is tumor invasiveness. While sahaquine abolished invasiveness and contributed to the loss of tumoroid viability, it did not markedly affect the abundance of secreted MMPs. In contrast, quercetin had limited effects on tumoroid viability, but decreased GBM invasion by inhibiting MMP secretion. Quercetin inhibits nuclear factor-κB (NF-κB) nuclear translocation, which could alter MMP expression[63,64] and enhance cell death through NF-κB-dependent regulation of apoptosis.

In an effort to reduce undesirable side effects in normal cells, selective HDAC inhibitors have been developed[65,66]. Ricolinostat (ACY-1215) is a selective HDAC6 inhibitor currently in clinical trials (phase I and II) in combination with pomalidomide for multiple myeloma[67]. Ricolinostat inhibits heat shock protein 90 deacetylation, resulting in an accumulation of unfolded proteins, disruption of protein homeostasis and cell death[68]. We show that sahaquine selectively inhibits HDAC6 at nanomolar concentrations, which distinguishes it from SAHA, which is non-selective at equimolar concentrations. Interestingly, sahaquine significantly reduced the abundance of heat shock protein 70 in GBM (Supplementary Fig. S10) and altered α-tubulin organization. We have previously shown that celastrol disrupts protein homeostasis[69] and the organization of the F-actin cytoskeleton in GBM[70]. Future studies will have to evaluate how sahaquine affects proteostasis in relation to cytoskeletal dynamics.

Many drugs currently in clinical trials aim at inhibiting proteins and proliferation pathways deregulated in GBM, notably HDAC6, EGFR, AKT, and ERK1/2[71–74]. Our in vitro studies showing enhanced ERK1/2 and AKT phosphorylation are corroborated by immunohistochemical data in tumor sections from GBM patients (Fig. 6a), also showing markedly stronger signals for HDAC6, EGFR, phosphorylated ERK1/2, and phosphorylated AKT compared to normal brain tissue (Fig. 6a). Sahaquine can decrease the abundance of EGFR, phosphorylated AKT, and phosphorylated ERK1/2 in GBM (Fig. 6b), thereby suggesting that similar hybrid molecules are viable candidates for GBM combination therapy. Interestingly, AKT deacetylation by HDAC6 promotes cancer growth and proliferation[75], indicating that sahaquine could reduce AKT activation through HDAC6 inhibition.

Drug resistance is a major problem in glioblastoma therapy[3,41]. A recent study of HDAC inhibitors in drug-resistant melanoma implicated increased levels of reactive oxygen species[76]. Combination of sahaquine with buthionine sulfoximine, which depletes endogenous glutathione levels[77], sensitized GBM cells to reactive oxygen species and enhanced cell death (Supplementary Fig. S11), although buthionine sulfoximine alone in the tested concentration had no effect on GBM viability. Further analysis of the effect of sahaquine on reactive oxygen species production in GBM is warranted.

Taken together, our study reveals sahaquine as a therapeutic agent affecting multiple cellular factors and processes that are critical for GBM treatment (Fig. 7). Sahaquine is superior to the clinical standard TMZ in reducing GBM and BTSC viability, invasiveness, and markers of key survival pathways. These effects are even more profound when sahaquine is combined with TMZ, buthionine sulfoximine, or quercetin. In conclusion, sahaquine is an effective cell death inducer which eliminates not only GBM cells but also BTSCs, thus suggesting that evaluation of sahaquine in combination with other drugs merit further investigations in patient-derived organoids, and eventually in humans.

Materials and methods

Synthesis of sahaquine

Sahaquine **5** was synthesized in four reaction steps (Fig. 1) adapted from the synthetic approach of Zhang et al[45]. Details of these steps are provided in the Supplementary Information. The first step included amide bond

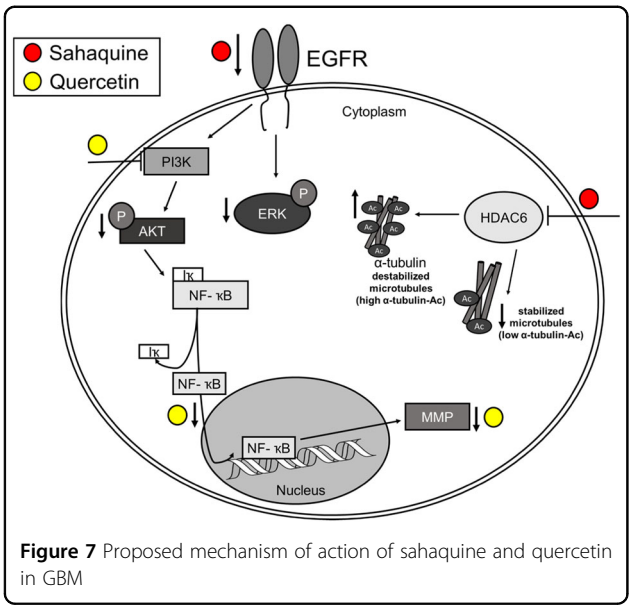

Figure 7 Proposed mechanism of action of sahaquine and quercetin in GBM

formation between mono-methyl glutarate (**1**, Sigma-Aldrich, St. Louis, MO, USA) and primaquine (Sigma-Aldrich, St. Louis, MO, USA), with 1-[*bis*(dimethylamino) methylene]-1*H*-1,2,3-triazolo[4,5-*b*]pyridinium 3-oxid hexafluorophosphate (HATU, Alfa Aesar, Thermo Fisher, Kandel, Germany) as a coupling agent and *N,N*-diisopropylethylamine (DIEA, Alfa Aesar, Thermo Fisher, Kandel, Germany) as a base. The prepared product **2** was further hydrolyzed with lithium hydroxide (Sigma-Aldrich, St. Louis, MO, USA) and gave carboxylic acid **3**. In the next step, **3** was coupled with *O*-benzylhydroxylamine (Sigma-Aldrich, St. Louis, MO, USA) in the presence of HATU/DIEA and yielded *O*-benzylhydroxamic acid **4**, which was deprotected by catalytic hydrogenation and gave the target compound **5** (sahaquine). All reactions proceeded at room temperature.

Cell culture and tissue samples

U251N human glioblastoma cells were originally obtained from the American Type Culture Collection. Cells were cultured in Dulbecco's modified Eagle's media (DMEM, Gibco, Thermo Fischer Scientific, Grand Island, NY, USA) supplemented with 5% (v/v) fetal bovine serum (Wisent, St. Bruno, Canada) and 1% (v/v) penicillin–streptomycin (Thermo Fisher Scientific, Eugene, OR, USA) at 37 °C with 5% CO_2 and 95% relative humidity, unless otherwise indicated. Glioblastoma samples were harvested under a protocol approved by the Montreal Neurological Hospital's research ethics board (NEU-10-066). Consent was given by all patients. At least 116 brain sections from GBM patients aged 55–76 and controls were used. Tissues were from the frontal, temporal, or parietal lobes of the cerebral cortex. Human BTSCs were expanded as neurospheres in complete NeuroCult^{TM} proliferation media (Stemcell Technologies, Vancouver, BC, Canada). NeuroCult^{TM} basal medium contained: NeuroCult^{TM} NS-A proliferation supplement (1/10), recombinant human epidermal growth factor EGF (20 ng/ml), recombinant human basic fibroblast growth factor (20 ng/ml), and heparin (2 μg/ml).

Cell counting assay

U251N cells were seeded in 96-well black plates (Costar, Corning, NY, USA) at 5,000 cells per well in 0.1 ml media and cultured for 24 h. Cells were treated with sahaquine (0.001, 1, 5, 10, 20, 25, 30, 40, and 50 μM), TMZ (0.001, 1, 10, 50, 100, 200, 300, 400, and 500 μM, Sigma-Aldrich, St. Louis, MO, USA), quercetin (0.001, 1, 10, 25, 50, 75, 100, 200, and 300 μM, Sigma-Aldrich, St. Louis, MO, USA), or SAHA (0.001, 0.1, 1, 2, 5, 8, 10, 25, and 50 μM, Cayman Chemical, Ann Arbor, MI, USA) for 24 or 72 h. Combination treatments included increasing concentrations of sahaquine (0.001, 1, 3, 5, 7, 10, 20, and 50 μM) with quercetin (100 μM), increasing concentrations of quercetin (0.001, 1, 10, 25, 50, 100, and 200 μM) with sahaquine (10 μM), TMZ (30 μM) with sahaquine (10 μM), quercetin (140 μM) or SAHA (1 μM), and buthionine sulfoximine (100 μM, Sigma-Aldrich, St. Louis, MO, USA) with sahaquine (10 μM) for 24 h or 72 h. Following treatment, cells were fixed with 4% paraformaldehyde (w/v, 10 min, BDH, Toronto, ON, Canada). Nuclei were labeled with Hoechst 33342 (10 μM, 10 min, Thermo Fisher Scientific, Eugene, OR, USA). Cells were washed with phosphate-buffered saline and imaged using a fluorescence microscope (Leica DMI4000B, Toronto, ON, Canada).

BTSC viability

48EF human brain tumor cells were seeded at 5,000 cells per well in 96-well plates (Sarstedt, Nümbrecht, Germany) and treated for 7 days. Cells were then imaged using light microscopy (Leica DMI4000B) and the surface areas of the neurospheres were measured in ImageJ (version 1.51s).

Scratch assay

U251N cells were seeded in 6-well plates (Sarstedt, Nümbrecht, Germany) at 1,500,000 cells per well in 1 ml media and cultured for 24 h. The scratch was performed by gently dragging a 200 μl pipette tip across the cell monolayer, after which cells were washed with phosphate-buffered saline and incubated in DMEM with or without treatment. Cytochalasin D (40 nM, Sigma-Aldrich, St. Louis, MO, USA) served as positive control. Predetermined areas of the wells were imaged using light microscopy immediately after the scratch (time = 0 h) and after 24 h. The cell-free area of the scratch was measured in ImageJ.

Cell invasion assay

U251N tumoroids were prepared using the hanging drop method[78]. Drops of 30,000 cells in 20 µl medium were pipetted onto the inner side of a 10 cm Petri dish (Thermo Fisher Scientific, Eugene, OR, USA) lid. The lid was quickly flipped to cover the Petri dish filled with 20 ml phosphate-buffered saline. Hanging drops were cultured at 37 °C for 48 h to allow tumoroids to form. Tumoroids were then gently scooped into a medium-filled Petri dish coated with 2% agarose and cultured for 48 h. Tumoroids were implanted in collagen gel (Advanced BioMatrix, San Diego, CA, USA) mixed with DMEM (1×) and sodium hydroxide (10 mM, Sigma-Aldrich, St. Louis, MO, USA). Gels were covered with 500 µl DMEM with or without treatment. Tumoroids were imaged using light microscopy immediately after implantation (time = 0 day) and after 4 days. The area of cell invasion was measured in ImageJ.

Immunocytochemistry

Following treatment, U251N human glioblastoma cells were fixed with 4% paraformaldehyde (10 min), and then permeabilized using 0.1% Triton X-100 (v/v, 10 min, Sigma-Aldrich, St. Louis, MO, USA). Blocking was performed with 10% goat serum (v/v, 1 h, Thermo Fisher Scientific, Eugene, OR, USA) in phosphate-buffered saline, and then samples were incubated with primary antibodies (acetyl-histone H3 K9/K14, 1/500, Cell Signalling, #9677; acetyl-α-tubulin K40, 1/500, Santa Cruz, sc-23950; α-tubulin, 1/1000, Abcam, ab7291) overnight at 4 °C in a humidified chamber. Samples were washed three times with phosphate-buffered saline with 5 min incubation between washes. Secondary antibodies (anti-rabbit Alexa Fluor 488, 1/500, Thermo Fisher Scientific, A11008; anti-mouse Alexa Fluor 647, 1/500, Thermo Fisher Scientific, A28181) were incubated with samples for 1 h in the dark, and then washed off three times with phosphate-buffered saline with 5 min incubation in between washes. Nuclei were labeled with Hoechst 33342 (10 µM, 10 min). Samples were mounted on microscope slides using Aqua-Poly/Mount (Polysciences, Warrington, PA, USA) and dried overnight before imaging with a fluorescence microscope (Leica DMI4000B).

Immunohistochemistry

Human brain sections were dewaxed in xylene, and then rehydrated in ethanol. Antigen retrieval was performed in citrate buffer using a decloaking chamber for 3 h. Samples were washed twice with double-distilled water, three times with phosphate-buffered saline, and then blocked with Protein Block (10 min, Spring Biosciences, Pleasanton, CA, USA). Samples were incubated with primary antibodies (HDAC6, 1/100, Santa Cruz, sc-11420; EGFR, 1/100, Oncogene Science Ab-1; phospho-AKT Ser473, Cell Signalling, #9271; phospho-p44/42 Erk1/2 Thr202/Tyr204, 1/100, Cell Signalling, #9101) overnight at 4 °C in a humidified chamber. Samples were washed twice with IF buffer (0.05% (v/v) Tween 20, 0.2% (v/v) Triton X-100 in phosphate-buffered saline). Secondary antibodies (anti-rabbit Alexa Fluor 647, 1/500, Thermo Fisher Scientific, A21245; anti-rabbit Alexa Fluor 488, 1/1000, Thermo Fisher Scientific, A27034; anti-mouse Alexa Fluor 647, 1/1000, Thermo Fisher Scientific, A-21235) diluted in 2% (w/v) bovine serum albumin (Sigma-Aldrich, St. Louis, MO, USA) in phosphate-buffered saline were incubated with samples for 1 h in the dark at room temperature. Samples were washed three times with IF buffer, and then nuclei were labeled with DAPI (4′,6-diamidino-2-phenylindole; 1 µg/ml, 5 min, Molecular Probes, Eugene, OR, USA). Samples were washed three times with phosphate-buffered saline, then mounted on microscope slides using mounting media (Dako, Mississauga, ON, Canada), and air-dried for at least 30 min. Samples were imaged using a fluorescence microscope (Leica DMI4000B).

Western blotting

Western blot analysis followed published procedures[70]. In brief, crude extracts were separated by sodium dodecyl sulfate–polyacrylamide gel electrophoresis (SDS-PAGE) and blotted onto nitrocellulose membranes. Blocked filters were probed with antibodies against acetyl-α-tubulin K40 (1/10,000, Sigma-Aldrich, St. Louis, MO, USA, #T7451), α-tubulin (1/1000, Santa Cruz, sc-5286), phospho-AKT Ser473 (1/2000, Santa Cruz, sc-7985), pan-AKT (1/1500, Cell Signaling, #9272), HDAC6 (1/1000, Santa Cruz, sc-11420), EGFR (1/1000, Santa Cruz, sc-03), phospho-ERK1/2 Thr202/Tyr204 (1/2000, Cell Signaling, #9106), pan-ERK1/2 (1/2000, Cell Signaling, #4695), and actin (1/100,000, Chemicon, MAB1501). Signals for enhanced chemiluminescence were acquired with a Bio-Rad ChemiDoc™ MP imaging system and quantified.

MTT assay

U251N cells were seeded in 24-well plates (Sarstedt, Nümbrecht, Germany) at 50,000 cells per well in 300 µl media and cultured for 24 h. Cells were treated with sahaquine (0.001, 1, 5, 10, 25, and 50 µM), TMZ (50, 100, 200, 300, 400, and 500 µM), quercetin (10, 50, 100, and 200 µM), or SAHA (0.1, 1, 2, 5, 8, 10, and 50 µM) for 72 h. Combination treatments included increasing concentrations of sahaquine (1, 10, and 50 µM) with a fixed concentration of quercetin (100 µM), or increasing concentrations of quercetin (10, 100, and 200 µM) with a fixed concentration of sahaquine (10 µM) for 72 h. Following treatment, MTT (Sigma-Aldrich, St. Louis, MO, USA) dissolved in phosphate-buffered saline was added to cells (0.5 mg/ml) for 1 h at 37 °C. After MTT-containing media were removed, dimethyl sulfoxide (0.5 ml) was added to each well to lyse cells and dissolve formazan.

Wells were sampled in triplicate and the optical density was measured at 595 nm using a microplate reader (Asys UVM 340, Biochrom, Holliston, MA, USA).

Gelatin zymography

U251N cells were seeded in 60-mm tissue culture dishes (Thermo Fisher Scientific, Rochester, NY, USA) at 1,500,000 cells per dish in 3 ml media and cultured for 24 h. Cells were treated in serum-deprived DMEM for 24 h. Following treatment, culture media were collected and concentrated 15-fold using 30 kDa centrifugal filters (Millipore, Cork, Ireland) following the manufacturer's recommendations. Concentrated media were separated by SDS-PAGE using gelatin (0.1%, w/v) and acrylamide (7.5%, w/v) gels under non-reducing conditions. Gels were washed for 30 min in renaturing solution (2.5% (v/v) Triton X-100 in double-distilled water) and 30 min in developing buffer (50 mM Tris, pH 7.8; 1% (v/v) Triton X-100; 1 µM $ZnCl_2$, 5 mM $CaCl_2$, adjusted to pH 7.45). Gels were then incubated in fresh developing buffer at 37 °C overnight. Gels were stained with 0.5% (w/v) Coomassie Blue G250 (Bio-Rad, Richmond, CA, USA) dissolved in 40% (v/v) ethanol and 10% (v/v) acetic acid for 1 h, and then destained in 40% ethanol and 10% acetic acid diluted in double-distilled water, until clear bands appeared. Quantification of MMP-9 and MMP-2 abundance (as band area) was done in ImageJ.

Tumoroid viability

U251N tumoroids were prepared using the liquid overlay system[79]. The 96-well cell culture plates were coated with 75 µl of 2% (w/v) agarose (Life Technologies, Gaithersburg, MD, USA) dissolved in serum-deprived DMEM. The agarose was cooled for 30 min, then cells were seeded at 5,000 cells per well in 200 µl media, and cultured for 4 days before treatment. Cells were treated for 7 days, and then imaged using a microscope (Leica DMI4000B). The surface area of tumoroids was analyzed in ImageJ.

Calcein-AM uptake

U251N cells were seeded in 96-well black plates at 5,000 cells per well in 0.1 ml media and cultured for 24 h before treatment. Cyclosporine A (Calbiochem, Toronto, Canada) served as a positive control for the inhibition of P-glycoprotein. Following treatment, cells were incubated in phenol-free Hanks' balanced Salt solution containing calcein-AM (0.5 µM, Thermo Fisher Scientific, Eugene, OR, USA) and propidium iodide (3 µM, Sigma-Aldrich, St. Louis, MO, USA) for 30 min at 37 °C. The media were replaced with fresh Hanks' balanced salt solution and cells were imaged using a fluorescence microscope (Leica DMI4000B). Cells positively labeled with propidium iodide were excluded from the analysis.

Statistics

Experiments were performed independently at least three times. Unless otherwise indicated, data are shown as mean (SD). Normality of data distribution was assessed by the Shapiro–Wilk test. For sample sizes larger than 30, the Central Limit Theorem allows the assumption of normal distribution. Equality of variances was assessed by Levene's test. If the assumptions of normality and homogeneity of variance were met, two-tailed one-way analysis of variance (ANOVA) with Tukey–Kramer's post hoc test were performed. If homogeneity of variance was not observed, Welch's ANOVA with the Games–Howell post hoc test were used. A p value smaller than 0.05 was considered statistically significant: $^{*}p < 0.05$, $^{**}p < 0.01$, and $^{***}p < 0.001$.

Acknowledgements

We wish to thank J. Choi and E. Gran for their contribution to initial experiments related to this study. D.M. thanks the Canadian Institute for Health Research (MOP-119425) and the Natural Sciences and Engineering Council of Canada (RGPIN 04994-15). K.P. is grateful to the Brilliant Night Foundation, and B.Z. thanks the Croatian Science Foundation (IP-2014-09-1501) for financial support.

Authors' contributions

D.M. designed and coordinated the project. M.B., I.Z., and U.S. performed the experiments. M.B., I.Z., D.M., and U.S. analyzed and discussed the data. D.M., U. S., P.U.L., K.P., B.Z., and Z.R. contributed with reagents or clinical samples and discussion. M.B., I.Z., and D.M. wrote the manuscript with the help from the rest of the authors.

Author details

[1]Department of Pharmacology and Therapeutics, McGill University, Montreal, QC, Canada. [2]Faculty of Pharmacy and Biochemistry, University of Zagreb, Zagreb, Croatia. [3]Department of Physiology, McGill University, Montreal, QC, Canada. [4]Brain Tumour Research Centre, Montreal Neurological Institute and Hospital, Department of Neurology and Neurosurgery, McGill University, Montreal, QC, Canada

Conflict of interest

The authors declare that they have no conflict of interest.

The online version of this article (https://doi.org/10.1038/s41420-018-0103-0) contains supplementary material, which is available to authorized users.

Received: 16 July 2018 Revised: 10 August 2018 Accepted: 21 August 2018
Published online: 26 September 2018

References

1. Weller, M. et al. European Association for Neuro-Oncology (EANO) guideline on the diagnosis and treatment of adult astrocytic and oligodendroglial gliomas. *Lancet Oncol.* **18**, e315–e329 (2017).
2. Weller, M. et al. MGMT promoter methylation in malignant gliomas: ready for personalized medicine? *Nat. Rev. Neurol.* **6**, 39–51 (2010).
3. Hegi, M. E. et al. MGMT gene silencing and benefit from temozolomide in glioblastoma. *N. Engl. J. Med.* **352**, 997–1003 (2005).

4. Erasimus, H., Gobin, M., Niclou, S. & Van Dyck, E. DNA repair mechanisms and their clinical impact in glioblastoma. *Mutat. Res. Rev. Mutat. Res* **769**, 19–35 (2016).
5. Johnstone, R. W. Histone-deacetylase inhibitors: novel drugs for the treatment of cancer. *Nat. Rev. Drug Discov.* **1**, 287–299 (2002).
6. Galanis, E. et al. Phase II trial of vorinostat in recurrent glioblastoma multiforme: a north central cancer treatment group study. *J. Clin. Oncol.* **27**, 2052–2058 (2009).
7. Hummel, T. R. et al. A pediatric phase 1 trial of vorinostat and temozolomide in relapsed or refractory primary brain or spinal cord tumors: a Children's Oncology Group Phase 1 Consortium Study. *Pediatr. Blood Cancer* **60**, 1452–1457 (2013).
8. Lee, E. Q. et al. Phase I study of vorinostat in combination with temozolomide in patients with high-grade gliomas: North American Brain Tumor Consortium Study 04-03. *Clin. Cancer Res.* **18**, 6032–6039 (2012).
9. Vorinostat and Radiation Therapy Followed by Maintenance Therapy With Vorinostat in Treating Younger Patients With Newly Diagnosed Diffuse Intrinsic Pontine Glioma—Full Text View—ClinicalTrials.gov. https://clinicaltrials.gov/ct2/show/NCT01189266 (accessed 31 May 2018).
10. Weathers, S.-P. & Gilbert, M. R. Advances in treating glioblastoma. *F1000Prime Rep.* **6**, 46 (2014).
11. Glozak, M. A. & Seto, E. Histone deacetylases and cancer. *Oncogene* **26**, 5420–5432 (2007).
12. Lee, D. H., Ryu, H.-W., Won, H.-R. & Kwon, S. H. Advances in epigenetic glioblastoma therapy. *Oncotarget* **8**, 18577–18589 (2017).
13. Grant, S., Easley, C. & Kirkpatrick, P. Vorinostat. *Nat. Rev. Drug Discov.* **6**, 21–22 (2007).
14. Bertrand, S., Hélesbeux, J.-J., Larcher, G. & Duval, O. Hydroxamate, a key pharmacophore exhibiting a wide range of biological activities. *Mini Rev. Med. Chem.* **13**, 1311–1326 (2013).
15. Gialeli, C., Theocharis, A. D. & Karamanos, N. K. Roles of matrix metalloproteinases in cancer progression and their pharmacological targeting. *FEBS J.* **278**, 16–27 (2011).
16. Corbet, C. & Feron, O. Tumour acidosis: from the passenger to the driver's seat. *Nat. Rev. Cancer* **17**, 577–593 (2017).
17. Mahoney, B. P., Raghunand, N., Baggett, B. & Gillies, R. J. Tumor acidity, ion trapping and chemotherapeutics. I. Acid pH affects the distribution of chemotherapeutic agents in vitro. *Biochem. Pharmacol.* **66**, 1207–1218 (2003).
18. Zhitomirsky, B. & Assaraf, Y. G. Lysosomal accumulation of anticancer drugs triggers lysosomal exocytosis. *Oncotarget* **8**, 45117–45132 (2017).
19. van Weert, A. W., Geuze, H. J., Groothuis, B. & Stoorvogel, W. Primaquine interferes with membrane recycling from endosomes to the plasma membrane through a direct interaction with endosomes which does not involve neutralisation of endosomal pH nor osmotic swelling of endosomes. *Eur. J. Cell Biol.* **79**, 394–399 (2000).
20. Kim, J.-H., Choi, A.-R., Kim, Y. K. & Yoon, S. Co-treatment with the anti-malarial drugs mefloquine and primaquine highly sensitizes drug-resistant cancer cells by increasing P-gp inhibition. *Biochem. Biophys. Res. Commun.* **441**, 655–660 (2013).
21. Yang, Z. J., Chee, C. E., Huang, S. & Sinicrope, F. A. The role of autophagy in cancer: therapeutic implications. *Mol. Cancer Ther.* **10**, 1533–1541 (2011).
22. Andres S. et al. Safety aspects of the use of quercetin as a dietary supplement. *Mol. Nutr. Food Res.* **62,** https://doi.org/10.1002/mnfr.201700447 (2018).
23. Srivastava, S. et al. Quercetin, a natural flavonoid interacts with DNA, arrests cell cycle and causes tumor regression by activating mitochondrial pathway of apoptosis. *Sci. Rep.* **6**, 24049 (2016).
24. Calgarotto, A. K. et al. Antitumor activities of Quercetin and Green Tea in xenografts of human leukemia HL60 cells. *Sci. Rep.* **8**, 3459 (2018).
25. Sun, S., Gong, F., Liu, P. & Miao, Q. Metformin combined with quercetin synergistically repressed prostate cancer cells via inhibition of VEGF/PI3K/Akt signaling pathway. *Gene* **664**, 50–57 (2018).
26. Zhang, X., Guo, Q., Chen, J. & Chen, Z. Quercetin enhances cisplatin sensitivity of human osteosarcoma cells by modulating microRNA-217-KRAS axis. *Mol. Cells* **38**, 638–642 (2015).
27. Zanini, C. et al. Inhibition of heat shock proteins (HSP) expression by quercetin and differential doxorubicin sensitization in neuroblastoma and Ewing's sarcoma cell lines. *J. Neurochem.* **103**, 1344–1354 (2007).
28. Bao, S. et al. Stem cell-like glioma cells promote tumor angiogenesis through vascular endothelial growth factor. *Cancer Res.* **66**, 7843–7848 (2006).
29. Chen, J., McKay, R. M. & Parada, L. F. Malignant glioma: lessons from genomics, mouse models, and stem cells. *Cell* **149**, 36–47 (2012).
30. Dagogo-Jack, I. & Shaw, A. T. Tumour heterogeneity and resistance to cancer therapies. *Nat. Rev. Clin. Oncol.* **15**, 81–94 (2018).
31. Johnson, B. E. et al. Mutational analysis reveals the origin and therapy-driven evolution of recurrent glioma. *Science* **343**, 189–193 (2014).
32. Chemicalize—Instant Cheminformatics Solutions. https://chemicalize.com/ (accessed 31 May 2018).
33. Holland, E. C. Glioblastoma multiforme: the terminator. *Proc. Natl. Acad. Sci. USA* **97**, 6242–6244 (2000).
34. Nakada, M., Okada, Y. & Yamashita, J. The role of matrix metalloproteinases in glioma invasion. *Front Biosci.* **8**, e261–e269 (2003).
35. Alaseem A. et al. Matrix metalloproteinases: a challenging paradigm of cancer management. *Semin. Cancer Biol.* https://doi.org/10.1016/j.semcancer.2017.11.008 (2017).
36. Jacobsen, J. A., Major Jourden, J. L., Miller, M. T. & Cohen, S. M. To bind zinc or not to bind zinc: an examination of innovative approaches to improved metalloproteinase inhibition. *Biochim. Biophys. Acta* **1803**, 72–94 (2010).
37. Bieliauskas, A. V. & Pflum, M. K. H. Isoform-selective histone deacetylase inhibitors. *Chem. Soc. Rev.* **37**, 1402–1413 (2008).
38. Schäfer, S. et al. Phenylalanine-containing hydroxamic acids as selective inhibitors of class IIb histone deacetylases (HDACs). *Bioorg. Med. Chem.* **16**, 2011–2033 (2008).
39. Sanchez-Vega, F. et al. Oncogenic signaling pathways in the Cancer Genome Atlas. *Cell* **173**, 321–337.e10 (2018).
40. Shinojima, N. et al. Prognostic value of epidermal growth factor receptor in patients with glioblastoma multiforme. *Cancer Res.* **63**, 6962–6970 (2003).
41. Lee, S. Y. Temozolomide resistance in glioblastoma multiforme. *Genes Dis.* **3**, 198–210 (2016).
42. Caporali, S. et al. DNA damage induced by temozolomide signals to both ATM and ATR: role of the mismatch repair system. *Mol. Pharmacol.* **66**, 478–491 (2004).
43. Yin, D. et al. Suberoylanilide hydroxamic acid, a histone deacetylase inhibitor: effects on gene expression and growth of glioma cells in vitro and in vivo. *Clin. Cancer Res.* **13**, 1045–1052 (2007).
44. Peters, K. B. et al. Phase I/II trial of vorinostat, bevacizumab, and daily temozolomide for recurrent malignant gliomas. *J. Neurooncol.* **137**, 349–356 (2018).
45. Zhang, X. et al. The discovery of colchicine-SAHA hybrids as a new class of antitumor agents. *Bioorg. Med. Chem.* **21**, 3240–3244 (2013).
46. Meunier, B. Hybrid molecules with a dual mode of action: dream or reality? *Acc. Chem. Res.* **41**, 69–77 (2008).
47. Cavalli, F. M. G. et al. Intertumoral heterogeneity within medulloblastoma subgroups. *Cancer Cell.* **31**, 737–754.e6 (2017).
48. Hunter, K. W., Amin, R., Deasy, S., Ha, N.-H. & Wakefield, L. Genetic insights into the morass of metastatic heterogeneity. *Nat. Rev. Cancer* **18**, 211–223 (2018).
49. Meacham, C. E. & Morrison, S. J. Tumour heterogeneity and cancer cell plasticity. *Nature* **501**, 328–337 (2013).
50. Lin, C.-C. J. et al. Identification of diverse astrocyte populations and their malignant analogs. *Nat. Neurosci.* **20**, 396–405 (2017).
51. Cancer Genome Atlas Research Network. Comprehensive genomic characterization defines human glioblastoma genes and core pathways. *Nature* **455**, 1061–1068 (2008).
52. Verhaak, R. G. W. et al. An integrated genomic analysis identifies clinically relevant subtypes of glioblastoma characterized by abnormalities in PDGFRA, IDH1, EGFR and NF1. *Cancer Cell* **17**, 98 (2010).
53. Sottoriva, A. et al. Intratumor heterogeneity in human glioblastoma reflects cancer evolutionary dynamics. *Proc. Natl. Acad. Sci. USA* **110**, 4009–4014 (2013).
54. Morrissy, A. S. et al. Spatial heterogeneity in medulloblastoma. *Nat. Genet.* **49**, 780–788 (2017).
55. Patel, A. P. et al. Single-cell RNA-seq highlights intratumoral heterogeneity in primary glioblastoma. *Science* **344**, 1396–1401 (2014).
56. Galli, R. et al. Isolation and characterization of tumorigenic, stem-like neural precursors from human glioblastoma. *Cancer Res.* **64**, 7011–7021 (2004).
57. Lee, J. et al. Tumor stem cells derived from glioblastomas cultured in bFGF and EGF more closely mirror the phenotype and genotype of primary tumors than do serum-cultured cell lines. *Cancer Cell* **9**, 391–403 (2006).
58. Singh, S. K. et al. Identification of human brain tumour initiating cells. *Nature* **432**, 396–401 (2004).
59. Liu, G. et al. Analysis of gene expression and chemoresistance of CD133+ cancer stem cells in glioblastoma. *Mol. Cancer* **5**, 67 (2006).
60. Bleau, A.-M. et al. PTEN/PI3K/Akt pathway regulates the side population phenotype and ABCG2 activity in glioma tumor stem-like cells. *Cell Stem Cell* **4**, 226–235 (2009).

61. Chen S.-F. et al. Nonadhesive culture system as a model of rapid sphere formation with cancer stem cell properties. *PLoS ONE* **7**, https://doi.org/10.1371/journal.pone.0031864 (2012).
62. Fouse, S. D., Nakamura, J. L., James, C. D., Chang, S. & Costello, J. F. Response of primary glioblastoma cells to therapy is patient specific and independent of cancer stem cell phenotype. *Neuro-Oncology* **16**, 361–371 (2014).
63. Bond, M., Chase, A. J., Baker, A. H. & Newby, A. C. Inhibition of transcription factor NF-kappaB reduces matrix metalloproteinase-1, -3 and -9 production by vascular smooth muscle cells. *Cardiovasc. Res.* **50**, 556–565 (2001).
64. Soubannier, V. & Stifani, S. NF-κB signalling in glioblastoma. *Biomedicines* **5**, https://doi.org/10.3390/biomedicines5020029 (2017).
65. Lee, J.-H. et al. Development of a histone deacetylase 6 inhibitor and its biological effects. *Proc. Natl. Acad. Sci. USA* **110**, 15704–15709 (2013).
66. Santo, L. et al. Preclinical activity, pharmacodynamic, and pharmacokinetic properties of a selective HDAC6 inhibitor, ACY-1215, in combination with bortezomib in multiple myeloma. *Blood* **119**, 2579–2589 (2012).
67. ACY-1215 (Ricolinostat) in Combination With Pomalidomide and Low-dose Dex in Relapsed-and-Refractory Multiple Myeloma—Full Text View—ClinicalTrials.gov. https://clinicaltrials.gov/ct2/show/NCT01997840 (accessed 31 May 2018).
68. Kekatpure, V. D., Dannenberg, A. J. & Subbaramaiah, K. HDAC6 modulates Hsp90 chaperone activity and regulates activation of aryl hydrocarbon receptor signaling. *J. Biol. Chem.* **284**, 7436–7445 (2009).
69. Boridy, S., Le, P. U., Petrecca, K. & Maysinger, D. Celastrol targets proteostasis and acts synergistically with a heat-shock protein 90 inhibitor to kill human glioblastoma cells. *Cell Death Dis.* **5**, e1216 (2014).
70. Maysinger, D., Moquin, A., Choi, J., Kodiha, M. & Stochaj, U. Gold nanourchins and celastrol reorganize the nucleo- and cytoskeleton of glioblastoma cells. *Nanoscale* **10**, 1716–1726 (2018).
71. Combs, S. E. et al. Treatment of primary glioblastoma multiforme with cetuximab, radiotherapy and temozolomide (GERT)—phase I/II trial: study protocol. *BMC Cancer* **6**, 133 (2006).
72. Emrich, J. G. et al. Radioiodinated (I-125) monoclonal antibody 425 in the treatment of high grade glioma patients: ten-year synopsis of a novel treatment. *Am. J. Clin. Oncol.* **25**, 541–546 (2002).
73. Quang, T. S. & Brady, L. W. Radioimmunotherapy as a novel treatment regimen: ^{125}I-labeled monoclonal antibody 425 in the treatment of high-grade brain gliomas. *Int. J. Radiat. Oncol. Biol. Phys.* **58**, 972–975 (2004).
74. ONC201 in Adults With Recurrent H3 K27M-mutant Glioma—Full Text View—ClinicalTrials.gov. https://clinicaltrials.gov/ct2/show/NCT03295396 (accessed 31 May 2018).
75. Iaconelli, J. et al. Lysine deacetylation by HDAC6 regulates the kinase activity of AKT in human neural progenitor cells. *ACS Chem. Biol.* **12**, 2139–2148 (2017).
76. Wang, L. et al. An acquired vulnerability of drug-resistant melanoma with therapeutic potential. *Cell* **173**, 1413–1425.e14 (2018).
77. Du, M., Zhang, L., Scorsone, K. A., Woodfield, S. E. & Zage, P. E. Nifurtimox is effective against neural tumor cells and is synergistic with buthionine sulfoximine. *Sci. Rep.* **6**, https://doi.org/10.1038/srep27458 (2016).
78. Werbowetski-Ogilvie, T. et al. Inhibition of medulloblastoma cell invasion by Slit. *Oncogene* **25**, 5103–5112 (2006).
79. Dhanikula, R. S., Argaw, A., Bouchard, J.-F. & Hildgen, P. Methotrexate loaded polyether–copolyester dendrimers for the treatment of gliomas: enhanced efficacy and intratumoral transport capability. *Mol. Pharm.* **5**, 105–116 (2008).

5. Fumardiamidi primakina i klorokina kao obećavajući antiplazmodijski agensi

molecules

MDPI

Article

Primaquine and Chloroquine Fumardiamides as Promising Antiplasmodial Agents

Maja Beus [1,†], Diana Fontinha [2,†], Jana Held [3], Zrinka Rajić [1,*], Lidija Uzelac [4], Marijeta Kralj [4], Miguel Prudêncio [2] and Branka Zorc [1,*]

1 University of Zagreb, Faculty of Pharmacy and Biochemistry, A. Kovačića 1, HR-10 000 Zagreb, Croatia
2 Instituto de Medicina Molecular, Faculdade de Medicina, Universidade de Lisboa, Av. Prof. Egas Moniz, 1649-028 Lisboa, Portugal
3 University of Tübingen, Institute of Tropical Medicine, Wilhelmstraße 27, 72074 Tübingen, Germany
4 Rudjer Bošković Institute, Division of Molecular Medicine, Laboratory of Experimental Therapy, 10 000 Zagreb, Croatia
* Correspondence: zrajic@pharma.hr (Z.R.); bzorc@pharma.hr (B.Z.); Tel.: +385-1-6394-477 (Z.R.); Fax: +385-1-485-62-01 (Z.R. & B.Z.)
† These authors contributed equally to this work.

Received: 15 July 2019; Accepted: 30 July 2019; Published: 1 August 2019

Abstract: This paper describes a continuation of our efforts in the pursuit of novel antiplasmodial agents with optimized properties. Following our previous discovery of biologically potent asymmetric primaquine (PQ) and halogenaniline fumardiamides (**1–6**), we now report their significant in vitro activity against the hepatic stages of *Plasmodium* parasites. Furthermore, we successfully prepared chloroquine (CQ) analogue derivatives (**11–16)** and evaluated their activity against both the hepatic and erythrocytic stages of *Plasmodium*. Our results have shown that PQ fumardiamides (**1–6)** exert both higher activity against *P. berghei* hepatic stages and lower toxicity against human hepatoma cells than the parent drug and CQ derivatives (**11–16)**. The favourable cytotoxicity profile of the most active compounds, **5** and **6**, was corroborated by assays performed on human cells (human breast adenocarcinoma (MCF-7) and non-tumour embryonic kidney cells (HEK293T)), even when glucose-6-phosphate dehydrogenase (G6PD) was inhibited. The activity of CQ fumardiamides on *P. falciparum* erythrocytic stages was higher than that of PQ derivatives, comparable to CQ against CQ-resistant strain *Pf*Dd2, but lower than CQ when tested on the CQ-sensitive strain *Pf*3D7. In addition, both sets of compounds showed favourable drug-like properties. Hence, quinoline fumardiamides could serve as a starting point towards the development of safer and more effective antiplasmodial agents.

Keywords: primaquine; chloroquine; antiplasmodial activity; cytotoxicity; fumardiamide

1. Introduction

Despite enormous efforts made by the scientific community, malaria remains a deadly disease, especially among pregnant women and children. According to the 2018 World Malaria Report, malaria is responsible for 266,000 deaths of children aged under five years worldwide [1]. In order to achieve the 2020 milestones of the WHO Global Technical Strategy for Malaria 2016–2030, which include a global reduction of at least 40% in malaria incidence and mortality rates, and disease elimination in at least 10 countries, substantial amounts of funding and research are required [2].

Malaria is caused by *Plasmodium* parasites, which infect their mammalian host upon the bite of an infected female *Anopheles* mosquito. Injected sporozoites travel to the liver, where they undergo an asymptomatic but obligatory phase of intra-hepatic replication. The liver stage of infection ends

with the release of thousands of merozoites into the blood, where they cyclically invade and replicate inside erythrocytes, causing the symptoms of malaria. Sexual forms of the parasites formed during this phase of infection can be ingested by a feeding mosquito, and subsequently undergo a developmental process that culminates in the formation of infective sporozoites, ready to start a new infection cycle [3].

Out of five *Plasmodium* species that cause malaria in humans, *P. vivax* and *P. ovale* can form hypnozoites in the liver, dormant forms of the parasite that can reactivate and cause clinical relapses of the disease, weeks or months after the primary infection [4,5]. Until July 2018, primaquine (PQ), an 8-aminoquinoline derivative, was the only drug effective against both the active hepatic stages of *Plasmodium* parasites, as well as *P. vivax* and *P. ovale* hypnozoites, registered worldwide. One of PQ's main downsides is its low oral bioavailability, underlaid by its rapid metabolic degradation to inactive carboxyprimaquine [6,7]. As a consequence, PQ is administered once daily for two weeks, but this regimen is associated with poor compliance, resulting in a lower drug effectiveness [8]. Tafenoquine (TQ) is another 8-aminoquinoline derivative, recently approved for the *P. vivax* malaria therapy in combination with a drug acting on the erythrocytic stage of the infection [9–11] as well as for prophylaxis of *P. falciparum* malaria. Due to its extremely long elimination half-life (approximately 15 days), only a single dose of TQ is required for the treatment of hypnozoites, which ensures better adherence to the therapy than PQ [12]. However, both drugs induce hemolysis in patients with congenital glucose-6-phosphate dehydrogenase (G6PD) deficiency [10,11]. Thus, novel therapies that target the hepatic stages of *Plasmodium* parasites, including hypnozoites, while having reduced hemotoxic properties, are needed.

This paper represents a continuation of our work on the derivatization of antiplasmodial drugs, which included the successful development and evaluation of around 150 PQ derivatives [13–19]. Recently, we have prepared a series of hybrid molecules **1**–**6** composed of PQ, fumaric acid, and halogenaniline fragments (Figure 1), and we evaluated their antimicrobial activity against various microorganisms, their biofilm eradication ability, and their cytostatic activity [20]. The analogues without carbon-carbon double bonds, i.e., derivatives of succinic acid, were also prepared and tested. In all of the biological assays performed, the activity of fumardiamides was superior to succindiamides, indicating the importance of the double bond conjugated to the carbonyl group (Michael acceptor) in the molecules. Since the antiplasmodial potential of these compounds has not been evaluated until now, the objective of this work was to assess their antiplasmodial activity in vitro against the hepatic and erythrocytic stages of *Plasmodium*. In order to estimate the impact of the quinoline core on the biological activity, we prepared the analogous compounds with the chloroquine (CQ) pharmacophore. Here, we disclose their synthesis and the evaluation of their antiplasmodial activity.

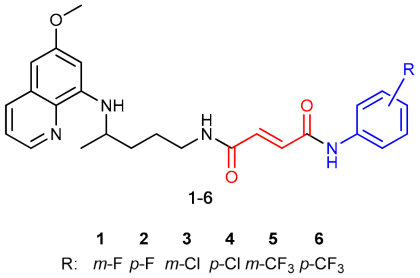

Figure 1. Hybrids **1**–**6** composed of PQ (black), fumaric acid (red) and halogenaniline (blue) fragments [20].

2. Results and Discussion

2.1. Chemistry

Analogous to PQ-based hybrids **1**–**6**, in fumardiamides **11**–**16**, one amide bond was achieved with CQ, and the other one with halogenanilines (*m*- and *p*-fluoroaniline, *m*- and *p*-chloroaniline, *m*- and

p-trifluoromethylaniline). A synthetic route developed earlier for the preparation of fumardiamides **1**–**6** was successfully applied here (Scheme 1).

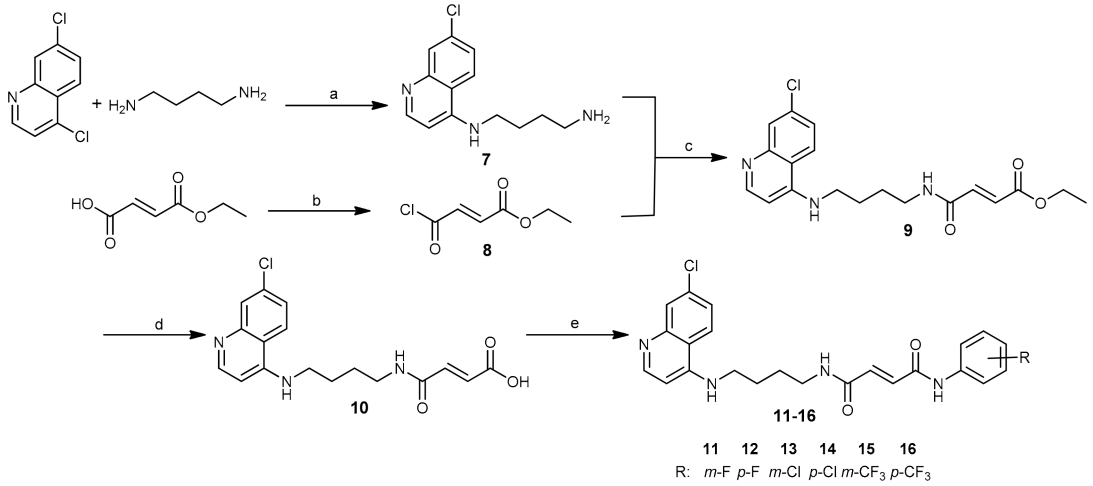

Scheme 1. Synthesis of chloroquine derivatives **11**–**16**. Reagents and conditions: a) MW, 95 °C, 1 h; b) $SOCl_2$, rt, 24 h; c) TEA, DCM, rt, 1 h; d) LiOH, MeOH, H_2O, rt, 1 h; e) halogenaniline, HATU, DIEA, DMF, rt, 2–24 h or MW, 65 °C, 1 h.

In short, the microwave-assisted method was applied for the first step to yield the primary amine **7** with the CQ core. Mono-ethyl fumarate was converted to the corresponding carboxylic acid chloride **8**, which reacted with the primary amino group of **7** to give the amidoester **9**. Basic hydrolysis of the product **9** by lithium hydroxide yielded the carboxylic acid **10**. In the last step, the coupling between the acid **10** and halogenanilines was accomplished by means of (1-[bis(dimethylamino)methylene]-1*H*-1,2,3-triazolo[4,5-*b*]pyridinium 3-oxid hexafluorophosphate (HATU) and *N*,*N*-diisopropylethylamine (DIEA). Purification of these compounds was carried out using crystallization methods and/or column chromatography. Yields for the first three reaction steps were high (73%−100%), but the yields varied from 25% to 91% for the last step. Taken together, our method offered title compounds **11**–**16** in good to moderate yields. All synthesized compounds were checked for purity and identified using elemental analysis, IR, ^{1}H and ^{13}C-NMR spectroscopy, and MS. The data obtained were in agreement with the proposed structures and are given in detail in the Supplementary Materials.

2.2. Antiplasmodial Activity

2.2.1. Erythrocytic Stages

We conducted the in vitro screening of the activity of PQ (**1**–**6**) and CQ (**11**–**16**) fumardiamides against the erythrocytic stages of the CQ-sensitive (*Pf*3D7) and CQ-resistant (*Pf*Dd2) *P. falciparum* strains. Both PQ and CQ were included as positive controls, and DMSO served as a negative control in these assays. PQ derivatives were poorly active, as only compound **2** displayed an IC_{50} value against *Pf*3D7 below 10 μM (IC_{50} = 7.74 μM). Such findings were not surprising, as PQ itself possesses only modest erythrocytic stage activity [21]. Moreover, the basic aliphatic amine required for such a type of activity is masked through the amide bond with fumaric acid. In contrast, the *Pf*3D7 strain was susceptible to CQ hybrids **11**–**16** in nanomolar concentrations. However, the most active compounds **14** and **16** were still less active than CQ (IC_{50} = 0.035 μM vs. 0.0037 μM). On the other hand, their activity against the *Pf*Dd2 strain was similar to that of CQ (Table 1). It is worth noting that *m*-derivatives **11**, **13**, and **15** have consistently shown higher activity than their *p*-substituted counterparts.

2.2.2. Hepatic Stages

Next, we examined the antiplasmodial activity of PQ (**1**–**6**) and CQ (**11**–**16**) derivatives against the hepatic stages of *P. berghei*, as well as toxicity to human hepatoma cells (Huh7) (Figure 2). PQ was included as a positive control, whereas DMSO served as a negative control in these assays. The results showed that PQ fumardiamides were markedly more active than the parent drug and their CQ counterparts. In addition, cell confluency measurements indicated that all PQ fumardiamides were non-toxic to human hepatoma cells. Such findings are in accordance with previous cytotoxicity studies of PQ fumardiamides on a panel of human cancer cell lines [20]. Conversely, CQ analogues displayed a higher level of toxicity than the PQ counterparts **1**–**6**. Additionally, IC_{50} values were determined for the most potent and promising PQ derivatives **3**–**6**. All four compounds exerted marked activities against hepatic parasites, with IC_{50} values ranging between 0.11 and 0.39 µM (Figure 3 and Table 1), which are at least an order of magnitude lower than the parent drug (IC_{50} = 8.4 ± 3.4 µM).

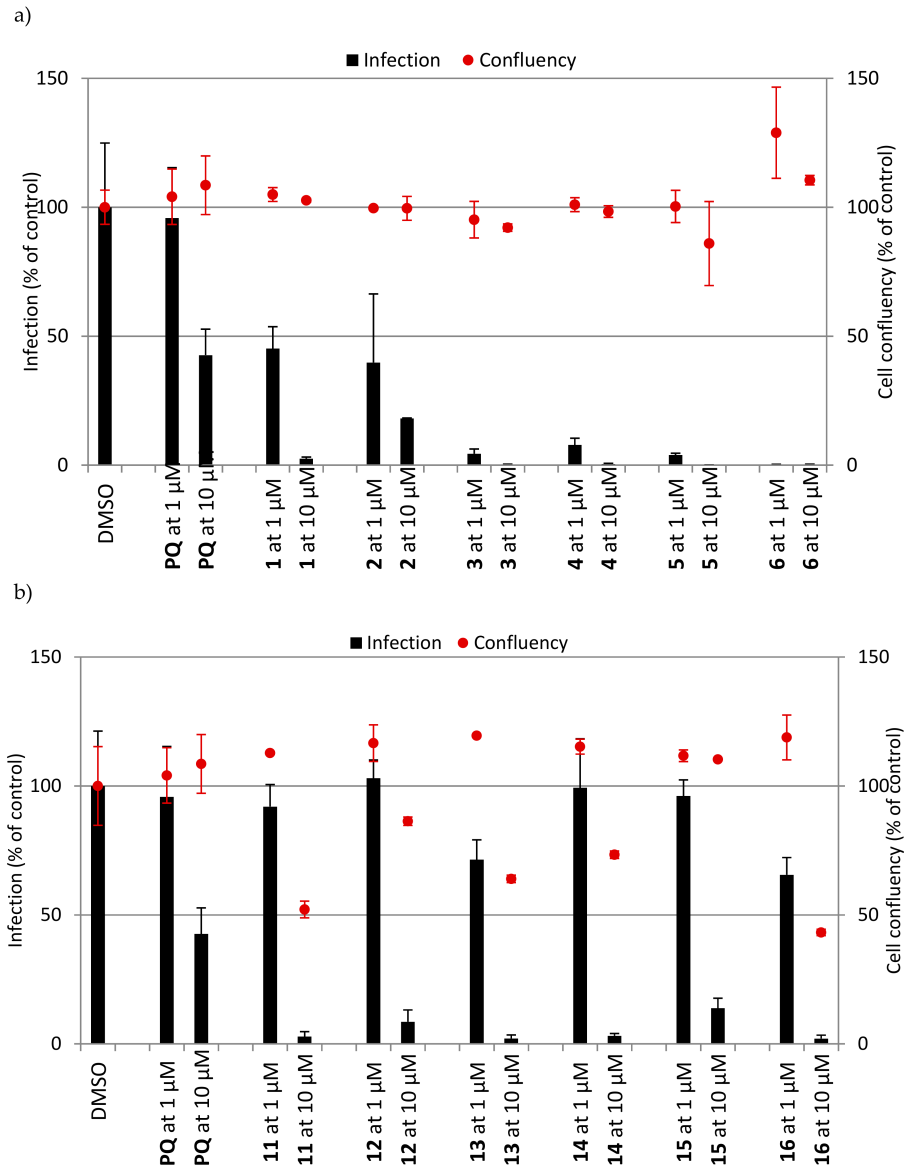

Figure 2. In vitro activity against *P. berghei* liver stages of (**a**) PQ derivatives **1**–**6** and (**b**) CQ derivatives **11**–**16** at 1 and 10 µM concentrations. Total parasite load (infection scale, bars) and cell viability (cell confluency scale, dots) are shown. Results were normalized to the negative control, dimethyl sulphoxide (DMSO), and are represented as mean ± SD, n = 1.

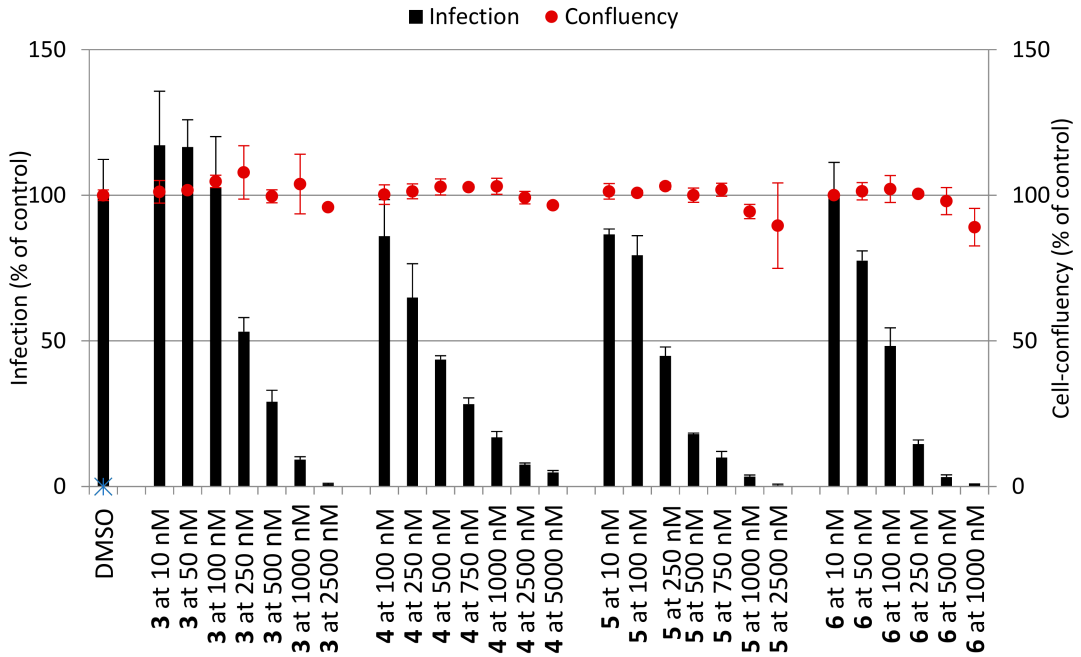

Figure 3. Dose-dependent response of the selected PQ derivatives against *P. berghei* hepatic stages. IC_{50} values are provided in Table 1.

Table 1. IC_{50} values for PQ (**1–6**) and CQ (**11–16**) fumardiamides against erythrocytic stages of two *P. falciparum* strains (*Pf*3D7 and *Pf*Dd2) and hepatic stages of *P. bergei.*

Compd.	Structure	IC_{50} [1] (μM) *Pf*3D7	IC_{50} (μM) *Pf*Dd2	IC_{50} (μM) *P. bergei*
1	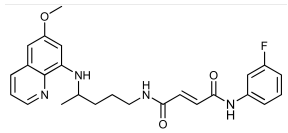	13.77	20	n.d. [2]
2	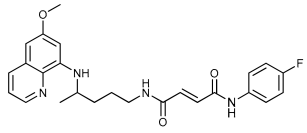	7.74	>13	n.d.
3	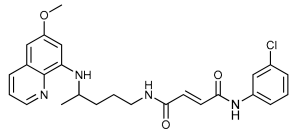	>13	13.58	0.27 ± 0.06 [3]
4	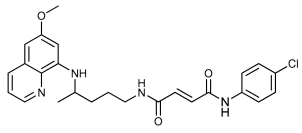	>13	>13	0.39 ± 0.01
5	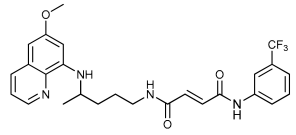	13.91	10.67	0.27 ± 0.08
6	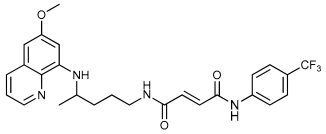	12.96	18.43	0.11 ± 0.02

Table 1. *Cont.*

Compd.	Structure	IC_{50} [1] (μM) *Pf*3D7	IC_{50} (μM) *Pf*Dd2	IC_{50} (μM) *P. bergei*
11	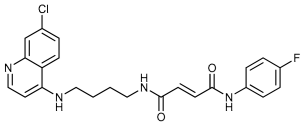	0.144	7.024	n.d.
12	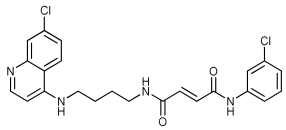	0.067	1.879	n.d.
13	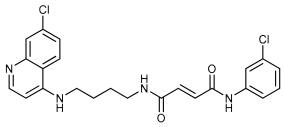	0.083	6.961	n.d.
14	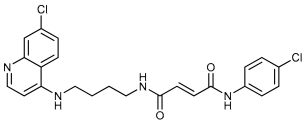	0.035	0.89	n.d.
15	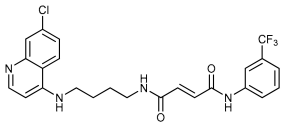	0.194	3.217	n.d.
16	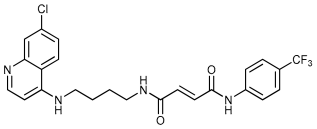	0.035	0.379	n.d.
PQ [4]		1.994	1.816	8.4 ± 3.4
CQ [5]		0.0037	0.241	n.d.

[1] IC_{50}, the concentration of the tested compound necessary for 50% growth inhibition. [2] n.d., not determined. [3] Results represent mean ± SD, $n = 1$. [4] PQ, primaquine. [5] CQ, chloroquine.

2.2.3. Cytotoxicity Assay in Human Cell Lines

Additional evaluation of the cytotoxicity of the most active PQ derivatives **5** and **6** was performed on two human cell lines from different tissues, MCF-7 (breast adenocarcinoma) and HEK293T (non-tumour embryonic kidney). Neither of the compounds displayed toxicity towards the tested cell lines (Table 2). Further, we tested whether the favourable cytotoxicity profile of PQ derivatives **5** and **6** was maintained in the glucose-6-phosphate dehydrogenase (G6PD)-deficient conditions, which were induced by the addition of the G6PD inhibitor 6-aminonicotinamide (6-AN) at a non-toxic concentration ($c = 1$ μM) to the cells [18]. No differences between 6-AN-treated and non-treated cell lines were observed in terms of growth inhibition (Table 2, Figure 4). Thus, these data suggest that derivatives **5** and **6** are promising lead compounds for the development of hepatic stage antiplasmodial compounds with an improved safety profile in G6PD-deficient patients as well.

Table 2. IC_{50} values for PQ fumardiamides **5** and **6** tested in vitro on MCF-7 and HEK293T cell lines, alone or in combination with 6-aminonicotinamide.

Compd.	IC_{50} [1] (μM) MCF-7	IC_{50} [2] (μM) HEK293T
5	≥100	≥100
6	≥100	≥100
6-AN + **5**	≥100	≥100
6-AN + **6**	≥100	≥100
6-AN	2 ± 0.3	10 ± 7

[1] IC_{50}, the concentration of the tested compound necessary for 50% growth inhibition. [2] 6-AN, 6-aminonicotinamide, c = 1 μM.

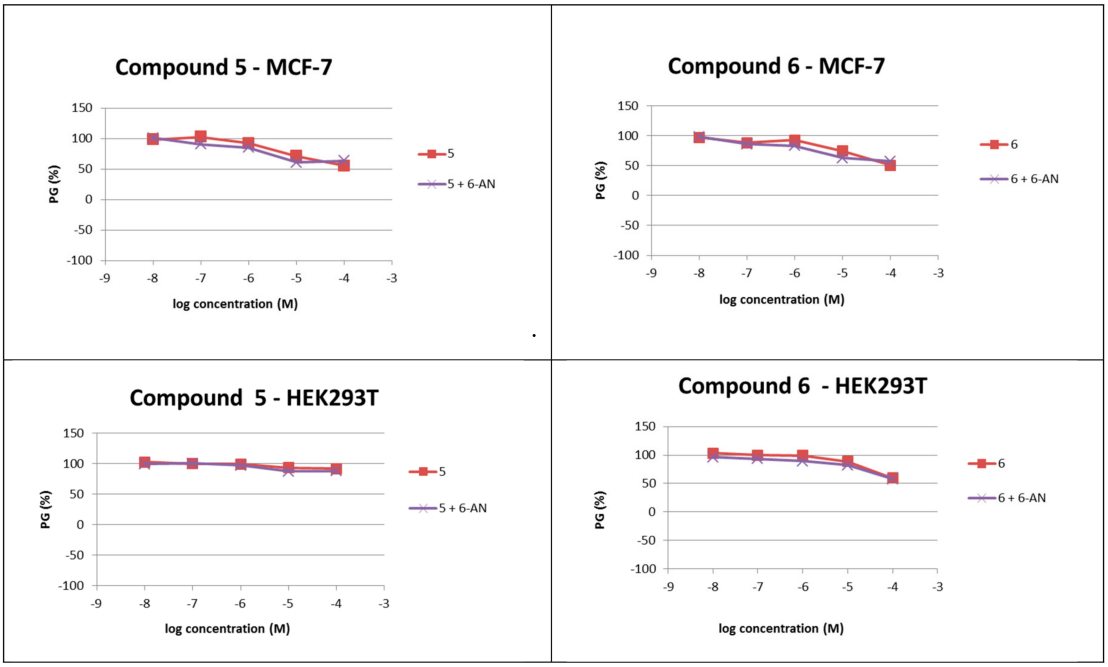

Figure 4. Dose-response profiles for compounds **5** and **6**, alone or in the combination with 6-aminonicotinamide, evaluated in vitro on MCF-7 and HEK293T cell lines.

2.2.4. Evaluation of Drug-Like Properties

The evaluation of the PQ fumardiamides' drug-likeness was reported earlier [20]. Thus, here we evaluated the drug-likeness of CQ derivatives **11–16**, by employing the Chemicalize.org software to calculate an array of physicochemical parameters, including the topological polar surface area (TPSA), the number of atoms, molecular weight (MW), the partition coefficient (log *P*), the H-bond donor (HBD), the H-bond acceptor (HBA), and molecular refractivity (MR) (Table 3) [22]. Our results show that all hybrids **11–16** fall within the Lipinski's and Gelovani's rules for prospective small molecular drugs (MW ≤ 500, log P ≤ 5, number of H-bond donors ≤ 5, number of H-bond acceptors ≤ 10, TPSA < 140 $Å^2$, MR within the range of 40 and 130 cm^3/mol, the number of atoms 20–70).

Both PQ and CQ hybrids were further analyzed through available filters for pan assay interference compounds (PAINS), which identify a substructure with an ability to interfere in any biological assay, based on various mechanisms [23]. Three computer programs, ZINC (http://zinc15.docking.org/PAINS/), PAINS Remover (http://www.cbligand.org/PAINS/), and SwissADME (http://www.swissadme.ch/), were employed for compounds **1–6** and **11–16**. In addition, we carried out the in silico identification of potential aggregators (Aggregator Advisor, http://advisor.docking.org). All tested compounds returned no PAINS and no aggregator alerts, thus showing that the selected hybrid compounds passed all filters. SwissADME bioavailability radars [24] of the most active compounds of both series, namely

compounds **6** and **16**, showed that all analyzed parameters are in the optimal range, with the exception of flexibility, which falls out of the set borders (Figure 5).

Table 3. Properties of novel compounds calculated with Chemicalize.org program [22]. The Lipinski's and Gelovani's parameters.

Compd.	Molecular Formula	Number of Atoms	MW	log *P*	HBD	HBA	Lipinski Score [1]	MR (cm^3/mol)	TPSA ($Å^2$)
11	$C_{23}H_{22}ClFN_4O_2$	53	440.90	3.57	3	4	4	122.34	83.12
12	$C_{23}H_{22}ClFN_4O_2$	53	440.90	3.57	3	4	4	122.34	83.12
13	$C_{23}H_{22}Cl_2N_4O_2$	53	457.36	4.03	3	4	4	126.93	83.12
14	$C_{23}H_{22}Cl_2N_4O_2$	53	457.36	4.03	3	4	4	126.93	83.12
15	$C_{24}H_{22}ClF_3N_4O_2$	56	490.91	4.30	3	4	4	128.10	83.12
16	$C_{24}H_{22}ClF_3N_4O_2$	56	490.91	4.30	3	4	4	128.10	83.12

MW—molecular weight; log *P*—partition coefficient; HBD—number of H-bond donors; HBA—number of H-bond acceptors; MR—molecular refractivity; TPSA—topological polar surface area; [1] out of four.

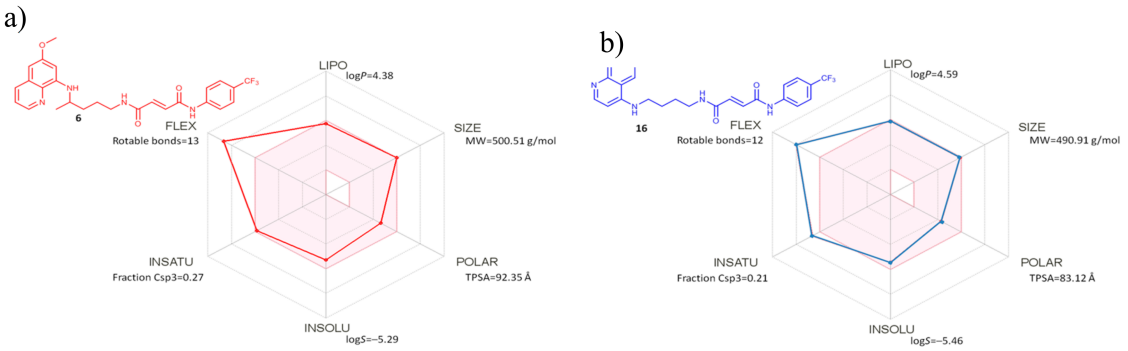

Figure 5. SwissADME bioavailability radars for the most active compounds: (**a**) PQ derivative **6** and (**b**) CQ derivative **16**. The pink area represents the optimal range for each property: lipophilicity (LIPO) (XLOGP3 between −0.7 and +5.0), molecular mass (SIZE) (between 150 and 500 g·mol^{-1}), polarity (POLAR) (TPSA between 20 and 130 Å^2), solubility (INSOLU) (log *S* not higher than 6), saturation (INSATU) (fraction of carbons in the sp^3 hybridization not less than 0.25), and flexibility (FLEX) (no more than nine rotatable bonds).

3. Materials and Methods

3.1. Chemistry

3.1.1. Materials and Methods

Melting points were determined on the SMP3 apparatus (Barloworld Scientific, Stone, UK) in open capillaries and are presented uncorrected. A CEM Discover microwave reactor was used for microwave reactions (CEM GmbH, Kamp-Lintfort, Germany). IR spectra were recorded on Spectrum One (Perkin-Elmer, Waltham, MS, USA) and UV-Vis spectra on Lambda 20 double beam spectrophotometers (Perkin-Elmer, UK). NMR ^{1}H and ^{13}C spectra were recorded at 25 °C on the NMR Avance 600 spectrometer (Bruker, Leipzig, Germany) at 300.13 or 600.13 and 75.47 or 150.9 MHz for ^{1}H and ^{13}C nuclei, respectively. Chemical shifts (δ) are reported in parts per million (ppm) relative to tetramethylsilane in the ^{1}H and the dimethyl sulfoxide (DMSO) residual peak as a reference in the ^{13}C spectra (39.51 ppm). Coupling constants (*J*) are reported in hertz (Hz). Mass spectra were collected on an HPLC-MS/MS instrument (HPLC, Agilent Technologies 1200 Series; MS, Agilent Technologies 6410 Triple Quad, Santa Clara, CA, USA) using electrospray ionization in the positive mode. Elemental analyses were performed on a CHNS LECO analyzer (LECO Corporation, St. Joseph, MI, USA). All compounds were routinely checked by TLC with Merck silica gel 60F-254 glass plates using dichloromethane/methanol 9.5:0.5, 9:1, 8.5:1.5, and cyclohexane/ethyl acetate/methanol 1:1:0.5

as the solvent systems. Spots were visualized by short-wave UV light and iodine vapour. Column chromatography was performed on silica gel at 0.063 to 0.200 mm (Sigma-Aldrich, St. Louis, Missouri, United States, USA) with the same eluents used in TLC.

All chemicals and solvents were of analytical grade and purchased from commercial sources. 4,7-Dichloroquinoline, 4-chloro-2,8-bis(trifluoromethyl)quinoline, butane-1,4-diamine, (*E*)-4-ethoxy-4-oxobut-2-enoic acid (mono-ethyl fumarate), 3-fluoroaniline, 4-fluoroaniline, 3-chloroaniline, 4-chloroaniline, 3-trifluoromethylaniline, 4-trifluoromethylaniline, triethylamine (TEA), DIEA, and HATU were purchased from Sigma-Aldrich. Anhydrous solvents were dried and redistilled prior to use.

3.1.2. Procedures for the Synthesis of Compounds **7**–**10**.

*N^1-(7-chloroquinolin-4-yl)butane-1,4-diaminediamine (**7**).* A mixture of 4,7-dichloroquinoline (0.599 g, 0.002 mol) and 1,4-diaminobutane (1.763 g, 0.02 mol) was stirred under microwave irradiation (300 W) at 95 °C. After 60 min, the reaction mixture was diluted with dichloromethane and extracted with 5% NaOH (4 × 40 mL) and washed with water (2 × 40 mL). The organic layer was dried over anhydrous sodium sulfate, filtrated, and evaporated under reduced pressure. The crude product **7** (0.499 g, 100%) was used in the further reaction without purification.

*(E)-ethyl 4-chloro-4-oxobut-2-enoate (Mono-ethyl fumarate chloride) (**8**).* A solution of 0.288 g mono-ethyl fumarate (2 mmol) in 7 mL thionyl chloride was kept overnight and evaporated under reduced pressure. The residue was trice triturated with dichloromethane and the solvent was evaporated again. Freshly prepared crude product **8** (0.315 g, 97%) was used in the further reaction without purification.

*Ethyl (E)-4-((4-((7-chloroquinolin-4-yl)amino)butyl)amino)-4-oxobut-2-enoate (**9**).* A solution of compound **7** (0.375 g, 1.5 mmol) and TEA (0.152 g, 1.5 mmol) in 10 mL of dichloromethane was added dropwise to a solution of mono-ethyl fumarate chloride **8** (0.288 g, 1.5 mmol) in 10 mL dichloromethane. The reaction mixture was stirred for 1 h at room temperature and extracted 3 times with brine. The organic layer was dried over sodium sulfate, filtered, and evaporated under reduced pressure. After purification by column chromatography (mobile phase dichloromethane/methanol 8.5:1.5) and crystallization from ether, 0.412 g (73%) of pale yellow solid **9** was obtained; mp 207–209 °C; IR (KBr): ν_{max} 2566, 3368, 3282, 3082, 2946, 2872, 2796, 1722, 1672, 1643, 1584, 1454, 1368, 1334, 1302, 1238, 1176, 1080, 1022, 974, 896, 850, 806, 766, 692, 666, 642, 570, 540 cm^{-1}; ^{1}H-NMR (DMSO-d_6) δ 8.56 (t, 1H, J = 5.5 Hz), 8.39 (d, 1H, J = 5.5 Hz), 8.29 (d, 1H, J = 9.1 Hz), 7.79 (d, 1H, J = 2.2 Hz), 7.49–7.39 (m, 2H,), 7.00 (d, 1H, J = 15.5 Hz), 6.56 (d, 1H, J = 15.5 Hz), 6.50 (d, 1H, J = 5.6 Hz), 4.18 (q, 2H, J = 7.1 Hz), 3.35-3.16 (m, 4H), 1.75–1.50 (m, 4H), 1.24 (t, 3H, J = 7.1 Hz); ^{13}C-NMR (DMSO-d_6) δ 165.08, 162.73, 151.41, 150.35, 148.51, 137.61, 133.61, 128.18, 127.02, 124.19, 124.14, 117.34, 98.67, 60.67, 42.04, 38.55, 26.48, 25.18, 14.01; ESI-MS: m/z calculated for $C_{19}H_{22}ClN_3O_3$: 375.13, found: 376.1 $(M + 1)^+$; Anal. Calcd. for $C_{19}H_{22}ClN_3O_3$: C, 60.72; H, 5.90; N, 11.18. Found: C, 60.58; H, 5.51; N, 11.38.

*(E)-4-((4-((7-chloroquinolin-4-yl)amino)butyl)amino)-4-oxobut-2-enoic acid (**10**).* A solution of 0.126 g (3 mmol) lithium hydroxide monohydrate in 10 mL water was added to a solution of 0.225 g (0.6 mmol) ester **9** in 10 mL methanol. The reaction mixture was stirred for 3 h at room temperature. Methanol was evaporated under reduced pressure and the aqueous residue was acidified with 10%-HCl to pH 1. The precipitated product was filtered and washed with water until neutral. 0.190 g (97%) of pale yellow solid **10** was obtained; mp 227–228 °C; IR (KBr): ν_{max} 3280, 3070, 3940, 2872, 2364, 2060, 1956, 1620, 1558, 1456, 1366, 1206, 1136, 1090, 984, 900, 816, 762, 658, 584 cm^{-1}; ^{1}H-NMR (DMSO-d_6) δ 8.47 (t, 1H, J = 5.5 Hz), 8.38 (d, 1H, J = 5.5 Hz), 8.27 (d, 1H, J = 9.1 Hz), 7.77 (d, 1H, J = 2.2 Hz), 7.52–7.33 (m, 2H), 6.88 (d, 1H, J = 15.5 Hz), 6.55–6.45 (m, 2H), 3.35–3.09 (m, 4H), 1.77–1.48 (m, 4H); ^{13}C-NMR (DMSO-d_6) δ 166.71, 163.21, 151.50, 150.32, 148.59, 136.60, 133.57, 130.12, 127.09, 124.18, 124.13, 117.36, 98.67, 42.05, 38.50, 26.55, 25.21; ESI-MS: m/z calculated for $C_{17}H_{18}ClN_3O_3$: 347.10, found: 348.0 $(M + 1)^+$; Anal. Calcd. $C_{17}H_{18}ClN_3O_3$: C, 58.71; H, 5.22; N, 12.08. Found: C, 59.12; H, 5.12; N, 11.97.

3.1.3. General Procedure for the Synthesis of Fumardiamides **11**–**16**

A solution of 0.094 g (0.27 mmol) compound **10**, 0.068 g (0.54 mmol) DIEA, and 0.103 g (0.27 mmol) HATU in 1 mL of *N*,*N*-dimethylformamide was stirred at room temperature. After 10 min, 0.297 mmol of the corresponding halogenaniline was added. The reaction mixture was stirred for 2 to 24 h at room temperature or for 2 h under microwave irradiation (300 W) at 65 °C. The solvent was evaporated under reduced pressure.

*(2E)-N′-{4-[(7-chloroquinolin-4-yl)amino]butyl}-N-(3-fluorophenyl)but-2-enediamide (***11***).* Reaction conditions: 2 h, room temperature. From the reaction of 0.094 g acid **10** and 0.033 g (0.297 mmol) 3-fluoroaniline and after purification by column chromatography (mobile phase dichloromethane/methanol 8.5:1.5) and crystallization from ether, 0.030 g (25%) of white solid **11** was obtained; mp 229–232 °C; IR (KBr): ν_{max} 3634, 3282, 3092, 2938, 3868, 1650, 1606, 1558, 1490, 1428, 1384, 1338, 1262, 1212, 1186, 1136, 1080, 1042, 1020, 970, 938, 902, 854, 810, 772, 716, 678, 594, 520 cm^{-1}; ^{1}H-NMR (DMSO-d_6) δ 10.77 (s, 1H), 8.68–8.40 (m, 4H), 7.92 (d, 1H, *J* = 1.4 Hz), 7.70 (d, 1H, *J* = 11.6 Hz), 7.62 (dd, 1H, *J* = 9.0, 1.7 Hz), 7.38 (m, 2H′), 7.03 (q, 2H, *J* = 15.1 Hz), 6.93 (t, 1H, *J* = 8.49 Hz), 6.72 (d, 1H, *J* = 6.4 Hz), 3.48–3.40 (m, 2H), 3.29–3.21 (m, 2H), 1.76–1.66 (m, 2H), 1.64–1.55 (m, 2H); ^{13}C-NMR (DMSO-d_6) δ 163.69–160.49 (d, *J* = 242.80 Hz), 163.39, 162.62, 154.77, 143.78, 140.61-140.46 (d, *J* = 11.38 Hz), 139.69, 137.42, 134.32, 132.39, 130.54–130.42 (d, *J* = 9.34 Hz), 126.47, 125.60, 119.96, 115.65, 115.18, 110.42–110.14 (d, *J* = 20.55), 106.33–105.98 (d, *J* = 20.55 Hz), 98.61, 42.73, 38.37, 26.34, 25.04; ESI-MS: *m*/*z* calculated for $C_{23}H_{22}ClFN_4O_2$: 440.14, found: 441.0 $(M + 1)^+$; Anal. Calcd. $C_{23}H_{22}ClFN_4O_2$: C, 62.66; H, 5.03; N, 12.71. Found: C, 62.70; H, 5.15; N, 12.79.

*(2E)-N′-{4-[(7-chloroquinolin-4-yl)amino]butyl}-N-(4-fluorophenyl)but-2-enediamide (***12***).* Reaction conditions: 2 h, room temperature. From the reaction of 0.094 g acid **10** and 0.033 g (0.297 mmol) 4-fluoroaniline and after extraction with ethyl acetate and crystallization from ether, 0.108 g (91%) of white solid **12** was obtained; mp 239 °C (decomp.); IR (KBr): ν_{max} 3284, 3072, 2956, 2932, 2864, 1636, 1582, 1542, 1510, 1452, 1406, 1368, 1334, 1278, 1212, 1172, 1140, 1080, 996, 934, 902, 834, 764, 690, 552, 516 cm^{-1}; ^{1}H-NMR (DMSO-d_6) δ 10.58 (s, 1H), 8.55 (t, 1H, *J* = 37 Hz), 8.41 (d, 1H, *J* = 5.6 Hz), 8.34 (d, 1H, *J* = 9.1 Hz), 7.80 (d, 1H, *J* = 2.1 Hz), 7.72 (dd, 2H, *J* = 9.0, 5.0 Hz), 7.59 (t, 1H, *J* = 5.47 Hz), 7.47 (dd, 1H, *J* = 9.0, 2.2 Hz), 7.17 (t, 2H, *J* = 9.13 Hz), 7.02 (q, 2H, *J* = 15.1 Hz), 6.53 (d, 1H, *J* = 5.7 Hz), 3.40–3.19 (m, 4H), 1.75–1.52 (m, 4H); ^{13}C-NMR (DMSO-d_6) δ 163.44, 162.23, 159.85-156.66 (d, *J* = 241.00 Hz), 150.96, 150.62, 148.03, 135.30, 133.97, 133.79, 132.60, 126.59, 124.35, 124.23, 121.14–121.03 (d, *J* = 7.71 Hz), 117.26, 115.56–115.27 (d, *J* = 22.77 Hz), 98.64, 42.09, 38.49, 26.56, 25.20; ESI-MS: *m*/*z* calculated for $C_{23}H_{22}ClFN_4O_2$: 440.14, found: 441.0 $(M + 1)^+$; Anal. Calcd. $C_{23}H_{22}ClFN_4O_2$: C, 62.66; H, 5.03; N, 12.71. Found: C, 62.45; H, 5.25; N, 12.53.

*(2E)-N-(3-chlorophenyl)-N′-{4-[(7-chloroquinolin-4-yl)amino]butyl}but-2-enediamide (***13***).* Reaction conditions: 16 h, room temperature. From the reaction of 0.094 g acid **10** and 0.038 g (0.297 mmol) 3-chloroaniline and after purification by column chromatography (mobile phase dichloromethane/methanol 8.5:1.5) and crystallization from ether, followed by crystallization from methanol, 0.032 g (26%) of white solid **13** was obtained; mp 232 °C (decomp.); IR (KBr): ν_{max} 3340, 3298, 3182, 3092, 3032, 2944, 2866, 2830, 2360, 1650, 1592 1542, 1482, 1426, 1334, 1234, 1214, 1170, 1142, 1078, 1034, 970, 900, 848, 808, 782, 678, 626, 588, 558 cm^{-1}; ^{1}H-NMR (DMSO-d_6) δ 10.67 (s, 1H), 8.56 (t, 1H, *J* = 5.5 Hz), 8.43 (d, 1H, *J* = 5.9 Hz), 8.38 (d, 1H, *J* = 9.1 Hz), 8.01–7.87 (m, 2H), 7.83 (d, 1H, *J* = 2.1 Hz), 7.66–7.46 (m, 2H), 7.37 (t, 1H, *J* = 8.1 Hz), 7.15 (dd, 1H, *J* = 7.9, 1.1 Hz), 7.02 (q, 2H, *J* = 14.5 Hz), 6.60 (d, 1H, *J* = 6.0 Hz), 3.42–3.32 (m, 2H), 3.29–3.19 (m, 2H), 1.76–1.53 (m, 4H); ^{13}C-NMR (DMSO-d_6) δ 163.34, 162.64, 151.57, 149.35, 146.10, 140.25, 134.66, 134.42, 133.14, 132.33, 130.56, 125.10, 124.79, 124.56, 123.53, 118.79, 117.78, 116.88, 98.66, 42.26, 38.50, 26.52, 25.18; ESI-MS: *m*/*z* calculated for $C_{23}H_{22}Cl_2N_4O_2$: 456.11, found: 457.0 $(M + 1)^+$; Anal. Calcd. $C_{23}H_{22}Cl_2N_4O_2$: C, 60.40; H, 4.85; N, 12.25. Found: C, 60.26; H, 4.62; N, 12.27.

(2E)-N-(4-chlorophenyl)-N′-{4-[(7-chloroquinolin-4-yl)amino]butyl}but-2-enediamide (**14**). Reaction conditions: 1 h, 65 °C, MW. From the reaction of 0.094 g acid **10** and 0.038 g (0.297 mmol) 4-chloroaniline and after crystallization from methanol, 0.088 g (71%) of white solid **14** was obtained; mp 237 °C (decomp.); IR (KBr): ν_{max} 3412, 3286, 3186, 3098, 3072, 2946, 2878, 2706, 2364, 1363, 1544, 1492, 1452, 1398, 1342, 1240, 1212, 1172, 1128, 1094, 1014, 986, 842, 76, 680, 584, 558, 506 cm^{-1}; ^{1}H-NMR (DMSO-d_6) δ 10.71 (s, 1H), 9.51 (t, 1H, J = 5.2 Hz), 8.66 (d, 1H, J = 9.2 Hz), 8.60 (t, 1H, J = 5.6 Hz), 8.55 (d, 1H, J = 7.1 Hz), 8.04 (d, 1H, J = 2.0 Hz), 7.75 (dd, 3H, J = 12.8, 5.5 Hz), 7.39 (d, 2H, J = 8.9 Hz), 7.02 (q, 2H, J = 15.1 Hz), 6.89 (d, 1H, J = 7.2 Hz), 3.6–3.5 (m, 2H), 3.27–3.14 (m, 2H), 1.79–1.66 (m, 2H), 1.65–1.53 (m, 2H); ^{13}C-NMR (DMSO-d_6) δ 163.43, 162.42, 155.17, 143.06, 138.87, 137.81, 134.13, 132.50, 128.73, 127.35, 126.68, 125.74, 120.87, 119.30, 115.50, 98.59, 42.79, 38.34, 26.32, 25.01; ESI-MS: m/z calculated for $C_{23}H_{22}Cl_2N_4O_2$: 456.11, found: 457.0 $(M + 1)^+$; Anal. Calcd. $C_{23}H_{22}Cl_2N_4O_2$: C, 60.40; H, 4.85; N, 12.25. Found: C, 60.34; H, 4.97; N, 12.13.

(2E)-N′-{4-[(7-chloroquinolin-4-yl)amino]butyl}-N-[3-(trifluoromethyl)phenyl]but-2-enediamide (**15**). Reaction conditions: 24 h, room temperature. From the reaction of 0.094 g acid **10** and 0.048 g (0.297 mmol) 3-trifluoroaniline and after purification by column chromatography (mobile phase dichloromethane/methanol 8.5:1.5) after crystallization from ether, 0.034 g (26%) of white solid **15** was obtained; mp 240 °C (decomp.); IR (KBr): ν_{max} 3418, 3210, 3072, 3002, 2958, 1620, 1550, 1490, 1414, 1312, 1182, 1136, 1068, 1022, 840, 656, 558 cm^{-1}; ^{1}H-NMR (DMSO-d_6) δ 10.81 (s, 1H), 9.26 (t, 1H, J = 5.2 Hz), 8.62–8.53 (m, 4H), 7.94 (d, 1H, J = 2.1 Hz), 7.86 (d, 1H, J = 8.4 Hz, 1H), 7.81 (dd, 1H, J = 9.1, 2.1 Hz), 7.62 (t, 1H, J = 8.0 Hz), 7.49 (d, 1H, J = 7.8 Hz), 7.04 (q, 2H, J = 14.88 Hz), 6.93 (d, 1H, J = 7.1 Hz), 3.61–3.54 (m, 2H), 3.32–3.25 (m, 2H), 1.81–1.70 (m, 2H), 1.68–1.58 (m, 2H); ^{13}C-NMR (DMSO-d_6) δ 163.31, 162.78, 155.08, 143.56, 139.54, 139.14, 137.77, 134.47, 132.27, 130.17, 129.64-129.38 (q, J = 26.85 Hz), 126.75, 125.45, 122.93, 122.71-120.00 (q, J = 274.54 Hz), 120.22, 119.67, 115.53, 115.36, 98.68, 42.85, 38.41, 26.34, 25.06; ESI-MS: m/z calculated for $C_{24}H_{22}ClF_3N_4O_2$: 490.14, found: 491.1 $(M + 1)^+$; Anal. Calcd. $C_{24}H_{22}ClF_3N_4O_2$: C, 58.72; H, 4.52; N, 11.41. Found: C, 58.90; H, 4.55; N, 11.58.

(2E)-N′-{4-[(7-chloroquinolin-4-yl)amino]butyl}-N-[4-(trifluoromethyl)phenyl]but-2-enediamide (**16**). Reaction conditions: 24 h, room temperature. From the reaction of 0.094 g acid **10** and 0.048 g (0.297 mmol) 4-trifluoroaniline and after crystallization from water, followed by crystallization from ether, 0.049 g (37%) of white solid **16** was obtained; mp 270 °C (decomp.); IR (KBr): ν_{max} 3254, 2972, 2914, 2836, 2760, 2722, 2546, 2488, 2426, 2362, 2098, 1976, 1712, 1610, 1590, 1544, 1472, 1442, 1398, 1324, 1210, 1154, 1104, 1066, 1018, 978, 956, 882, 842, 802, 768, 686, 650, 592, 508 cm^{-1}; ^{1}H-NMR (DMSO-d_6) δ 10.92 (s, 1H), 9.30 (t, 1H, J = 2.54 Hz), 8.71–8.57 (m, 2H), 8.54 (d, 1H, J = 6.9 Hz), 8.01 (d, 1H, J = 2.0 Hz), 7.91 (d, 2H, J = 8.5 Hz), 7.73 (dd, 3H, J = 14.2, 5.2 Hz), 7.06 (q, 2H, J = 15.1 Hz), 6.86 (d, 1H, J = 7.0 Hz), 3.57–3.49 (m, 2H), 3.29–3.21 (m, 2H), 1.77–1.67 (m, 2H), 1.64–1.54 (m, 2H); ^{13}C-NMR (DMSO-d_6) δ 163.35, 162.88, 155.08, 143.26, 142.39, 139.08, 137.70, 134.62, 132.29, 126.65, 126.17, 125.70, 123.95–123.52 (q, J = 25.48 Hz), 122.53–118.93 (q, J = 270.75 Hz), 119.48–119.33 (q, J = 10.26), 115.54, 98.61, 42.79, 38.38, 26.33, 25.03; ESI-MS: m/z calculated for $C_{24}H_{22}ClF_3N_4O_2$: 490.14, found: 491.1 $(M + 1)^+$; Anal. Calcd. $C_{24}H_{22}ClF_3N_4O_2$: C, 58.72; H, 4.52; N, 11.41. Found: C, 58.96; H, 4.73; N, 11.67.

3.2. In Vitro Drug Sensitivity Assay Against Erythrocytic Stages of P. falciparum

Antiplasmodial activity of fumardiamides **1**–**6** and **11**–**16** was tested in a drug sensitivity assay against two laboratory *P. falciparum* strains (3D7—CQ-sensitive, and Dd2—CQ-resistant), as previously described, using the histidine-rich protein 2 (HRP2) assay [25,26]. In brief, 96-well plates were pre-coated with the tested compounds in a three-fold dilution before ring stage parasites were added in complete culture medium at a hematocrit of 1.5% and a parasitaemia of 0.05%. After three days of incubation at 37 °C, 5% CO_2, and 5% oxygen, plates were frozen until analyzed by HRP2-ELISA. All compounds were evaluated in duplicate in at least two independent experiments. The IC_{50} was determined by analysing the nonlinear regression of log concentration-response curves using the drc-package v0.9.0 of R v2.6.1 [27].

3.3. In Vitro Activity Against P. berghei Hepatic Stages

In vitro activity of the tested compounds against the liver stage of *P. berghei* infection was assessed as previously described [28,29]. Briefly, Huh7 cells, a human hepatoma cell line, were routinely cultured in 1640 Roswell Park Memorial Institute (RPMI) medium supplemented with 10% (v/v) fetal bovine serum, 1% (v/v) glutamine, 1% (v/v) penicillin/streptomycin, 1% non-essential amino acids, and 10 mM 4-(2-hydroxyethyl)-1-piperazineethanesulfonic acid (HEPES). For drug screening experiments, Huh7 cells were seeded at 1×10^4 cell/well of a 96-well plate and incubated overnight at 37 °C with 5% CO_2. Next, 10 mM stock solutions of test compounds were prepared in DMSO and were serially diluted in infection medium, i.e., culture medium supplemented with gentamicin (50 µg/mL) and amphotericin B (0.8 µg/mL), in order to obtain the test concentrations. On the day of the infection, the culture medium was replaced with serial dilutions of the test compounds and incubated for 1 h at 37 °C with 5% CO_2. Next, 1×10^4 firefly luciferase-expressing *P. berghei* sporozoites, freshly isolated from the salivary glands of female infected *Anopheles stephensi* mosquitoes, were added to the cultures, plates were centrifuged at 1800× *g* for 5 min at room temperature, and incubated at 37 °C with 5% CO_2.

To assess the effect of each compound concentration in cell viability, at 46 hours post-infection (hpi), cultures were incubated with Alamar Blue (Thermo Fisher Scientific, Waltham, MA, USA), according to the manufacturer's recommendations. Parasite load was then assessed by the bioluminescence assay (Biotium, Fremont, CA, USA), using the multi-plate reader Infinite M200 (Tecan, Männedorf, Switzerland). Nonlinear regression analysis was employed to fit the normalized results of the dose–response curves, and IC_{50} values were determined using GraphPad Prism 6.0 (GraphPad Software, La Jolla California USA).

3.4. Cytotoxicity Assay in Human Cell Lines

The experiments were carried out on 2 human cell lines: MCF-7 (breast carcinoma) and HEK293T (embryonic kidney). MCF-7 and HEK293T cells were cultured as monolayers and maintained in Dulbecco's modified Eagle medium (DMEM), supplemented with 10% fetal bovine serum (FBS), 2 mM L-glutamine, 100 U/mL penicillin, and 100 µg/mL streptomycin in a humidified atmosphere with 5% CO_2 at 37 °C. The panel cell lines were inoculated in parallel onto a series of standard 96-well microtiter plates on day 0, at 1×10^4 to 3×10^4 cells/mL, depending on the doubling time of a specific cell line. Test compounds were then added in five 10-fold dilutions (10^{-8} to 10^{-4} M) alone or in combination with 6-AN (c = 1 µM) and incubated for a further 72 hours. Working dilutions were freshly prepared on the day of the testing.

After 72 hours of incubation, the cell growth rate was evaluated by performing the MTT assay [18]. The absorbance was directly proportional to cell viability. Each test point was performed in quadruplicate in three individual experiments. The IC_{50} values were calculated from the dose–response curves using linear regression analysis. Each result is a mean value from at least two separate experiments.

4. Conclusions

The antiplasmodial potential of previously prepared PQ fumardiamides **1**–**6** and novel CQ analogues **11**–**16** was evaluated against the hepatic and erythrocytic stages of *Plasmodium* parasites. The evaluation of the compounds' activity against *P. berghei* hepatic stages in vitro revealed that: i) PQ hybrids show markedly higher activities than PQ itself, ii) PQ derivatives display higher activity than CQ fumardiamides, and iii) PQ fumardiamides are non-toxic to human hepatoma cells, whereas their CQ analogues exert higher levels of toxicity. The most active PQ derivatives **5** and **6** showed low cytotoxicity towards human cells (MCF-7 and HEK293T), which was also founnd when G6PD was inhibited. CQ fumardiamides displayed higher activity than PQ derivatives against *P. falciparum* erythrocytic stages in vitro. It is encouraging that the activity of the most active CQ derivatives **14** and **16** against the CQ-resistant strain, *Pf*Dd2, was comparable to that of the parent drug. Taken together,

our results indicate that the quinoline core influences the profile of activity/toxicity for PQ and CQ fumardiamides. Due to their biological profile and favourable drug-like properties, quinoline fumardiamides could provide a strong basis for further optimisation towards the development of novel and safer antiplasmodial drugs.

Supplementary Materials: Spectra of all compounds are available online. Figure S1: Structural formula, MS, IR, ^{1}H and ^{13}C spectra of compounds **9**–**16**. Table S1: Analytical and spectral data of compounds **9**–**16**, Table S2: ^{1}H and ^{13}C NMR spectra of compounds **9**–**16**.

Author Contributions: Conceptualization, Z.R. and B.Z.; methodology, M.B., D.F., J.H., L.U., M.K., and M.P.; writing—original draft, Z.R. and B.Z.

Funding: The authors thank Filipa Teixeira for mosquito production and infection. The authors acknowledge the financial support by the Croatian Science Foundation (research projects IP-2014-09-1501 and IP-2013-5660) and University of Zagreb (support for 2018), and by the Portuguese Foundation for Science and Technology (grant PTDC-SAU-INF-29550-2017). The work of doctoral student Maja Beus has been fully supported by the Young researcher's career development project – training of doctoral students of the Croatian Science Foundation founded by the European Union from the European Social Fund. D.F. was supported by FEEI and FCT-MEC. M.P. is supported by a Stimulus of Scientific Employement 2018 grant of Fundação para a Ciência e Tecnologia, Portugal.

Conflicts of Interest: The authors declare no conflict of interest.

Abbreviations

6-AN, 6-aminonicotinamide; CQ, chloroquine; DCM, dichloromethane; DIEA, *N*,*N*-diisopropylethylamine; DMEM, Dulbecco's modified Eagle's medium; DMSO, dimethyl sulfoxide; FBS, foetal bovine serum; G6PD, glucose-6-phosphate dehydrogenase, HATU, 1-[bis(dimethylamino)methylene]-1*H*-1,2,3-triazolo[4,5-*b*]pyridinium 3-oxide hexafluorophosphate; HEK293T, non-tumour embryonic kidney cell line; Huh7, human hepatoma cell line; HBA, number of H-bond acceptors; HBD, number of H-bond donors; HRP2, histidine-rich protein 2; IC_{50}, the concentration of the tested compound necessary for 50% growth inhibition; log *P*, partition coefficient; MCF-7, breast adenocarcinoma cell line; MR, molar refractivity; MTT, (3-(4,5-dimethylthiazol-2-yl)-2,5-diphenyltetrazolium bromide; MW, microwave irradiation; PAINS, pan assay interference compounds; PQ, primaquine; RPMI, Roswell Park Memorial Institute; $SOCl_2$, thionyl chloride, TEA, triethylamine, TQ, tafenoquine; TPSA, topological polar surface area.

References

1. World Health Organization. *World Malaria Report 2018*; World Health Organization: Geneva, Switzerland, 2018.
2. World Health Organization. *Global Technical Strategy for Malaria 2016–2030*; World Health Organization: Geneva, Switzerland, 2015.
3. Prudêncio, M.; Rodriguez, A.; Mota, M.M. The silent path to thousands of merozoites: The Plasmodium liver stage. *Nat. Rev. Microbiol.* **2006**, *4*, 849–856. [CrossRef] [PubMed]
4. Campo, B.; Vandal, O.; Wesche, D.L.; Burrows, J.N. Killing the hypnozoite drug discovery approaches to prevent relapse in Plasmodium vivax. *Pathog. Glob. Health* **2015**, *109*, 107–122. [CrossRef] [PubMed]
5. White, N.J. Determinants of relapse periodicity in Plasmodium vivax malaria. *Malar J.* **2011**, *10*, 297. [CrossRef] [PubMed]
6. Vale, N.; Moreira, R.; Gomes, P. Primaquine revisited six decades after its discovery. *Eur. J. Med. Chem.* **2009**, *44*, 937–953. [CrossRef] [PubMed]
7. Pybus, B.S.; Marcsisin, S.R.; Jin, X.; Deye, G.; Sousa, J.C.; Li, Q.; Caridha, D.; Zeng, Q.; Reichard, G.A.; Ockenhouse, C.; et al. The metabolism of primaquine to its active metabolite is dependent on CYP 2D6. *Malar. J.* **2013**, *12*, 212. [CrossRef]
8. Leslie, T.; Rab, M.A.; Ahmadzai, H.; Durrani, N.; Fayaz, M.; Kolaczinski, J.; Rowland, M. Compliance with 14-day primaquine therapy for radical cure of vivax malaria a randomized placebo-controlled trial comparing unsupervised with supervised treatment. *Trans. R. Soc. Trop. Med. Hyg.* **2004**, *98*, 168–173. [CrossRef]
9. Rajapakse, S.; Rodrigo, C.; Fernando, S.D. Tafenoquine for preventing relapse in people with *Plasmodium vivax* malaria. *Cochrane Database Syst. Rev.* **2015**, *29*, CD010458. [CrossRef]
10. Lacerda, M.V.G.; Llanos-Cuentas, A.; Krudsood, S.; Lon, C.; Saunders, D.L.; Mohammed, R.; Yilma, D.; Pereira, D.; Espino, F.E.J.; Mia, R.Z.; et al. Single-dose tafenoquine to prevent relapse of *Plasmodium vivax* malaria. *N. Engl. J. Med.* **2019**, *380*, 215–228. [CrossRef]

11. Llanos-Cuentas, A.; Lacerda, M.V.G.; Hien, T.T.; Vélez, I.D.; Namaik-Larp, C.; Chu, S.S.; Villegas, M.F.; Val, F.; Monteiro, W.M.; Brito, M.A.M.; et al. Tafenoquine versus primaquine to prevent relapse of *Plasmodium vivax* malaria. *N Engl. J. Med.* **2019**, *380*, 229–241. [CrossRef]
12. Llanos-Cuentas, A.; Lacerda, M.V.G.; Rueangweerayut, R.; Krudsood, S.; Gupta, S.K.; Kochar, S.K.; Arthur, P.; Chuenchom, N.; Möhrle, J.J.; Duparc, S.; et al. Tafenoquine plus chloroquine for the treatment and relapse prevention of *Plasmodium vivax* malaria (DETECTIVE): A multicentre, double-blind, randomised, phase 2b dose-selection study. *Lancet* **2014**, *383*, 1049–1058. [CrossRef]
13. Pavić, K.; Perković, I.; Cindrić, M.; Pranjić, M.; Martin-Kleiner, I.; Kralj, M.; Schols, D.; Hadjipavlou-Litina, D.; Katsori, A.-M.; Zorc, B. Novel semicarbazides and ureas of primaquine with bulky aryl or hydroxyalkyl substituents, Synthesis, cytostatic and antioxidative activity. *Eur. J. Med. Chem.* **2014**, *86*, 502–514.
14. Perković, I.; Antunović, M.; Marijanović, I.; Pavić, K.; Ester, K.; Kralj, M.; Vlainić, J.; Kosalec, I.; Schols, D.; Hadjipavlou-Litina, D.; et al. Novel urea and bis-urea primaquine derivatives with hydroxyphenyl and halogenphenyl substituents: Synthesis and biological evaluation. *Eur. J. Med. Chem.* **2016**, *124*, 622–636. [CrossRef]
15. Pavić, K.; Perković, I.; Gilja, P.; Kozlina, F.; Ester, K.; Kralj, M.; Schols, D.; Hadjipavlou-Litina, D.; Pontiki, E.; Zorc, B. Design, synthesis and biological evaluation of novel primaquine-cinnamic acid conjugates of amide and acylsemicarbazide type. *Molecules* **2016**, *21*, 1629. [CrossRef]
16. Pavić, K.; Perković, I.; Pospíšilová, Š.; Machado, M.; Fontinha, D.; Prudêncio, M.; Jampilek, J.; Coffey, A.; Endersen, L.; Rimac, H.; et al. Primaquine hybrids as promising antimycobacterial and antimalarial agents. *Eur. J. Med. Chem.* **2018**, *143*, 769–779. [CrossRef]
17. Vlainić, J.; Kosalec, I.; Pavić, K.; Hadjipavlou-Litina, D.; Pontiki, E.; Zorc, B. Insights into biological activity of ureidoamides with primaquine and amino acid moieties. *J. Enzym. Inhib. Med. Chem.* **2018**, *33*, 376–382. [CrossRef]
18. Levatić, J.; Pavić, K.; Perković, I.; Uzelac, L.; Ester, K.; Kralj, M.; Kaiser, M.; Rottmann, M.; Supek, F.; Zorc, B. Machine learning prioritizes synthesis of primaquine ureidoamides with high antimalarial activity and attenuated cytotoxicity. *Eur. J. Med. Chem.* **2018**, *146*, 651–667. [CrossRef]
19. Beus, M.; Rajić, Z.; Maysinger, D.; Mlinarić, Z.; Antunović, M.; Marijanović, I.; Fontinha, D.; Prudêncio, M.; Held, J.; Olgen, S.; et al. SAHA-primaquine hybrids (sahaquines) as potential anticancer and antimalarial compounds. *Chem. Open* **2018**, *7*, 624–638.
20. Rajić, Z.; Beus, M.; Michnova, H.; Vlainić, J.; Persoons, L.; Kosalec, I.; Jampilek, J.; Schols, D.; Keser, T.; Zorc, B. Asymmetric primaquine and halogenaniline fumardiamides as novel biologically active Michael acceptors. *Molecules* **2018**, *23*, 1724. [CrossRef]
21. Pérez, B.; Teixeira, C.; Albuquerque, I.S.; Gut, J.; Rosenthal, P.J.; Prudêncio, M.; Gomes, P. Primacins, *N*-cinnamoyl-primaquine conjugates, with improved liver-stage antimalarial activity. *Med. Chem. Commun.* **2012**, *3*, 1170–1172. [CrossRef]
22. *Chemicalize, 2017*; ChemAxon Ltd.: Budapest, Hungary, 2017. Available online: https://chemicalize.com (accessed on 15 April 2019).
23. Baell, J.B.; Holloway, G.A. New substructure filters for removal of pan assay interference compounds (PAINS) from screening libraries and for their exclusion in bioassays. *J. Med. Chem.* **2010**, *53*, 2719–2740. [CrossRef]
24. Swiss ADME Programs, Swiss Institute of Bioinformatics, Lausanne, Switzerland. Available online: http://www.swissadme.ch (accessed on 10 April 2019).
25. Held, J.; Gebru, T.; Kalesse, M.; Jansen, R.; Gerth, K.; Müller, R.; Mordmüller, B. Antimalarial activity of the myxobacterial macrolide chlorotonil A. *Antimicrob. Agents Chemother.* **2014**, *58*, 6378–6384. [CrossRef]
26. Noedl, H.; Bronnert, J.; Yingyuen, K.; Attlmayr, B.; Kollaritsch, H.; Fukuda, M. Simple histidine-rich protein 2 double-site sandwich enzyme-linked immunosorbent assay for use in malaria drug sensitivity testing. *Antimicrob. Agents Chemother.* **2005**, *49*, 3575–3577. [CrossRef]
27. R Core Team. *A Language and Environment for Statistical Computing*; R Foundation for Statistical Computing: Vienna, Austria, 2018; Available online: https://www.R-project.org/ (accessed on 25 March 2019).
28. Machado, M.; Sanches-Vaz, M.; Cruz, J.P.; Mendes, A.M.; Prudêncio, M. Inhibition of Plasmodium hepatic infection by antiretroviral compounds. *Front. Cell. Infect. Microbiol.* **2017**, *7*, 1–9. [CrossRef]

29. Ploemen, I.H.J.; Prudêncio, M.; Douradinha, B.G.; Ramesar, J.; Fonager, J.; Gemert, G.J.; Luty, A.J.F.; Hermsen, C.C.; Sauerwein, R.W.; Baptista, F.G.; et al. Visualisation and quantitative analysis of the rodent malaria liver stage by real time imaging. *PLoS ONE* **2009**, *4*, e7881. [CrossRef]

Sample Availability: Samples of the compounds are not available from the authors.

6. RASPRAVA

Kao što je rečeno u Uvodu, učinkovitost lijekova iz skupine antimalarika i njihovih derivata u terapiji karcinoma intenzivno se proučava. Istraživanja koja se provode na Zavodu za farmaceutsku kemiju također su usmjerena k tom cilju. Tijekom nekoliko godina sintetizirano je oko 200 novih derivata primakina kao potencijalnih citostatika, a njihov pregled dan je u revijalnom članku (160). Mnogi od tih spojeva pokazuju antiproliferativno djelovanje u niskim mikromolarnim ili nanomolarnim koncentracijama prema različitim staničnim linijama karcinoma ili selektivno djelovanje na pojedine stanične linije, prije svega na stanice adenokarinoma dojke, MCF-7.

Kombinacija (hibridizacija) dvaju farmakofora ili dvije molekule ljekovite tvari u jedinstvenu molekulu jedan je od pristupa u razvoju novih lijekova (161). Najvažnija prednost hibrida je u potencijalnom djelovanju na više meta, čime bi se mogla povećati njihova učinkovitost, a smanjiti toksičnost i interakcije između lijekova (162, 163). Kombinacijom dvaju molekula s citotoksičnim djelovanjem na stanice karcinoma moglo bi se postići sinergističko djelovanje, što bi u konačnici rezultiralo povoljnijim učinkom za pacijenta. S obzirom da stanice karcinoma posjeduju razne proteine, enzime ili signalne putove kojima mogu zaobići djelovanje citostatika, kombinacija lijekova različitih mehanizama djelovanja mogla bi dovesti do smanjene pojavnosti rezistencije (164). U okviru ove disertacije, pomoću koncepta hibridnih spojeva, dizajnirani su i sintetizirani sahakini, novi spojevi koji predstavljaju kombinaciju antimalarika primakina i citostatika SAHA-e (vorinostata) te im je ispitano citostatsko djelovanje (Slika 12). Prvi cilj bila je sinteza sahakina kojima je varirana duljina i vrsta poveznice između primakinskog prstena i terminalne hidroksamske kiseline. Kasnije je serija proširena spojevima kojima je promijenjena terminalna funkcionalna skupina i/ili kinolinski prsten kako bi se dobio bolji uvid u odnos strukture i djelovanja (Shema 11).

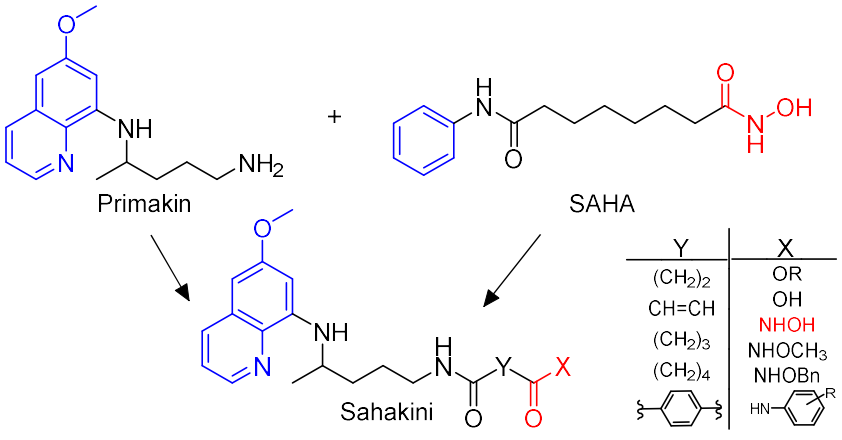

Slika 12. Dizajniranje sahakina.

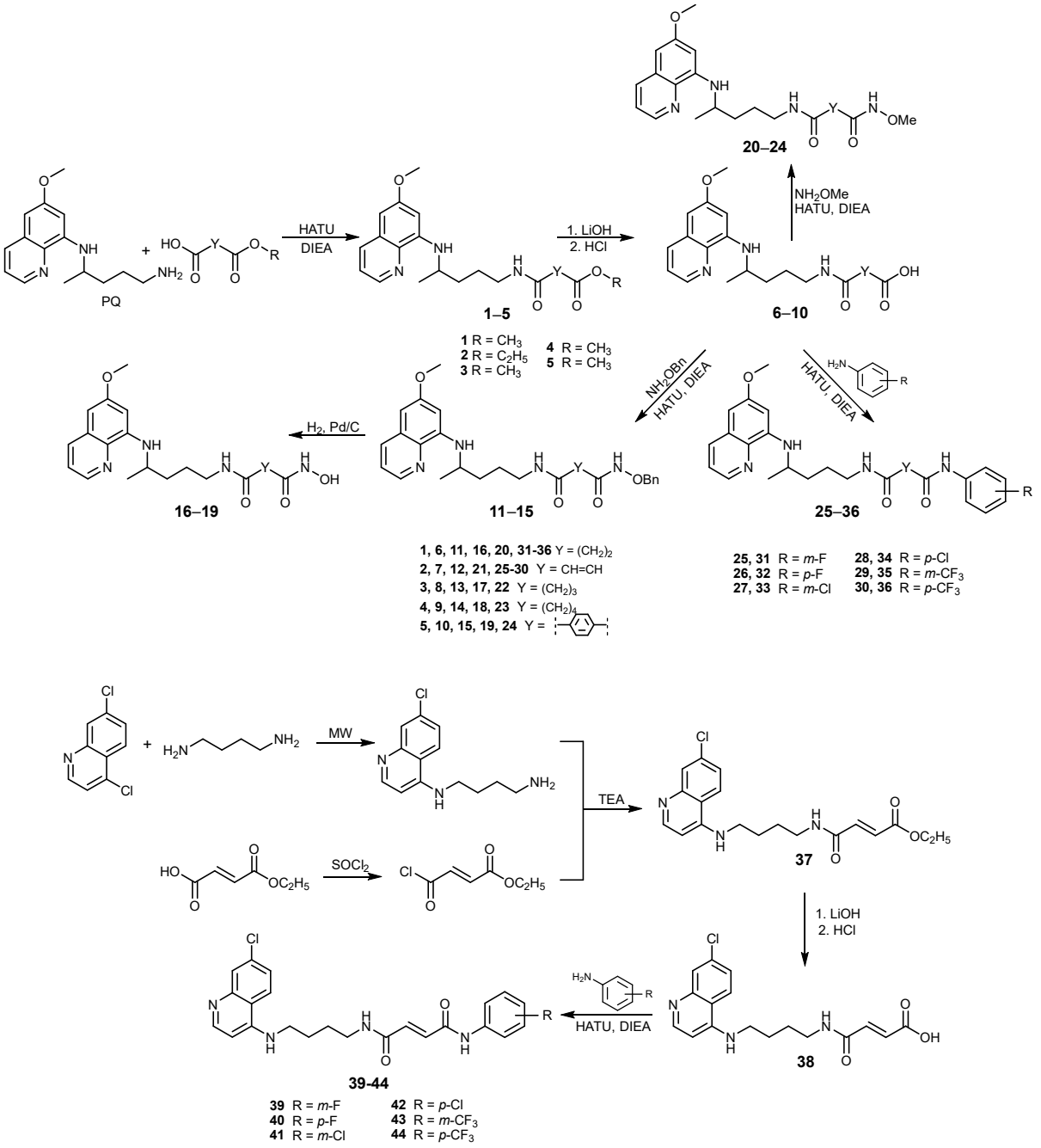

Shema 11. Sinteza sahakina.

Prva serija sahakina bila je serija derivata primakina od 24 spoja koji su se međusobno razlikovali po duljini/vrsti poveznice te po terminalnoj funkcionalnoj skupini (esterskoj, karboksilnoj skupini, *O*-benzil-, *O*-metil- i nesupstituiranoj hidroksamskoj kiselini). Sinteza počinje reakcijom primakina s monoesterima dikarboksilnih kiselina (monometil-sukcinat, monoetil-fumarat, monometil-glutarat, monometil-adipat i monometil-tereftalat) u prisutnosti HATU-s kao *coupling* reagensa i DIEA. Reakcija monoetil-fumarata s primakinom u prisutnosti HATU/DIEA nije dala očekivani produkt **2**. Međutim, spoj **2** je dobiven reakcijom

kiselinskog klorida monoetil-fumarata i primakina. Amido-esteri **1**–**5** podvrgnuti su hidrolizi uz litijev hidroksid, čime su dobivene amido-karboksilne kiseline **6**–**10**, koje su u idućem koraku reagirale sa zaštićenim hidroksilaminima. Aktivacija karboksilne kiseline provedena je kao i u prvom koraku – uz HATU i DIEA. Produkti reakcija s *O*-benzil- ili *O*-metilhidroksilaminom bili su *O*-benzilhidroksamske kiseline **11**–**15**, odnosno *O*-metilhidroksamske kiseline **20**–**24**. Nesupstituirane hidroksamske kiseline **16**–**19** dobivene su katalitičkom hidrogenolizom odgovarajućih *O*-benzilhidroksamskih kiselina. Hidroksamska kiselina s fumarnom kiselinom u središnjem dijelu nije dobivena jer je hidrogeniranjem odgovarajućeg prekursora došlo do adicije vodika na dvostruku vezu te je kao produkt dobivena sukcinil-hidroksamska kiselina **16**. Sve reakcije dale su produkte čija su iskorištenja varirala od srednjih do visokih, pri čemu su najviša iskorištenja imale reakcije u prva dva sintetska koraka (70–97 %), a najniža reakcije sinteze *O*-benzilhidroksamske kiseline (40–61 %).

Nedavnom registracijom lijekova koji se ireverzibilno vežu za biološke mete kovalentim vezama, porastao je interes za dizajniranje takvih lijekova. Jedni od prvih odobrenih ireverzibilnih inhibitora bili su afatinib, neratinib i osimertinib (inhibitori receptora epidermalnog faktora rasta), te ibrutinib (inhibitor Brutonove tirozin kinaze) (165, 166). Navedeni lijekovi su Michaelovi akceptori, tj. u svojoj strukturi sadrže α,β-nezasićene karbonilne skupine, zbog čega mogu sudjelovati u ireverzibilnoj hetero-Michaelovoj adiciji s cisteinskim ostacima specifičnog proteina. Stvaranje tiolnih adukata jedan je od glavnih puteva kovalentne inhibicije proteina i također glavni put deaktivacije kovalentnih inhibitora nakon stvaranja adukata sa staničnim tiolima, kao što je glutation. Također, dokazano je da spojevi koji podliježu selektivnoj kovalentnoj inhibiciji imaju sposobnost nadvladavanja rezistencije na lijekove (167–169). Uzimajući navedene činjenice u obzir, dizajnirana je druga serija sahakina, diamida **25**–**30**, s fumarnom kiselinom u središnjem dijelu koja sadrži dvostruku vezu C=C konjugiranu s karbonilnom skupinom zbog čega može sudjelovati u reakcijama Michaelove adicije (170). Amidne veze u tim diamidima ostvarene su na jednoj strani s primakinom, a na drugoj s odgovarajućim halogeniranim anilinom. Za provjeru važnosti konjugiranog sustava C=C–CO za biološki učinak, sintetizirani su i analogni derivati jantarne kiseline (zasićene kiseline s istim brojem C-atoma kao i fumarna kiselina). Za pripravu sahakina **25**–**36** korištene su amido-karboksilne kiseline **6** i **7** te sljedeći halogenanilini: *m*-fluoroanilin, *p*-fluoroanilin, *m*-kloroanilin, *p*-kloroanilin, *m*-trifluormetilanilin i *p*-trifluormetilanilin. U ovoj seriji sintetizirano je ukupno 12 sahakina. Općenito su iskorištenja

reakcija sinteze derivata jantarne kiseline bila viša od analognih derivata fumarne kiseline (49–90 % za derivate jantarne, odnosno 31–58 % za derivate fumarne kiseline). Također, *p*-derivati su dobiveni u nešto boljim iskorištenjima nego *m*-derivati.

Svi sahakini ispunjavaju Lipinskijevo pravilo broja 5 i Gelovanijeva pravila ($M_r \leq 500$, log $P \leq 5$, broj donora u vodikovoj vezi ≤ 5, broj akceptora u vodikovoj vezi ≤ 10, TPSA < 140 Å^2, MR unutar raspona od 40 do 130 cm^3/mol, ukupan broj atoma 20–70), pa bi se nakon peroralne primjene trebali apsorbirati. Jedino sahakin **15** s tereftalnom kiselinom u razmaknici neznatno odstupa od navedenih pravila. Tijek kemijskih reakcija i čistoća produkata praćeni su tankoslojnom kromatografijom, a njihove strukture potvrđene su uobičajenim spektroskopskim metodama (IR, ^{1}H i ^{13}C NMR, MS) te elementarnom analizom koja je služila i za potvrdu čistoće (Prilozi 1).

Sahakini **1**–**24** testirani su na stanicama osteosarkoma (U2OS), hepatocelularnog karcinoma (HepG2), adenokarcinoma dojke (MCF-7), glioblastoma (U251N) i na normalnim stanicama (embrionalne stanice bubrega, Hek293). Navedena biološka ispitivanja provedena su na Biološkom odsjeku Prirodoslovno-matematičkog fakulteta u Zagrebu. Nesupstituirane hidroksamske kiseline **16**–**19** pokazale su aktivnost prema svim ispitanim staničnim linijama u niskim mikromolarnim koncentracijama koje su varirale od 1,6 do 5,4 μM. S druge strane, najmanje aktivne bile su amido-karboksilne kiseline **6**–**9** koje nisu inhibirale rast niti jedne stanične linije. Samo je derivat tereftalne kiseline **10** inhibirao rast MCF-7 stanica. Amido-esteri **1**–**5** pokazali su slabu aktivnost, a *O*-benzil- i *O*-metilhidroksamske kiseline **11**–**15**, odnosno **20**–**24** pokazale su aktivnost samo prema MCF-7 staničnoj liniji. Općenito su MCF-7 stanice bile najosjetljivije od svih ispitanih staničnih linija, a njihov rast inhibirala je većina ispitanih sahakina. Velika selektivnost derivata primakina na tu staničnu liniju primijećena je i u prijašnjim istraživanjima provedenim u Zavodu za farmaceutsku kemiju (160, 164, 172). HepG2 stanice bile su najotpornije na djelovanje sahakina. Jedini spojevi koji su inhibirali rast HepG2 stanica bile su nesupstituirane hidroksamske kiseline i *O*-benzilhidroksamski derivat adipinske kiseline **14**. Djelovanje spojeva ispitano je i na zdravim stanicama, Hek293 staničnoj liniji, kako bi se ispitala selektivnost. Sedam sahakina inhibiralo je rast Hek293 stanica, uključujući i nesupstituirane hidroksamske kiseline, ali u koncentracijama višim od onih koje su potrebne za inhibiciju rasta stanica karcinoma.

Sahakini **25**–**36** testirani su *in vitro* na devet staničnih linija karcinoma, tri od karcinoma solidnog tipa (stanice adenokarcinoma gušterače, Capan-1, kolorektalnog karcinom, HCT-116,

i karcinoma pluća, NCI-H460), a preostalih šest staničnih linija bile su stanice kronične mijeloične leukemije (Hap1), akutne limfoblastičke leukemije (DND-41), akutne mijeloične leukemije (HL-60), kronične mijeloične leukemije (K-562), multiplog mijeloma (MM.1S) te stanice ne-Hodkinovog limfoma (Z-138). Navedena biološka ispitivanja provedena su na Rega Institute for Medical Research KU Leuven (Belgija). Sahakini sa supstituentima u *meta*-položaju bili aktivniji od analognih *para*-supstituiranih spojeva. Najaktivniji je bio sahakin **25**, *m*-fluoranilinski derivat s fumarnom poveznicom koji je inhibirao rast svih ispitanih staničnih linija u niskim mikromolarnim koncentracijama s IC_{50} vrijednostima od 5,7 do 31,2 μM. Druga dva *meta*-derivata, sahakini **27** i **29**, pokazali su selektivno citostatsko djelovanje prema staničnoj liniji DND-41. IC_{50} vrijednosti iznosile su 8,4 μM za *m*-kloranilinski, odnosno 8,9 μM za *m*-trifluormetilanilinski derivat. Analogni derivati sa supstituentima u *para*-položaju nisu inhibirali rast DND-41 stanica. Najosjetljivija je bila stanična linija DND-41 čiji su rast inhibirala sva tri *meta*-derivata s IC_{50} vrijednostima manjim od 10 μM, a najotpornije su bile stanične linije HL-60 i MM.1S čiji je rast inhibirao jedino *m*-fluoranilinski derivat. Derivati jantarne kiseline nisu inhibirali rast tumorskih stanica što ukazuje na važnost Michaelovog akceptora u strukturi za citostatsko djelovanje.

Jedan od najagresivnijih oblika malignih bolesti je glioblastom, najčešći oblik tumora mozga u odraslih (37). Nakon kirurškog odstranjivanja tumora, slijedi zračenje uz kemoterapiju kako bi se uništile stanice raka preostale nakon operacije (43). Jedini lijek koji je trenutno odobren za liječenje glioblastoma je temozolomid (37). Međutim, preživljavanje je u prosjeku 14–16 mjeseci, a samo mali postotak pacijenata preživi 5 godina nakon dijagnoze (48) jer stanice karcinoma vrlo brzo razviju rezistenciju na temozolomid povećavajući količine enzima MGMT (47). S obzirom da su HDAC enzimi pretjerano eksprimirani u glioblastomu te da njihov mehanizam djelovanja ne ovisi o MGMT-u i drugim mehanizmima rezistencije glioblastoma na terapiju, HDAC inhibitori potencijalni su citostatici za terapiju glioblastoma (173–175). Trenutno je registrirano nekoliko HDAC inhibitora: SAHA, panobinostat i belinostat (75, 91, 101), s hidroksamskom skupinom kao farmakoforom koja kompleksira ione cinka u aktivnom središtu HDAC-a (77). Osim HDAC-a, ovi lijekovi inhibiraju i MMP enzime, koji također sadrže ion cinka u aktivnom mjestu. Ti enzimi su pretjerano eksprimirani u karcinomu te potiču njegov rast, proliferaciju, migraciju i metastaziranje (52, 72, 73). Zbog toga se SAHA trenutno nalazi u kliničkim ispitivanjima za terapiju glioblastoma bilo u monoterapiji ili u kombinaciji s drugim kemoterapeuticima ili zračenjem (176–179).

Učinak najaktivnijeg sahakina, N^1-hidroksi-N^5-(4-((6-metoksikinolin-8-il)amino)pentil)-glutaramida (**17**), detaljno je testiran na U251N stanicama. Njegova IC_{50} vrijednost nakon 72 h iznosila je 10 μM što je tri puta niže od vrijednosti temozolomida. Analogni sahakini, koji u svojoj strukturi nemaju hidroksamsku kiselinu, nisu imali nikakvo inhibitorno djelovanje na stanice glioblastoma što ukazuje na važnost hidroksamske skupine. Djelovanje sahakina **17** ispitano je *in vitro* u 2D modelu koji je jednostavniji i brži, te u 3D modelu (na tzv. tumoroidima), koji bolje predstavljaju model tumora: otporniji su i daju potpuniju informaciju o prodiranju ispitivanog spoja u tumor. Sahakin **17** je nakon 7 dana smanjio veličinu tumoroida stanica glioblastoma za 37 % (Slika S1 u Prilozima 2). Važnu ulogu u ponovnoj pojavnosti glioblastoma imaju matične stanice tumora koje su prisutne u mikrookolišu karcinoma. One vrlo često zaostaju nakon tumorske resekcije, a imaju mogućnost razvoja u stanice glioblastoma te se mogu dalje širiti i razmnožavati (41, 42). Nakon 4 dana, sahakin **17** je u 10 μM koncentraciji uspješno uništio agregate matičnih stanica tumora, za razliku od temozolomida koji je u 10 puta većoj koncentraciji imao manji utjecaj. Stanice glioblastoma vrlo rijetko metastaziraju izvan mozga, ali zato mogu migrirati ili prodirati u moždano tkivo i stvarati nove tumorske lezije (180). Zbog toga je praćen učinak sahakina **17** na migraciju stanica u stvorenu pukotinu te učinak na invazivnost tumorskih stanica mjerenjem radijalnog širenja stanica iz 3D tumoroida nasađenih u kolagenski matriks. Iako nije imao učinka na migraciju stanica, sahakin **17** je smanjio invaziju stanica za preko 50 % u odnosu na kontrolu. Kako bi mogle lakše prodirati u tkivo, stanice karcinoma izlučuju MMP enzime koji mogu razgraditi izvanstanični matriks. MMP-2 i MMP-9 su jedini enzimi koji mogu razgraditi fibrilarni kolagen koji sudjeluje u izgradnji izvanstaničnog matriksa i, kao što je spomenuto, u svojem aktivnom središtu sadrže atom cinka (77). Metodom zimografije ispitan je učinak sahakina **17** na ekspresiju MMP-2 i MMP-9. Rezultati ukazuju da ispitani sahakin ne utječe na ekspesiju MMP-9, dok ekspresiju MMP-2 smanjuje za oko 40 % (Slika S2 u Prilozima 2). Da bismo bolje razlučili mehanizam djelovanja sahakina na inhibiciju invazije, testirali smo njegov učinak na aktivnost HDAC6. HDAC6 je jedini HDAC enzim koji se nalazi isključivo u citosolu stanice, zbog čega djeluje na proteine citosola, kao što su α-tubulin, kortaktin i Hsp90. Deacetilacijom α-tubulina i kortaktin sudjeluje u kontroli citoskeleta i poticanju migracije stanica, dok deacetilacijom Hsp90 omogućava njegovu funkciju šaperona (65, 67). Još jedna od posebnosti HDAC6 u odnosu na ostale HDAC enzime je šire vezno mjesto zbog čega je moguće dizajnirati selektivne HDAC6 inhibitore (181). HDAC inhibitori koji se trenutno nalaze u upotrebi nisu selektivni te djeluju i na druge mete što kao posljedicu može imati ozbiljne nuspojave (83, 96, 105, 106). Za razliku od SAHA-e, sahakin **17** ima dva

aromatska prstena u strukturi zbog čega bi lakše mogao ući u vezno mjesto HDAC6 jer je sterički prevelik za ostale HDAC-ove. Metodom imunocitokemije dokazano je da sahakin **17** selektivno inhibira HDAC6 u nanomolarnim koncentracijama, dok SAHA neselektivno inhibira i HDAC klase I i HDAC6. Posljedično, sahakin **17** uzrokuje reorganizaciju α-tubulina i tako ometa invaziju stanica karcinoma (Slika S3 u Prilozima 2). Osim što primakin u strukturi sahakina **17** ima ulogu u selektivnosti prema HDAC6 enzimu, dokazano je da primjena primakina inhibira P-glikoprotein i tako smanjuje rezistenciju stanica karcinoma na djelovanje citostatika (144). Sahakin **17** je smanjio aktivnost P-glikoproteina u stanicama glioblastoma u koncentraciji od 10 μM, dok je SAHA pokazala slabiju inhibitornu aktivnost u istoj koncentraciji (Slika S4 u Prilozima 2).

U glioblastomu je vrlo često povećana ekspresija receptora za epidermalni faktora rasta (engl. *epidermal growth factor receptor*, EGFR), kinaze koji ima ulogu u tumorigenezi i rezistenciji tumora na terapiju (182). To čini EGFR zanimljivom metom za razvoj novih lijekova i zbog toga se danas nekoliko EGFR inhibitora nalazi u kliničkim ispitivanjima za terapiju glioblastoma (183, 184). Djelovanje sahakina **17** na ekspresiju EGFR ispitano je Western blot metodom. Također je ispitano utječe li primjena sahakina na aktivaciju nizvodnih meta EGFR-a, fosforilaciju AKT i ERK1/2. Sahakin **17** je utjecao na smanjenje ekspresije EGFR-a, p-AKT i p-ERK1/2. Koncentracije ukupnog AKT i ERK1/2 ostale su nepromijenjene na temelju čega se može zaključiti da je smanjena aktivacija AKT i ERK1/2 posljedica inhibicije EGFR-a sahakinom **17**.

Klorokin je drugi antimalarik iz skupine derivata kinolina koji se nalazi u kliničkim ispitivanjima za terapiju karcinoma (131). Za razliku od primakina, on je derivat 4--aminokinolina i djeluje na eritrocitnu fazu malarije (123). Osim za terapiju malarije, klorokin se već dulje vrijeme nalazi u pretkliničkim ispitivanjima kao inhibitor autofagije (132). Iako se još ne zna točan mehanizam djelovanja, uočeno je da klorokin ometa fuziju lizosoma s autofagom čime sprječava nastajanje autofagosoma, proces ključan za odvijanje autofagije (185).

Na temelju rezultata bioloških ispitivanja, sintetizirana je zadnja serija sahakina **39**–**44** u kojima je primakinska jezgra zamijenjena klorokinskom, a zadržana je poveznica na bazi fumarne kiseline. Sinteza je počela kondenzacijom 4,7-diklorokinolina s 1,4-diaminobutanom potpomognutom mikrovalovima kako bi se dobio analog klorokina s primarnom amino

skupinom. Dobiveni produkt reagirao je s kiselinskim kloridom monoetil-fumarata. Amido--ester **37** podvrgnut je hidrolizi uz litijev hidroksid pri čemu je nastala amido-karboksilna kiselina **38**. Konačni spojevi, tj. fumardiamidi **39**–**44**, dobiveni su reakcijom halogenanilina sa spojem **38** u prisutnosti HATU i DIEA. Kao i u prethodnoj seriji sahakina, u ovoj seriji korišteni su *m*-fluoroanilin, *p*-fluoroanilin, *m*-kloroanilin, *p*-kloroanilin, *m*-trifluormetilanilin i *p*-trifluormetilanilin. Iskorištenja u prve tri reakcije bila su relativno visoka (teorijsko iskorištenje za reakciju kondenzacije, 73 % za amido-ester i 97 % za amido-karboksilnu kiselinu). Međutim, iskorištenja u reakcijama dobivanja amida varirala su od 25 do 91 %. Općenito, iskorištenja sinteze *para*-derivata bila su bolja od iskorištenja analognih *meta*-derivata.

Citostatsko djelovanje sahakina **39**–**44** ispitano je na staničnim linijama karcinoma pluća nemalih stanica (H460), HCT-116 i MCF-7, a na Hek293 stanicama ispitan je učinak na zdrave stanice (186). Navedena biološka ispitivanja provedena su na Zavodu za molekularnu medicinu Instituta Ruđer Bošković u Zagrebu. Svi spojevi pokazali su citostatsko djelovanje u niskim mikromolarnim ili čak nanomolarnim koncentracijama. Najosjetljivije su bile MCF-7 stanice, ali spojevi su u relativnom sličnim koncentracijama djelovali i na HCT-116. Spojevi su također djelovali i na Hek293 stanice, ali u većim koncentracijama od onih koje su bile potrebne za citostatski učinak na stanice karcinoma. Najaktivniji je bio sahakin **44**, derivat *p*-trifluormetilanilina, čija je IC_{50} vrijednost bila u nanomolarnim koncentracijama, odnosno 0.4 ± 0.1 μM za MCF-7 stanice i 0.3 ± 0.1 μM za HCT-116 stanice. Najmanje aktivan bio je sahakin **43**, derivat *m*-trifluormetilanilina, iako je i on inhibirao rast stanica karcinoma u nižim mikromolarnim koncentracijama.

Zbog različitog citostatskog djelovanja, pojedini sahakini mogu poslužiti kao spojevi-uzori u daljnjem dizajniranju i razvoju spojeva za terapiju određenih karcinoma, pri čemu su zanimljiviji sahakini koji pokazuju selektivno djelovanje prema jednoj staničnoj liniji karcinoma. Također, ispitivanjem djelovanja na zdravim stanicama (Hek293) može se dobiti uvid u potencijalno djelovanje ispitivanog spoja na zdrave stanice u organizmu. Ukoliko spoj ima selektivno djelovanje u *in vitro* uvjetima, veće su šanse da će taj spoj imati i manje nuspojava u daljnjim *in vivo* i kliničkim ispitivanjima.

Iako klorokin i primakin ispoljavaju slabo citostatsko djelovanje, modifikacijom njihovih molekula moguće je pojačati antiproliferativni učinak. U okviru ove doktorske disertacije sintetizirani su sahakini – hibridni spojevi, derivati primakina/klorokina s različitim funkcionalnim skupinama i razmaknicama. Sahakini s nesupstituiranom hidroksamskom

skupinom te *meta*-halogenanilinski derivati bili su najaktivniji. Izborom funkcionalne skupine može se utjecati na aktivnost, ali i na selektivnost spojeva. Primakinski derivat *m*-fluoranilina bio je najaktivniji u amidnoj seriji sahakina, ali je bio neselektivan. S druge strane, zamjenom atoma fluora atomom klora ili trifluormetilnom skupinom, dobiveni su sahakini sa selektivnim djelovanjem. Velik utjecaj na djelovanje ima i kinolinski prsten u strukturi spojeva. Derivati klorokina bili su citotoksičniji od analognih derivata primakina. Posjedovali su aktivnost u vrlo niskim mikromolarnim koncentracijama. Međutim, derivati klorokina su neselektivno djelovali na sve ispitane stanične linije, zbog čega su derivati primakina zanimljiviji kandidati za potencijalne nove citostatike. Nadalje, na citostatsko djelovanje sahakina utjecao je i izbor poveznice. Sahakini s nezasićenom dikiselinom u poveznici bili su aktivniji od analognih derivata sa zasićenom poveznicom. S druge stane, prekratka ili prerigidna poveznica, s jantarnom, odnosno tereftalatnom kiselinom, rezultirala je slabljenjem ili gubitkom citostatskog djelovanja.

Iz svega navedenog može se zaključiti da su modifikacijom kinolinskog prstena, vrste i duljine poveznice, te funkcionalne skupine u sahakinima, dobiveni spojevi vrlo različitog citostatskog djelovanja. S obzirom da su stanice adenokarcinoma dojke MCF-7 i glioblastoma U251N bile najpodložnije djelovanju sahakina, ovi spojevi mogu biti zanimljivi kandidati za vodeće spojeve u razvoju citostatskih lijekova za terapiju karcinoma dojke i glioblastoma.

7. ZAKLJUČCI

U sklopu ovog doktorskog rada:

- Dizajnirano je i sintetizirano 44 nova spoja, sahakina, kao potencijalnih citostatika.
- Sahakini su građeni iz tri ključna dijela: kinolinskog prstena (dio molekule primakina ili klorokina), središnjeg dijela (dikarboksilne kiseline: jantarne, fumarne, glutarne, adipinske, tereftalne) te završnog dijela s dodatnom funkcionalnom skupinom (esterskom, karboksilnom, amidnom te *O*-benzil-, *O*-metil- ili nesupstituiranom hidroksamskom kiselinom).
- Sinteza sahakina uključuje dva ključna kondenzacijska koraka ostvarena pomoću standardnog *coupling* reagensa HATU-a u prisutnosti DIEA.
- Derivati primakina imali su bolja iskorištenja od analognih klorokinskih derivata.
- Strukture novih spojeva potvrđene su uobičajenim analitičkim i spektroskopskim metodama (talište, CHN analiza, ^{1}H i ^{13}C NMR, MS).
- Programom Chemicalize.org izračunata su njihova *drug-like* svojstva.
- Ispitano je citostatsko djelovanje sahakina na 14 tumorskih staničnih linija (Capan-1, HCT-116, NCI-H460, Hap1, DND-41, HL-60, K-562, MM.1S, Z-138, U2OS, HepG2, MCF-7, H460, U251N). Najosjetljivije su MCF-7 i U251N stanične linije.
- Funkcionalna skupina u završnom dijelu sahakina značajno utječe na biološku aktivnost: najaktivniji su sahakini iz podskupine hidroksamskih kiselina (IC_{50} u niskom mikromolarnom području), a najmanje aktivni sahakinini s karboksilnom skupinom.
- Sahakini s fumardiamidnom poveznicom pokazuju puno jače djelovanje od analoga s jantarnom kiselinom, što ukazuje na važnost α,β-nezasićene karbonilne skupine.
- U sahamidima amidnog tipa, položaj supstituenta u halogenanilinu utječe na citostatsko djelovanje: *meta*-derivati aktivniji su od analognih derivata s *para*-supstituentima.
- Najaktivniji spoj je N^1-hidroksi-N^5-(4-((6-metoksikinolin-8-il)amino)pentil)-glutaramid, hidroksamska kiselina s primakinskom jezgrom i glutarnom kiselinom u poveznici. Njegov mehanizam djelovanja ispitan je na U251N, stanicama glioblastoma. Dokazano je da ovaj spoj selektivno inhibira HDAC6, invaziju tumorskih stanica, smanjuje ekspresiju MMP-2 i EGFR, smanjuje aktivaciju AKT i ERK1/2, ubija stanice glioblastoma u 3D staničnom tumorskom modelu te matične stanice tumora mozga.
- Rezultati ukazuju na sahakine kao potencijalne vodeće spojeve u razvoju citostatskih lijekova za terapiju karcinoma dojke i glioblastoma.

Rezultati istraživanja provedenih u okviru ovog doktorskog rada objavljeni su u četiri znanstvena rada i 13 kongresnih priopćenja.

8. POPIS LITERATURE

(1) Bray F, Ferlay J, Soerjomataram I, Siegel RL, Torre LA, Jemal A. Global cancer statistics 2018: GLOBOCAN estimates of incidence and mortality worldwide for 36 cancers in 185 countries. *CA Cancer J Clin*, 2018, 68, 394–424.

(2) World Health Organisation. Cancer. https://www.who.int/en/news-room/fact-sheets/detail/cancer, pristupljeno 07. 12. 2019.

(3) Hassanpour SH, Mohammadamin D. Review of cancer from perspective of molecular. *J Cancer Res Pract*, 2017, 4, 127–129.

(4) Hanahan D, Weinberg RA. Hallmarks of cancer: the next generation. *Cell*, 2011, 144, 646–674.

(5) Rajabi M, Mousa SA. The role of angiogenesis in cancer Treatment. *Biomedicines*, 2017, 5, pii: E34.

(6) Baeriswyl V, Christofori G. The angiogenic switch in carcinogenesis. *Semin Cancer Biol*, 2009, 19, 329–337.

(7) Kessenbrock K, Plaks V, Werb Z. Matrix metalloproteinases: Regulators of the tumor microenvironment. *Cell*, 2010, 141, 52–67.

(8) Ferrara N. Vascular endothelial growth factor. *Arterioscler Thromb Vasc Biol*, 2009, 29, 789–791.

(9) Son B, Lee S, Youn H, Kim E, Kim W, Youn B. The role of tumor microenvironment in therapeutic resistance. *Oncotarget*, 2017, 8, 3933–3945.

(10) Longley DB, Johnston PG. Molecular mechanisms of drug resistance. *J Pathol*, 2005, 205, 275–292.

(11) Curtin NJ. DNA repair dysregulation from cancer driver to therapeutic target. *Nat Rev*, 2012, 12, 801–817.

(12) Nosengo N. Can you teach old drugs new tricks? *Nature*, 2015, 534, 314–316.

(13) Chong CR, Sullivan DJ Jr. New uses for old drugs. *Nature*, 2007, 488, 645–646.

(14) New Global Cancer Data: GLOBOCAN 2018. https://www.uicc.org/new-global-cancer-data-globocan-2018, pristupljeno 09. 12. 2019.

(15) Rak dojke – statistika. http://www.onkologija.hr/rak-dojke/rak-dojke-statistika/, pristupljeno 09. 12. 2019.

(16) Gomez-Raposo C, Zambrana Tevar F, Sereno Moyano M, Lopez Gomez M, Casado E. Male breast cancer. *Cancer Treat Rev*, 2010, 36, 451–457.

(17) Breast Cancer: Statistics. https://www.cancer.net/cancer-types/breast-cancer/statistics/2015, pristupljeno 09. 12. 2019.

(18) Russo J, Russo IH. The role of estrogen in the initiation of breast cancer. *J Steroid Biochem Mol Biol*, 2006, 102, 89–96.

(19) Davies C, Pan H, Godwin J, Gray R, Arriagada R, Raina V, Abraham M, Medeiros Alencar VH, Badran A, Bonfill X, Bradbury J, Clarke M, Collins R, Davis SR, Delmestri A, Forbes JF, Haddad P, Hou MF, Inbar M, Khaled H, Kielanowska J, Kwan WH, Mathew BS, Mittra I, Müller B, Nicolucci A, Peralta O, Pernas F, Petruzelka L, Pienkowski T, Radhika R, Rajan B, Rubach MT, Tort S, Urrútia G, Valentini M, Wang Y, Peto R. Adjuvant Tamoxifen: Longer Against Shorter (ATLAS) Collaborative Group. Long-term effects of continuing adjuvant tamoxifen to 10 years versus stopping at 5 years after diagnosis of oestrogen receptor-positive breast cancer: ATLAS, a randomised trial. *Lancet*, 2013, 381, 805–816.

(20) Foulkes WD, Smith IE, Reis-Filho JS. Triple-negative breast cancer. *N Engl J Med*, 2010, 363, 1938–1948.

(21) WebMd. Types of Breast Cancer. https://www.webmd.com/breast-cancer/guide/breast-cancer-types-er-positive-her2-positive#1, pristupljeno 09. 12. 2019.

(22) Cardoso F, Kyriakides S, Ohno S, Penault-Llorca F5, Poortmans P, Rubio IT, Zackrisson S, Senkus E. Early breast cancer: ESMO clinical practice guidelines for diagnosis, treatment and follow-up. *Ann Oncol*, 2019, pii: mdz173.

(23) Cardoso F, Senkus E, Costa A, Papadopoulos E, Aapro M, André F, Harbeck N, Aguilar Lopez B, Barrios CH, Bergh J, Biganzoli L, Boers-Doets CB, Cardoso MJ, Carey LA, Cortés J, Curigliano G, Diéras V, El Saghir NS, Eniu A, Fallowfield L, Francis PA, Gelmon K, Johnston SRD, Kaufman B, Koppikar S, Krop IE, Mayer M, Nakigudde G, Offersen BV, Ohno S, Pagani O, Paluch-Shimon S, Penault-Llorca F, Prat A, Rugo HS, Sledge GW, Spence D, Thomssen C, Vorobiof DA, Xu B40, Norton L, Winer EP. 4th ESO-ESMO International Consensus Guidelines for Advanced Breast Cancer (ABC 4). *Ann Oncol*, 2018, 29, 1634–1657.

(24) Bulut N, Altundag K. Does estrogen receptor determination affect prognosis in early stage breast cancers? *Int J Clin Exp Med,* 2015, 8, 21454–21459.

(25) Lumachi F, Luisetto G, Basso SM, Basso U, Brunello A, Camozzi V. Endocrine therapy of breast cancer. *Curr Med Chem*, 2011, 18, 513–522.

(26) Fisher B, Costantino JP, Wickerham DL, Cecchini RS, Cronin WM, Robidoux A, Bevers TB, Kavanah MT, Atkins JN, Margolese RG, Runowicz CD, James JM, Ford LG, Wolmark N. Tamoxifen for prevention of breast cancer: report of the National Surgical Adjuvant Breast and Bowel Project P-1 Study. *J Natl Cancer Inst*, 1998, 90, 1371–1388.

(27) Early Breast Cancer Trialists' Collaborative Group. Tamoxifen for early breast cancer: an overview of the randomised trials. *Lancet*, 1998, 351, 1451–1467.

(28) Fisher B, Dignam J, Bryant J, Wolmark N. Five versus more than five years of tamoxifen for the lymph-node negative breast cancer: updated findings from the National Surgical Adjuvant Breast and Bowel Project B-14 randomized trial. *J Natl Cancer Inst,* 2001, 93, 684–690.

(29) Abrams JS. Tamoxifen: five versus ten years – is the end in sight? *J Natl Cancer Inst,* 2001, 93, 662–664.

(30) Clinical Guidelines for the Management of Breast Cancer, https://www.england.nhs.uk/mids-east/wp-content/uploads/sites/7/2018/02/guidelines-for-the-management-of-breast-cancer-v1.pdf, pristupljeno 10. 12. 2019.

(31) Hormonal Therapy Side Effects Comparison Chart, https://www.breastcancer.org/treatment/hormonal/comp_chart, pristupljeno 10. 12. 2019.

(32) Chemotherapy for Breast Cancer, https://www.cancer.org/cancer/breast-cancer/treatment/chemotherapy-for-breast-cancer.html, pristupljeno 10. 12. 2019.

(33) Waks AG, Winer EP. Breast cancer treatment: A review. *JAMA*, 2019, 321, 288–300.

(34) Chemotherapy Side Effects, https://www.cancer.org/treatment/treatments-and-side-effects/treatment-types/chemotherapy/chemotherapy-side-effects.html, pristupljeno 17. 3. 2020.

(35) Breast Cancer: Types of Treatment, https://www.cancer.net/cancer-types/breast-cancer/types-treatment, pristupljeno 10. 12. 2019.

(36) Agnihotri S, Burrell KE, Wolf A, Jalali S, Hawkins C, Rutka JT, Zadeh G. Glioblastoma, a brief review of history, molecular genetics, animal models and novel therapeutic strategies. *AITE*, 2013, 61, 25–25.

(37) Weller M, van den Bent M, Tonn JC, Stupp R, Preusser M, Cohen-Jonathan-Moyal E, Henriksson R, Rhun EL, Balana C, Chinot O, Bendszus M, Reijneveld JC, Dhermain F, French P, Marosi C, Watts C, Oberg I, Pilkington G, Baumert BG, Taphoorn MJB, Hegi M, Westphal M, Reifenberger G, Soffietti R, Wick W; European Association for Neuro-Oncology (EANO) Task Force on Gliomas. European Association for Neuro-Oncology (EANO) guideline on the diagnosis and treatment of adult astrocytic and oligodendroglial gliomas. *Lancet Oncol*, 2017, 18, e315–e329.

(38) MedScape. Neurologic Manifestations of Glioblastoma Multiforme, https://emedicine.medscape.com/article/1156220-overview, pristupljeno 11. 12. 2019.

(39) Zhang X, Zhang W, Cao WD, Cheng G, Zhang YQ. Glioblastoma multiforme: Molecular characterization and current treatment strategy (Review). *Exp Ther Med*, 2012, 3, 9–14.

(40) Davis ME. Glioblastoma: overview of disease and treatment. *Clin J Oncol Nurs*, 2016, 20, S2–8.

(41) Eyüpoglu IY, Buchfelder M, Savaskan NE. Surgical resection of malignant gliomas-role in optimizing patient outcome. *Nat Rev Neurol*, 2013, 9, 141–151.

(42) Eyüpoglu IY, Savaskan NE. Epigenetics in brain tumors: HDACs take center stage. *Curr Neuropharmacol*, 2016, 14, 48–54.

(43) Scott J, Tsai YY, Chinnaiyan P, Yu HH. Effectiveness of radiotherapy for elderly patients with glioblastoma. *Int J Radiat Oncol Biol Phys*, 2011, 81, 206–206.

(44) Glas M, Rath BH, Simon M, Reinartz R, Schramme A, Trageser D, Eisenreich R, Leinhaas A, Keller M, Schildhaus HU, Garbe S, Steinfarz B, Pietsch T, Steindler DA, Schramm J, Herrlinger U, Brüstle O, Scheffler B. Residual tumor cells are unique cellular targets in glioblastoma. *Ann Neurol*, 2010, 68, 264–269.

(45) Newlands ES, Blackledge GR, Slack JA, Rustin GJ, Smith DB, Stuart NS, Quarterman CP, Hoffman R, Stevens MF, Brampton MH. Phase I trial of temozolomide (CCRG 81045: M&B 39831: NSC 362856). *Br J Cancer,* 1992, 65, 287–291.

(46) Tsang LL, Farmer PB, Gescher A, Slack JA. Characterisation of urinary metabolites of temozolomide in humans and mice and evaluation of their cytotoxicity. *Cancer Chemother. Pharmacol*, 1990, 26, 429–436.

(47) Hegi ME, Diserens AC, Gorlia T, Hamou MF, de Tribolet N, Weller M, Kros JM, Hainfellner JA, Mason W, Mariani L, Bromberg JE, Hau P, Mirimanoff RO, Cairncross JG, Janzer RC, Stupp R. MGMT gene silencing and benefit from temozolomide in glioblastoma. *N Engl J Med*, 2005, 352, 997–1003.

(48) Weathers SP, Gilbert MR. Advances in treating glioblastoma. *F1000Prime Rep*, 2014, 6, 46.

(49) Vermeulen M, Eberl HC, Matarese F, Marks H, Denissov S, Butter F, Lee KK, Olsen JV, Hyman AA, Stunnenberg HG, Mann M. Quantitative interaction proteomics and genome-wide profiling of epigenetic histone marks and their readers. *Cell*, 2010, 142, 967–980.

(50) Kouzarides T. Chromatin modifications and their function. *Cell*, 2007, 128, 693–705.

(51) Dokmanovic M, Clarke C, Marks PA. Histone deacetylase inhibitors: overview and perspectives. *Mol Cancer Res*, 2007, 5, 981–989.

(52) Ropero S, Esteller M. The role of histone deacetylases (HDACs) in human cancer. *Mol Oncol*, 2007, 1, 19–25.

(53) Tang Y, Zhao W, Chen Y, Zhao Y, Gu W. Acetylation is indispensable for p53 activation. *Cell*, 2008, 133, 612–626.

(54) Pearson M, Carbone R, Sebastiani C, Cioce M, Fagioli M, Saito S, Higashimoto Y, Appella E, Minucci S, Pandolfi PP, Pelicci PG. PML regulates p53 acetylation and premature senescence induced by oncogenic Ras. *Nature*, 2000, 406, 207–210.

(55) Yang XJ, Grégoire S. Class II histone deacetylases: from sequence to function, regulation, and clinical implication. *Mol Cell Biol*, 2005, 25, 2873–2884.

(56) Verdin E, Dequiedt F, Kasler HG. Class II histone deacetylases: versatile regulators. *Trends Genet*, 2003, 19, 286–293.

(57) Gregoretti IV, Lee YM, Goodson HV. Molecular evolution of the histone deacetylase family: functional implications of phylogenetic analysis. *J Mol Biol*, 2004, 338, 17–31.

(58) Bertos NR, Wang AH, Yang XJ. Class II histone deacetylases: structure, function, and regulation. *Biochem Cell Biol*, 2001, 79, 243–52.

(59) Zhang CL, McKinsey TA, Chang S, Antos CL, Hill JA, Olson EN. Class II histone deacetylases act as signal-responsive repressors of cardiac hypertrophy. *Cell*, 2002, 110, 479–488.

(60) Vega RB, Matsuda K, Oh J, Barbosa AC, Yang X, Meadows E, McAnally J, Pomajzl C, Shelton JM, Richardson JA, Karsenty G, Olson EN. Histone deacetylase 4 controls chondrocyte hypertrophy during skeletogenesis. *Cell*, 2004, 119, 555–566.

(61) Dequiedt F, Kasler H, Fischle W, Kiermer V, Weinstein M, Herndier BG, Verdin E. HDAC7, a thymus-specific class II histone deacetylase, regulates Nur77 transcription and TCR-mediated apoptosis. *Immunity*, 2003, 18, 687–698.

(62) Urbich C, Rossig L, Kaluza D, Potente M, Boeckel JN, Knau A, Diehl F, Geng JG, Hofmann WK, Zeiher AM, Dimmeler S. HDAC5 is a repressor of angiogenesis and determines the angiogenic gene expression pattern of endothelial cells. *Blood*, 2009. 113, 5669–5679.

(63) Valenzuela-Fernández A, Cabrero JR, Serrador JM, Sánchez-Madrid F. HDAC6: a key regulator of cytoskeleton, cell migration and cell-cell interactions. *Trends Cell Biol*, 2008, 18, 291–297.

(64) Boyault C, Gilquin B, Zhang Y, Rybin V, Garman E, Meyer-Klaucke W, Matthias P, Müller CW, Khochbin S. HDAC6-p97/VCP controlled polyubiquitin chain turnover. *EMBO J*, 2006, 25, 3357–3366.

(65) Hurst DR, Mehta A, Moore BP, Phadke PA, Meehan WJ, Accavitti MA, Shevde LA, Hopper JE, Xie Y, Welch DR, Samant RS. Breast cancer metastasis suppressor 1 (BRMS1) is stabilized by the Hsp90 chaperone. *Biochem Biophys Res Commun*, 2006, 348, 1429–1435.

(66) Qian DZ, Kachhap SK, Collis SJ, Verheul HM, Carducci MA, Atadja P, Pili R. Class II histone deacetylases are associated with VHL-independent regulation of hypoxia-inducible factor 1 alpha. *Cancer Res*, 2006, 66, 8814–8821.

(67) Cabrero JR, Serrador JM, Barreiro O, Mittelbrunn M, Naranjo-Suárez S, Martín-Cófreces N, Vicente-Manzanares M, Mazitschek R, Bradner JE, Avila J, Valenzuela-Fernández A, Sánchez-Madrid F. Lymphocyte chemotaxis is regulated by histone deacetylase 6, independently of its deacetylase activity. *Mol Biol Cell*, 2006, 17, 3435–3445.

(68) Park JH, Kim SH, Choi MC, Lee J, Oh DY, Im SA, Bang YJ, Kim TY. Class II histone deacetylases play pivotal roles in heat shock protein 90-mediated proteasomal degradation of vascular endothelial growth factor receptors. *Biochem Biophys Res Commun*, 2008, 368, 318–322.

(69) Gao L, Cueto MA, Asselbergs F, Atadja P. Cloning and functional characterization of HDAC11, a novel member of the human histone deacetylase family. *J Biol Chem*, 2002, 277, 25748–25755.

(70) Yanginlar C, Logie C. HDAC11 is a regulator of diverse immune functions. *Biochim Biophys Acta Gene Regul Mech*, 2018, 1861, 54–59.

(71) Yuan L, Chen X, Cheng L, Rao M, Chen K, Zhang N, Meng J, Li M, Yang LT, Yang PC, Wang X, Song J. HDAC11 regulates interleukin-13 expression in CD4+ T cells in the heart. *J Mol Cell Cardiol*, 2018, 122, 1–10.

(72) Glozak MA, Seto E. Histone deacetylases and cancer. *Oncogene*, 2007, 26, 5420–5432.

(73) Yixuan L, Seto E. HDACs and HDAC Inhibitors in Cancer Development and Therapy. *Cold Spring Harb Perspect Med*, 2016, 6, a026831.

(74) Suraweera A, O'Byrne KJ, Richard DJ. Combination therapy with Histone deacetylase inhibitors (HDACi) for the treatment of cancer: Achieving the full therapeutic potential of HDACi. *Front Oncol*. 2018, 8, 92.

(75) Duvic M, Dimopoulos M. The safety profile of vorinostat (suberoylanilide hydroxamic acid) in hematologic malignancies: A review of clinical studies. *Cancer Treat Rev*, 2016, 43, 58–66.

(76) Medscape, Vorinostat. https://reference.medscape.com/drug/zolinza-vorinostat-342102#6, pristupljeno 18. 12. 2019.

(77) Muri EM, Nieto MJ, Sindelar RD, Williamson JS. Hydroxamic acids as pharmacological agents. *Curr Med Chem*, 2002, 9, 1631–1653.

(78) Marks P, Rifkind RA, Richon VM, Breslow R, Miller T, Kelly WK. Histone deacetylases and cancer: causes and therapies. *Nat Rev Cancer*, 2006, 1, 194–202.

(79) Bubna, AK. Vorinostat – an overview. *Indian J Dermatol*, 2016, 60, 419.

(80) Khan O, La Thangue NB. HDAC inhibitors in cancer biology: emerging mechanisms and clinical applications. *Immunol Cell Biol*, 2012, 90, 85–94.

(81) Duvic M, Talpur R, Ni X, Zhang C, Hazarika P, Kelly C, Chiao JH, Reilly JF, Ricker JL, Richon VM, Frankel SR. Phase 2 trial of oral vorinostat (suberoylanilide hydroxamic acid, SAHA) for refractory cutaneous T-cell lymphoma (CTCL). *Blood*, 2007, 109, 31–39.

(82) Vorinostat (Zolinza) for cutaneous T-Cell lymphoma. *Med Lett Drugs Ther,* 2007, 49, 23–24.

(83) Shultz MD, Cao X, Chen CH, Cho YS, Davis NR, Eckman J, Fan J, Fekete A, Firestone B, Flynn J, Green J, Growney JD, Holmqvist M, Hsu M, Jansson D, Jiang L, Kwon P, Liu G, Lombardo F, Lu Q, Majumdar D, Meta C, Perez L, Pu M, Ramsey T, Remiszewski S, Skolnik S, Traebert M, Urban L, Uttamsingh V, Wang P, Whitebread S, Whitehead L, Yan-Neale Y, Yao YM, Zhou L, Atadja P. Optimization of the in vitro cardiac safety of hydroxamate-based histone deacetylase inhibitors. *J Med Chem*, 2011, 54, 4752–4772.

(84) Vorinostat Pregnancy and Breastfeeding Warnings. https://www.drugs.com/pregnancy/vorinostat.html, pristupljeno 19. 12. 2019.

(85) van Tilburg CM, Milde T, Witt R, Ecker J, Hielscher T, Seitz A, Schenk JP, Buhl JL, Riehl D, Frühwald MC, Pekrun A, Rossig C, Wieland R, Flotho C, Kordes U, Gruhn B, Simon T, Linderkamp C, Sahm F, Taylor L, Freitag A, Burhenne J, Foerster KI, Meid AD, Pfister SM, Karapanagiotou-Schenkel I, Witt O. Phase I/II intra-patient dose escalation study of vorinostat in children with relapsed solid tumor, lymphoma, or leukemia. *Clin Epigenetics*, 2019, 11, 188.

(86) Hummel TR, Wagner L, Ahern C, Fouladi M, Reid JM, McGovern RM, Ames MM, Gilbertson RJ, Horton T, Ingle AM, Weigel B, Blaney AM. A pediatric phase 1 trial of vorinostat and temozolomide in relapsed or refractory primary brain or spinal cord tumors: A children's oncology group phase 1 consortium study. *Pediatr Blood Cancer*, 2013, 60, 1452–1457.

(87) Breslow R, Marks PA, Rifkind RA, Jursic B. Potent inducers of terminal differentiation and methods of use thereof, 1991. US patent 5, 369, 108.

(88) Reuben RC, Wife RL, Breslow R, Rifkind RA, Marks PA. A new group of potent inducers of differentiation in murine erythroleukemia cells. *Proc Natl Acad Sci U S A*. 1976, 73, 862–866.

(89) Mai A, Esposito M, Sbardella G, Massa S. A new facile and expeditious synthesis of *N*-hydroxy-N^1-phenyloctanediamide, a potent inducer of terminal cytodifferentiation. *OPPI Briefs*, 2001, 33, 391–394.

(90) Gediya LK, Chopra P, Purushottamachar P, Maheshwari N, Njar VC. A new simple and high-yield synthesis of suberoylanilide hydroxamic acid and its inhibitory effect alone or in combination with retinoids on proliferation of human prostate cancer cells. *J Med Chem*, 2005, 48, 5047–5051.

(91) Poole RM. Belinostat: first global approval. *Drugs*, 2014, 74, 1543–1554.

(92) West AC, Johnstone RW. New and emerging HDAC inhibitors for cancer treatment. *J Clin Invest*, 2014, 124, 30–39.

(93) Gimsing P. Belinostat: a new broad acting antineoplastic histone deacetylase inhibitor. *Expert Opin Investig Drugs*, 2009, 18, 501–508.

(94) Finn PW, Loza E, Carstensen E. The Discovery and Development of Belinostat. U: Fischer J, Childers WE (ed.), Successful Drug Discovery, vol 2. 2016, WILEY-VCH Verlag GmbH & Co. KGaA, 31–57.

(95) Lee HZ, Kwitkowski VE, Del Valle PL, Ricci MS, Saber H, Habtemariam BA, Bullock J, Bloomquist E, Li Shen Y, Chen XH, Brown J, Mehrotra N, Dorff S, Charlab R, Kane RC, Kaminskas E, Justice R, Farrell AT, Pazdur 2. FDA approval: Belinostat for the treatment of patients with relapsed or refractory peripheral T-cell lymphoma. *Clin Cancer Res*, 2015, 21, 2666–2670.

(96) Sawas A, Radeski D, O'Connor OA. Belinostat in patients with refractory or relapsed peripheral T-cell lymphoma: a perspective review. *Ther Adv Hematol*, 2015, 6, 202–208.

(97) Belinostat Pregnancy and Breastfeeding Warnings, https://www.drugs.com/pregnancy/belinostat.html, pristupljeno 22. 12. 2019.

(98) Reisch H, Leeming P, Raje P. Methods of synthesis of certain hydroxamic acid compounds, 2009. WO 2009/040517 A2.

(99) Yang L, Xiaowen X, Zhang Y. Simple and efficient synthesis of belinostat. *Synth Commun*, 2010, 40, 2520–2524.

(100) Bao X, Song D, Qiao X, Zhao X, Chen G. The development of an effective synthetic route of belinostat. *Org Process Res Dev*, 2016, 20, 1482–1488.

(101) Drug Trials Snapshot: FARYDAK (panobinostat), https://www.fda.gov/drugs/drug-approvals-and-databases/drug-trials-snapshot-farydak-panobinostat, pristupljeno 25. 12. 2019.

(102) Moore D. Panobinostat (Farydak): A novel option for the treatment of relapsed or relapsed and refractory multiple myeloma. *P T*, 2016, 41, 296–300.

(103) Andreu-Vieyra CV, Berenson JR. The potential of panobinostat as a treatment option in patients with relapsed and refractory multiple myeloma. *Ther Adv Hematol*, 2014, 5, 197–210.

(104) Atadja P. Development of the pan-DAC inhibitor panobinostat (LBH589): successes and challenges. *Cancer Lett*, 2009, 280, 233–241.

(105) Khot A, Dickinson M, Prince HM. Panobinostat in lymphoid and myeloid malignancies. *Expert Opin Investig Drugs*, 2013, 22, 1211–1223.

(106) Giver CR, Jaye DL, Waller EK, Kaufman JL, Lonial S. Rapid recovery from panobinostat (LBH589)-induced thrombocytopenia in mice involves a rebound effect of bone marrow megakaryocytes. *Leukemia*, 2011, 25, 362–365.

(107) Singh A, Patel VK, Jain DK, Patel P, Rajak H. Panobinostat as pan-deacetylase inhibitor for the treatment of pancreatic cancer: Recent progress and future prospects. *Oncol Ther*, 2016, 4, 73–89.

(108) Panobinostat Pregnancy and Breastfeeding Warnings, https://www.drugs.com/pregnancy/panobinostat.html#ref_pregnancy, pristupljeno 26. 12. 2019.

(109) Bair KW, Green MA, Perez LB, Remiszewski SW, Sambucetti L, Versace RW, Sharma SK. Preparation of hydroxamic acids as deacetylase inhibitors, 2002. WO 02/22577 A2.

(110) Chen S, Zhang P, Chen H, Zhang P, Yu Y, Gan Z. An improved and efficient synthesis of panobinostat. *J Chem Res*, 2018, 42, 471–473.

(111) World malaria report 2019. https://www.who.int/news-room/feature-stories/detail/world-malaria-report-2019/, pristupljeno 10. 3. 2020.

(112) Prudêncio M, Rodriguez A, Mota MM. The silent path to thousands of merozoites: The *Plasmodium* liver stage. *Nat Rev Microbiol*, 2006, 4, 849–856.

(113) Cowman AF, Healer J, Marapana D, Marsh K. Malaria: Biology and disease. *Cell*, 2016, 167, 610–624.

(114) WHO. Guidelines for the treatment of malaria. Third edition, 2015.

(115) WHO Model Lists of Essential Medicines, https://www.who.int/medicines/publications/essentialmedicines/en/, pristupljeno 26. 12. 2019.

(116) Kaur K, Jain M, Khan SI, Jacob MR, Tekwani BL, Singh S, Singh PP, Jain R. Amino acid, dipeptide and pseudodipeptide conjugates of ring-substituted 8-aminoquinolines: synthesis and evaluation of anti-infective, β-haematin inhibition and cytotoxic activities*, Eur J Med Chem*, 2012, 52, 230–241.

(117) Primaquine Pregnancy and Breastfeeding Warnings, https://www.drugs.com/pregnancy/primaquine.html, pristupljeno 26. 12. 2019.

(118) Vale N, Moreira R, Gomes P. Primaquine revisited six decades after its discovery. *Eur J Med Chem*, 2009, 44, 937–953.

(119) Pybus BS, Marcsisin SR, Jin X, Deye G, Sousa JC, Li Q, Caridha D, Zeng Q, Reichard GA, Ockenhouse C, Bennett J, Walker LA, Ohrt C, Melendez V. The metabolism of primaquine to its active metabolite is dependent on CYP 2D6. *Malar J*, 2013, 12, e212

(120) Marcsisin SR, Reichard G, Pybus BS. Primaquine pharmacology in the context of CYP 2D6 pharmacogenomics: current state of the art. *Pharmacol Ther*, 2016, 161, 1e10.

(121) Payne D. Spread of chloroquine resistance in Plasmodium falciparum. *Parasitol Today*, 1987, 3, 241–246.

(122) Mushtaque M. Reemergence of chloroquine (CQ) analogs as multi-targeting antimalarial agents: a review. *Eur J Med Chem*, 2015, 90, 280–295.

(123) Hempelmann E. Hemozoin biocrystallization in *Plasmodium falciparum* and the antimalarial activity of crystallization inhibitors. *Parasitol Research*, 2007, 100, 671–676.

(124) Chloroquine Dosage, https://www.drugs.com/dosage/chloroquine.html#Usual_Adult_Dose_for_Malaria_Prophylaxis, pristupljeno 26. 12. 2019.

(125) Aralen Side Effects, https://www.rxlist.com/aralen-side-effects-drug-center.htm, pristupljeno 26. 12. 2019.

(126) Costedoat-Chalumeau N, Dunogué B, Leroux G, Morel N, Jallouli M, Le Guern V, Piette JC, Brézin AP, Melles RB, Marmor MF. A Critical review of the effects of hydroxychloroquine and chloroquine on the eye. *Clin Rev Allergy Immunol*, 2015, 49, 317–326.

(127) Rainsford KD, Parke AL, Clifford-Rashotte M, Kean WF. Therapy and pharmacological properties of hydroxychloroquine and chloroquine in treatment of systemic lupus erythematosus, rheumatoid arthritis and related diseases. *Inflammopharmacology*, 2015, 23, 231–269.

(128) Chloroquine Drug Interactions, https://www.drugs.com/drug-interactions/chloroquine.html, pristupljeno 26. 12. 2019.

(129) Johnson MW, Vine AK. Hydroxychloroquine therapy in massive total doses without retinal toxicity. *Am J Ophthalmol*, 1987, 104, 139–144.

(130) Curtin NJ. DNA repair dysregulation from cancer driver to therapeutic target. *Nat Rev*, 2012, 12, 801–817.

(131) ClinicalTrials.gov, https://clinicaltrials.gov/ct2/home, pristupljeno 27. 12. 2019.

(132) Yoon YH, Cho KS, Hwang JJ, Lee SJ, Choi JA, Koh JY. Induction of lysosomal dilatation, arrested autophagy, and cell death by chloroquine in cultured ARPE-19 cells. *Invest Ophthalmol Vis Sci*, 2010, 51, 6030–6037.

(133) Cheng C, Wang T, Song Z, Peng L, Gao M, Hermine O, Rousseaux S, Khochbin S, Mi JQ, Wang J. Induction of autophagy and autophagy-dependent apoptosis in diffuse large B-cell lymphoma by a new antimalarial artemisinin derivative, SM1044. *Cancer Med*. 2017, 26, 1–17.

(134) Shi TT, Yu XX, Yan LJ, Xiao HT. Research progress of hydroxychloroquine and autophagy inhibitors on cancer. *Cancer Chemother Pharmacol*. 2017, 79, 287–294.

(135) Efferth T, Sauerbrey A, Olbrich A, Gebhart E, Rauch P, Weber HO, Hengstler JG, Halatsch ME, Volm M, Tew KD, Ross DD, Funk JO. Molecular modes of action of artesunate in tumor cell lines. *Mol Pharmacol*, 2003, 64, 382–394.

(136) Karnak D, Xu L. Chemosensitization of prostate cancer by modulating Bcl-2 family proteins. *Curr Drug Targets*, 2010, 11, 699–707.

(137) Lu YY, Chen TS, Wang XP, Li L. Single-cell analysis of dihydroartemisinin-induced apoptosis through reactive oxygen species-mediated caspase-8 activation and mitochondrial pathway in ASTC-a-1 cells using fluorescence imaging techniques. *J Biomed Opt*, 2010, 15, 046028.

(138) Aung W, Sogawa C, Furukawa T, Saga T. Anticancer effect of dihydroartemisinin (DHA) in a pancreatic tumor model evaluated by conventional methods and optical imaging. *Anticancer Res*, 2011, 31, 1549–1558.

(139) Lijuan W. Effect of artesunate on human endometrial carcinoma. *J Med Coll PLA*, 2010, 25, 143–151.

(140) Efferth T, Giaisi M, Merling A, Krammer PH, Li-Weber M. Artesunate induces ROS-mediated apoptosis in doxorubicin-resistant T leukemia cells. *PLoS One*, 2007, 1, e693.

(142) Hwang YP, Yun HJ, Kim HG, Han EH, Lee GW, Jeong HG. Suppression of PMA-induced tumor cell invasion by dihydroartemisinin via inhibition of

PKCalpha/Raf/MAPKs and NF-kappaB/AP-1-dependent mechanisms. *Biochem Pharmacol*, 2010, 79, 1714–1726.

(142) Anfosso L, Efferth T, Albini A, Pfeffer U. Microarray expression profiles of angiogenesis-related genes predict tumor cell response to artemisinins. *Pharmacogenomics J*, 2006, 6, 269–278.

(143) Zhou HJ, Wang WQ, Wu GD, Lee J, Li A. Artesunate inhibits angiogenesis and downregulates vascular endothelial growth factor expression in chronic myeloid leukemia K562 cells. *Vascul Pharmacol*, 2007, 47, 131–138.

(144) Choi AR, Kim JH, Kim YK, Yoo, S. Co-treatment with the anti-malarial drugs mefloquine and primaquine highly sensitizes drug-resistant cancer cells by increasing P-gp inhibition. *Biochem Biophys Res Commun*, 2013, 441, 655–660.

(145) Manic G, Obrist F, Kroemer G, Vitale I, Galluzzi L. Chloroquine and hydroxychloroquine for cancer therapy. *Mol Cell Oncol*, 2014, 1, e29911.

(146) Jutten B, Keulers TG, Schaaf MB, Savelkouls K, Theys J, Span PN, Vooijs MA, Bussink J, Rouschop KM. EGFR overexpressing cells and tumors are dependent on autophagy for growth and survival. *Radiother Oncol*, 2013, 108, 479–483.

(147) Kim EL, Wüstenberg R, Rübsam A, Schmitz-Salue C, Warnecke G, Bücker EM, Pettkus N, Speidel D, Rohde V, Schulz-Schaeffer W, Deppert W, Giese A. Chloroquine activates the p53 pathway and induces apoptosis in human glioma cells. *Neuro Oncol*, 2010, 12, 389–400.

(148) Song YJ, Zhang SS, Guo XL, Sun K, Han ZP, Li R, Zhao QD, Deng WJ, Xie XQ, Zhang JW, Wu MC, Wei LX. Autophagy contributes to the survival of CD133+ liver cancer stem cells in the hypoxic and nutrient-deprived tumor microenvironment. *Cancer Lett*, 2013, 339, 70–81.

(149) Hu T, Li P, Luo Z, Chen X, Zhang J, Wang C, Chen P, Dong Z. Chloroquine inhibits hepatocellular carcinoma cell growth *in vitro* and *in vivo*. *Oncol Rep*, 2016, 35, 43–49.

(150) Sun K, Guo X, Zhao Q, Jing Y, Kou X, Xie X, Zhou Y, Cai N, Gao L, Zhao X, Zhang S, Song J, Li D, Deng W, Li R, Wu M, Wei L. Paradoxical role of autophagy in the dysplastic and tumor-forming stages of hepatocarcinoma development in rats. *Cell Death Dis*, 2013, 4, e501.

(151) Zheng Y, Zhao YL, Deng X, Yang S, Mao Y, Li Z, Jiang P, Zhao X, Wei Y. Chloroquine inhibits colon cancer cell growth in vitro and tumor growth in vivo via induction of apoptosis. *Cancer Invest*, 2009, 27, 286–292.

(152) Lakhter AJ, Sahu RP, Sun Y, Kaufmann WK, Androphy EJ, Travers JB, Naidu SR. Chloroquine promotes apoptosis in melanoma cells by inhibiting BH3 domain-mediated PUMA degradation. *J Invest Dermatol*, 2013, 133, 2247–2254.

(153) Jiang PD, Zhao YL, Deng XQ, Mao YQ, Shi W, Tang QQ, Li ZG, Zheng YZ, Yang SY, Wei YQ. Antitumor and antimetastatic activities of chloroquine diphosphate in a murine model of breast cancer. *Biomed Pharmacother*, 2010, 64, 609–614.

(154) Sotelo J, Briceño E, López-González MA. Adding chloroquine to conventional treatment for glioblastoma multiforme: a randomized, double-blind, placebo-controlled trial. *Ann Intern Med*, 2006, 144, 337–343.

(155) Martinez-Outschoorn UE, Pavlides S, Whitaker-Menezes D, Daumer KM, Milliman JN, Chiavarina B, Migneco G, Witkiewicz AK, Martinez-Cantarin MP, Flomenberg N, Howell A, Pestell RG, Lisanti MP, Sotgia F. Tumor cells induce the cancer associated fibroblast phenotype via caveolin-1 degradation: implications for breast cancer and DCIS therapy with autophagy inhibitors. *Cell Cycle*, 2010, 9, 2423–2433.

(156) IDO2 Genetic Status Informs the Neoadjuvant Efficacy of Chloroquine (CQ) in Brain Metastasis Radiotherapy (ClinicalTrials.gov Identifier: NCT01727531), https://clinicaltrials.gov/ct2/show/NCT01727531, pristupljeno: 28. 12. 2019.

(157) Adjuvant Effect of Chloroquine on Gemcitabine (ClinicalTrials.gov Identifier: NCT01777477), https://clinicaltrials.gov/ct2/show/NCT01777477, pristupljeno: 28. 12. 2019.

(158) Chloroquine in Combination With Carboplatin/Gemcitabine in Advanced Solid Tumors (ClinicalTrials.gov Identifier: NCT02071537), https://clinicaltrials.gov/ct2/show/NCT02071537, pristupljeno: 28. 12. 2019.

(159) Chloroquine With Taxane Chemotherapy for Advanced or Metastatic Breast Cancer After Anthracycline Failure (CAT) (ClinicalTrials.gov Identifier: NCT01446016) (https://clinicaltrials.gov/ct2/show/NCT01446016, pristupljeno: 29. 12. 2019.

(160) Zorc B, Perković I, Pavić K, Rajić Z, Beus M. Primaquine derivatives: Modifications of the terminal amino group. *Eur J Med Chem*, 2019, 182, 111640.

(161) Bérubé G. An overview of molecular hybrids in drug discovery. *Expert Opin Drug Discov*, 2016, 11, 281–305.

(162) Zhang X, Zhang J, Tong L, Luoa Y, Sub M, Zangb Y, Lib J, Lua W, Chen Y. The discovery of colchicine-SAHA hybrids as a new class of antitumor agents. *Bioorg Med Chem*, 2013, 21, 3240–3244.

(163) Shaveta MS, Singh P. Hybrid molecules: The privileged scaffolds for various pharmaceuticals. *Eur J Med Chem*, 2016, 29, 500–536.

(164) Fortin S, Bérubé G. Advances in the development of hybrid anticancer drugs. *Expert Opin Drug Discov*, 2013, 8, 1029–1047.

(165) Minami Y, Shimamura T, Shah K, LaFramboise T, Glatt KA, Liniker E, Borgman CL, Haringsma HJ, Feng W, Weir BA, Lowell AM, Lee JC, Wolf J, Shapiro GI, Wong KK, Meyerson M, Thomas RK. The major lung cancer-derived mutants of ERBB2 are oncogenic and are associated with sensitivity to the irreversible EGFR/ERBB2 inhibitor HKI-272. *Oncogene*, 2007, 26, 5023–5027.

(166) Baselga J, Coleman RE, Cortés J, Janni W. Advances in the management of HER2-positive early breast cancer. *Crit Rev Oncol Hematol*, 2017, 119, 113–122.

(167) Copeland RA, Pompliano DL, Meek TD. Drug-target residence time and its implications for lead optimization. *Nat Rev Drug Discovery*, 2006, 5, 730–739.

(168) Duplan V, Hoshino M, Li W, Honda T, Fujita M. In situ observation of thiol Michael addition to a reversible covalent drug in a crystalline sponge. *Angew Chem Int Ed Engl*, 2016, 55, 4919–4923.

(169) Barf T, Kaptein A. Irreversible protein kinase inhibitors: balancing the benefits and risks. *J Med Chem*, 2012, 55, 6243–6262.

(170) Noordzij GJ, Wilsens CHRM. Cascade aza-Michael addition-cyclizations; Toward renewable and multifunctional carboxylic acids for melt-polycondensation. *Front Chem*, 2019, 7, 729.

(171) Šimunović M, Perković I, Zorc B, Ester K, Kralj M, Hadjipavlou-Litina D, Pontiki E. Urea and carbamate derivatives of primaquine: Synthesis, cytostatic and antioxidant activities. *Bioorg Med Chem*, 2009, 17, 5605–5613.

(172) Perković I, Tršinar S, Žanetić J, Kralj M, Martin-Kleiner I, Balzarini J, Hadjipavlou-Litina D, Katsori AM, Zorc B. Novel 1-acyl-4-substituted semicarbazide derivatives of primaquine − synthesis, cytostatic, antiviral and antioxidative studies. *J Enzyme Inhib Med Chem*, 2013, 28, 601–610.

(173) Lee HD, Ryu HW, Won HR, Kwon SH. Advances in epigenetic glioblastoma therapy. *Oncotarget*, 2017, 8, 18577–18589.

(174) Kim YZ. Altered histone modifications in gliomas. *Brain Tumor Res Treat*, 2014, 2, 7–21.

(175) Lee P, Murphy B, Miller R, Menon V, Banik NL, Giglio P, Lindhorst SM, Varma AK, Vandergrift WA, Patel SJ, Das A. Mechanisms and clinical significance of histone

deacetylase inhibitors: epigenetic glioblastoma therapy. *Anticancer Res*, 2015, 35, 615–625.

(176) Galanis E, Jaeckle KA, Maurer MJ, Reid JM, Ames MM, Hardwick JS, Reilly JF, Loboda A, Nebozhyn M, Fantin VR, Richon VM, Scheithauer B, Giannini C, Flynn PJ, Moore DF, Zwiebel J, Buckner JC. Phase II trial of Vorinostat in recurrent glioblastoma multiforme: A north central cancer treatment group study. *J Clin Oncol*, 2009, 27, 2052–2058.

(177) Wen PY, Puduvalli VK, Kuhn JG, Lamborn KR, Cloughesy TF, Chang SM, Drappatz J, Yung WK, Gilbert MR, Robins HI, Lieberman FS, Lassman AB, McGovern RM, Xu J, Desideri S, Ye X, Ames MM, Espinoza-Delgado I, Prados MD, Wen PY. Phase I study of vorinostat in combination with temozolomide in patients with malignant gliomas. *Clin Cancer Res*, 2012, 18, 6032–6039.

(178) Hummel TR, Wagner L, Ahern C, Fouladi M, Reid JM, McGovern RM, Ames MM, Gilbertson RJ, Horton T, Ingle AM, Weigel B, Blaney SM. A pediatric phase I trial of vorinostat and temozolomide in relapsed or refractory primary brain or spinal cord tumors: a children's oncology group phase I consortium study. *Pediatr Blood Cancer*, 2013, 60, 1452–1457.

(179) Chinnaiyan P, Chowdhary S, Potthast L, Prabhu A, Tsai Y, Sarcar B, Kahali S, Brem S, Yu M, Rojiani A, Murtagh R, Pan E. Phase I trial of vorinostat combined with bevacizumab and CPT-11 in recurrent glioblastoma. *Neuro Oncol*, 2012, 14, 93–100.

(180) Holland EC. Glioblastoma multiforme: the terminator. *Proc Natl Acad Sci USA*, 2000, 97, 6242–6244.

(181) Schäfer S, Saunders L, Eliseeva E, Velena A, Jung M, Schwienhorst A, Strasser A, Dickmanns A, Ficner R, Schlimme S, Sippl W, Verdin E, Jung M. Phenylalanine-containing hydroxamic acids as selective inhibitors of class IIb histone deacetylases (HDACs). *Bioorg Med Chem*, 2008, 16, 2011–2033.

(182) Shinojima N, Tada K, Shiraishi S, Kamiryo T, Kochi M, Nakamura H, Makino K, Saya H, Hirano H, Kuratsu J, Oka K, Ishimaru Y, Ushio Y. Prognostic value of epidermal growth factor receptor in patients with glioblastoma multiforme. *Cancer Res*, 2003, 63, 6962–6970.

(183) Combs SE, Heeger S, Haselmann R, Edler L, Debus J, Schulz-Ertner D. Treatment of primary glioblastoma multiforme with cetuximab, radiotherapy and temozolomide (GERT)–phase I/II trial: study protocol. *BMC Cancer*, 2006, 6, 133.

(184) Emrich JG, Brady LW, Quang TS, Class R, Miyamoto C, Black P, Rodeck U. Radioiodinated (I-125) monoclonal antibody 425 in the treatment of high-grade glioma patients: ten-year synopsis of a novel treatment. *Am J Clin Oncol*, 2002, 25, 541–546.

(185) Mauthe M, Orhon I, Rocchi C, Zhou X, Luhr M, Hijlkema KJ, Coppes RP, Engedal N, Mari M, Reggiori F. Chloroquine inhibits autophagic flux by decreasing autophagosome-lysosome fusion. *Autophagy*, 2018, 14, 1435–1455.

(186) Zorc B, Rajić Z, Perković I. Antiproliferative evaluation of various aminoquinoline derivatives. *Acta Pharm*, 2019, 69, 661–672.

9. PRILOZI

Prilog 1. IR, NMR i MS spektri.

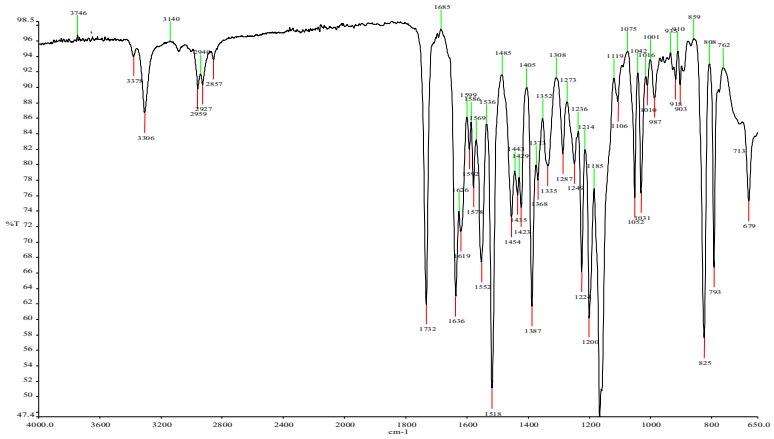

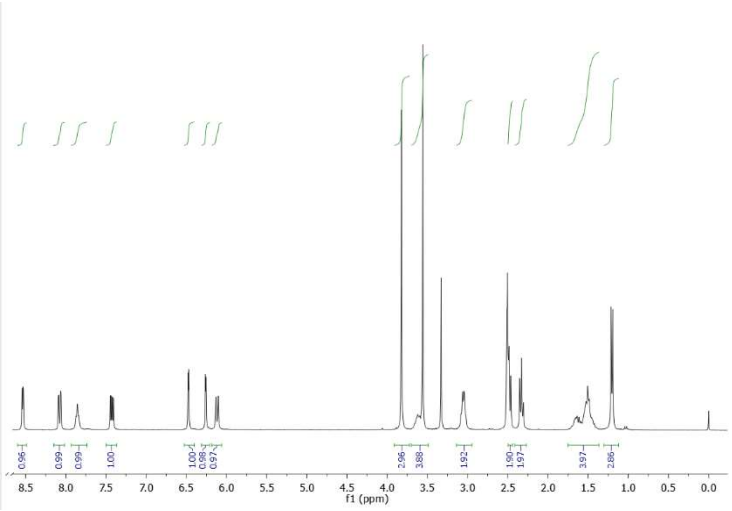

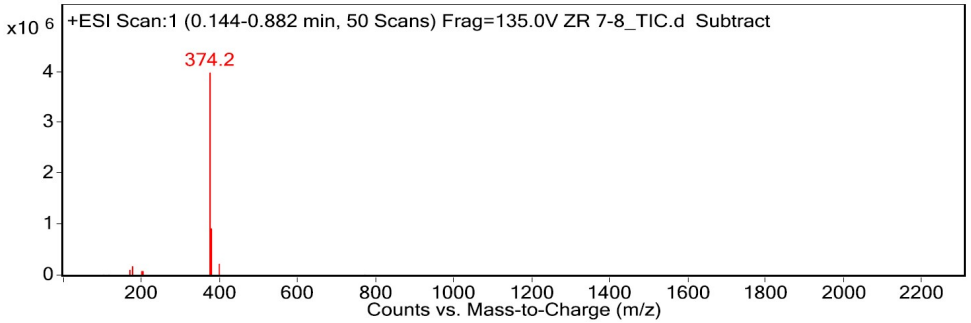
+ESI Scan:1 (0.144-0.882 min, 50 Scans) Frag=135.0V ZR 7-8_TIC.d Subtract
x10 6
374.2
Counts vs. Mass-to-Charge (m/z)

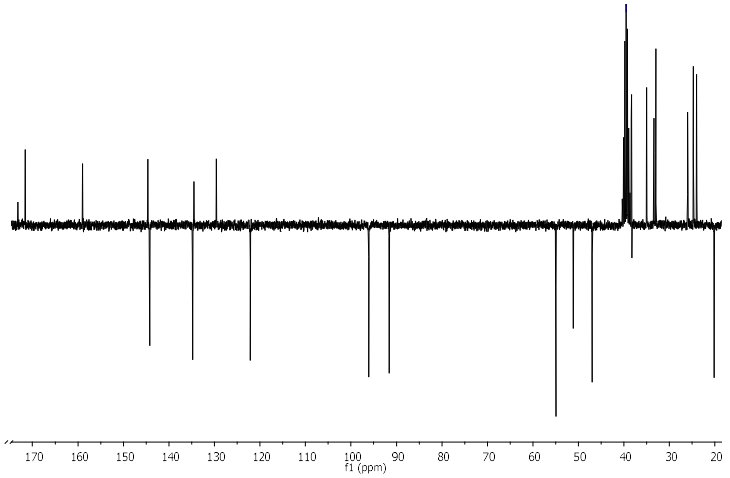

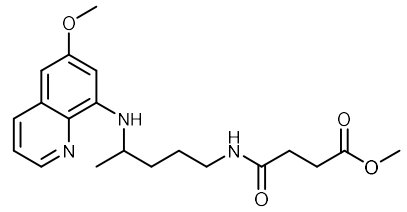
O
NH
N
H
N
O
O
O

1

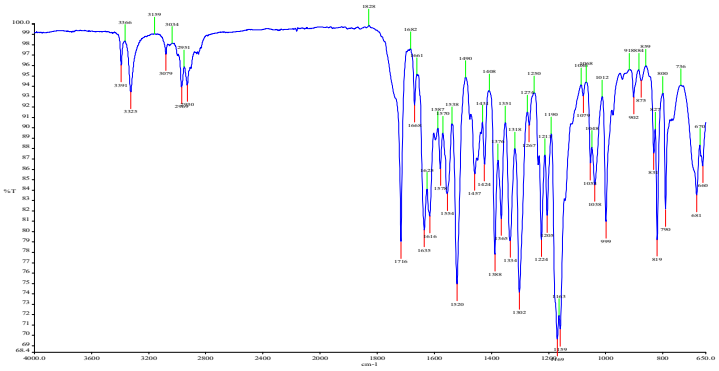

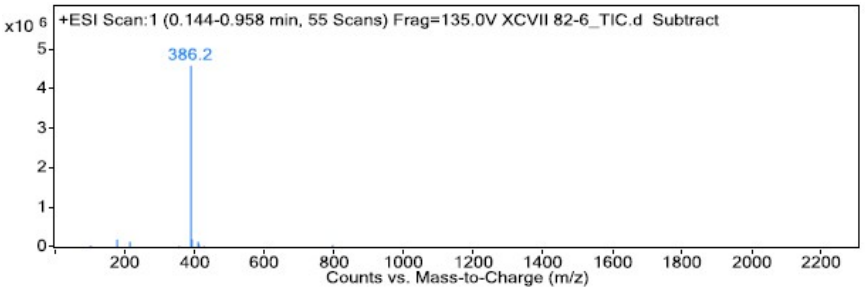
+ESI Scan:1 (0.144-0.958 min, 55 Scans) Frag=135.0V XCVII 82-6_TIC.d Subtract
x10 6
386.2
Counts vs. Mass-to-Charge (m/z)

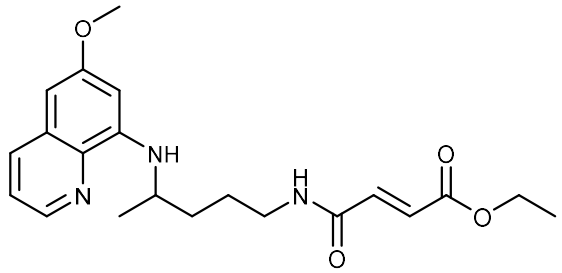
O
NH
N
H
N
O
O
O

2

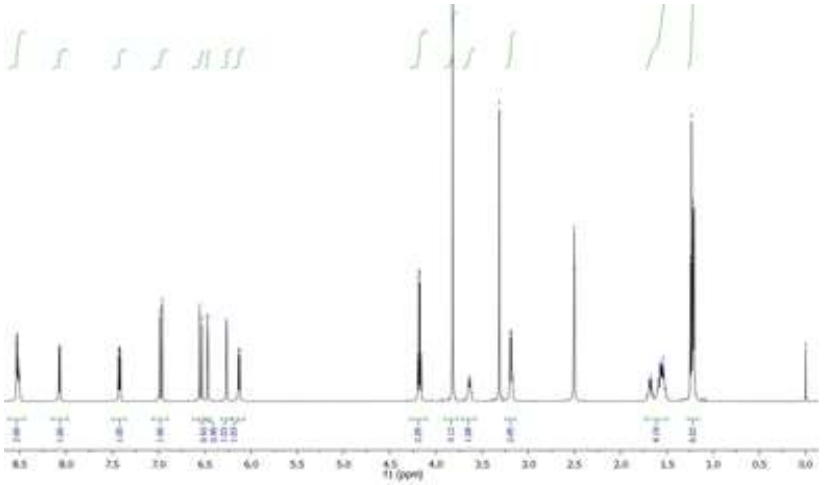
f1 (ppm)

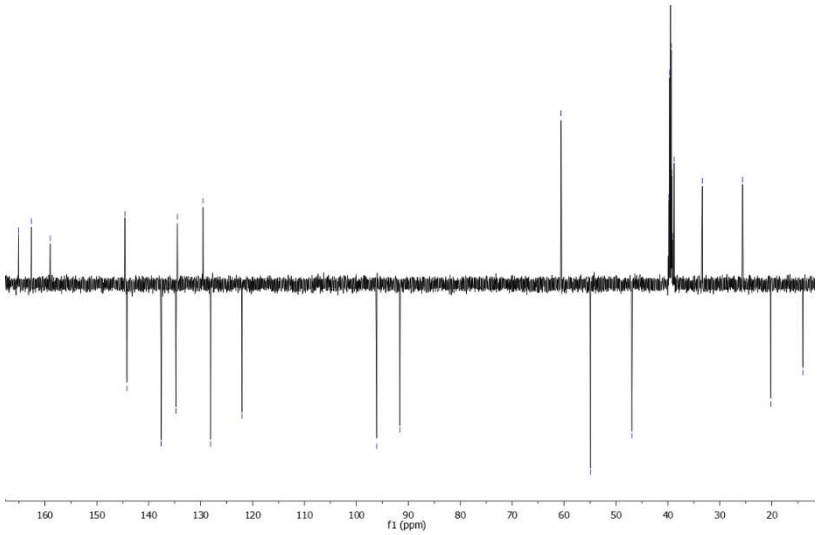
f1 (ppm)

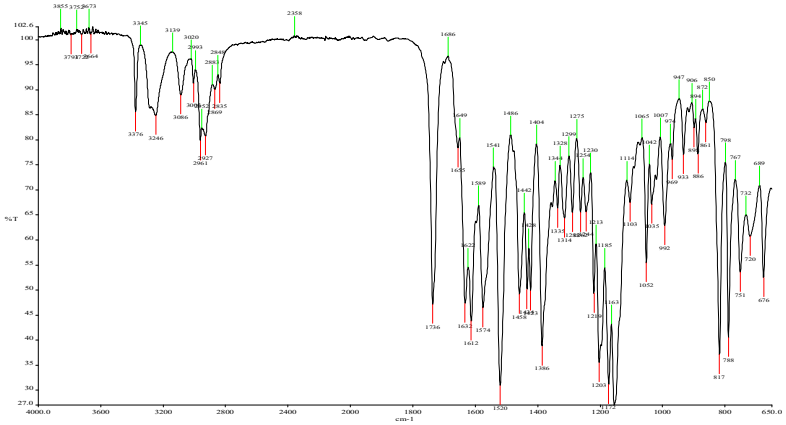

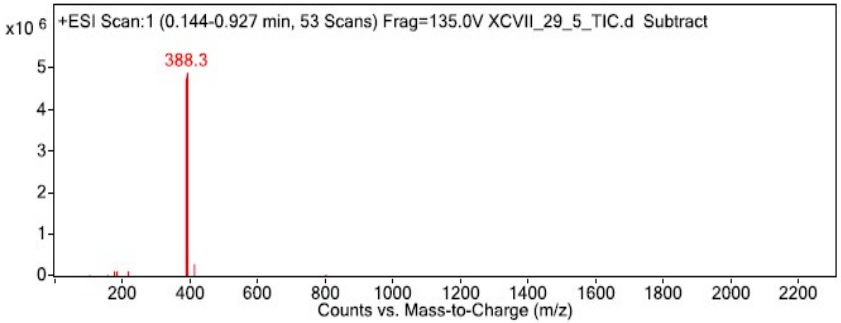
+ESI Scan:1 (0.144-0.927 min, 53 Scans) Frag=135.0V XCVII_29_5_TIC.d Subtract
x10 6
388.3
Counts vs. Mass-to-Charge (m/z)

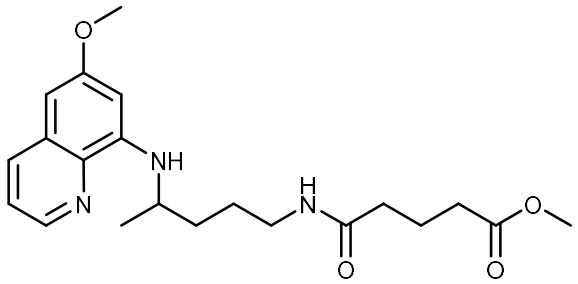
O
NH
N
H
N
O
O
O

3

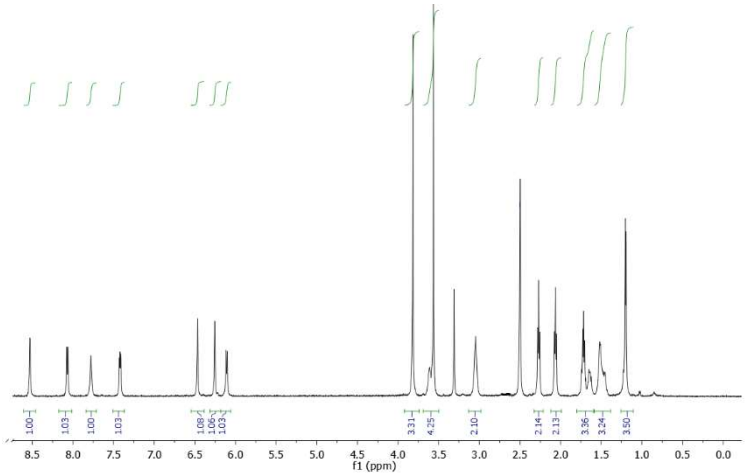
f1 (ppm)

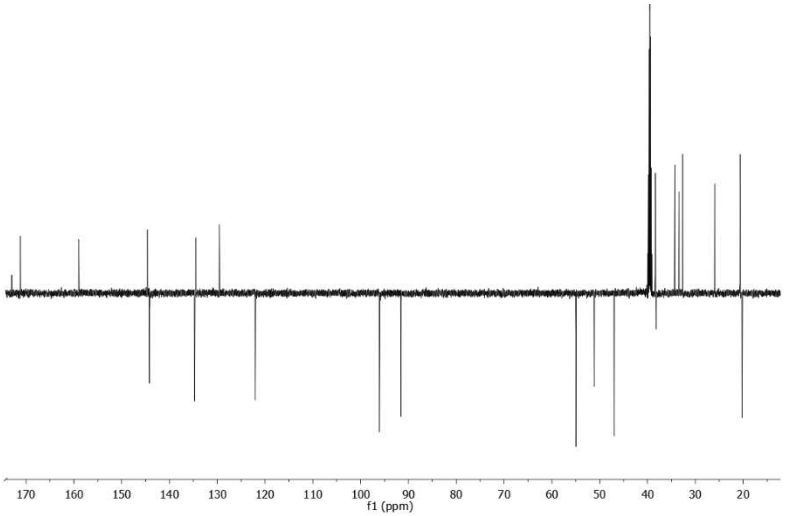
f1 (ppm)

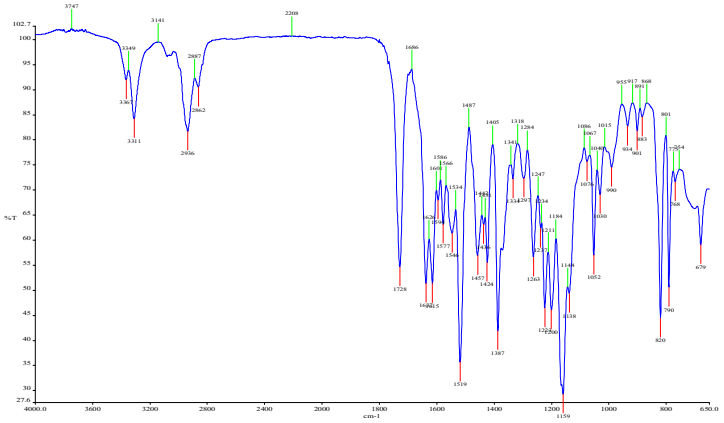

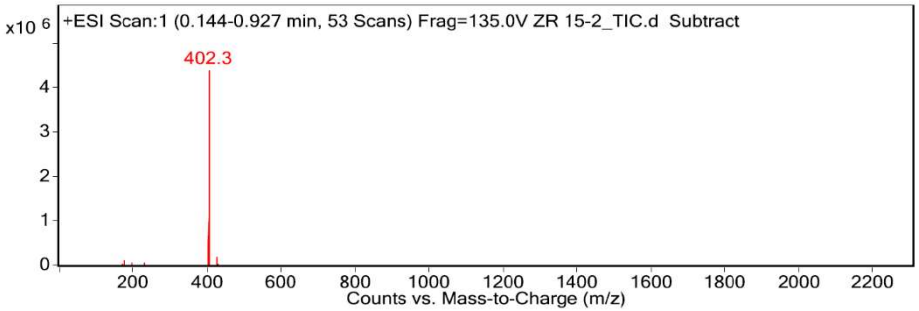
+ESI Scan:1 (0.144-0.927 min, 53 Scans) Frag=135.0V ZR 15-2_TIC.d Subtract
x10 6
402.3
Counts vs. Mass-to-Charge (m/z)

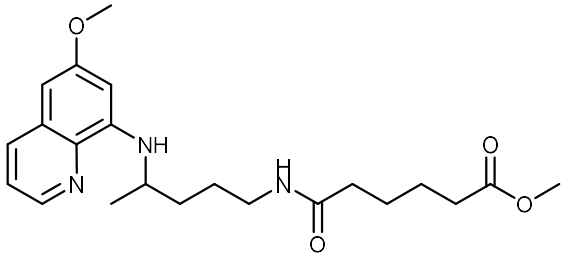
O
NH
N
H
N
O
O

4

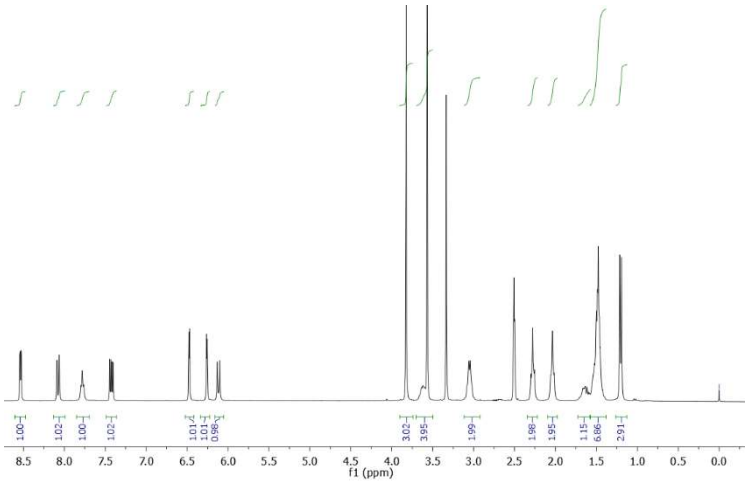
f1 (ppm)

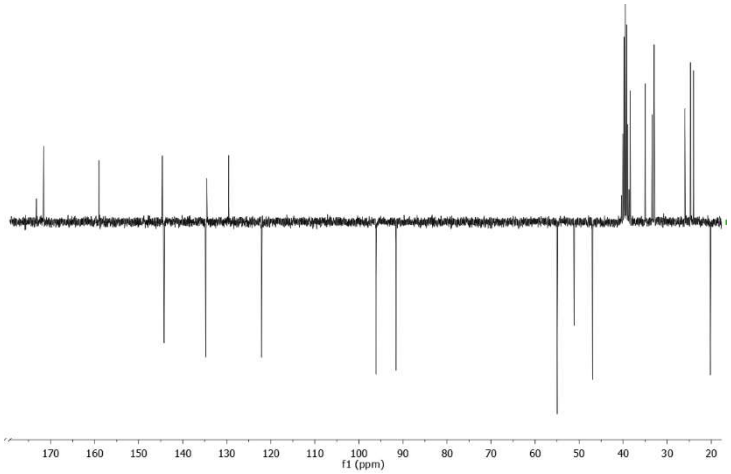
f1 (ppm)

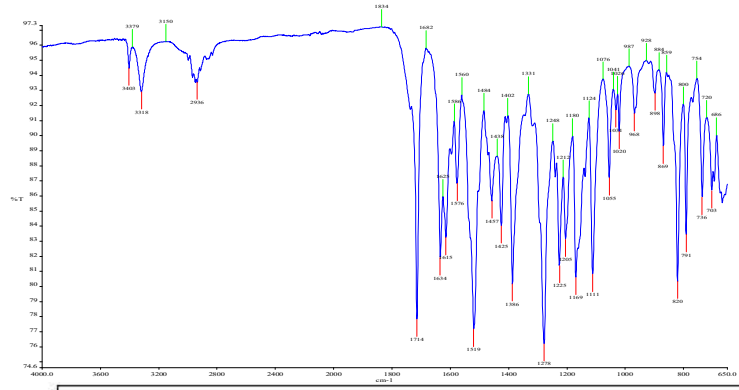

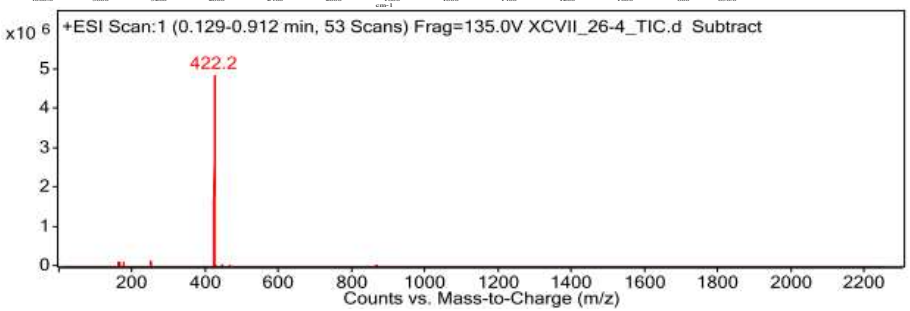
x10 6
+ESI Scan:1 (0.129-0.912 min, 53 Scans) Frag=135.0V XCVII_26-4_TIC.d Subtract
422.2
Counts vs. Mass-to-Charge (m/z)

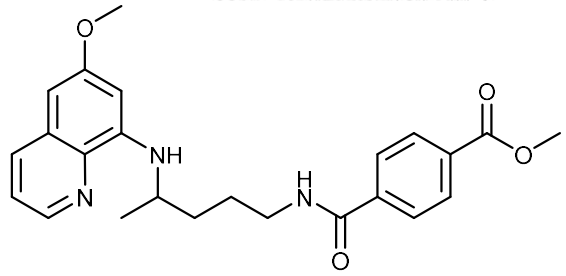
O
NH
N
H
N
O
O
O

5

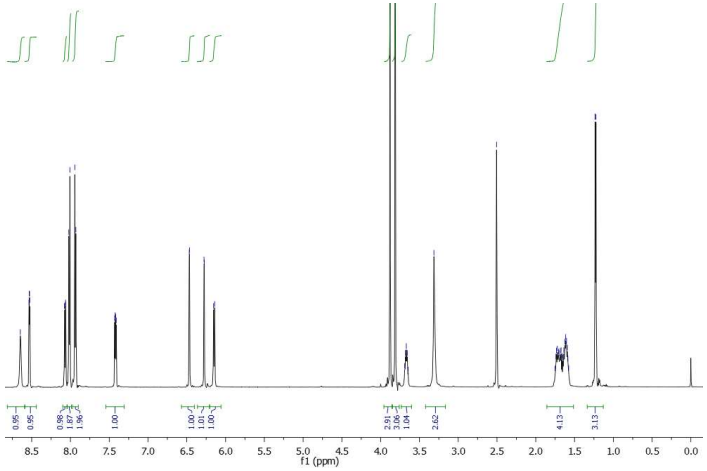
f1 (ppm)

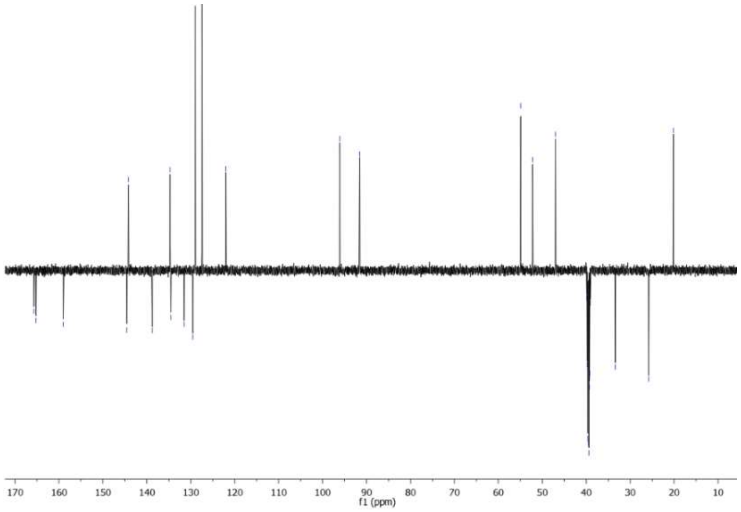
f1 (ppm)

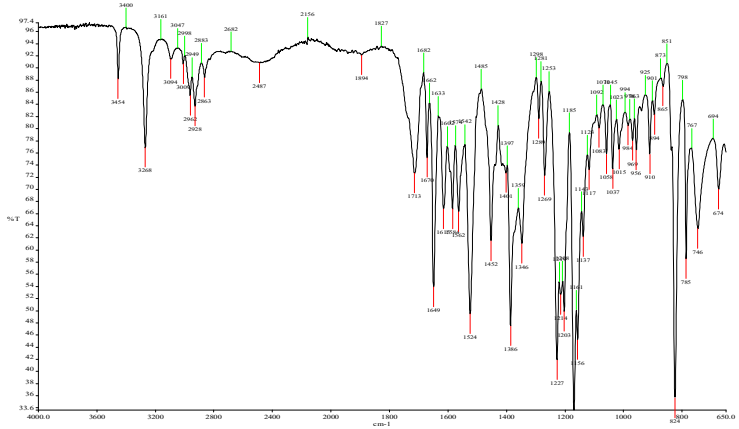

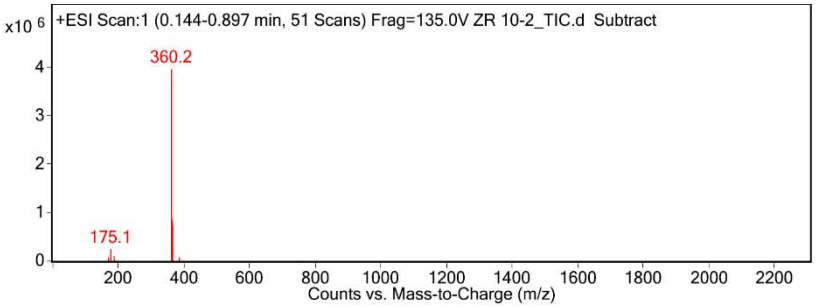
x10 6
+ESI Scan:1 (0.144-0.897 min, 51 Scans) Frag=135.0V ZR 10-2_TIC.d Subtract
360.2
175.1
Counts vs. Mass-to-Charge (m/z)

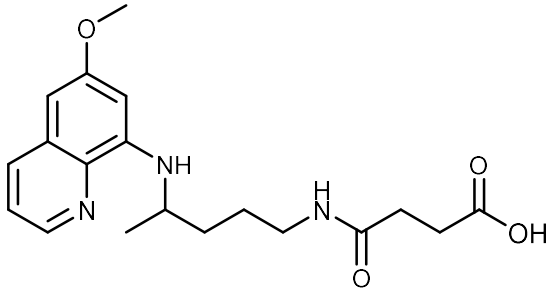
O
NH
N
H
N
O
O
OH

6

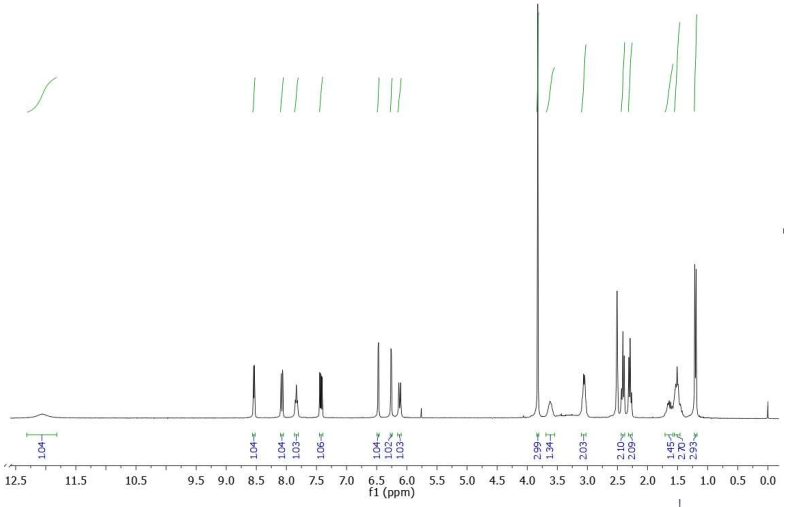
f1 (ppm)

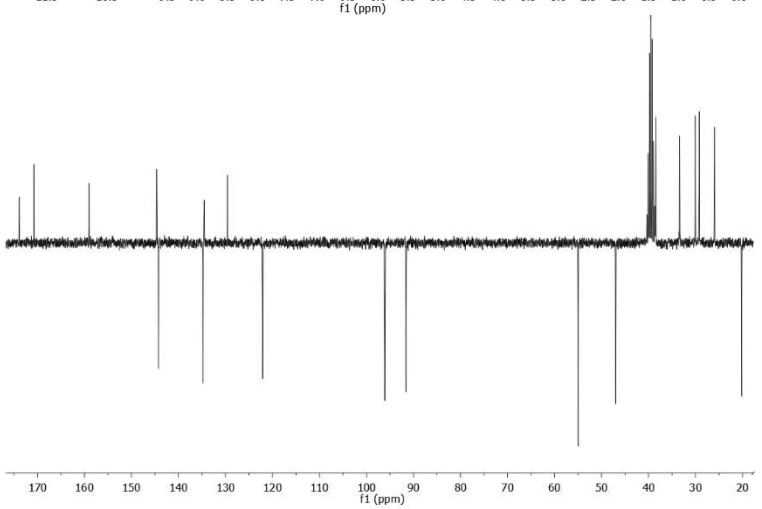
f1 (ppm)

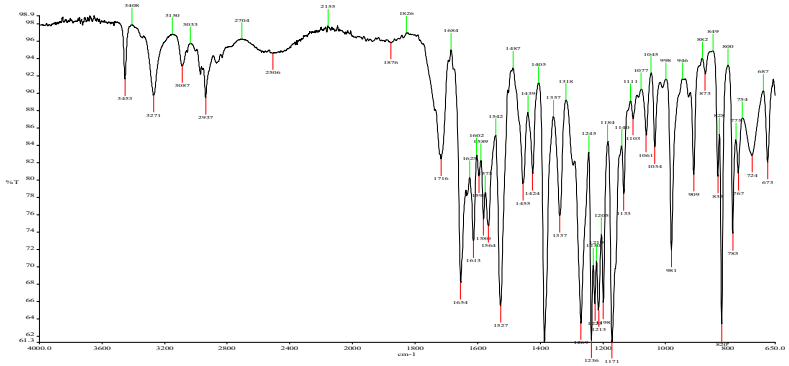

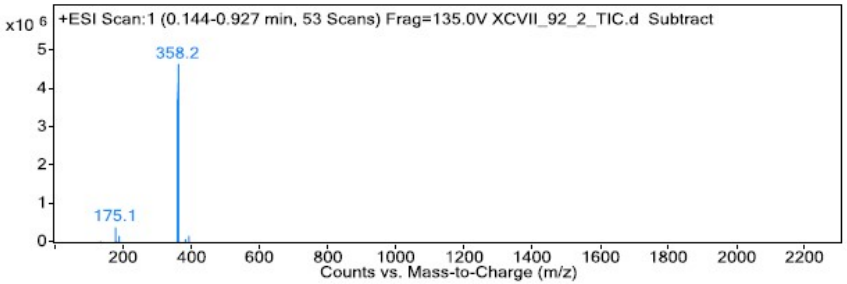
x10 6
+ESI Scan:1 (0.144-0.927 min, 53 Scans) Frag=135.0V XCVII_92_2_TIC.d Subtract
358.2
175.1
Counts vs. Mass-to-Charge (m/z)

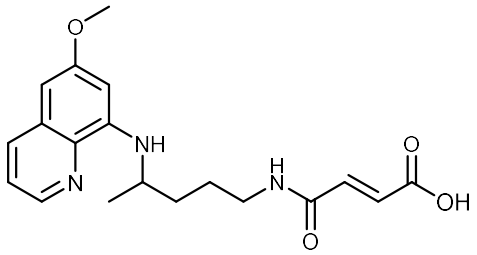
O
NH
N
H
N
O
O
OH

7

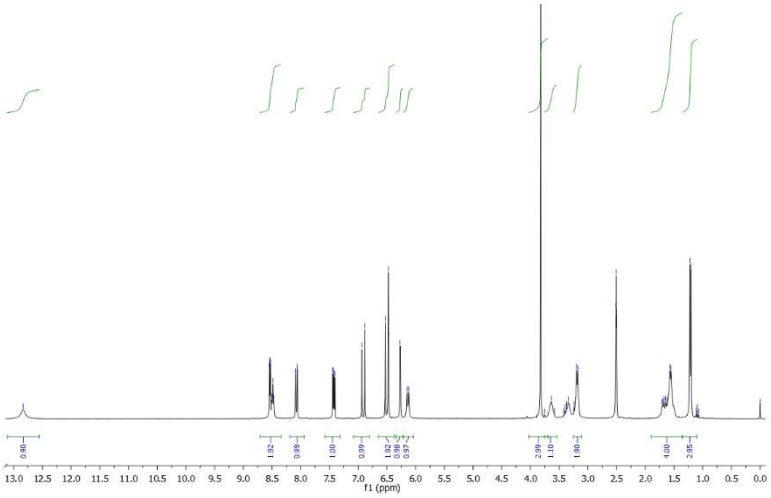
f1 (ppm)

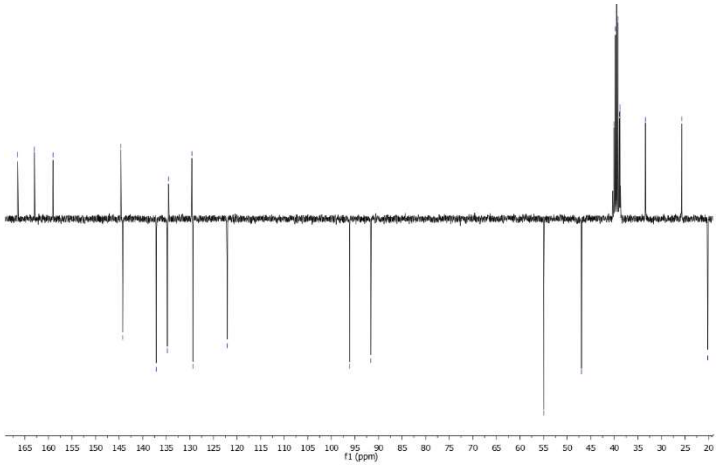
f1 (ppm)

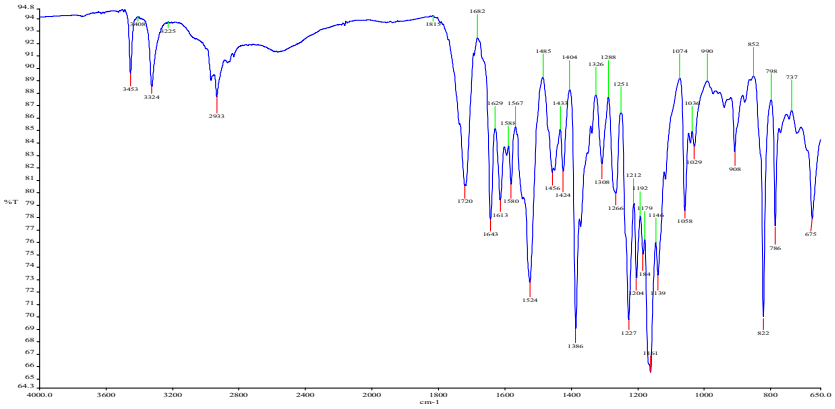

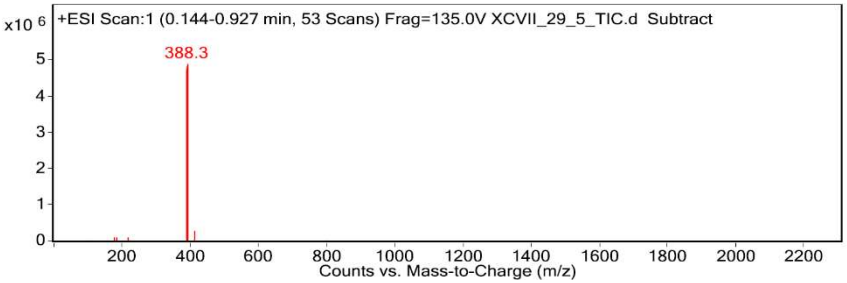
x10 6
+ESI Scan:1 (0.144-0.927 min, 53 Scans) Frag=135.0V XCVII_29_5_TIC.d Subtract
388.3
Counts vs. Mass-to-Charge (m/z)

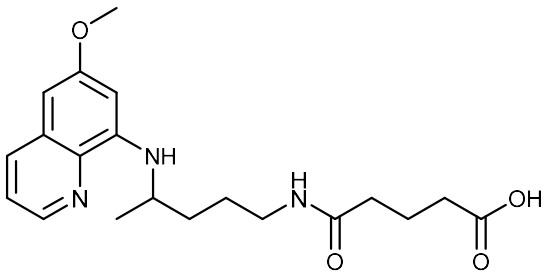
O
NH
N
H
N
O
OH
O

8

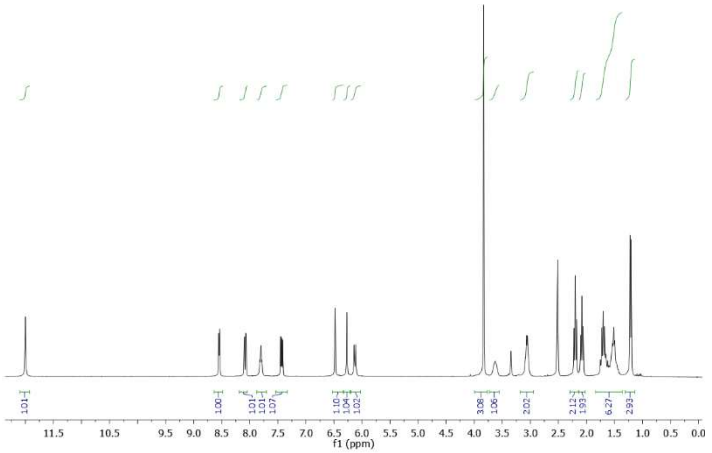
f1 (ppm)

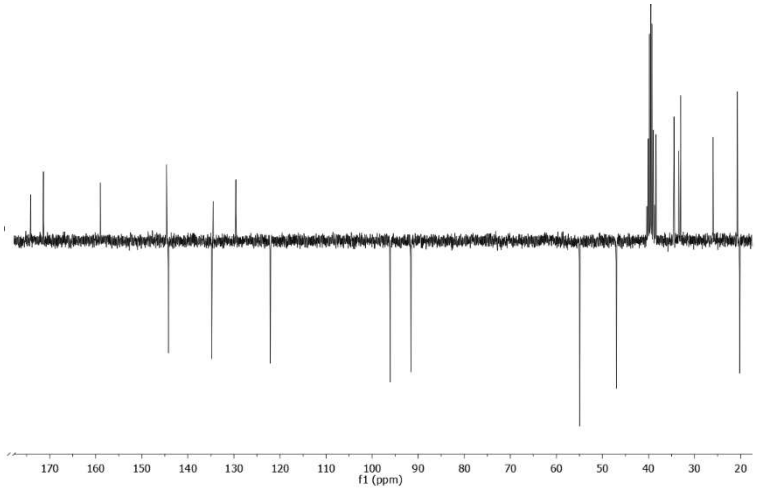
f1 (ppm)

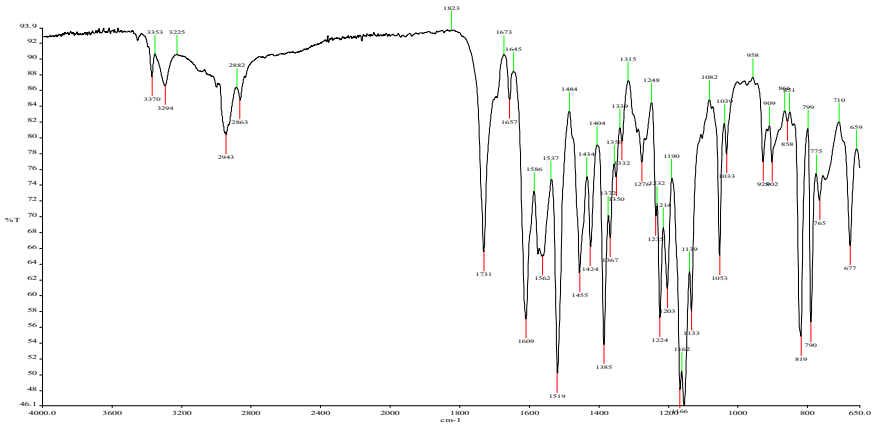

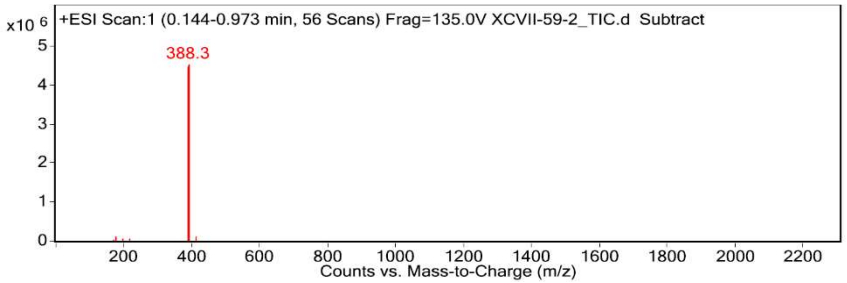
+ESI Scan:1 (0.144-0.973 min, 56 Scans) Frag=135.0V XCVII-59-2_TIC.d Subtract
x10 6
388.3
Counts vs. Mass-to-Charge (m/z)

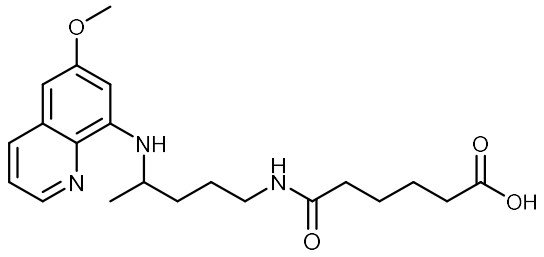
O
NH
N
H
N
O
O
OH

9

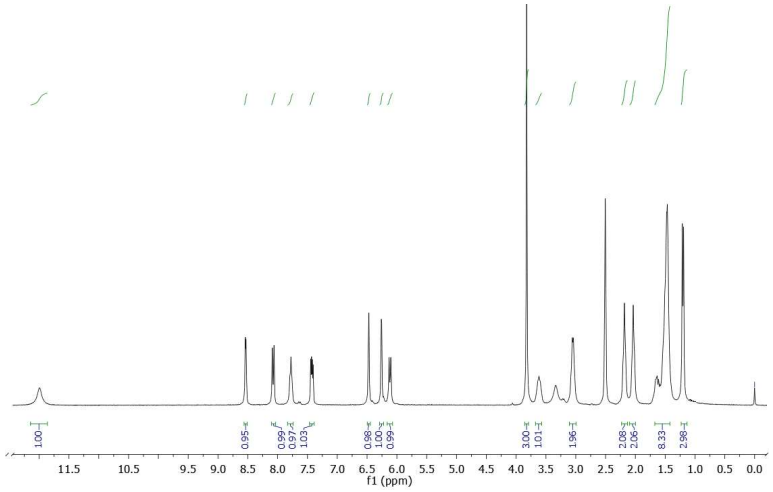
f1 (ppm)

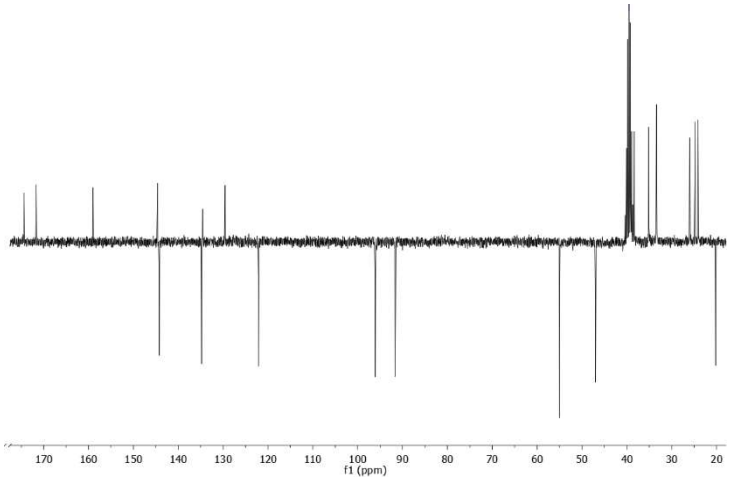
f1 (ppm)

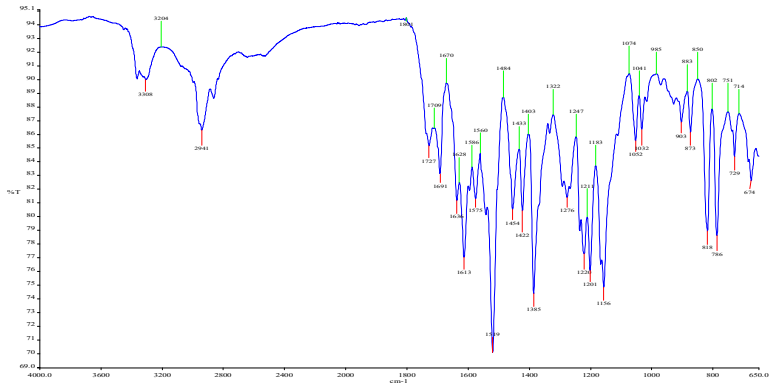

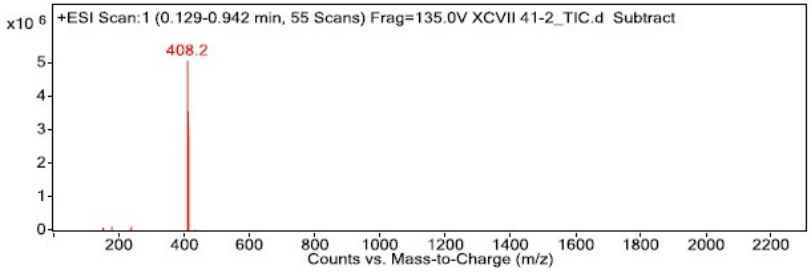
+ESI Scan:1 (0.129-0.942 min, 55 Scans) Frag=135.0V XCVII 41-2_TIC.d Subtract
x10 6
408.2
Counts vs. Mass-to-Charge (m/z)

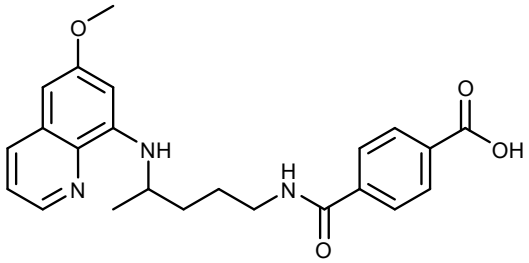
O
NH
N
H
N
O
OH
O

10

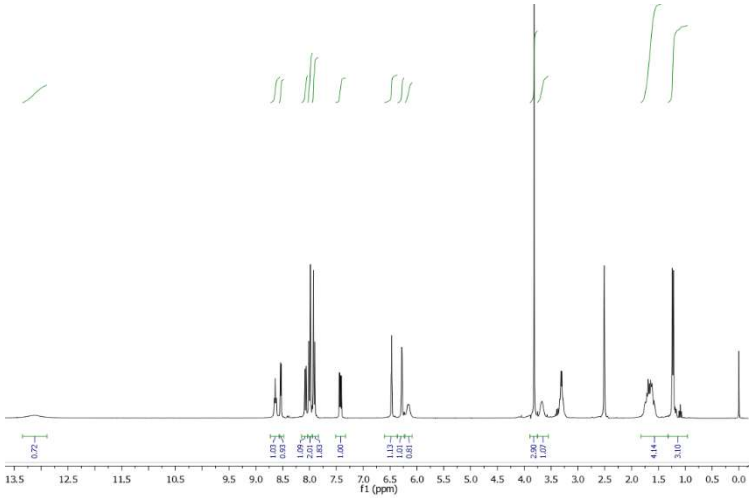
f1 (ppm)

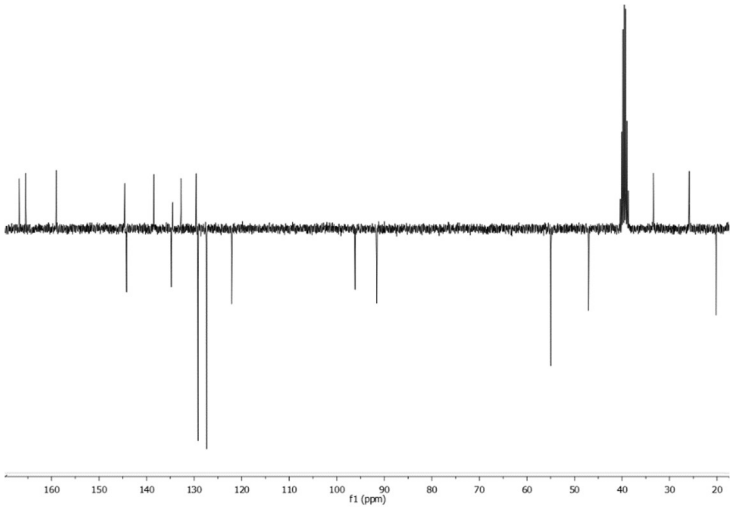
f1 (ppm)

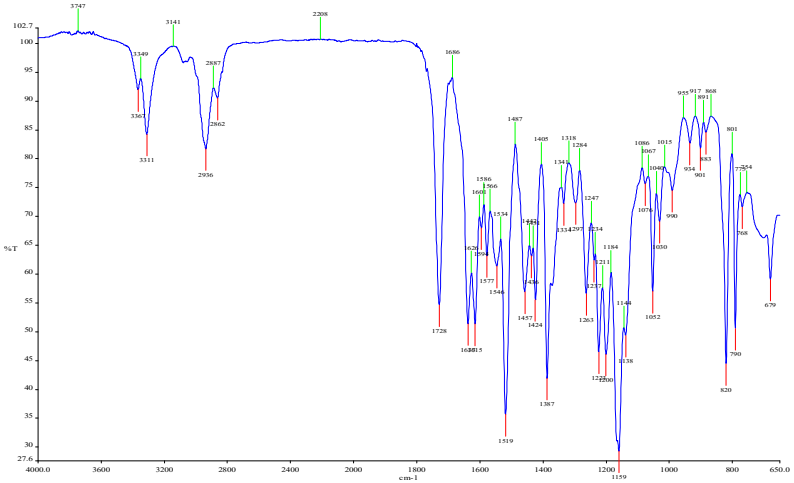

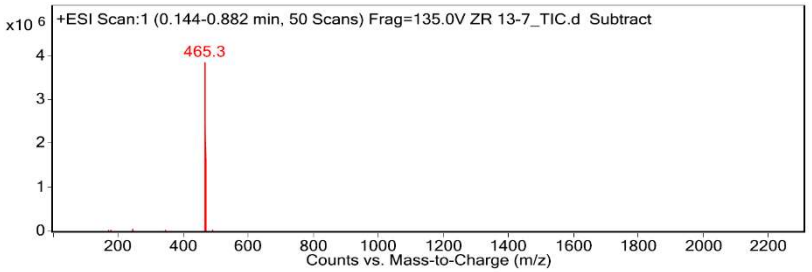
+ESI Scan:1 (0.144-0.882 min, 50 Scans) Frag=135.0V ZR 13-7_TIC.d Subtract
x10 6
465.3
Counts vs. Mass-to-Charge (m/z)

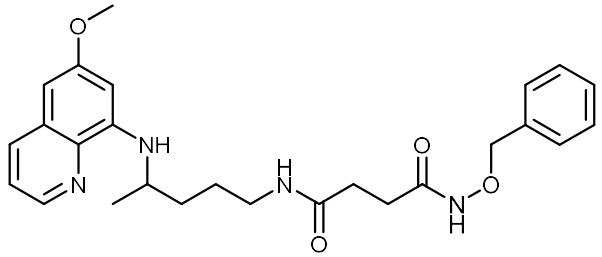
O
NH
N
H
N
O
O
N
H
O

11

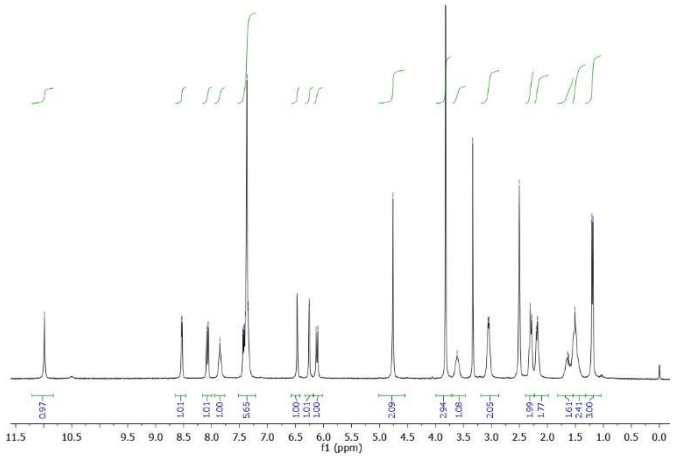
f1 (ppm)

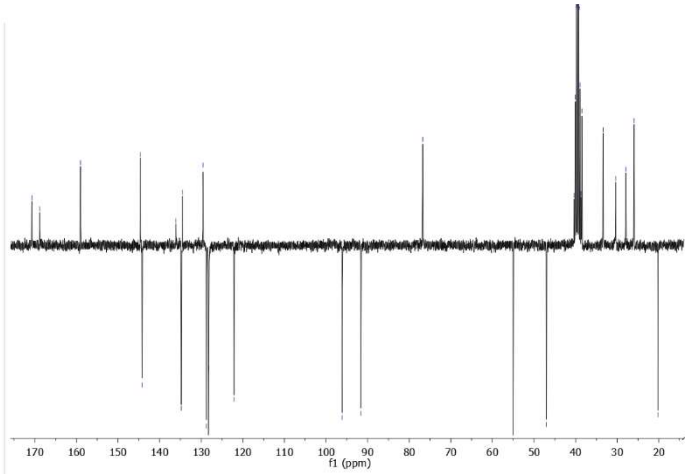
f1 (ppm)

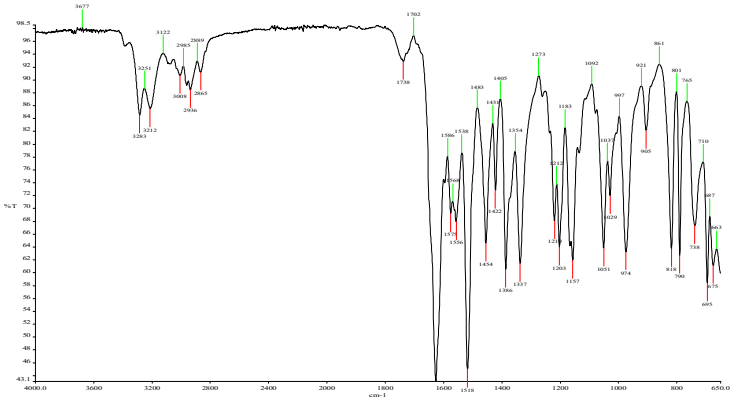

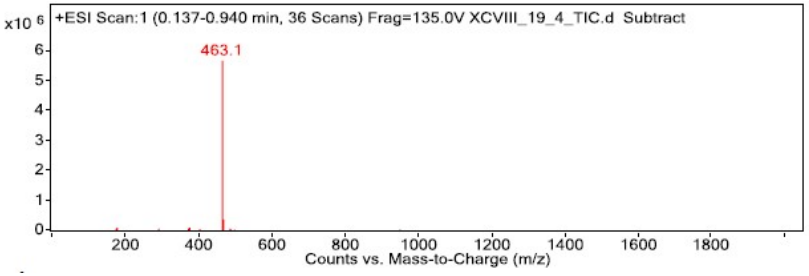
x10 6
+ESI Scan:1 (0.137-0.940 min, 36 Scans) Frag=135.0V XCVIII_19_4_TIC.d Subtract
463.1
Counts vs. Mass-to-Charge (m/z)

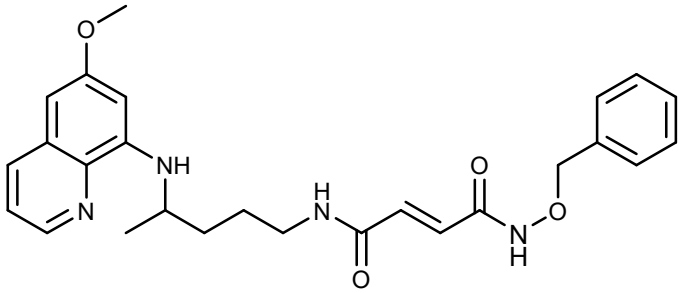
O
NH
N
H
N
O
O
N
H
O

12

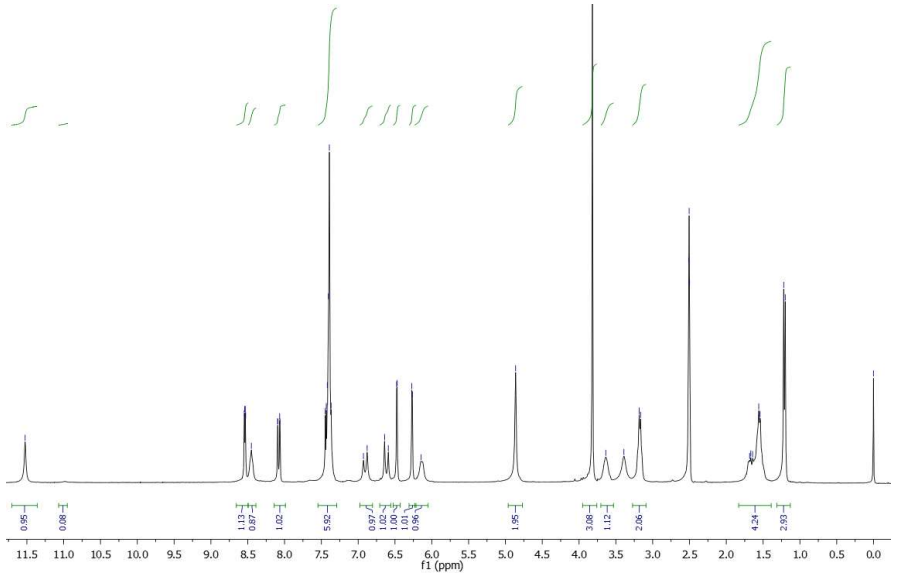
f1 (ppm)

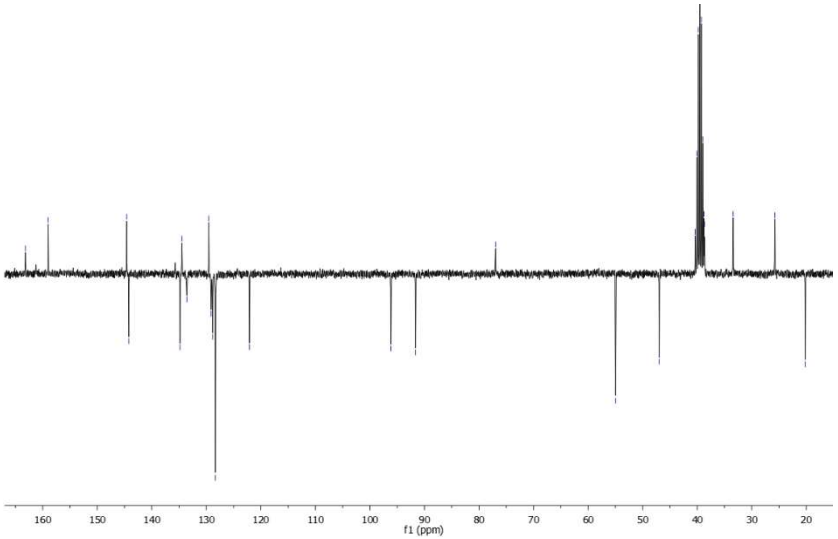
f1 (ppm)

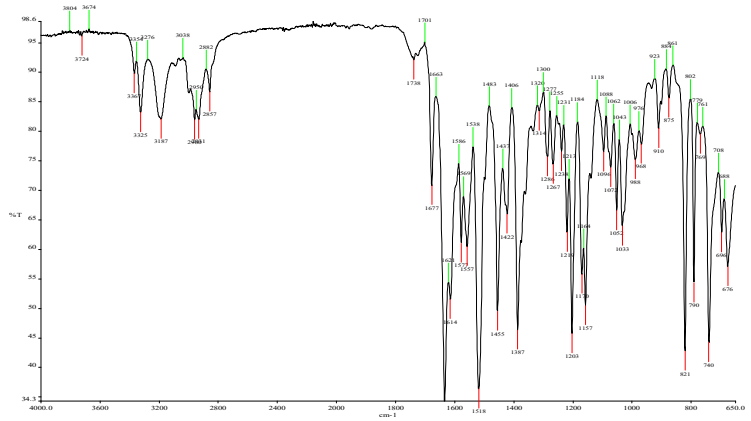

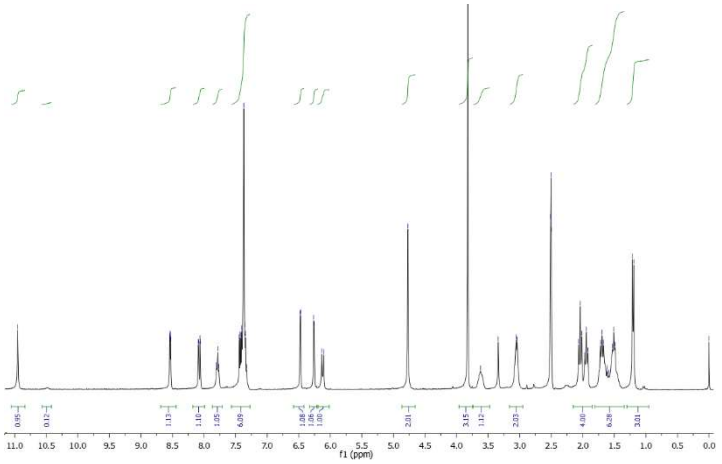

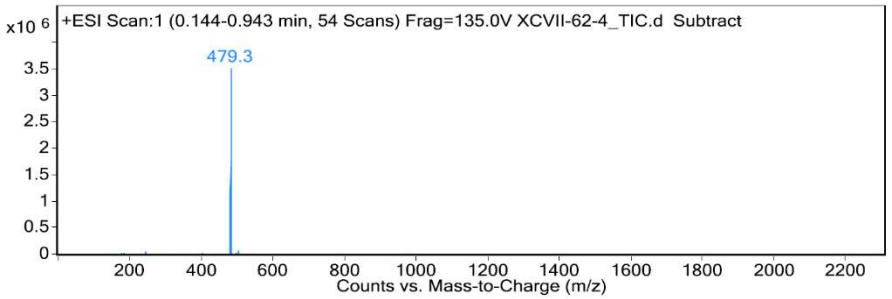
x10 6
+ESI Scan:1 (0.144-0.943 min, 54 Scans) Frag=135.0V XCVII-62-4_TIC.d Subtract
479.3
Counts vs. Mass-to-Charge (m/z)

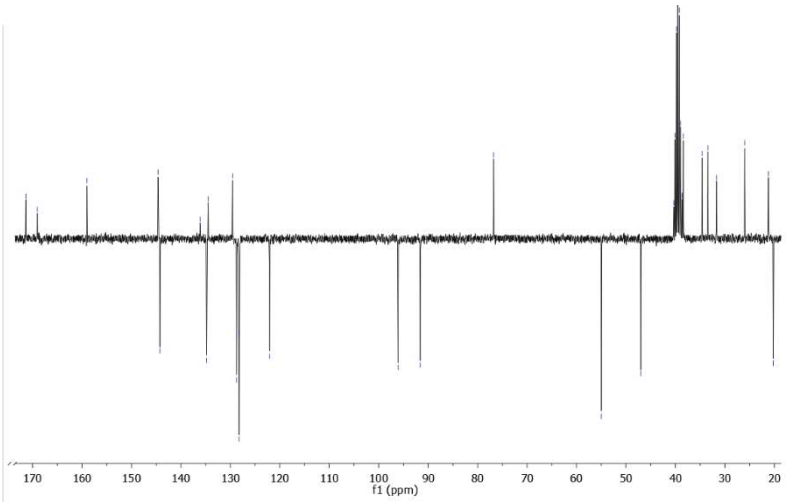

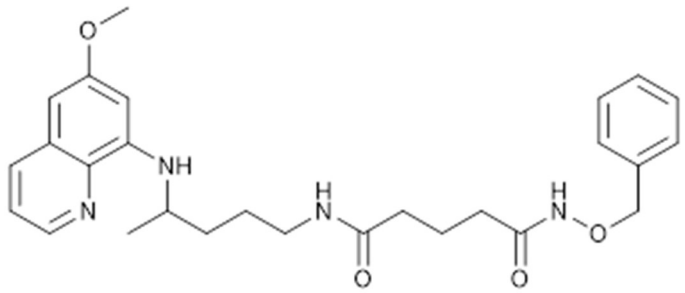
O
NH
N
H
N
O
H
N
O
O

13

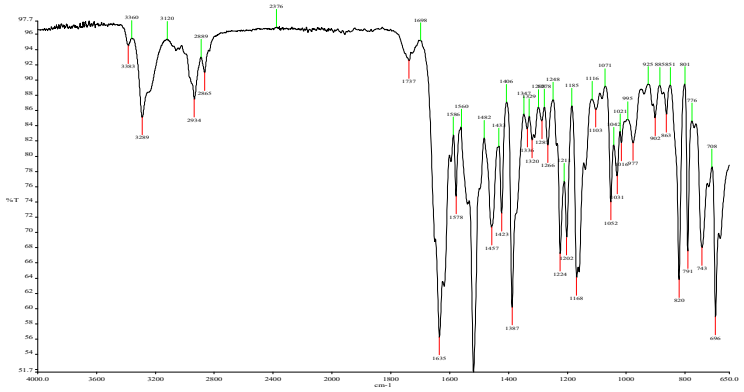

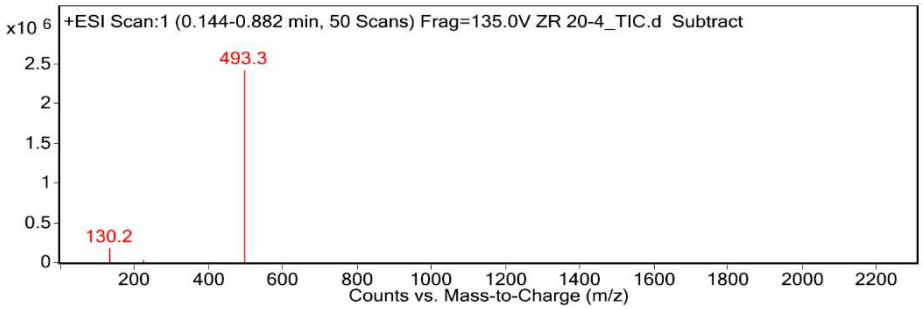
x10 6
+ESI Scan:1 (0.144-0.882 min, 50 Scans) Frag=135.0V ZR 20-4_TIC.d Subtract
493.3
130.2
Counts vs. Mass-to-Charge (m/z)

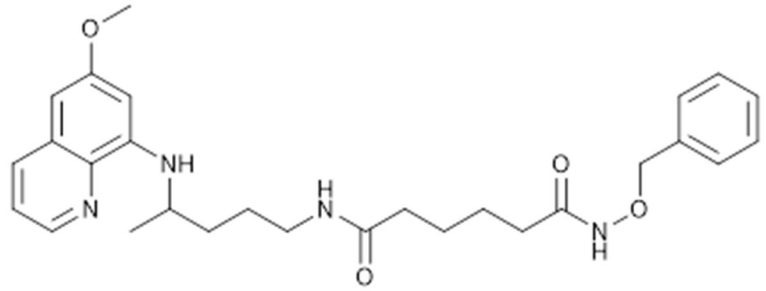
O
NH
N
H
N
O
O
N
H
O

14

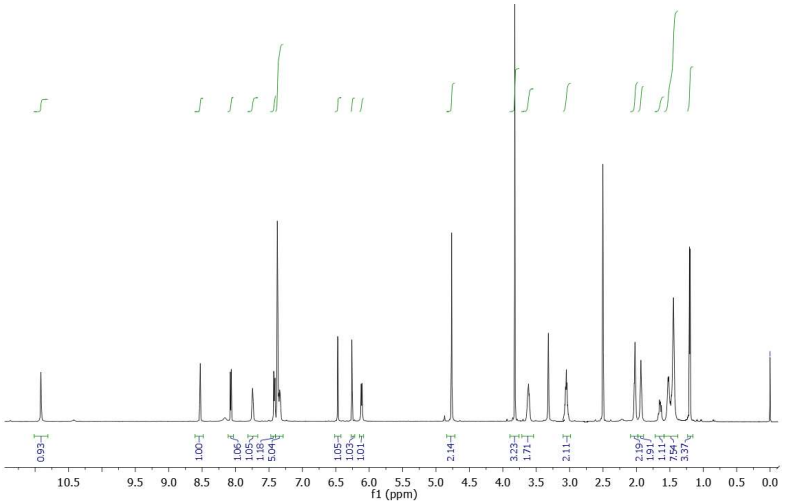
f1 (ppm)

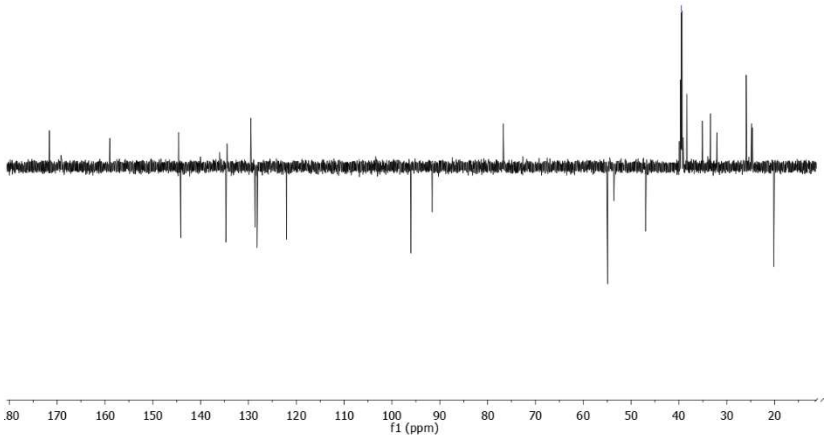
f1 (ppm)

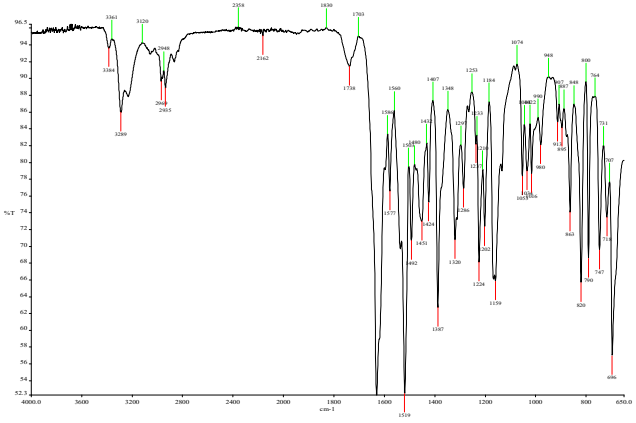

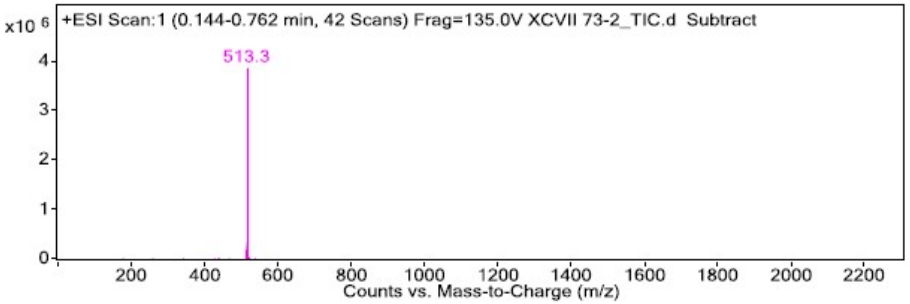
+ESI Scan:1 (0.144-0.762 min, 42 Scans) Frag=135.0V XCVII 73-2_TIC.d Subtract
x10 6
513.3
Counts vs. Mass-to-Charge (m/z)

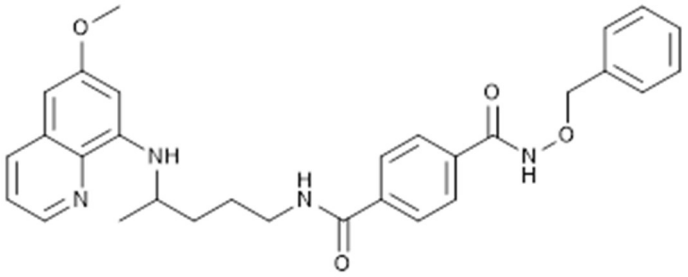

15

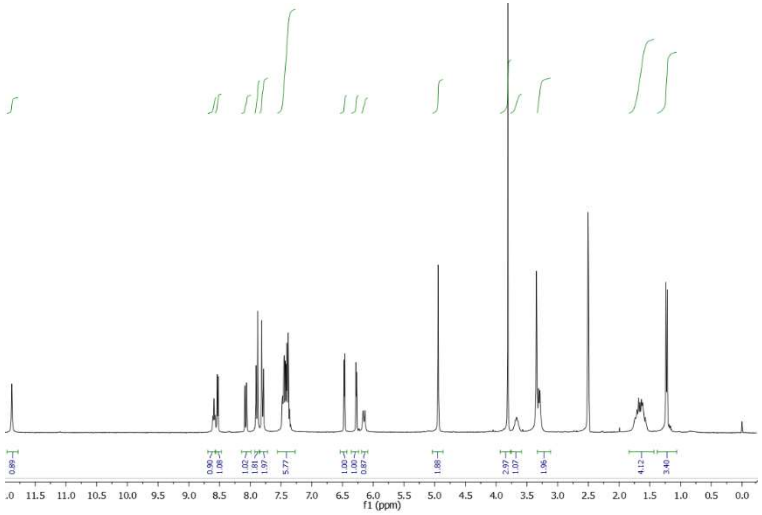
f1 (ppm)

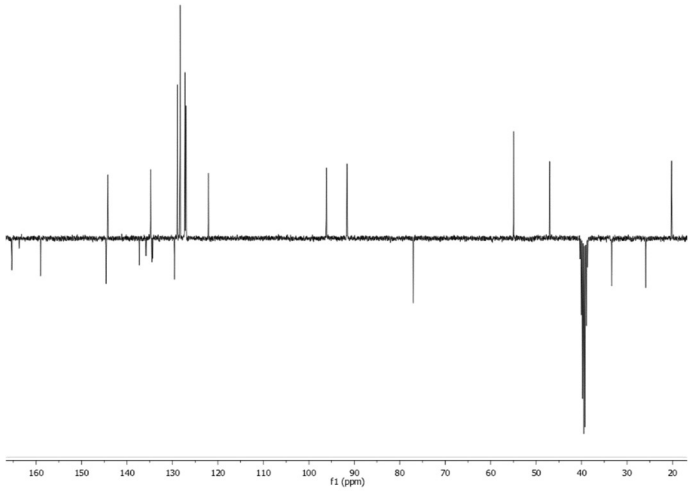
f1 (ppm)

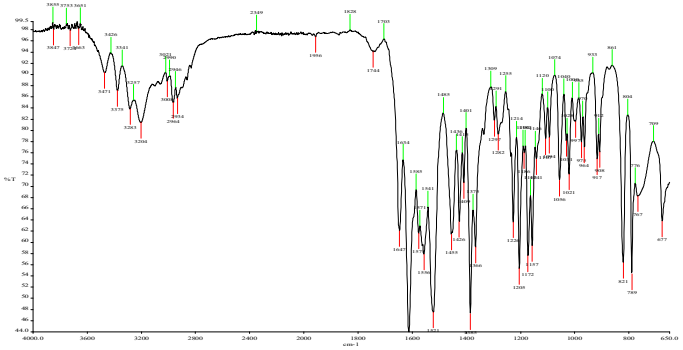

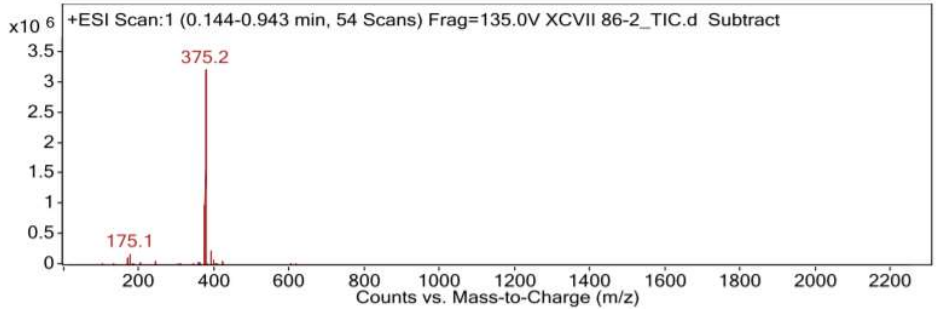
x10 6
+ESI Scan:1 (0.144-0.943 min, 54 Scans) Frag=135.0V XCVII 86-2_TIC.d Subtract
375.2
175.1
Counts vs. Mass-to-Charge (m/z)

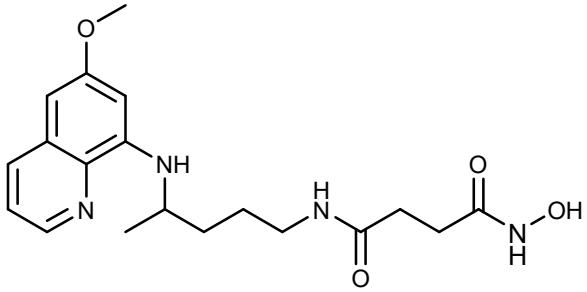
O
NH
N
H
N
O
O
N
H
OH

16

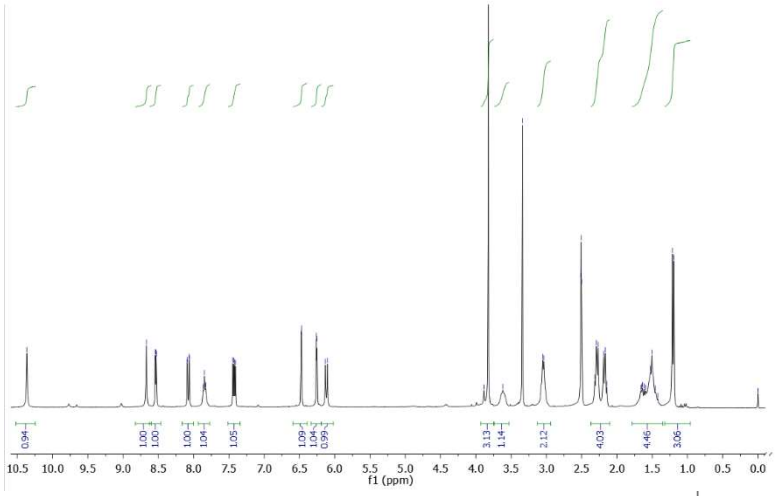
f1 (ppm)

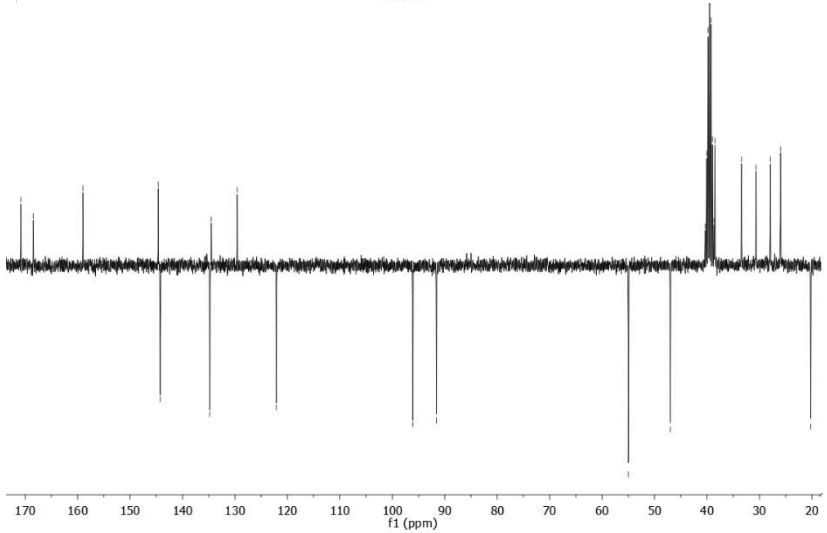
f1 (ppm)

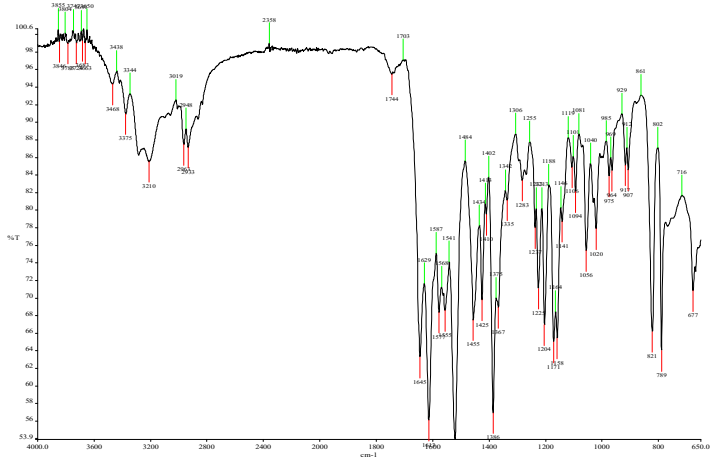

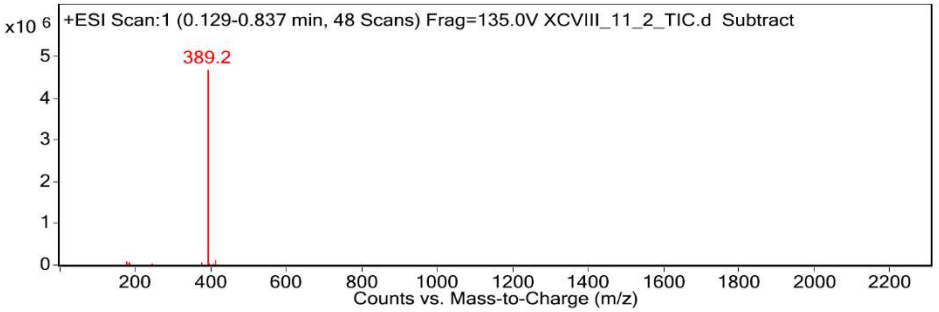
x10 6
+ESI Scan:1 (0.129-0.837 min, 48 Scans) Frag=135.0V XCVIII_11_2_TIC.d Subtract
389.2
Counts vs. Mass-to-Charge (m/z)

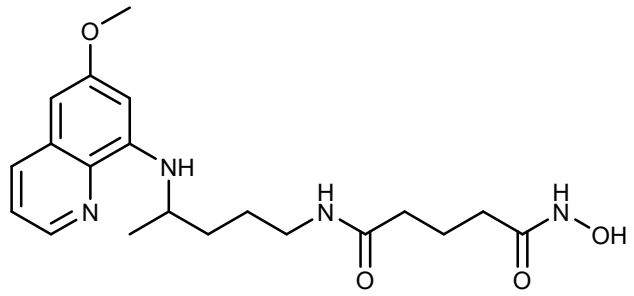
O
NH
N
H
N
O
H
N
OH
O

17

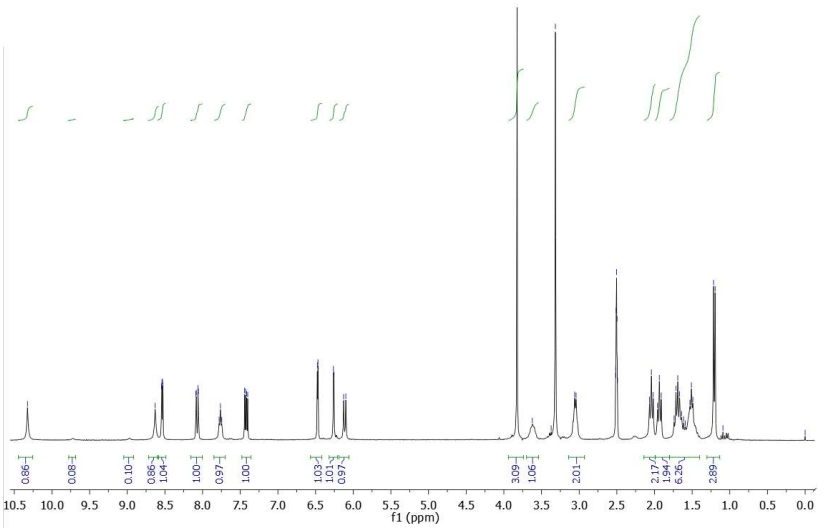
f1 (ppm)

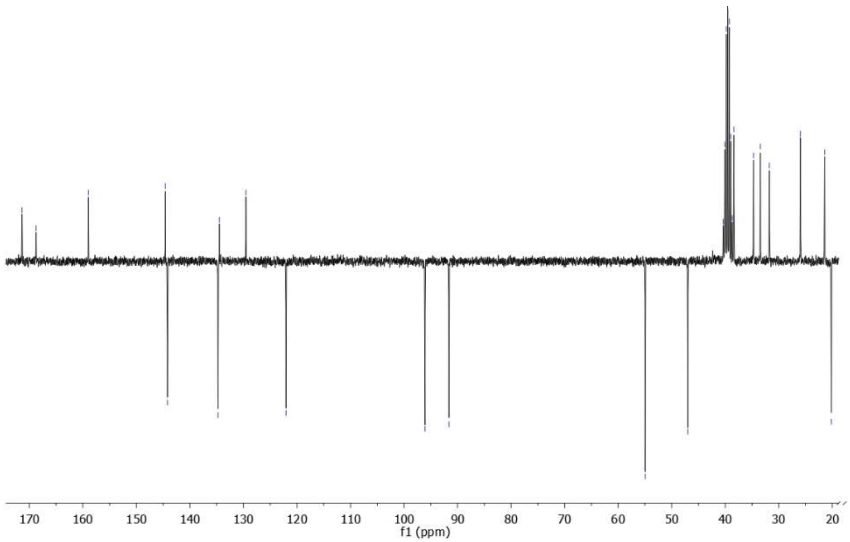
f1 (ppm)

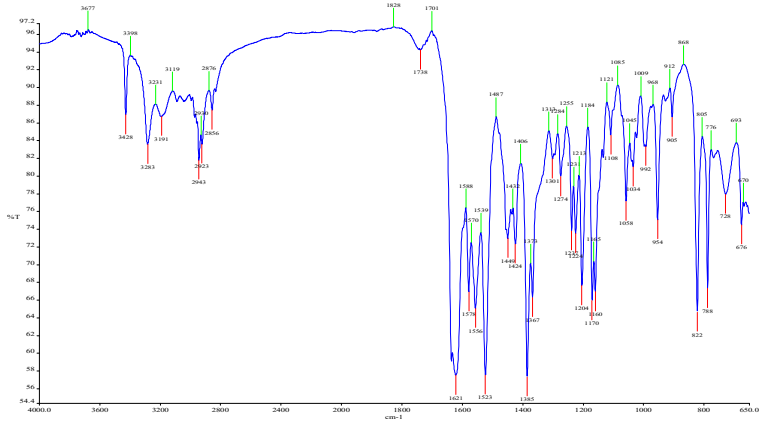

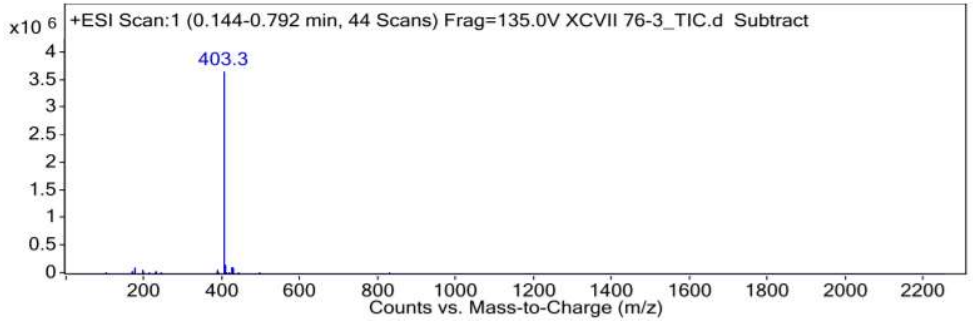
+ESI Scan:1 (0.144-0.792 min, 44 Scans) Frag=135.0V XCVII 76-3_TIC.d Subtract
x10 6
403.3
Counts vs. Mass-to-Charge (m/z)

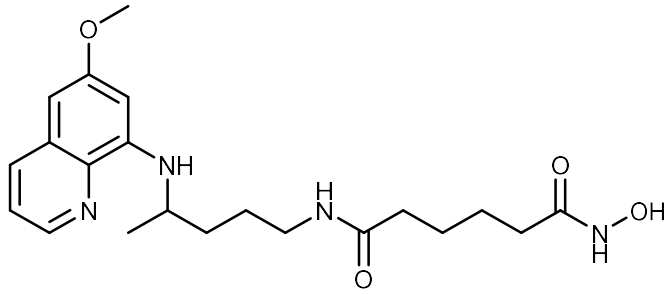
O
NH
N
H
N
O
O
N
H
OH

18

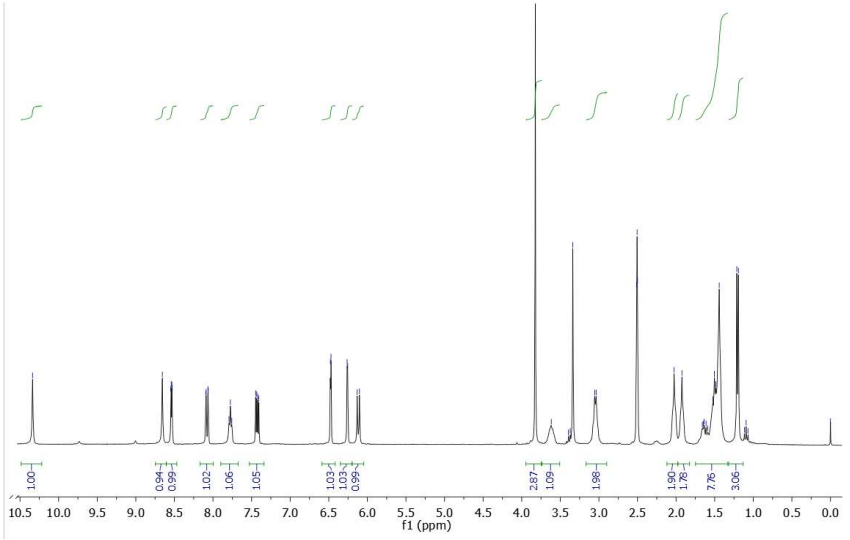
f1 (ppm)

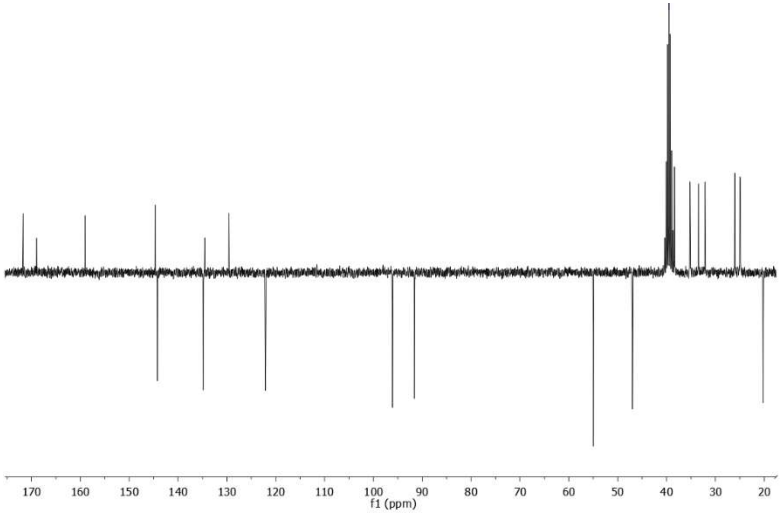
f1 (ppm)

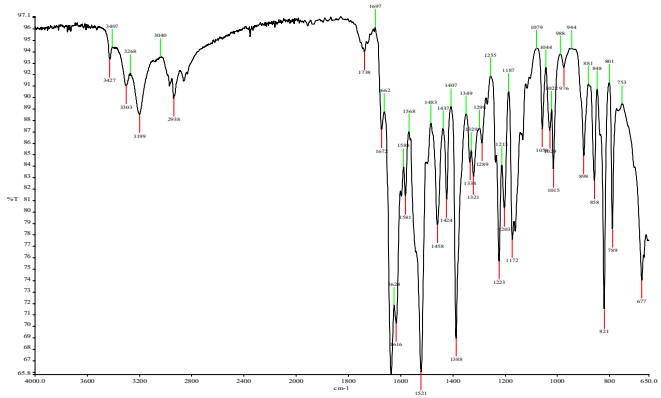

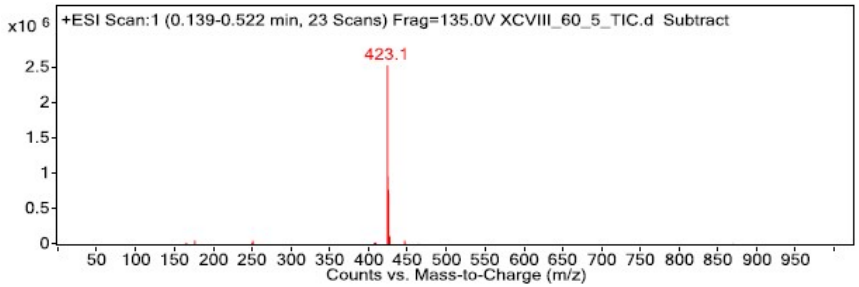
x10 6
+ESI Scan:1 (0.139-0.522 min, 23 Scans) Frag=135.0V XCVIII_60_5_TIC.d Subtract
423.1
2.5
2
1.5
1
0.5
0
50 100 150 200 250 300 350 400 450 500 550 600 650 700 750 800 850 900 950
Counts vs. Mass-to-Charge (m/z)

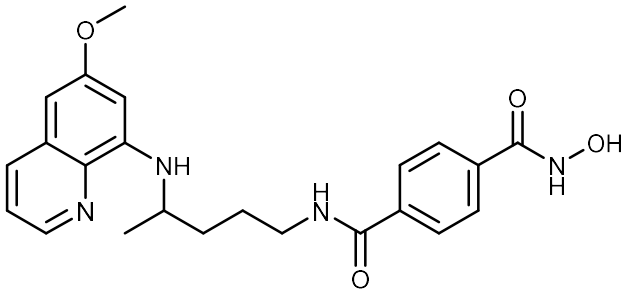
O
NH
N
H
N
O
N
OH
H

19

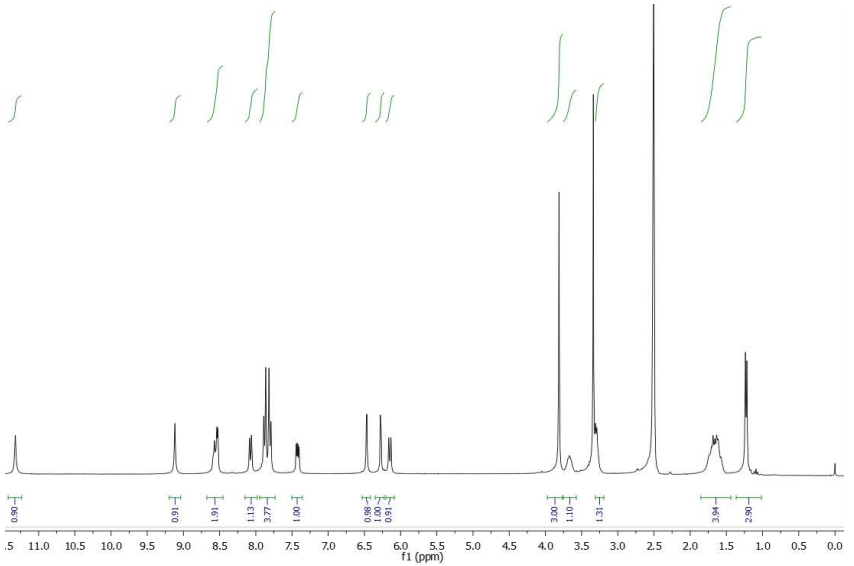
0.90
0.91
1.91
1.13
3.77
1.00
0.98
1.00
0.91
3.00
1.10
1.31
3.94
2.90
.5 11.0 10.5 10.0 9.5 9.0 8.5 8.0 7.5 7.0 6.5 6.0 5.5 5.0 4.5 4.0 3.5 3.0 2.5 2.0 1.5 1.0 0.5 0.0
f1 (ppm)

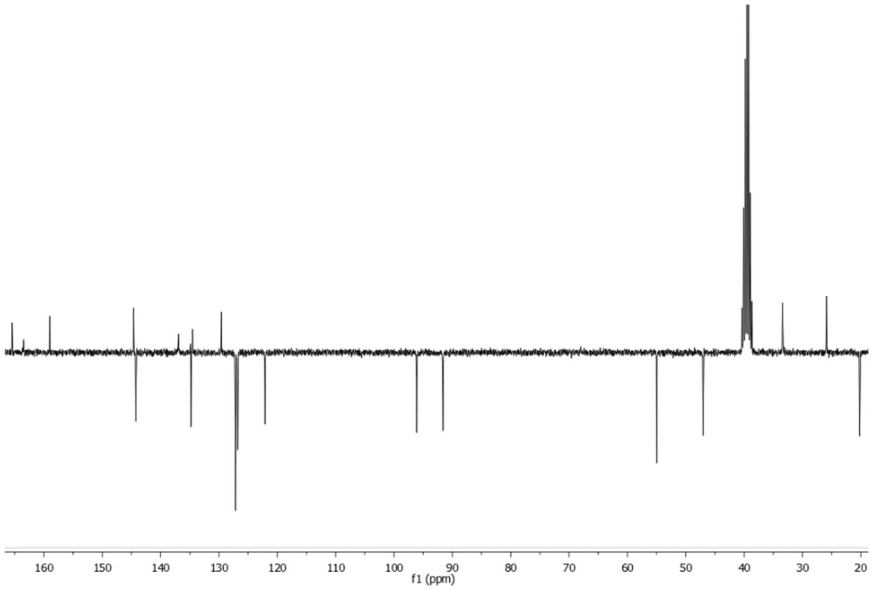
160 150 140 130 120 110 100 90 80 70 60 50 40 30 20
f1 (ppm)

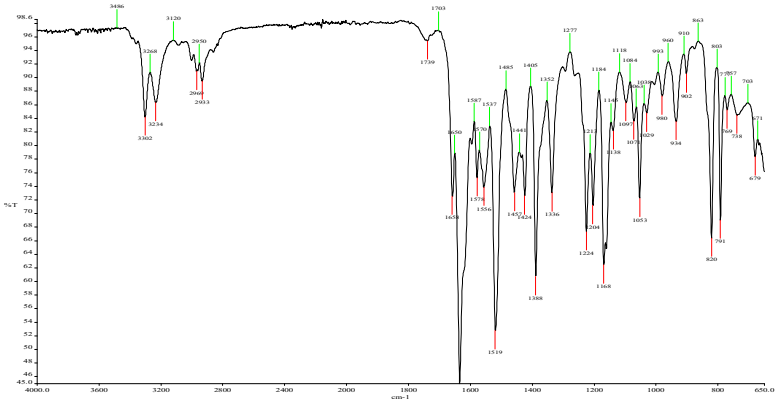

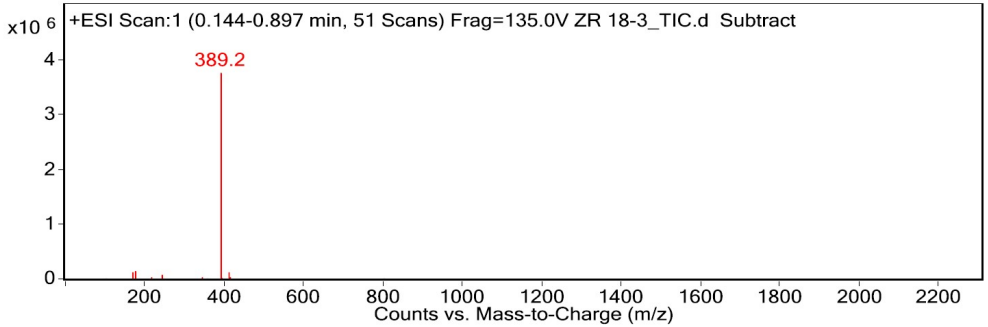
x10 6
+ESI Scan:1 (0.144-0.897 min, 51 Scans) Frag=135.0V ZR 18-3_TIC.d Subtract
389.2
Counts vs. Mass-to-Charge (m/z)

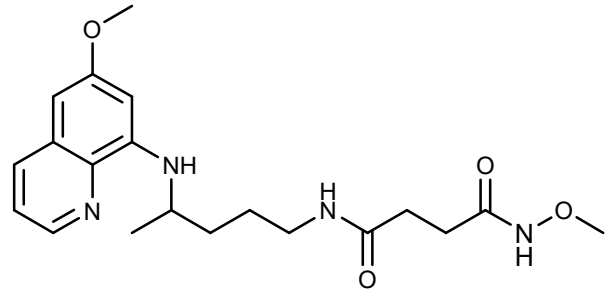
O
NH
N
H
N
O
O
N
H
O

20

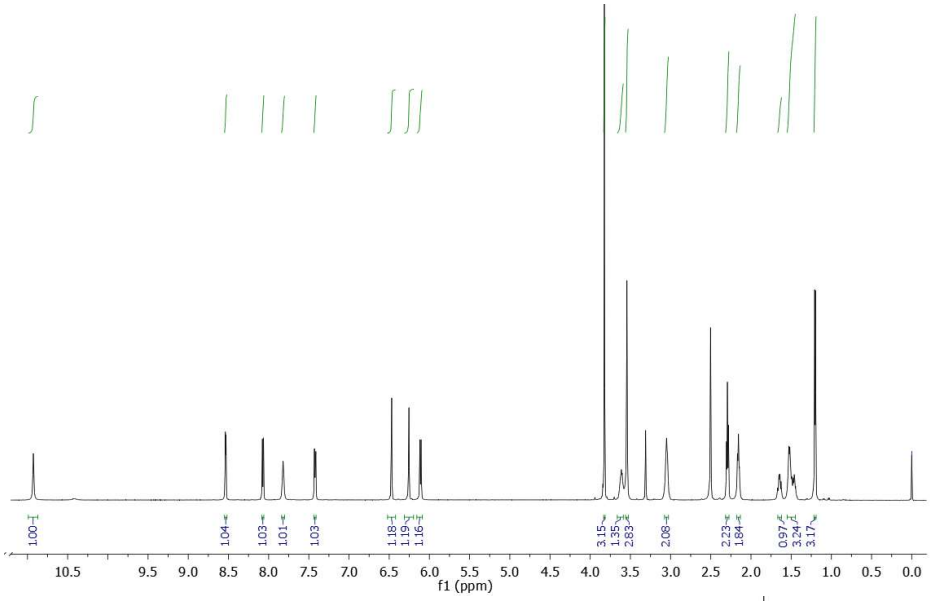
f1 (ppm)

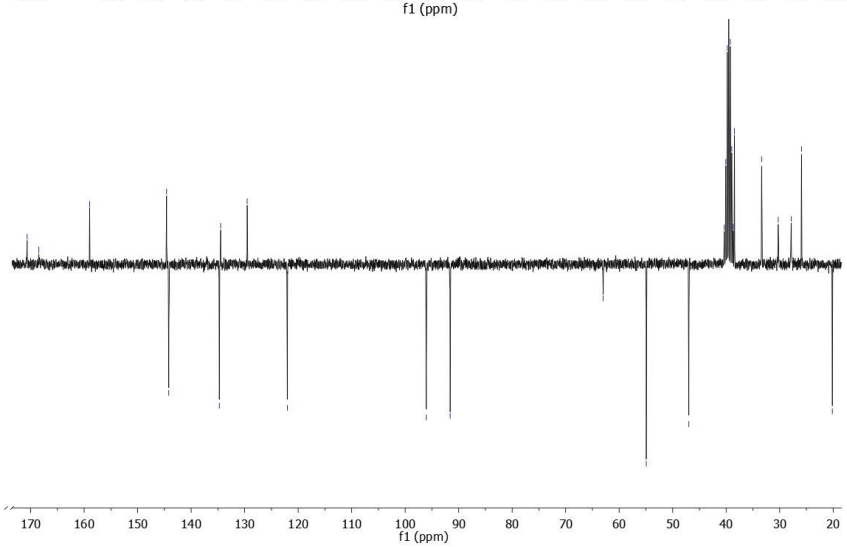
f1 (ppm)

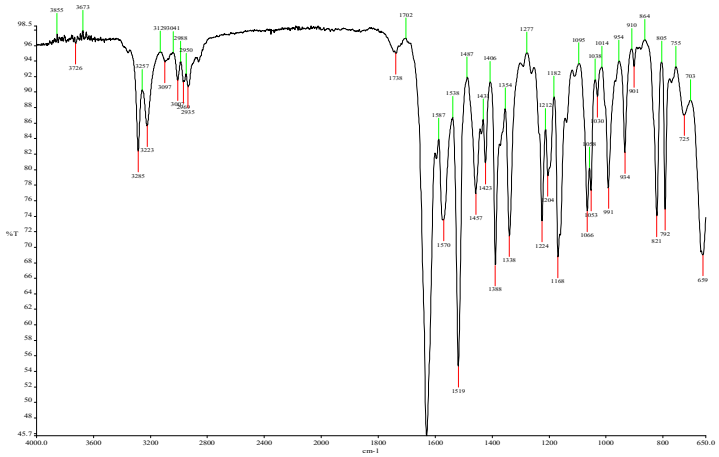

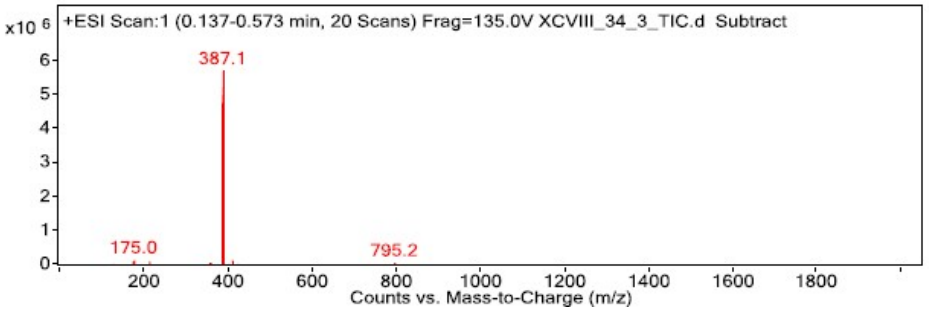
+ESI Scan:1 (0.137-0.573 min, 20 Scans) Frag=135.0V XCVIII_34_3_TIC.d Subtract
x10 6
387.1
175.0
795.2
Counts vs. Mass-to-Charge (m/z)

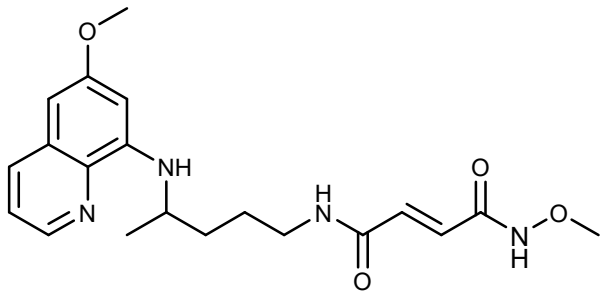
O
NH
N
H
N
O
O
N
H
O

21

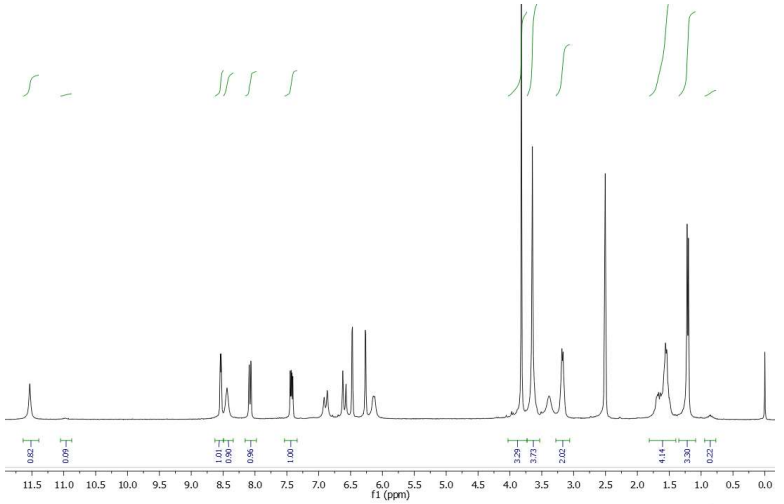
f1 (ppm)

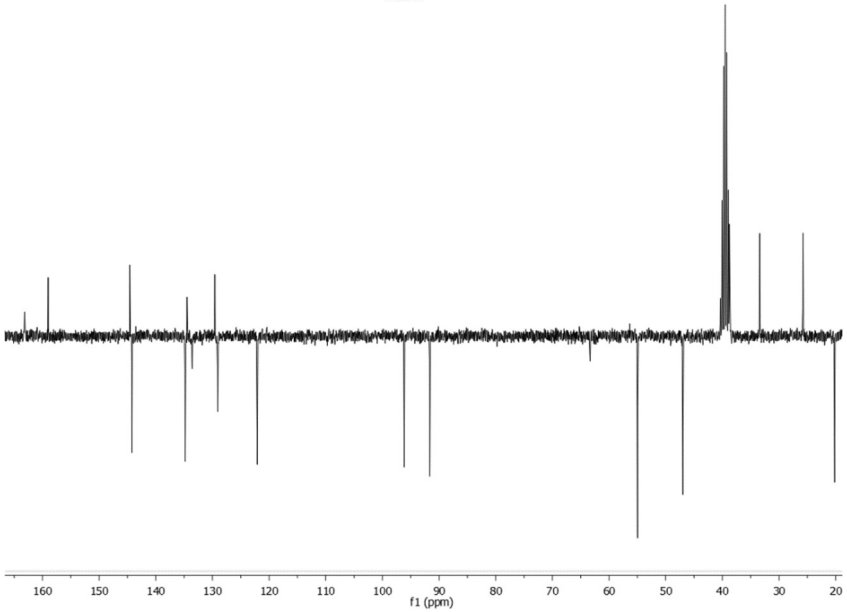
f1 (ppm)

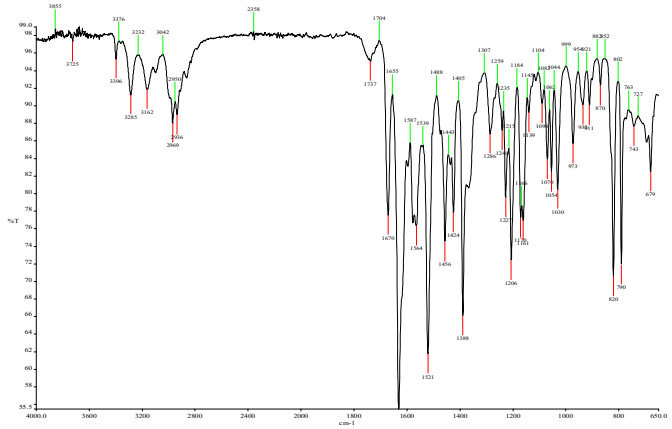

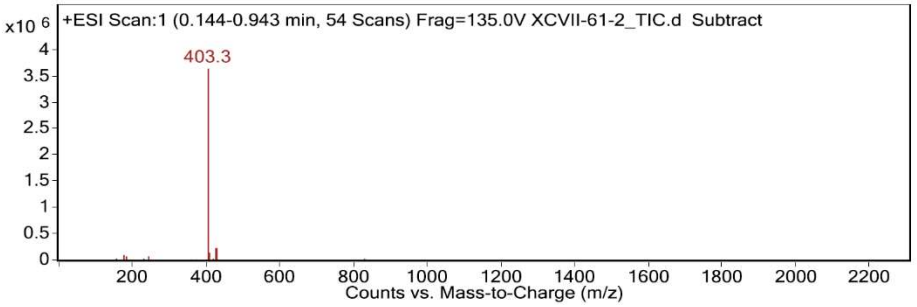
+ESI Scan:1 (0.144-0.943 min, 54 Scans) Frag=135.0V XCVII-61-2_TIC.d Subtract
x10 6
403.3
Counts vs. Mass-to-Charge (m/z)

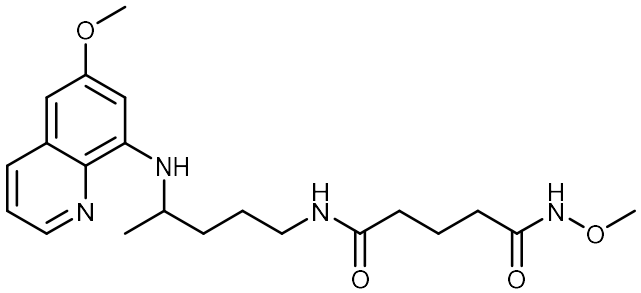

22

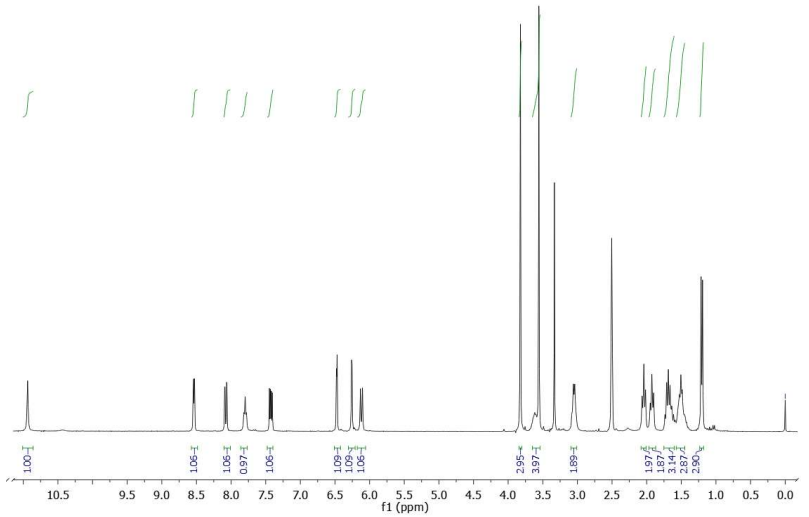
f1 (ppm)

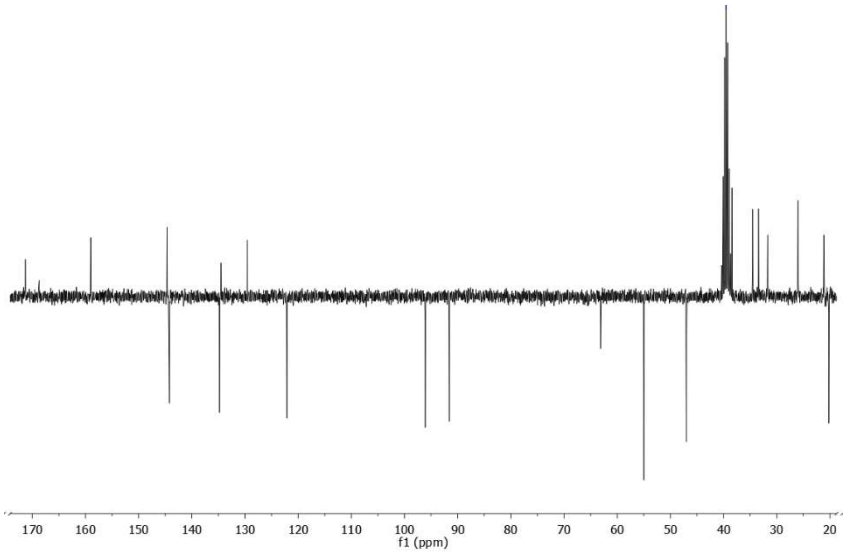
f1 (ppm)

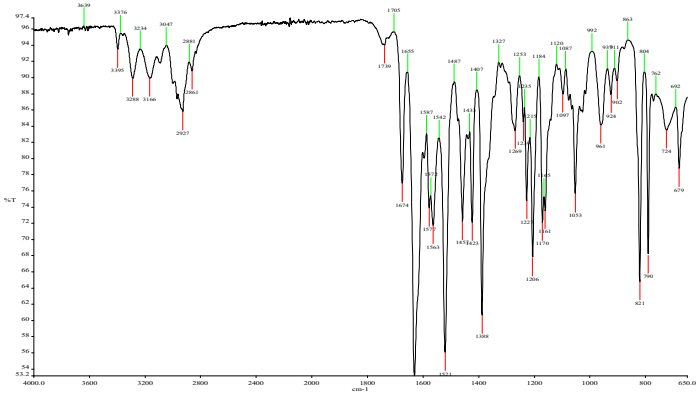

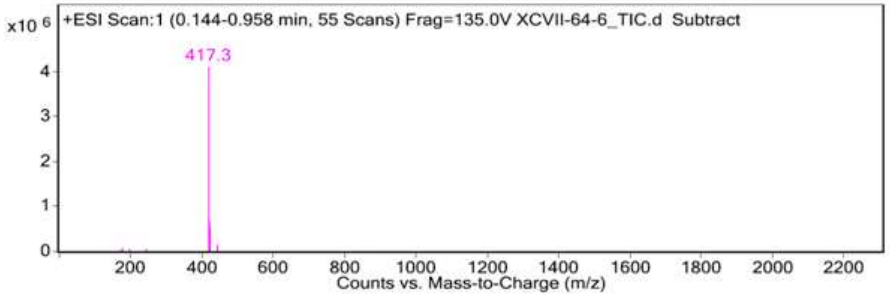
x10 6
+ESI Scan:1 (0.144-0.958 min, 55 Scans) Frag=135.0V XCVII-64-6_TIC.d Subtract
417.3
Counts vs. Mass-to-Charge (m/z)

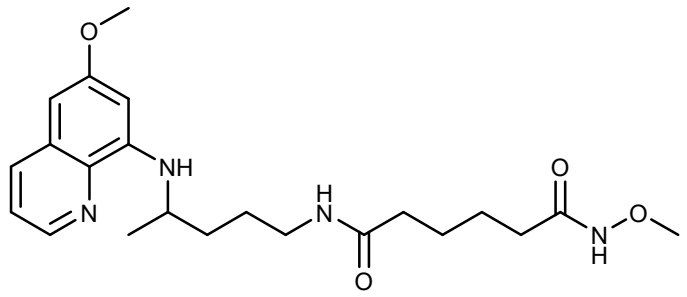
O
NH
N
H
N
O
O
N
H
O

23

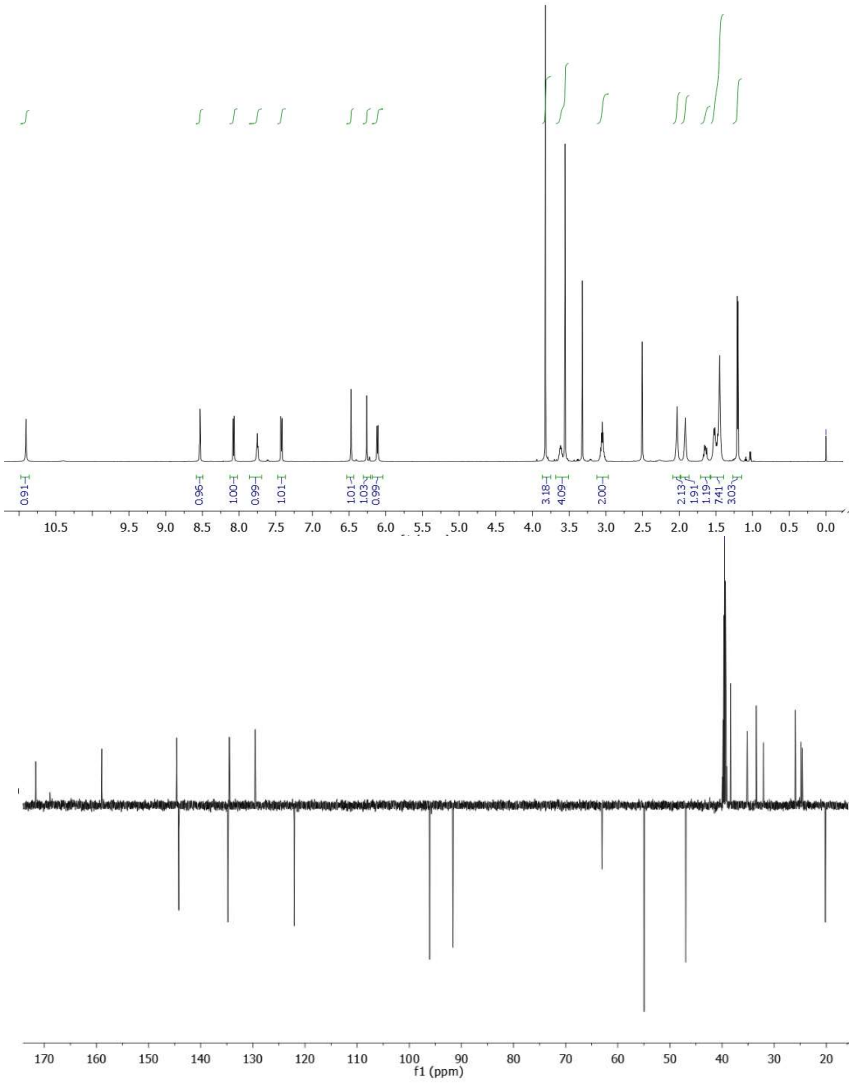
f1 (ppm)

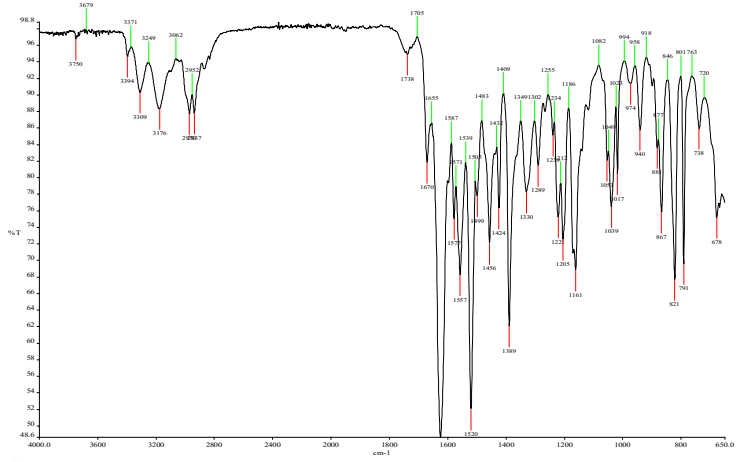

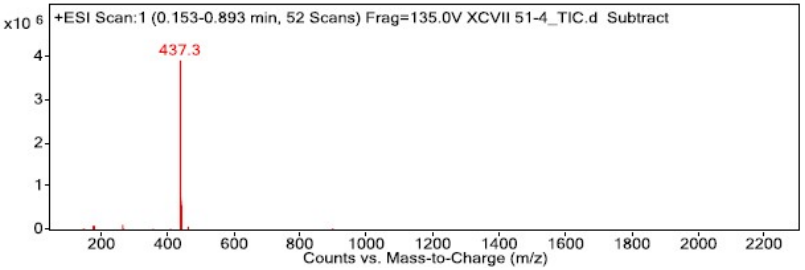
+ESI Scan:1 (0.153-0.893 min, 52 Scans) Frag=135.0V XCVII 51-4_TIC.d Subtract
x10 6
437.3
Counts vs. Mass-to-Charge (m/z)

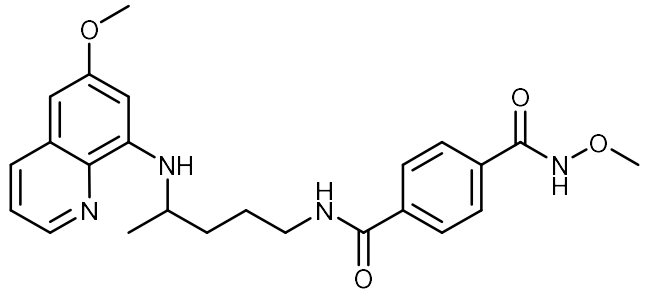
O
NH
N
H
N
O
O
N
H
O

24

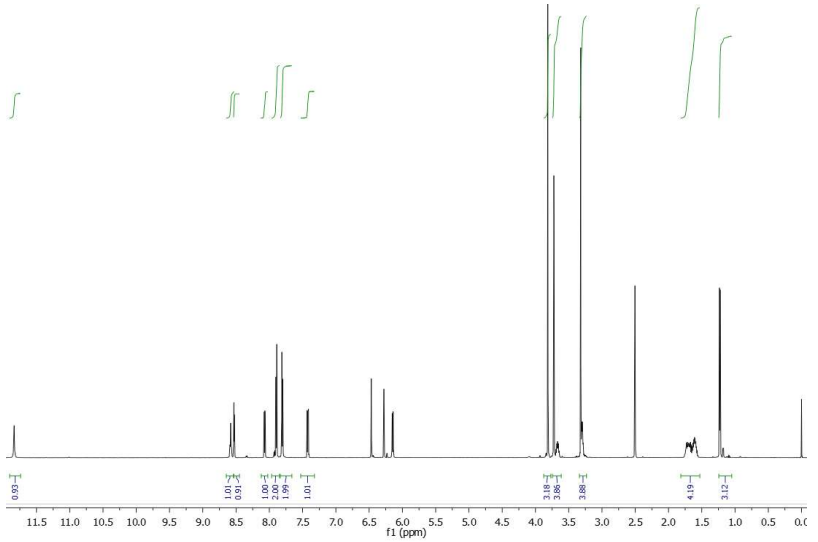
f1 (ppm)

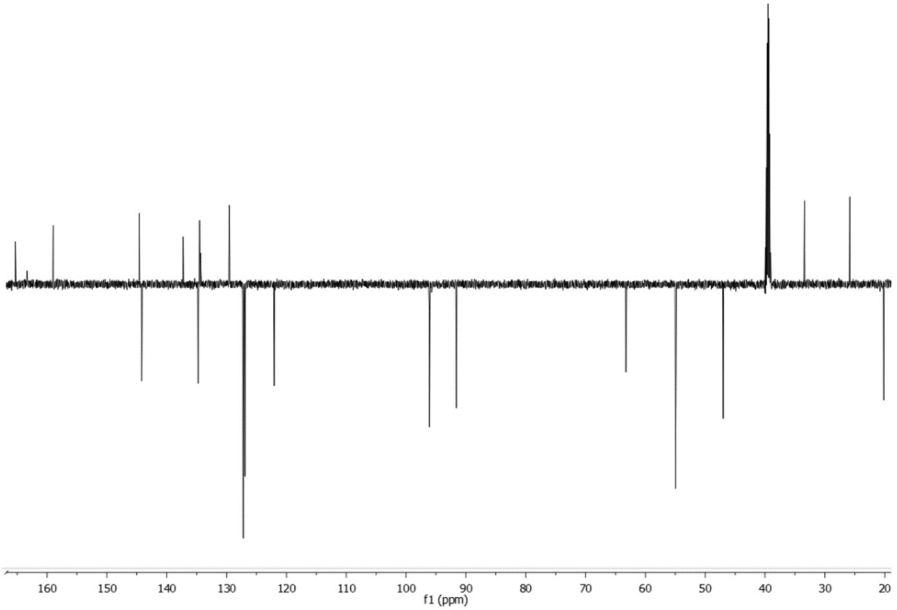
f1 (ppm)

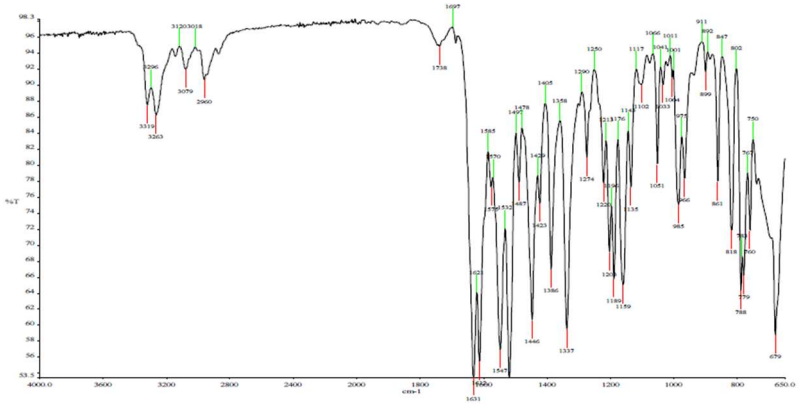

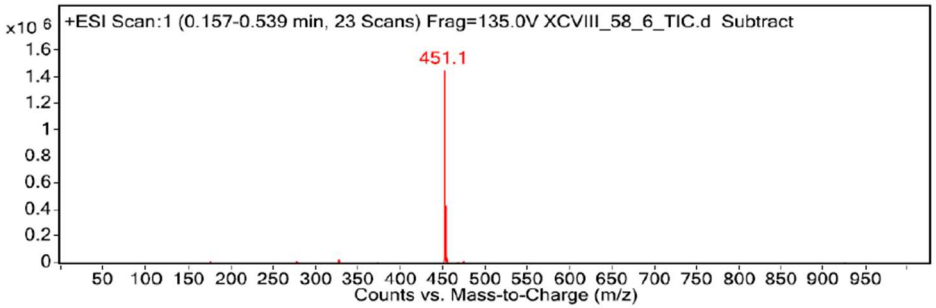
+ESI Scan:1 (0.157-0.539 min, 23 Scans) Frag=135.0V XCVIII_58_6_TIC.d Subtract
x10 6
451.1
Counts vs. Mass-to-Charge (m/z)

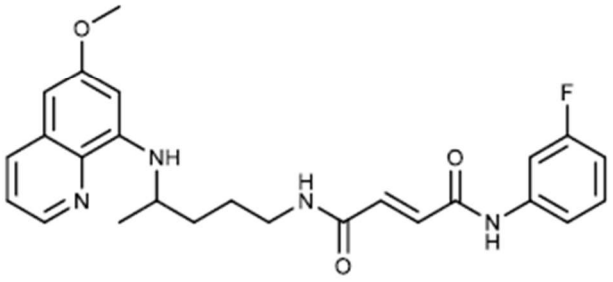
O
NH
N
H
N
O
O
N
H
F

25

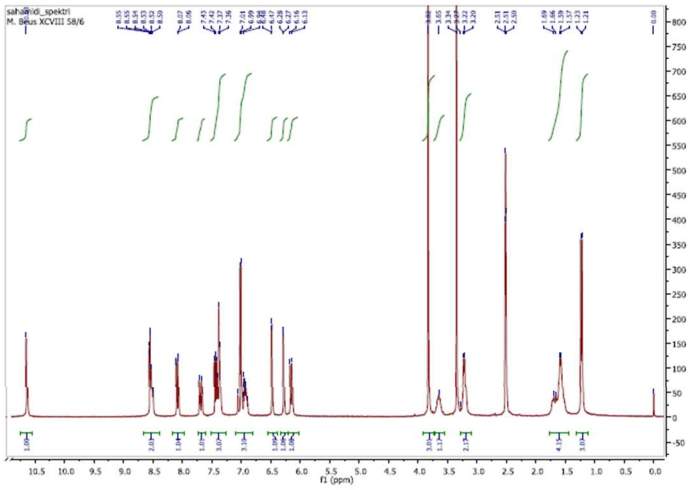

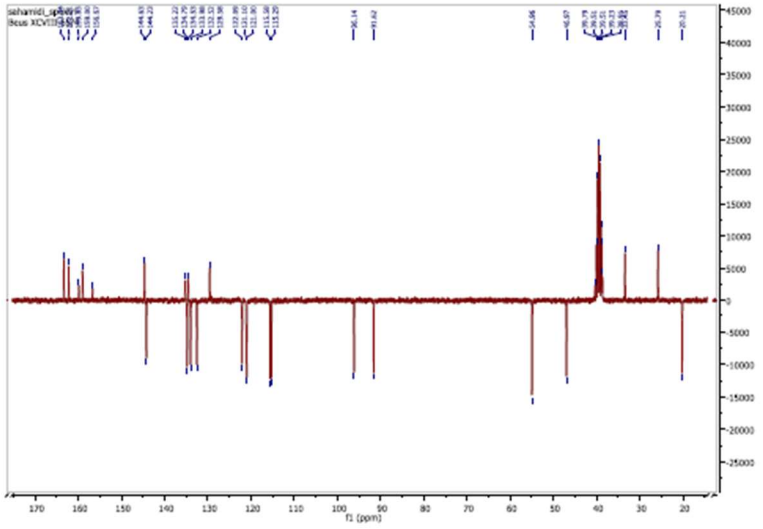

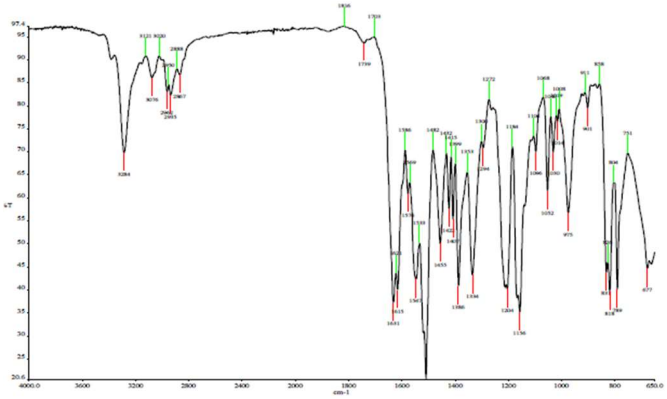

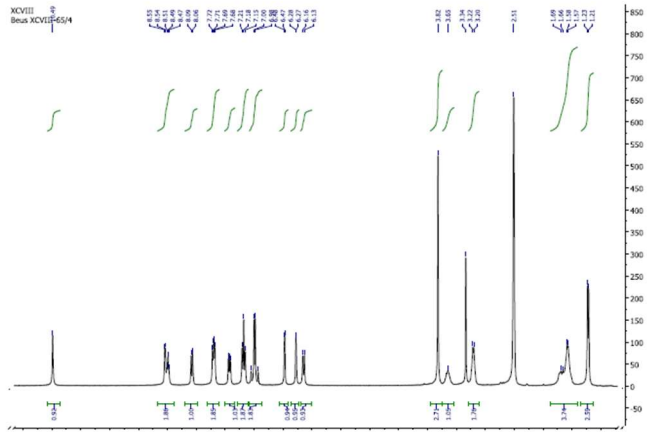

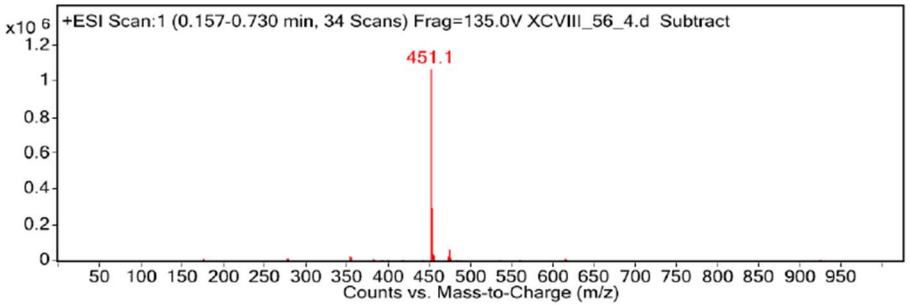
+ESI Scan:1 (0.157-0.730 min, 34 Scans) Frag=135.0V XCVIII_56_4.d Subtract
x10 6
451.1
Counts vs. Mass-to-Charge (m/z)

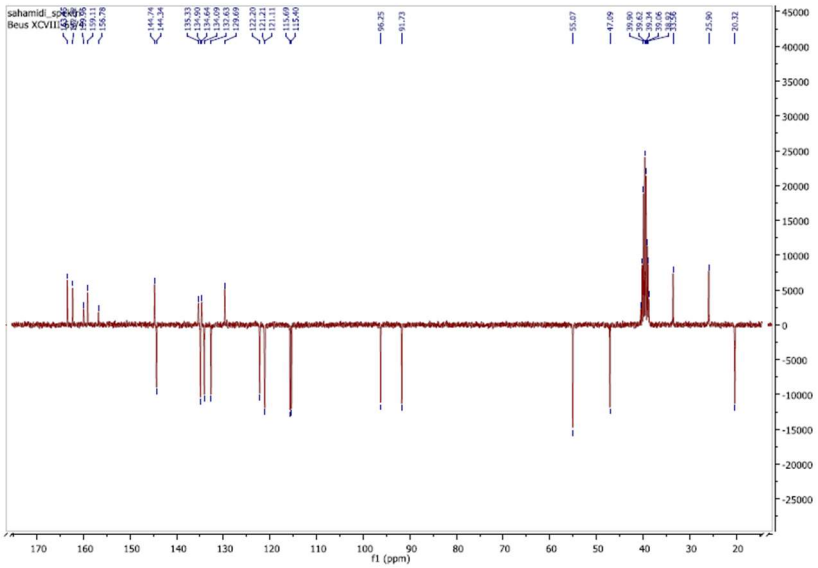

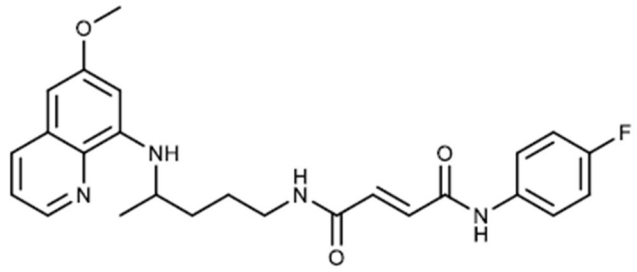
O
NH
N
H
N
O
O
N
H
F

26

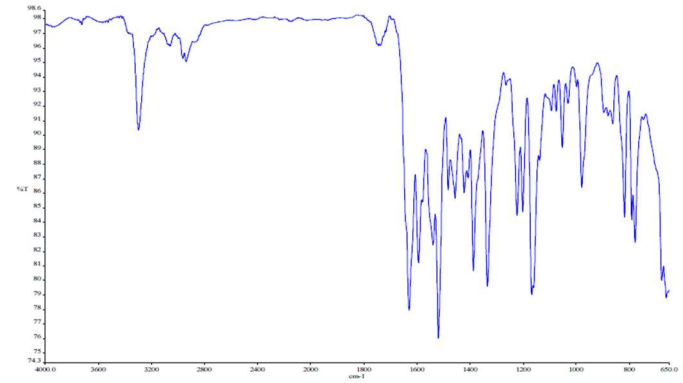

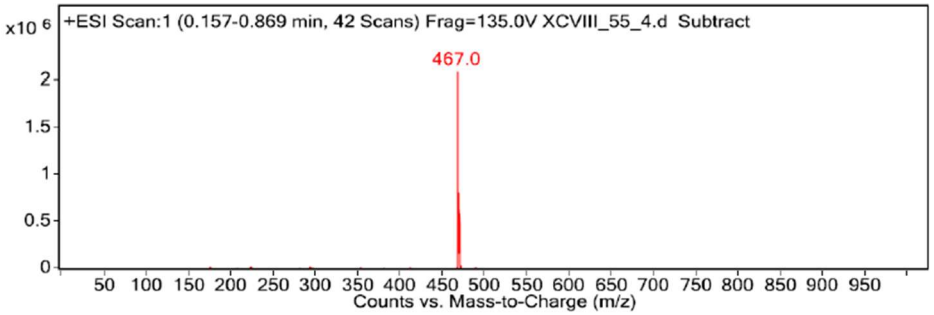
x10 6
+ESI Scan:1 (0.157-0.869 min, 42 Scans) Frag=135.0V XCVIII_55_4.d Subtract
467.0
Counts vs. Mass-to-Charge (m/z)

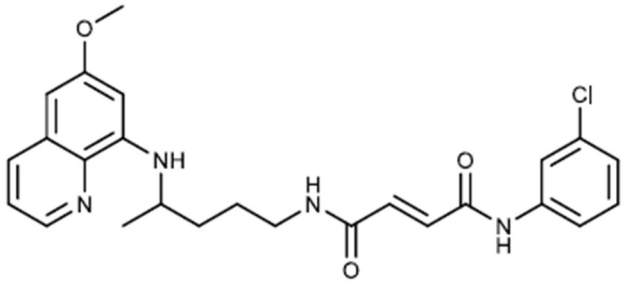
O
NH
N
H
N
O
O
N
H
Cl

27

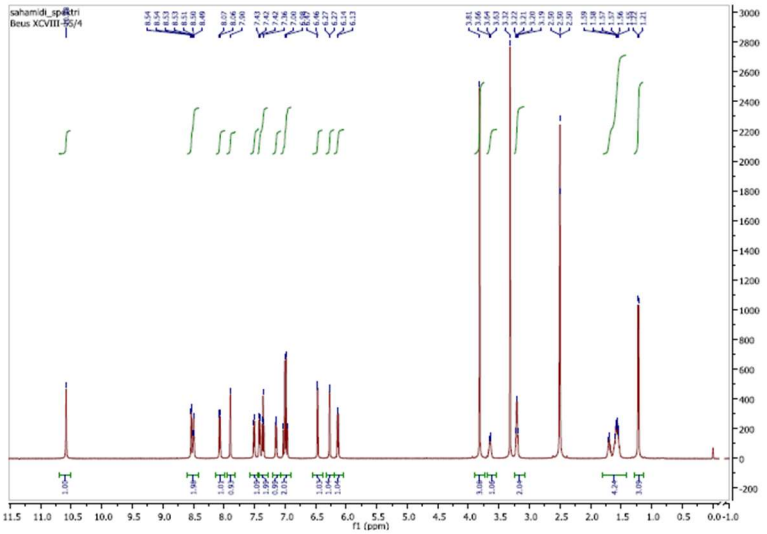

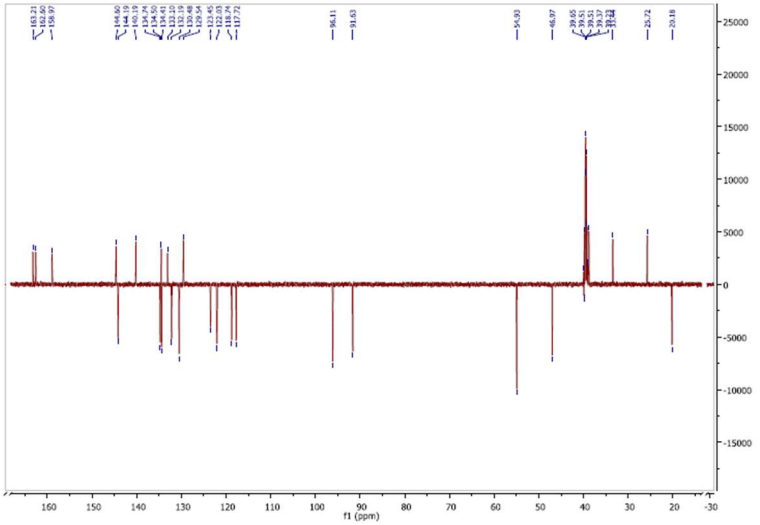

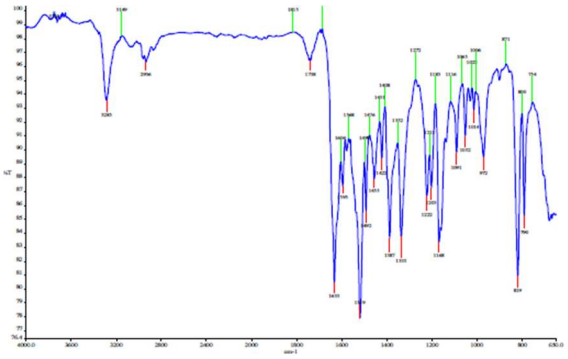

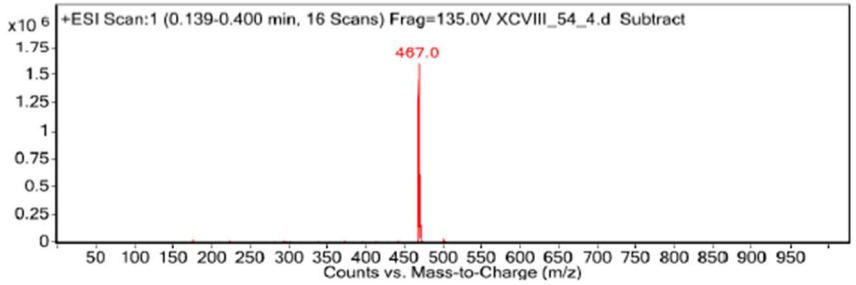
+ESI Scan:1 (0.139-0.400 min, 16 Scans) Frag=135.0V XCVIII_54_4.d Subtract
x10 6
467.0
Counts vs. Mass-to-Charge (m/z)

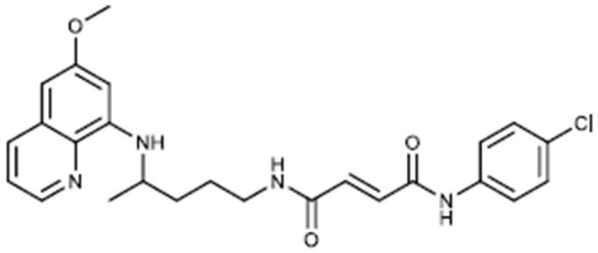
O
NH
N
H
N
O
O
N
H
Cl

28

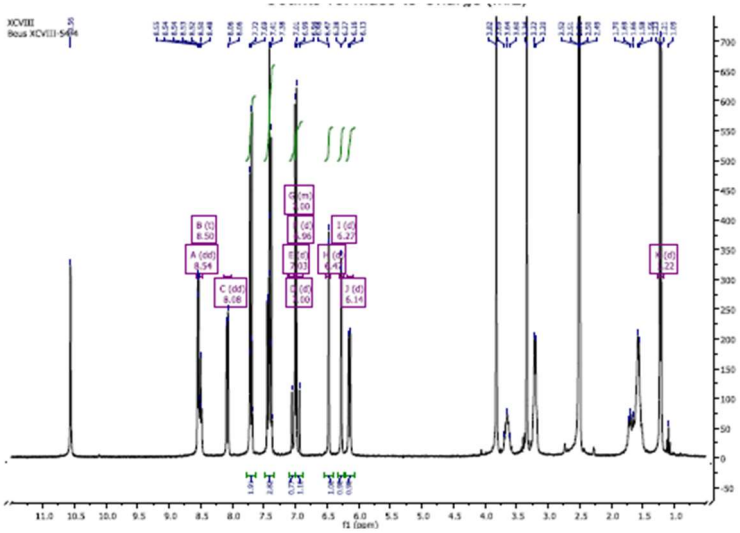

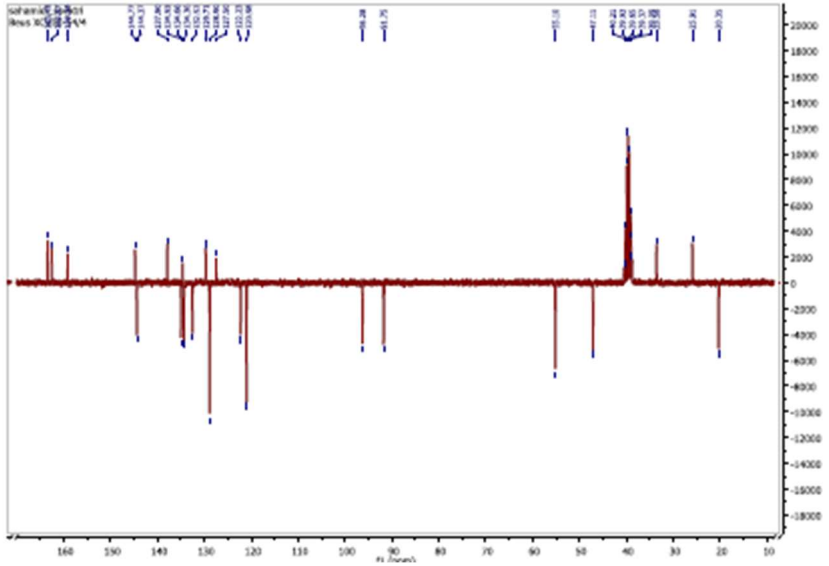

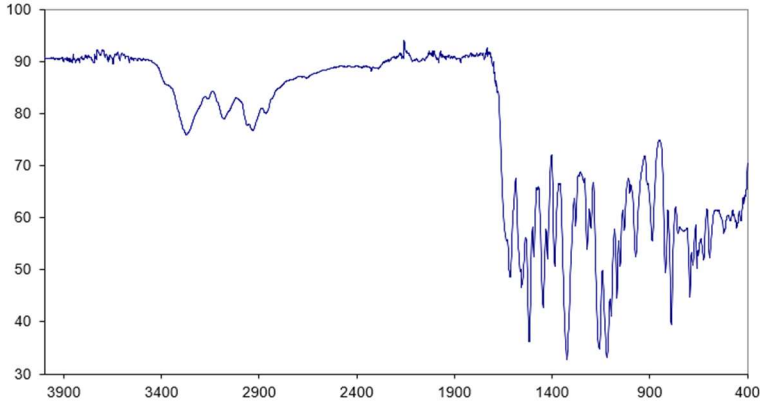
100
90
80
70
60
50
40
30
3900
3400
2900
2400
1900
1400
900
400

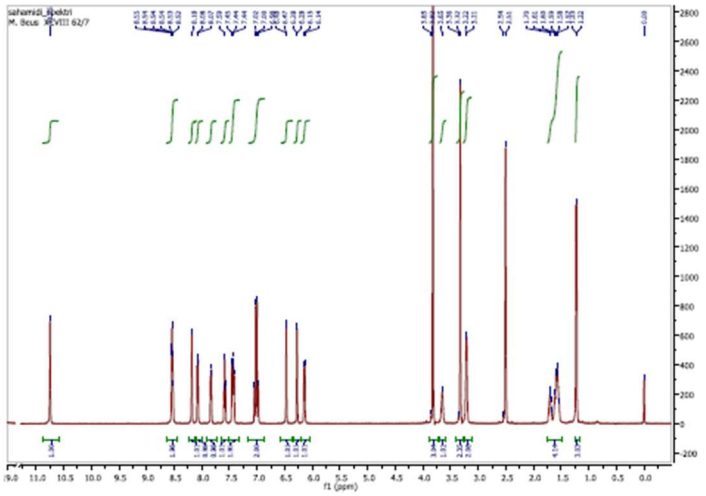

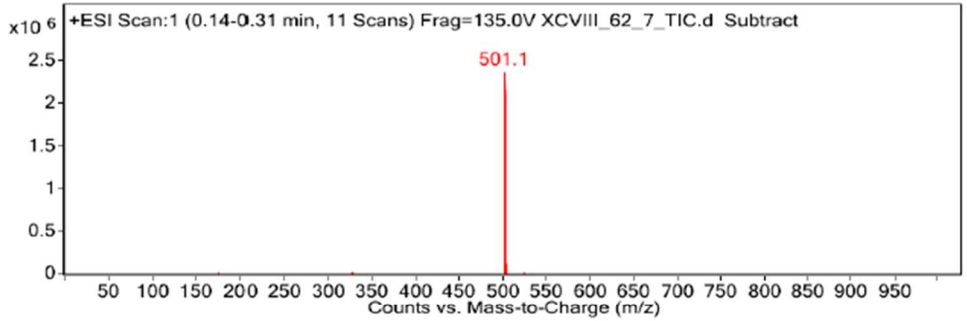
x10 6
+ESI Scan:1 (0.14-0.31 min, 11 Scans) Frag=135.0V XCVIII_62_7_TIC.d Subtract
501.1
2.5
2
1.5
1
0.5
0
50 100 150 200 250 300 350 400 450 500 550 600 650 700 750 800 850 900 950
Counts vs. Mass-to-Charge (m/z)

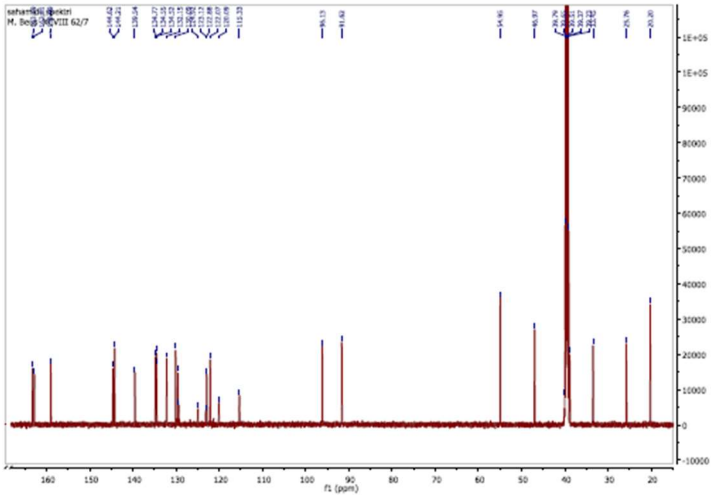

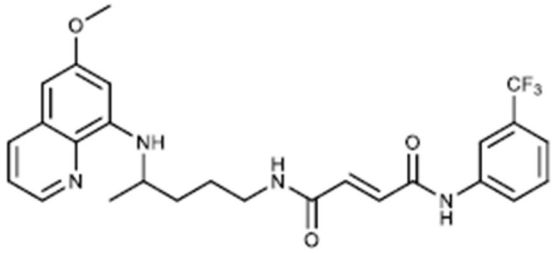
O
NH
N
H
N
O
O
N
H
CF3

29

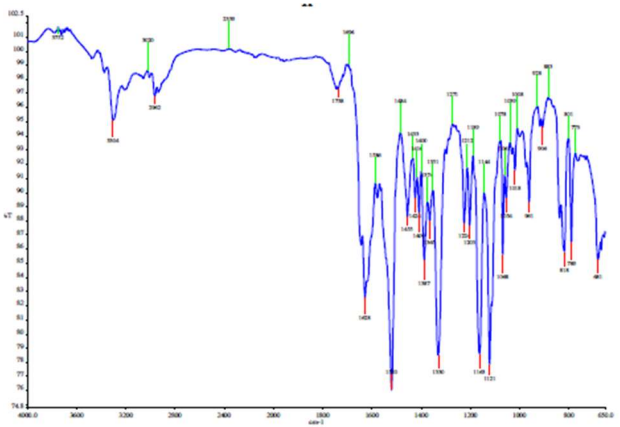

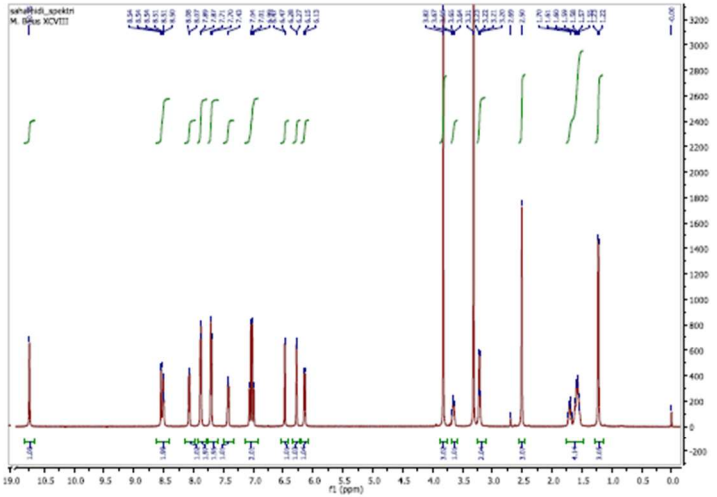

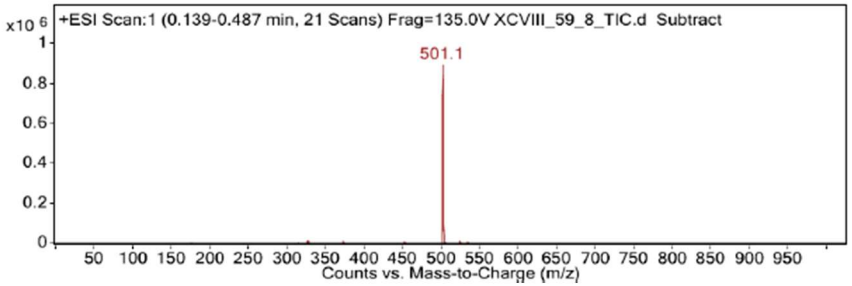
x10 6
+ESI Scan:1 (0.139-0.487 min, 21 Scans) Frag=135.0V XCVIII_59_8_TIC.d Subtract
501.1
Counts vs. Mass-to-Charge (m/z)

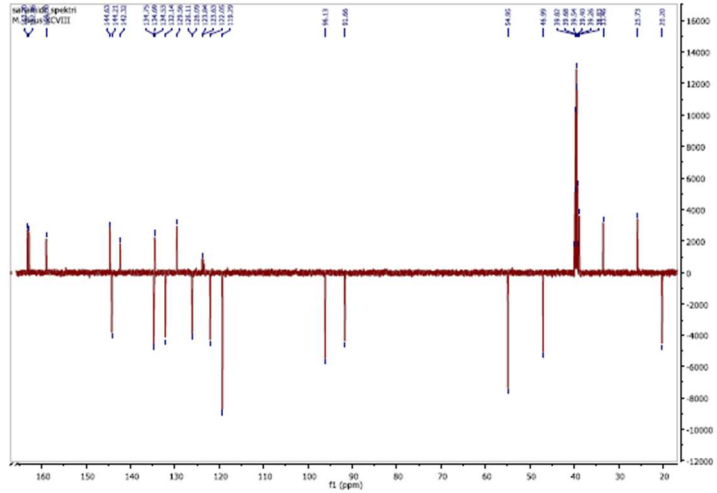

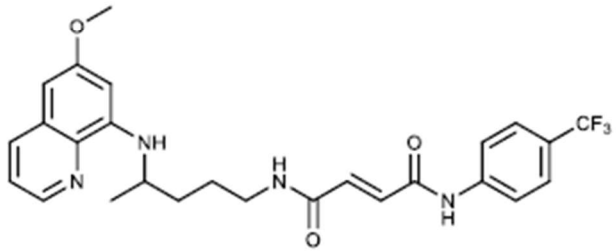
O
NH
N
H
N
O
O
N
H
CF3

30

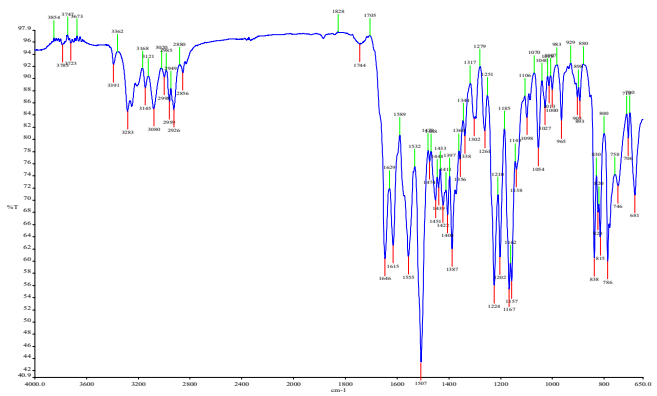

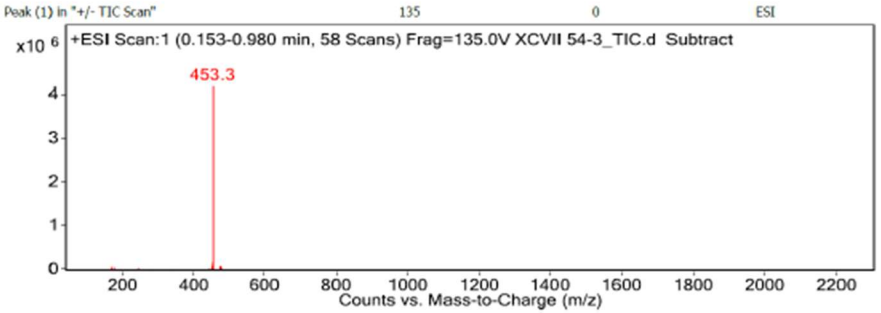
Peak (1) in "+/- TIC Scan" 135 0 ESI
+ESI Scan:1 (0.153-0.980 min, 58 Scans) Frag=135.0V XCVII 54-3_TIC.d Subtract
x10 6
453.3
Counts vs. Mass-to-Charge (m/z)

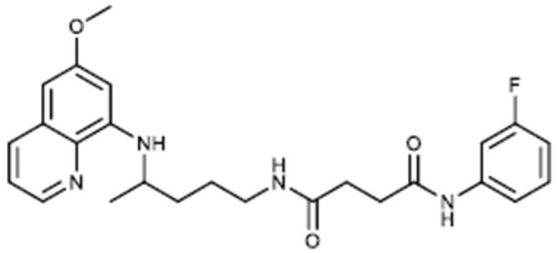
O
NH
N
H
N
O
O
N
H
F

31

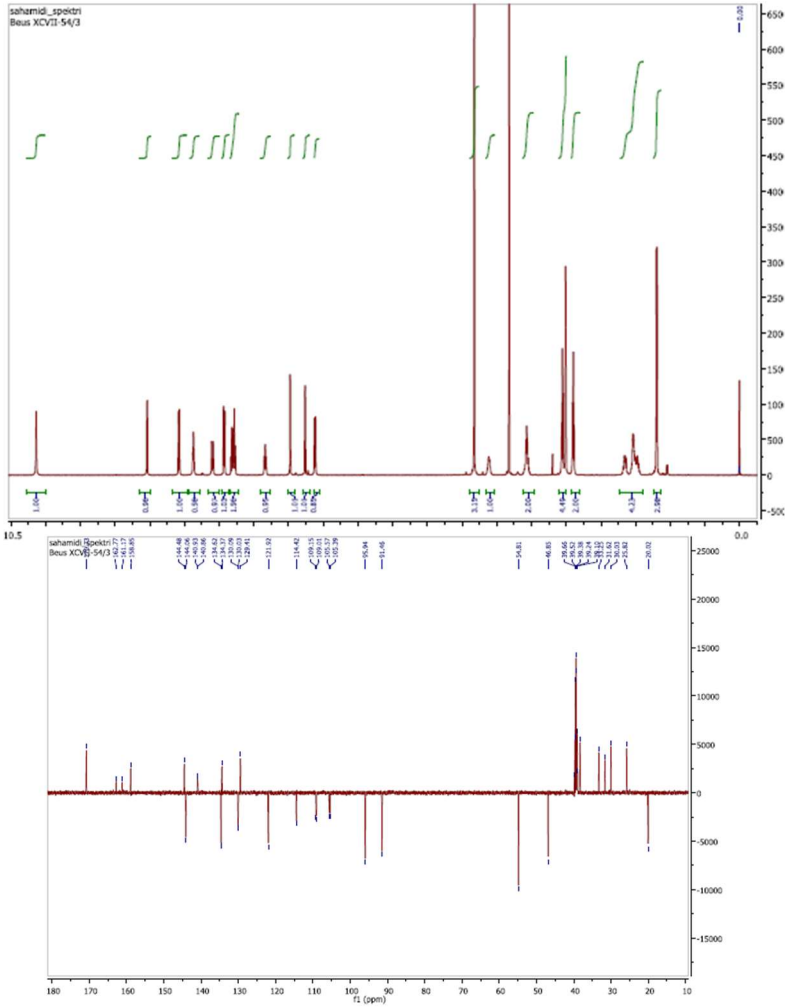
sahamidi_spektri
Beus XCVII-54/3
f1 (ppm)

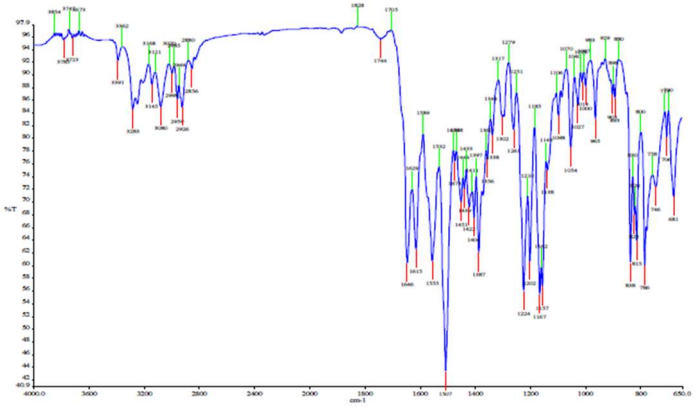

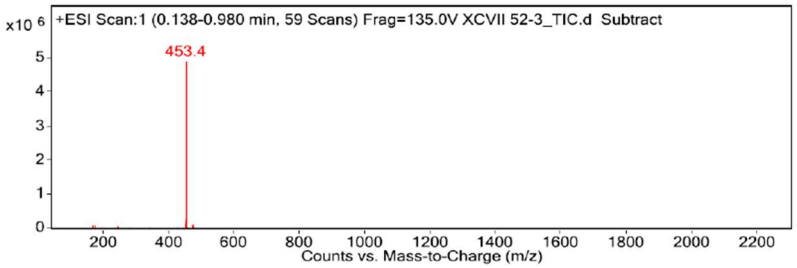
x10 6
+ESI Scan:1 (0.138-0.980 min, 59 Scans) Frag=135.0V XCVII 52-3_TIC.d Subtract
453.4
Counts vs. Mass-to-Charge (m/z)

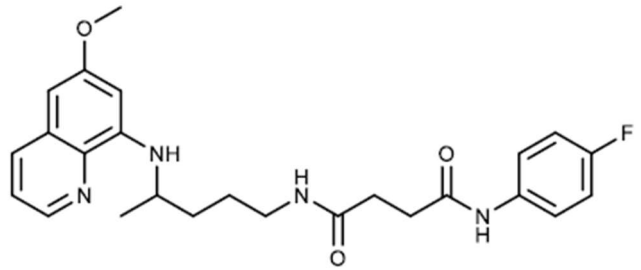
O
NH
N
H
N
O
O
N
H
F

32

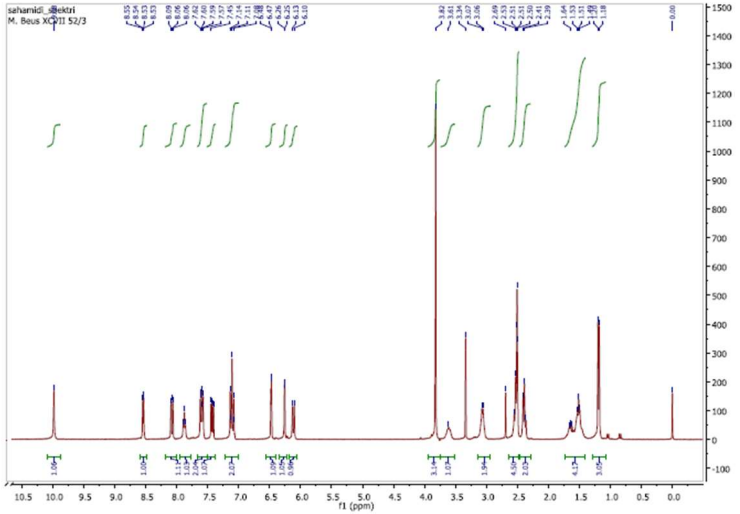
f1 (ppm)

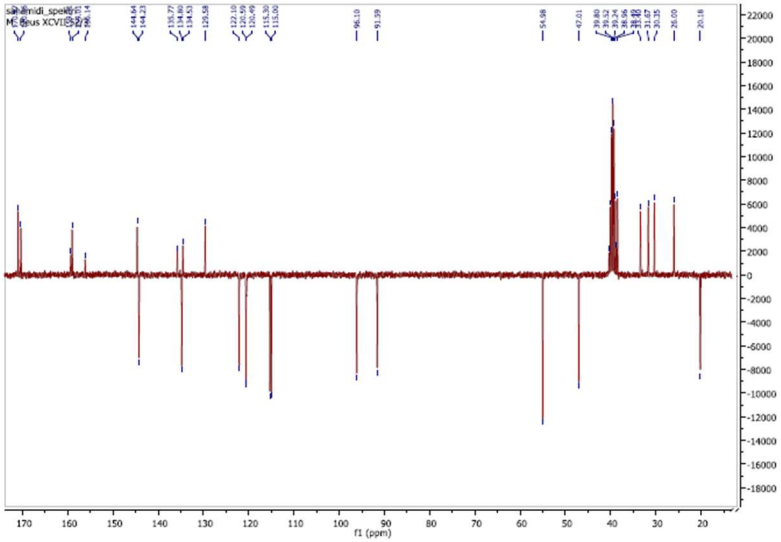
f1 (ppm)

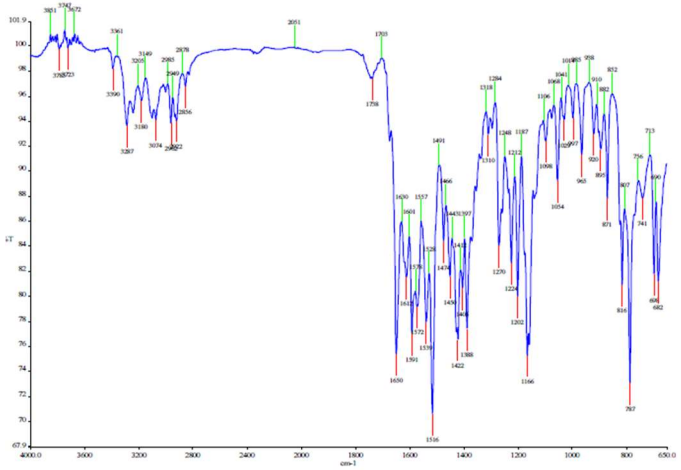

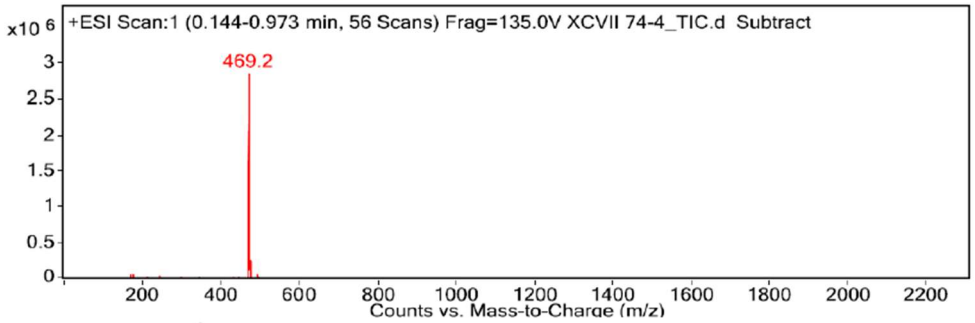
+ESI Scan:1 (0.144-0.973 min, 56 Scans) Frag=135.0V XCVII 74-4_TIC.d Subtract
x10 6
469.2
Counts vs. Mass-to-Charge (m/z)

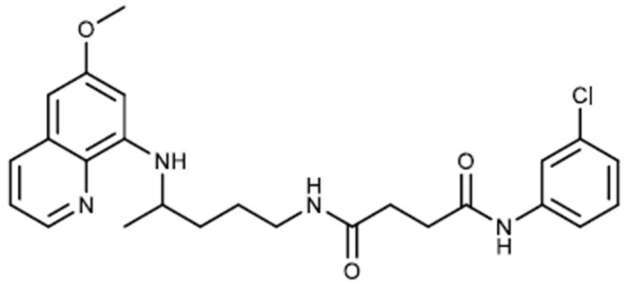
O
NH
N
H
N
O
O
N
H
Cl

33

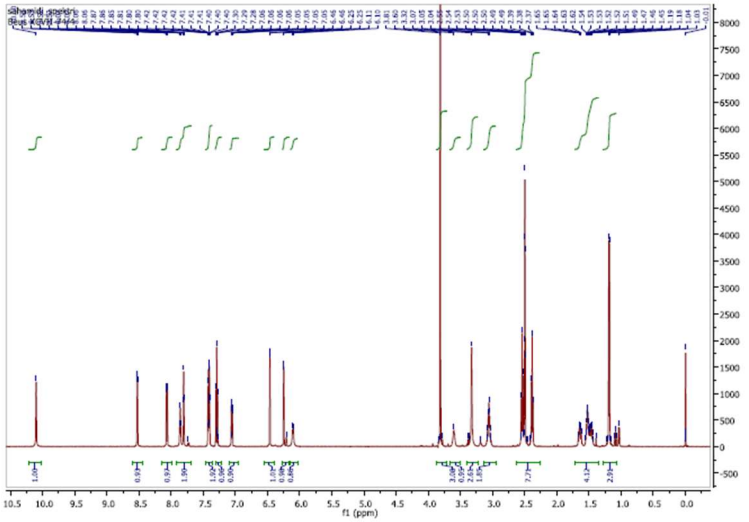

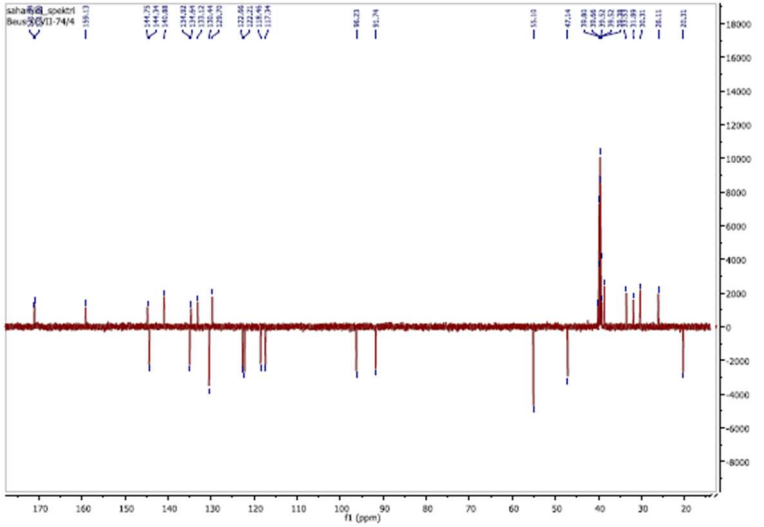

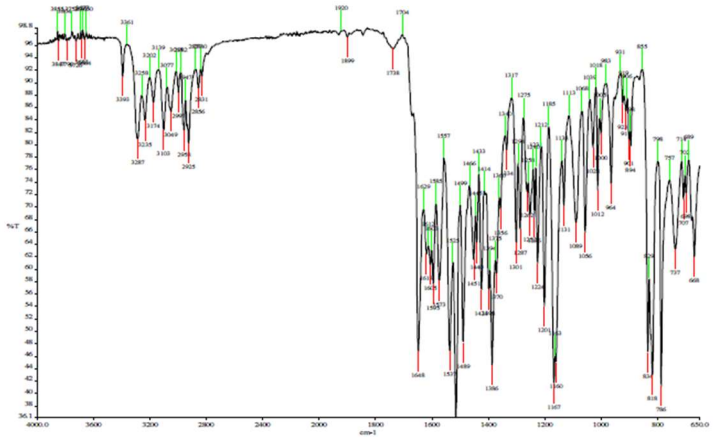

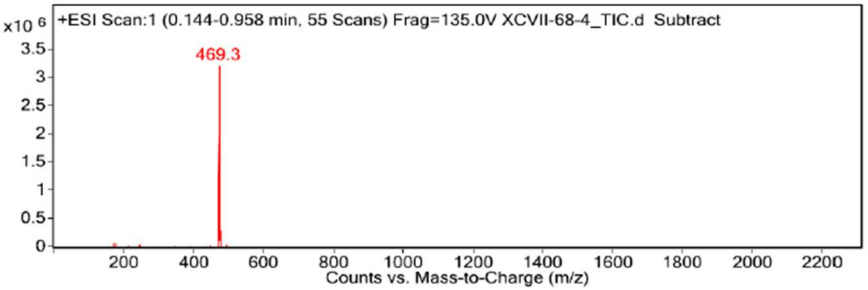
x10 6
+ESI Scan:1 (0.144-0.958 min, 55 Scans) Frag=135.0V XCVII-68-4_TIC.d Subtract
469.3
Counts vs. Mass-to-Charge (m/z)

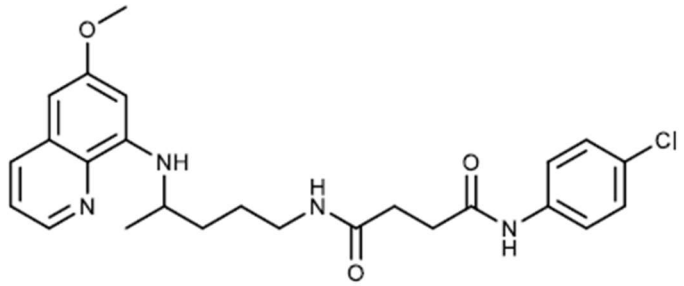
O
NH
N
H
N
O
O
N
H
Cl

34

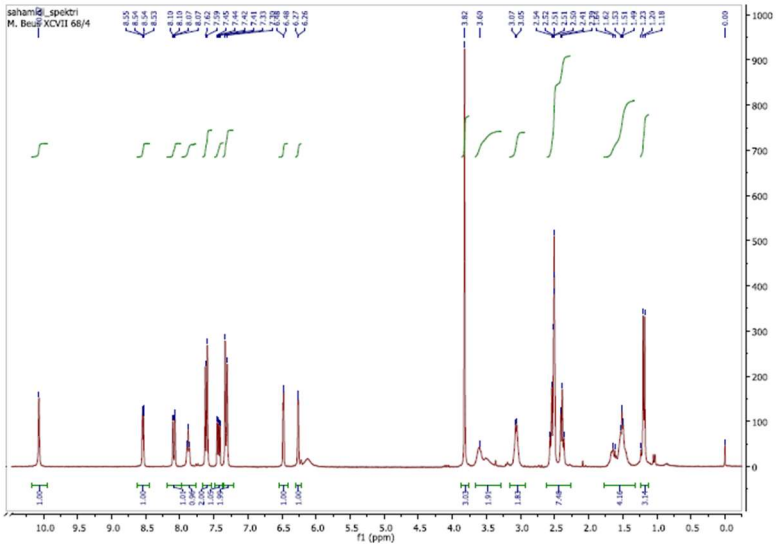
f1 (ppm)

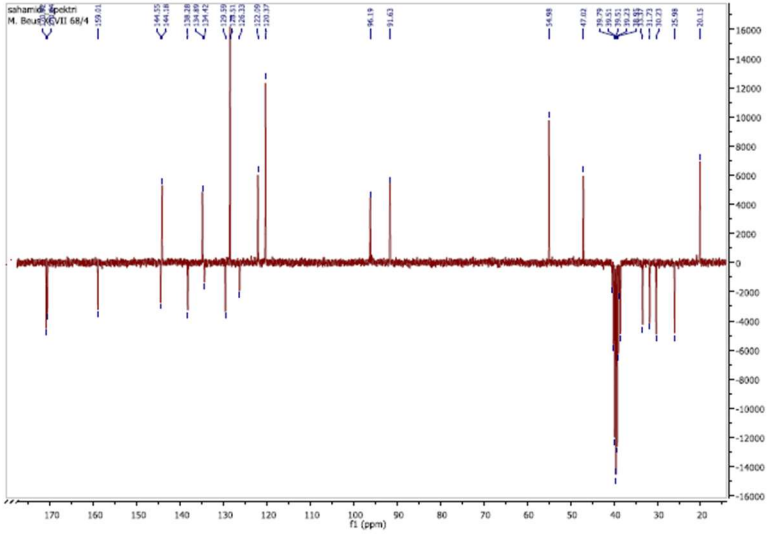
f1 (ppm)

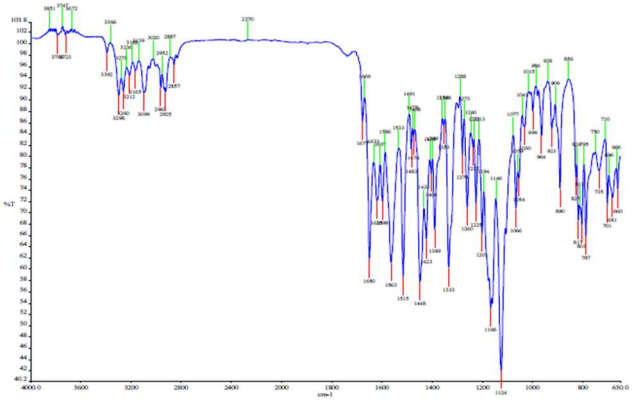

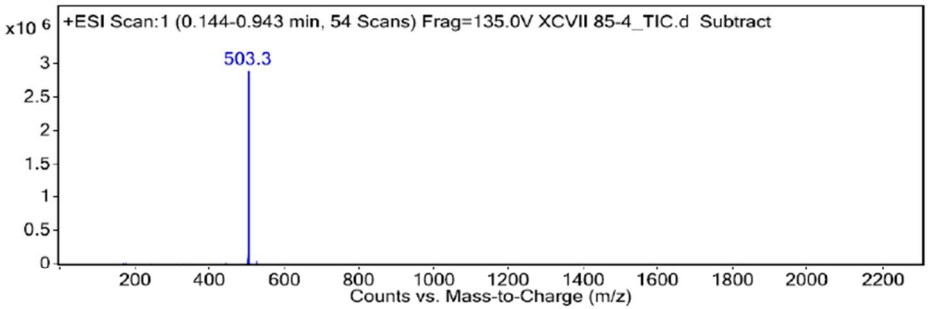
+ESI Scan:1 (0.144-0.943 min, 54 Scans) Frag=135.0V XCVII 85-4_TIC.d Subtract
x10 6
503.3
Counts vs. Mass-to-Charge (m/z)

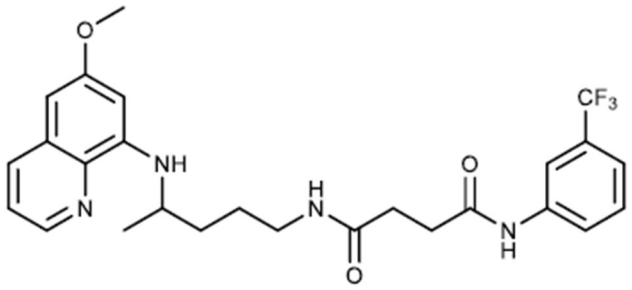
O
NH
N
H
N
O
O
N
H
CF3

35

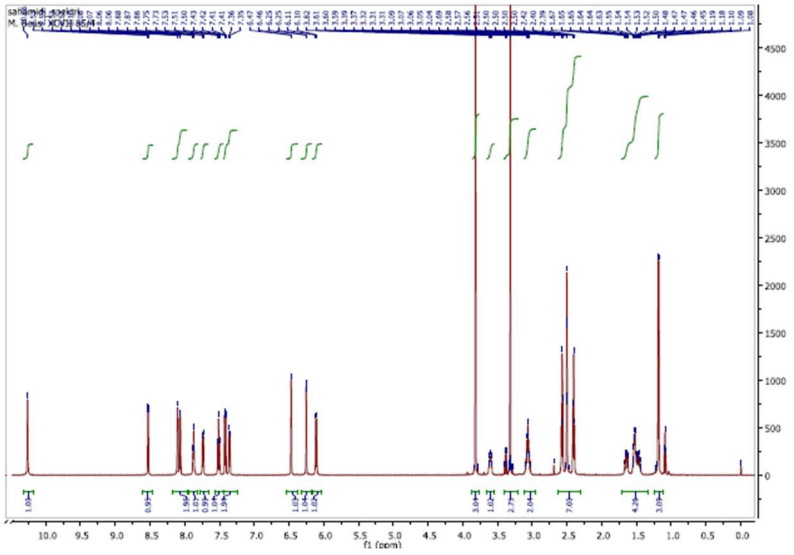

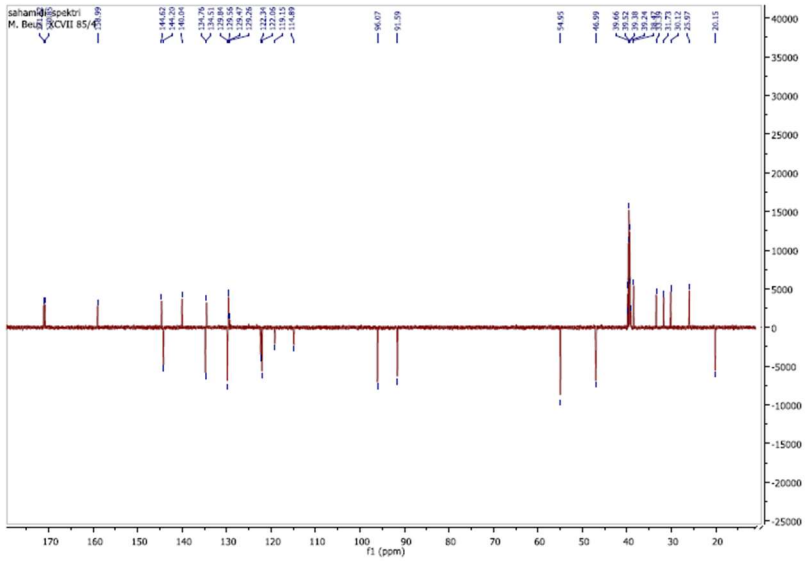

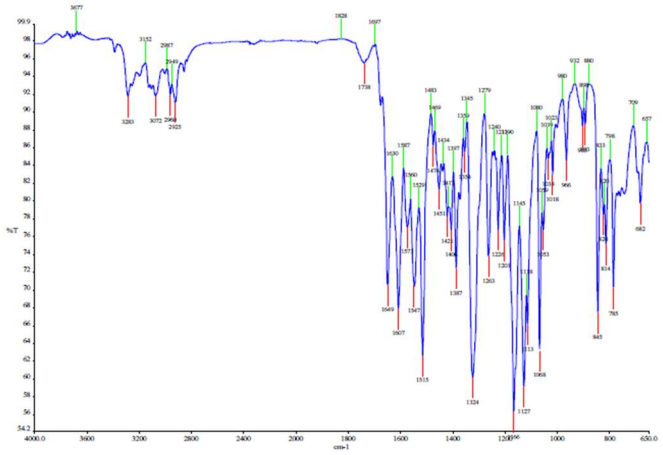

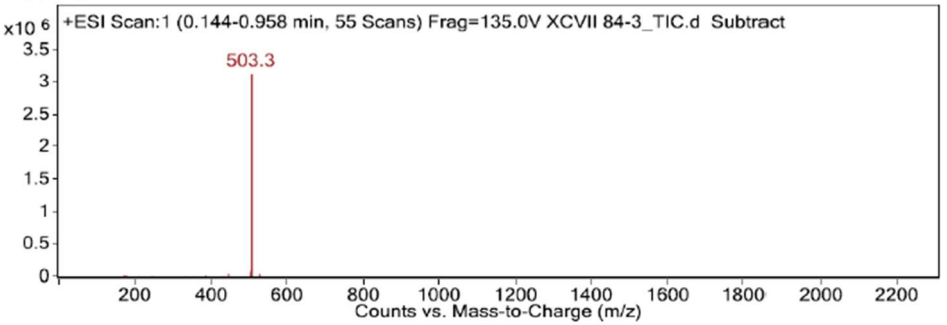
+ESI Scan:1 (0.144-0.958 min, 55 Scans) Frag=135.0V XCVII 84-3_TIC.d Subtract
x10 6
503.3
Counts vs. Mass-to-Charge (m/z)

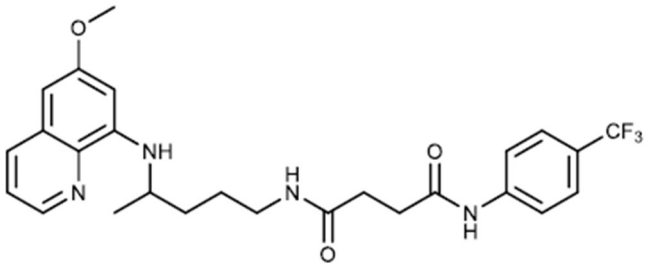
O
NH
N
H
N
O
O
N
H
CF3

36

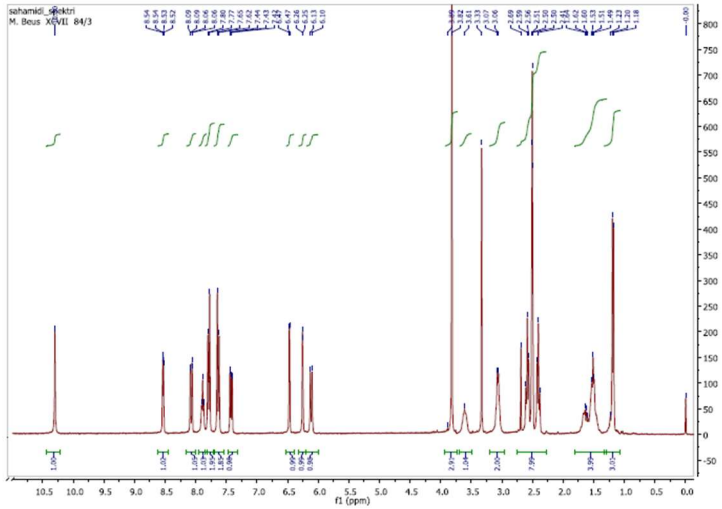

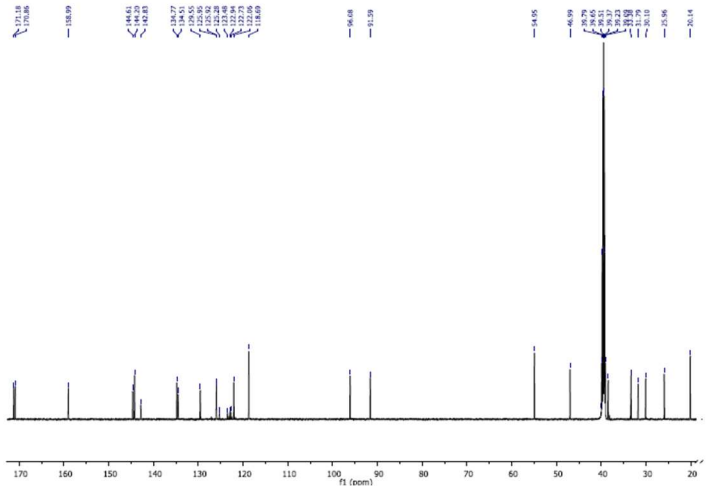

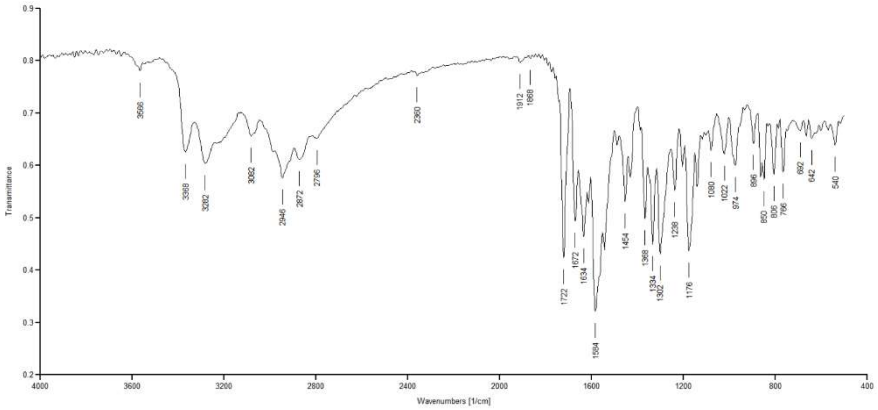
Transmittance
Wavenumbers [1/cm]
3566
3388
3262
3062
2946
2872
2796
2360
1912
1868
1722
1672
1634
1584
1454
1368
1334
1302
1256
1176
1080
1022
974
896
850
835
796
692
642
540

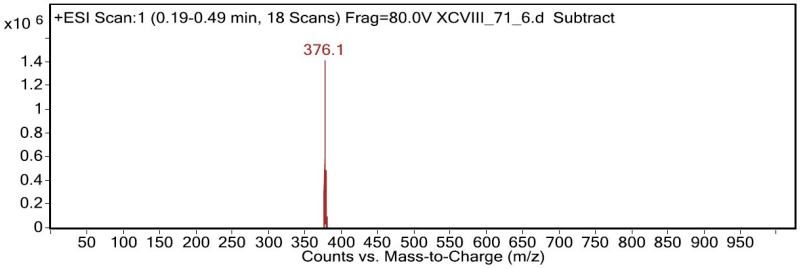
x10 6
+ESI Scan:1 (0.19-0.49 min, 18 Scans) Frag=80.0V XCVIII_71_6.d Subtract
376.1
Counts vs. Mass-to-Charge (m/z)

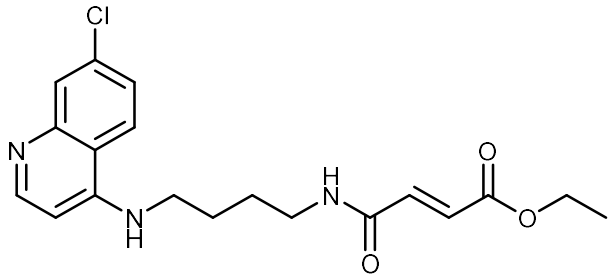
Cl
N
N
H
H
O
O
O

37

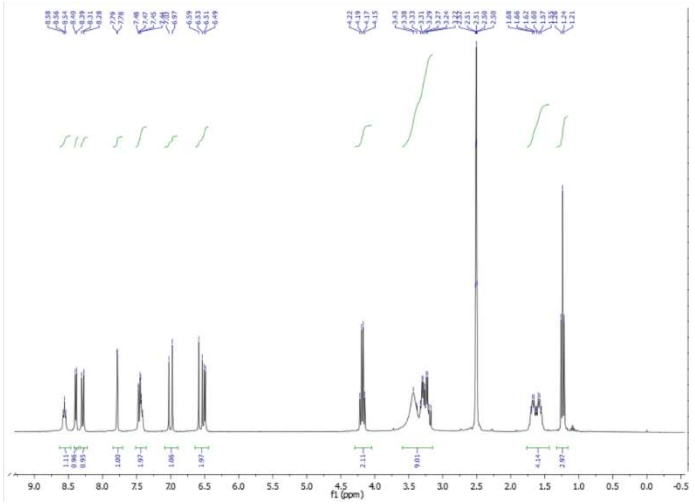
f1 (ppm)

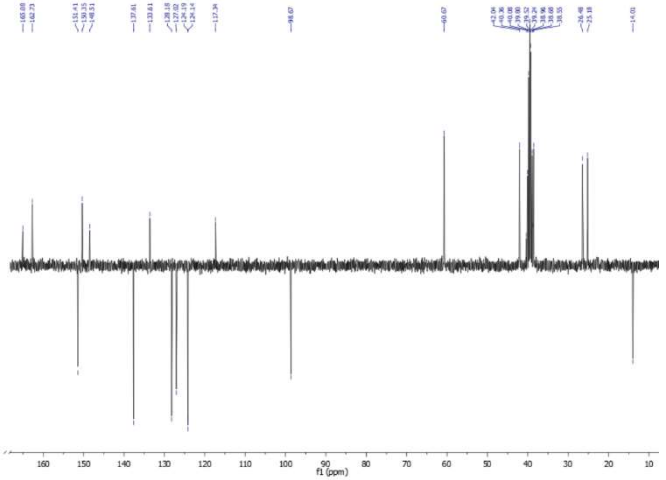
f1 (ppm)

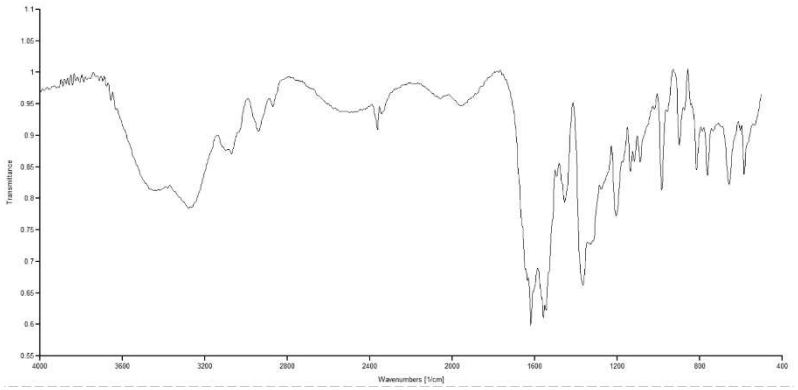
Transmittance
Wavenumbers [1/cm]

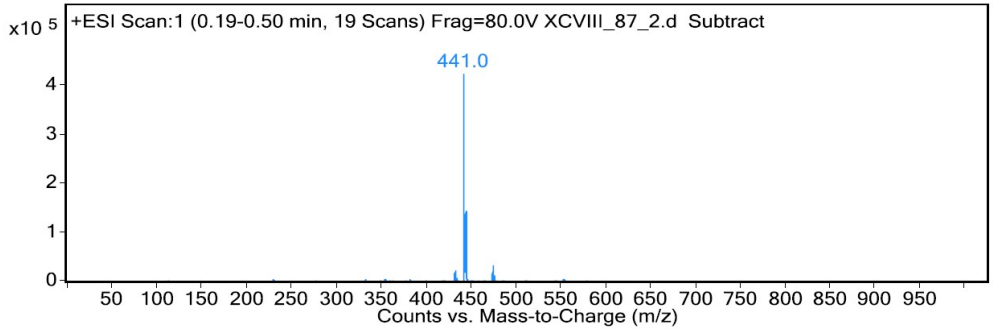
x10 5
+ESI Scan:1 (0.19-0.50 min, 19 Scans) Frag=80.0V XCVIII_87_2.d Subtract
441.0
Counts vs. Mass-to-Charge (m/z)

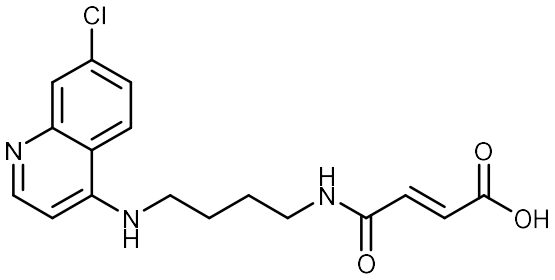
Cl
N
H
N
H
O
O
OH

38

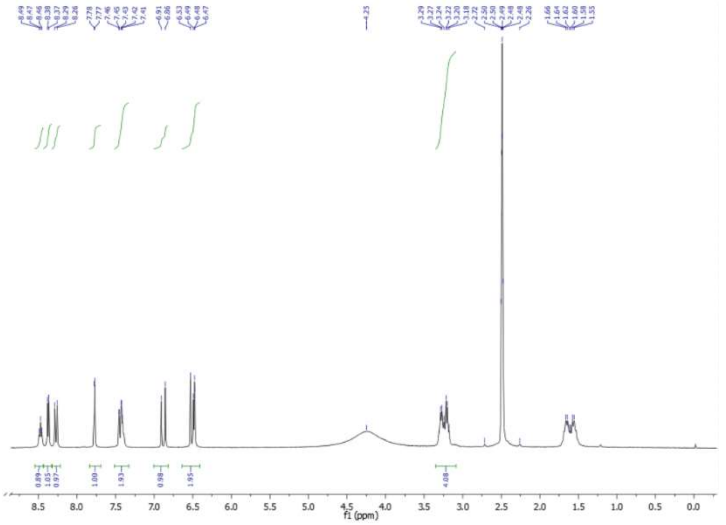
f1 (ppm)

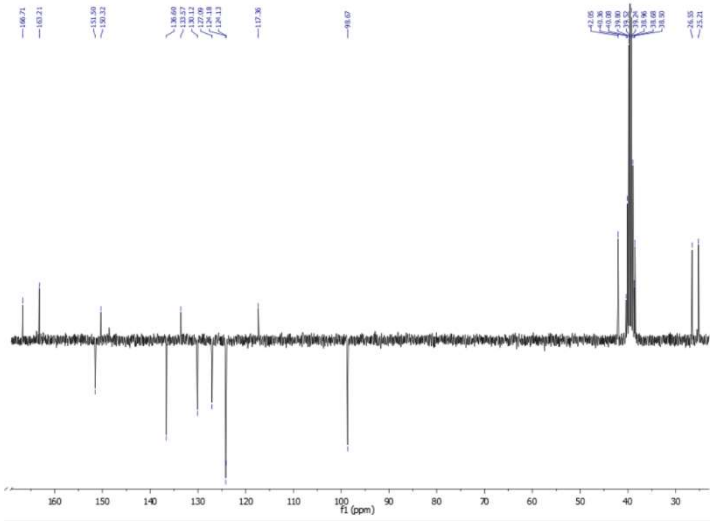
f1 (ppm)

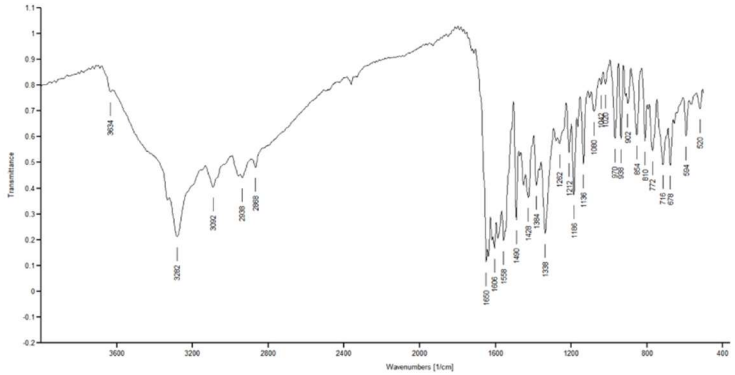

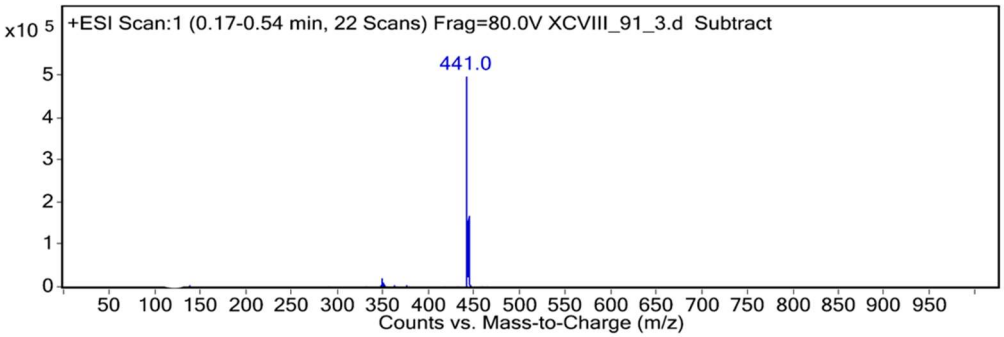
x10 5
+ESI Scan:1 (0.17-0.54 min, 22 Scans) Frag=80.0V XCVIII_91_3.d Subtract
441.0
Counts vs. Mass-to-Charge (m/z)

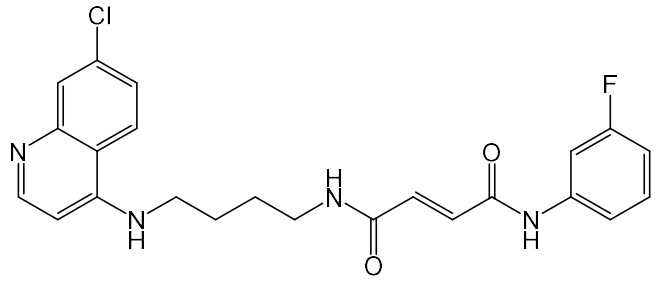
Cl
F
N
H
N
O
N
H
O

39

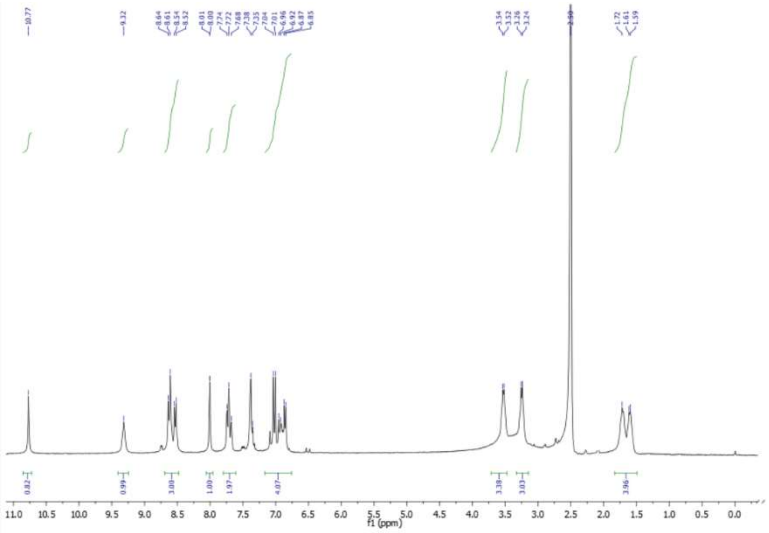

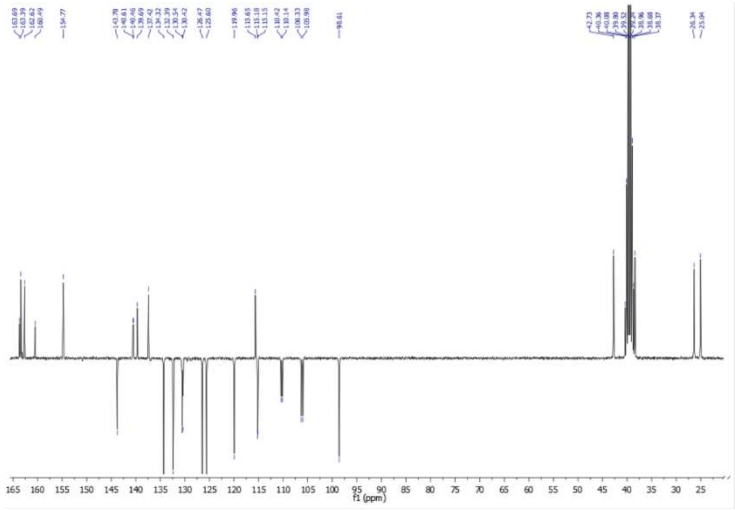

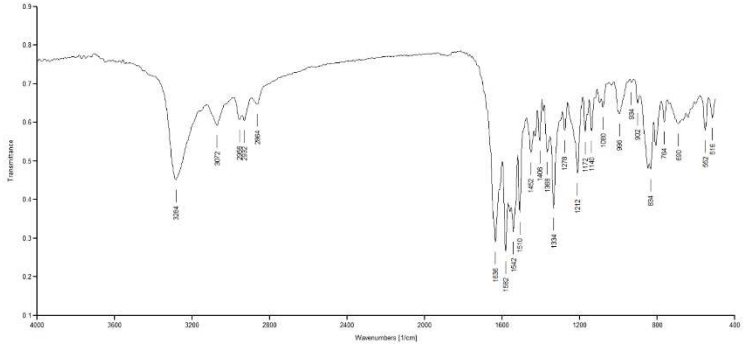

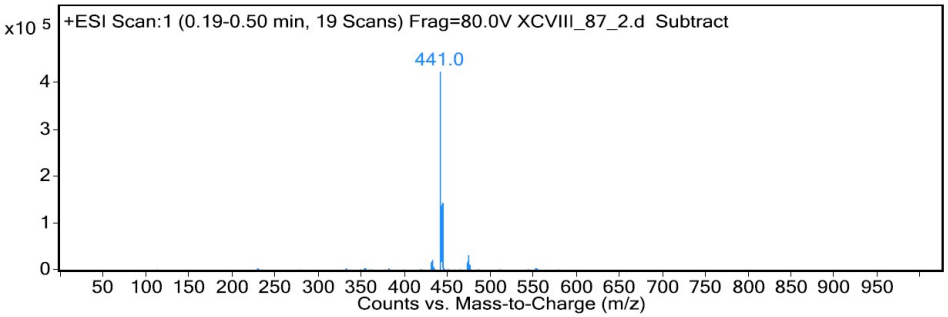
x10 5
+ESI Scan:1 (0.19-0.50 min, 19 Scans) Frag=80.0V XCVIII_87_2.d Subtract
441.0
Counts vs. Mass-to-Charge (m/z)

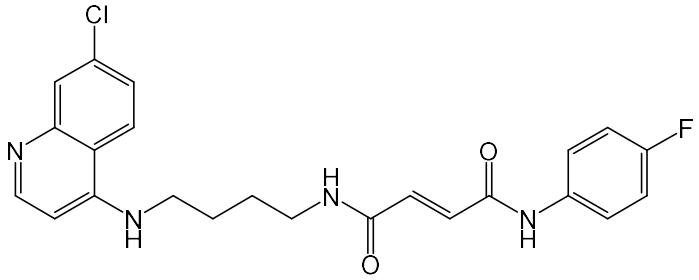
Cl
N
H
N
O
H
N
O
F

40

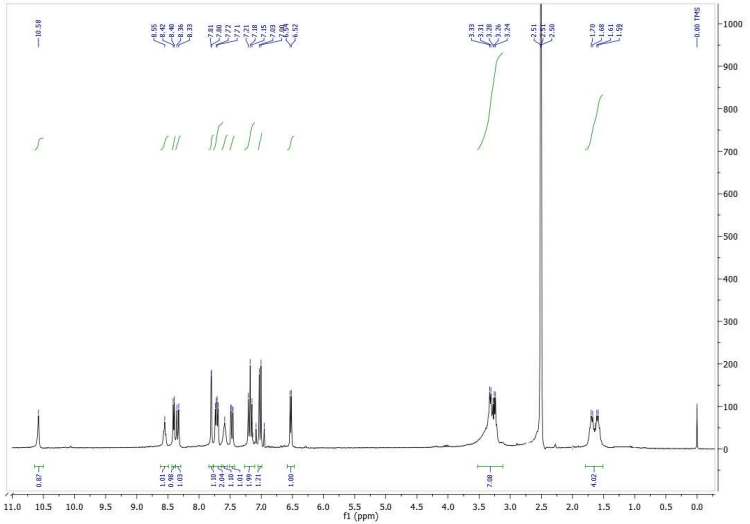
f1 (ppm)

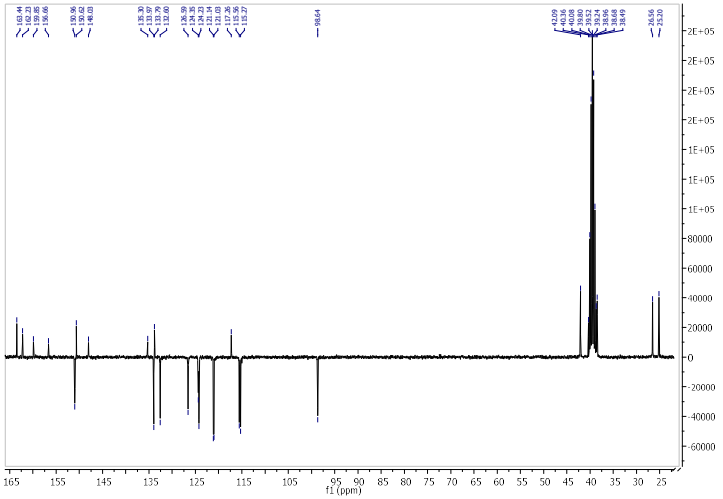
f1 (ppm)

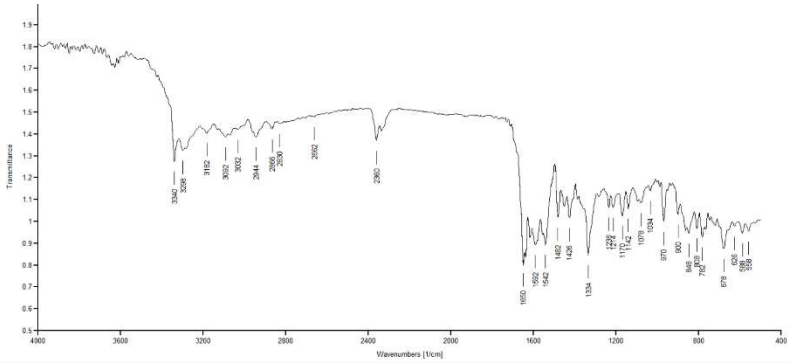

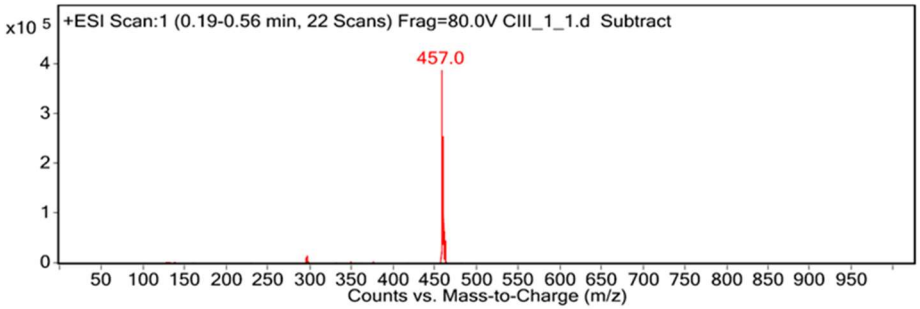
x10 5
+ESI Scan:1 (0.19-0.56 min, 22 Scans) Frag=80.0V CIII_1_1.d Subtract
457.0
Counts vs. Mass-to-Charge (m/z)

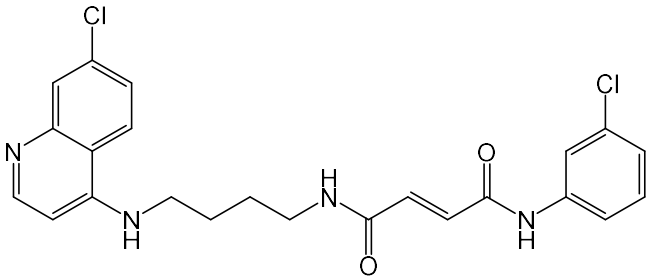
Cl
N
H
N
O
H
N
O
Cl

41

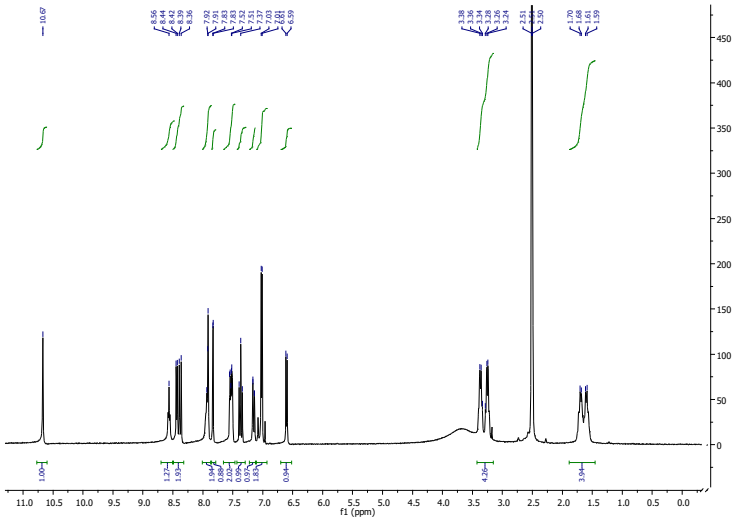
f1 (ppm)

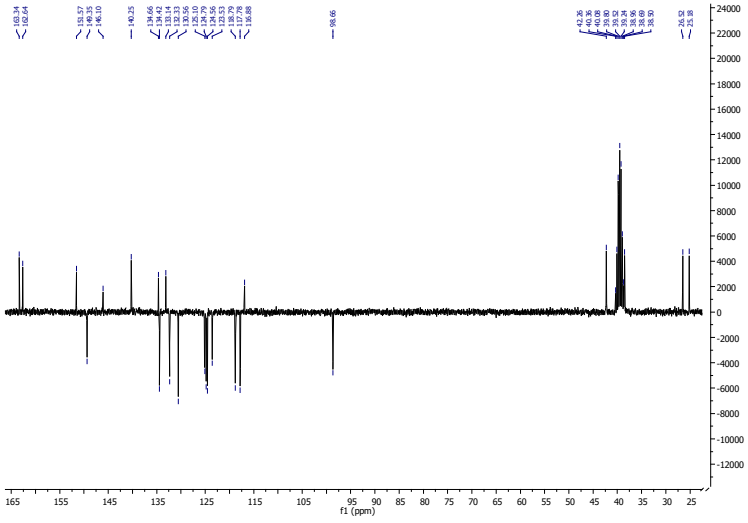
f1 (ppm)

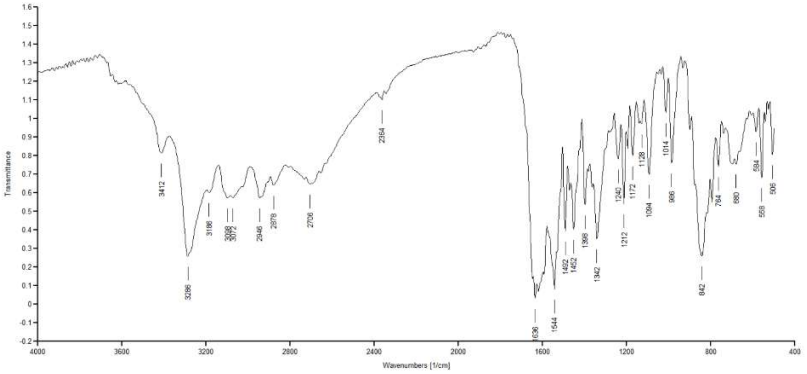
Transmittance
Wavenumbers [1/cm]
3412
3286
3186
3099
3057
2946
2879
2726
2564
1636
1544
1492
1452
1386
1342
1312
1240
1172
1138
1094
1014
966
842
784
680
634
559
505

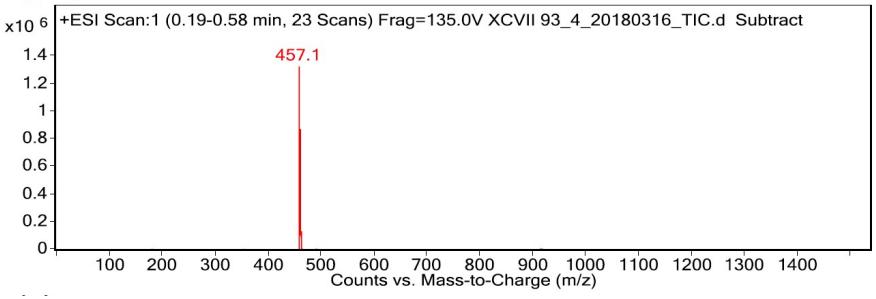
x10 6
+ESI Scan:1 (0.19-0.58 min, 23 Scans) Frag=135.0V XCVII 93_4_20180316_TIC.d Subtract
457.1
Counts vs. Mass-to-Charge (m/z)

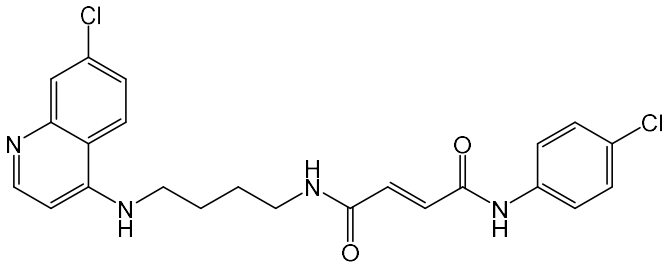
Cl
N
H
N
O
H
N
O
Cl

42

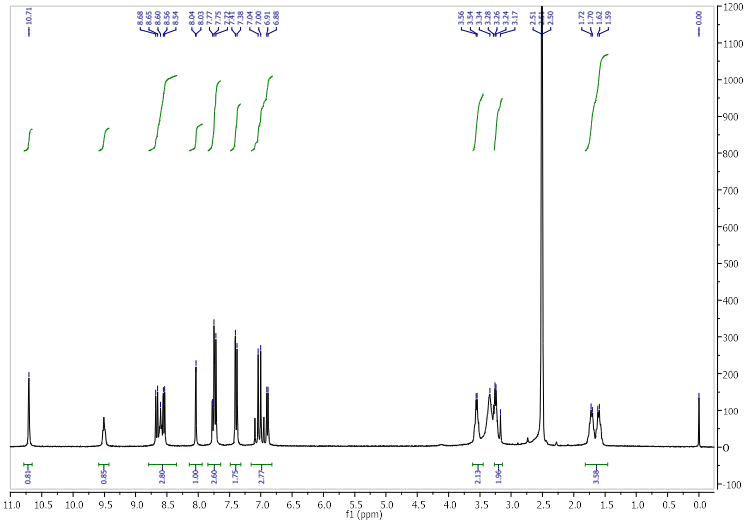
f1 (ppm)

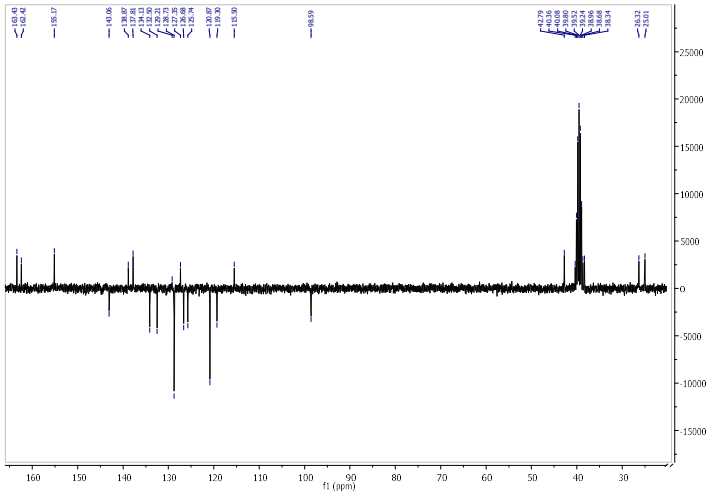
f1 (ppm)

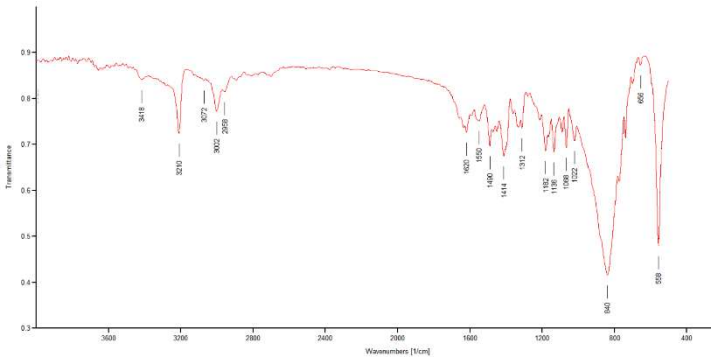

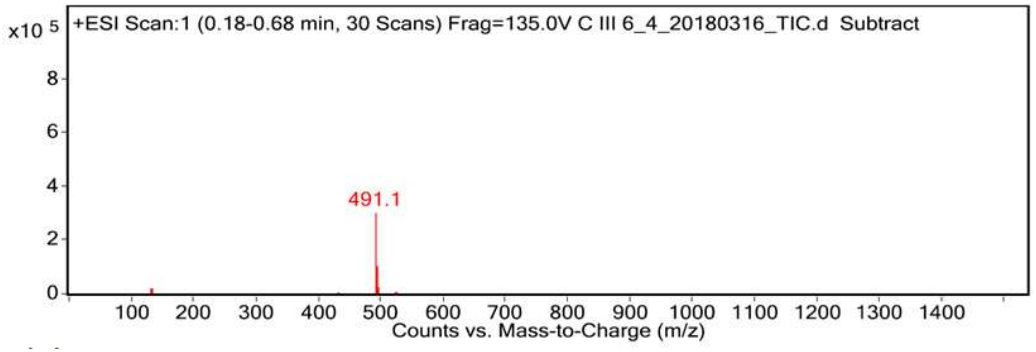
+ESI Scan:1 (0.18-0.68 min, 30 Scans) Frag=135.0V C III 6_4_20180316_TIC.d Subtract
x10 5
491.1
Counts vs. Mass-to-Charge (m/z)

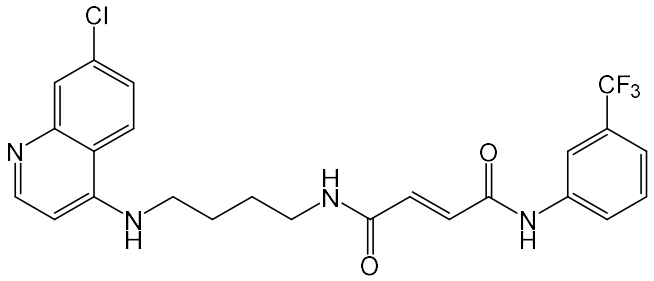
Cl
N
H
N
O
H
N
O
CF3

43

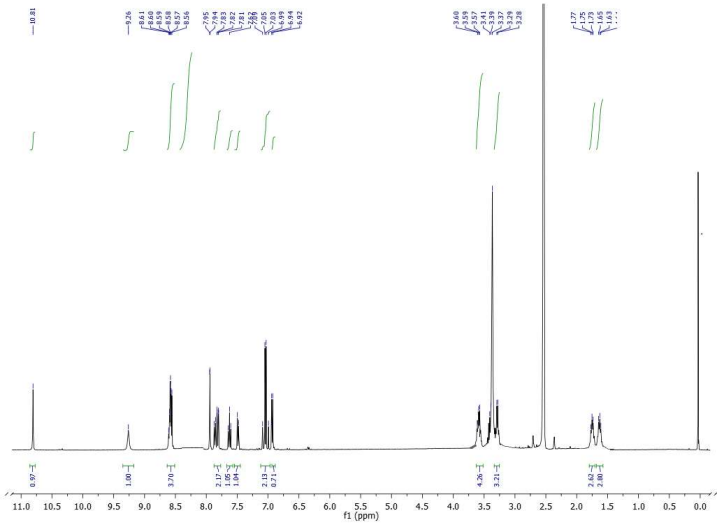

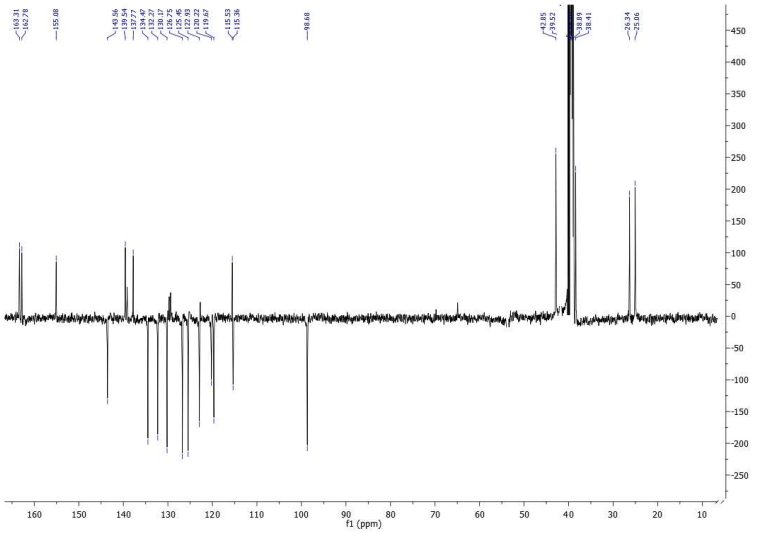

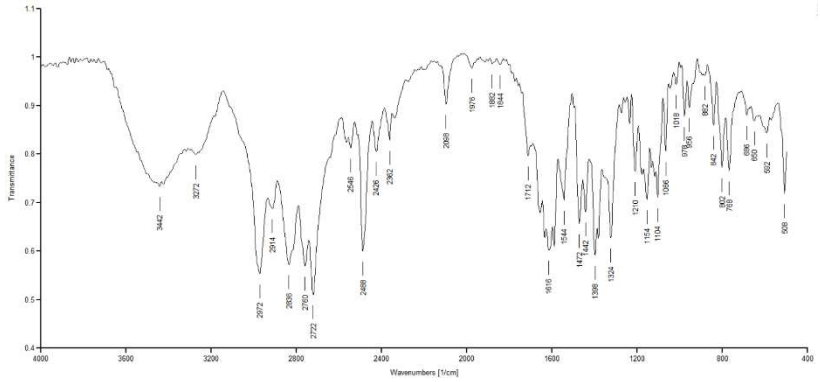
Transmittance
Wavenumbers [1/cm]

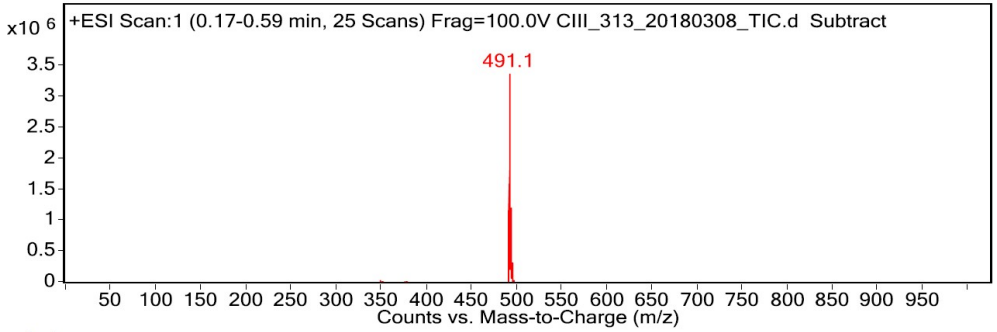
x10 6
+ESI Scan:1 (0.17-0.59 min, 25 Scans) Frag=100.0V CIII_313_20180308_TIC.d Subtract
491.1
Counts vs. Mass-to-Charge (m/z)

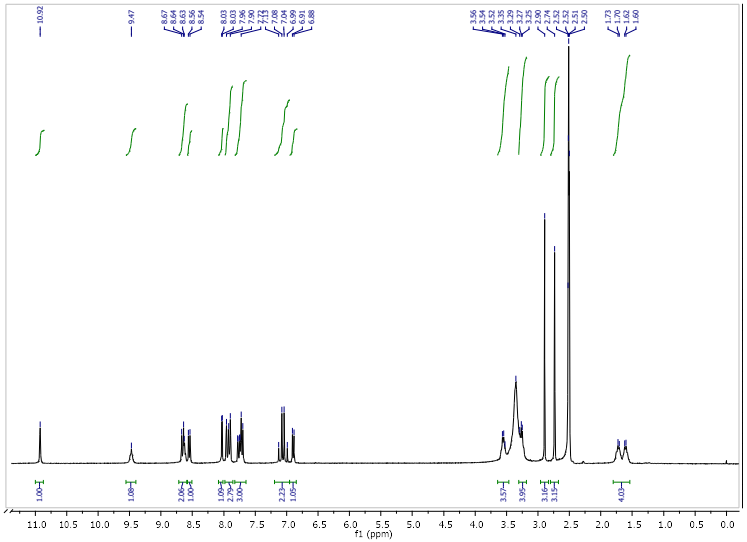
f1 (ppm)

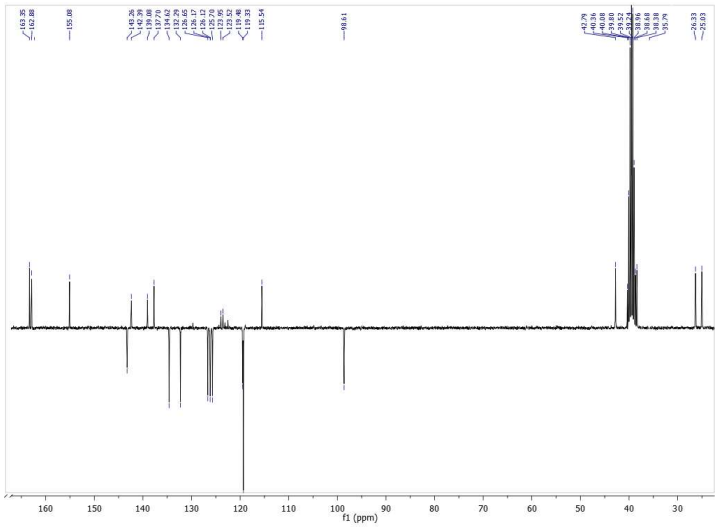
f1 (ppm)

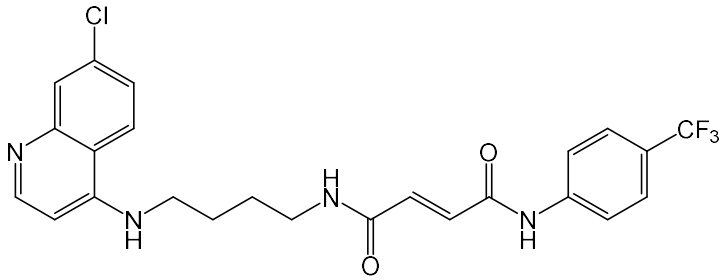
Cl
N
H
N
H
N
O
O
CF3

44

9.2. Prilog 2. Inhibicija proliferacije i invazije stanica glioblastoma, te mehanizam djelovanja sahakina **17**.

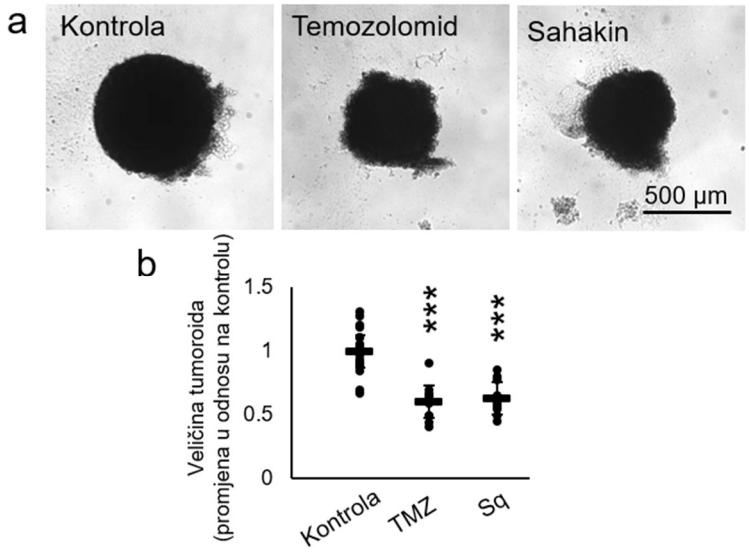

Slika S1. a) Reprezentativni mikrografi tumoroida glioblastoma nakon što su izloženi djelovanju temozolomida (TMZ, 100 µM, n = 13) ili sahakina **17** (Sq, 10 µM, n = 13) kroz 7 dana. b) Veličina tumoroida je procijenjena temeljeno na 2D mikrografu. Svaka točka predstavlja vrijednost koja je normalizirana u odnosu na kontrolu. Vodoravne linije predstavljaju srednju vrijednost od barem tri neovisna ispitivanja (***p < 0.001, one-way ANOVA i Tukey-Kramerov post hoc test).

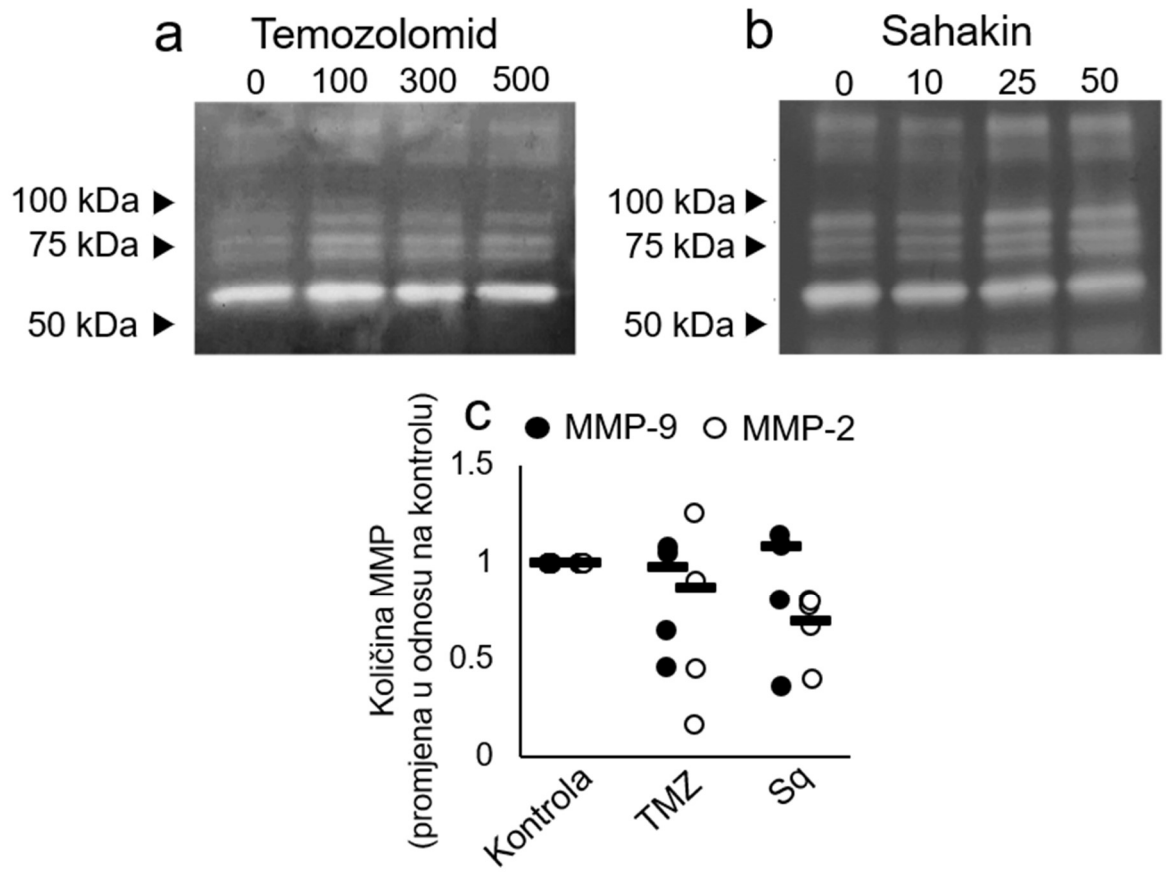

Slika S2. Zimografi stanica glioblastoma tretiranih a) temozolomidom (TMZ, 100, 300, 500 μM) i b) sahakinom **17** (Sq, 1, 10, 25 μM) nakon 24 h. c) Kvantifikacija MMP-9 i MMP-2 iz zimografa (TMZ, 100 μM, $n = 5$; Sq, 10 μM, $n = 5$). Svaka točka predstavlja vrijednost koja je normalizirana u odnosu na kontrolu. Vodoravne linije predstavljaju srednju vrijednost od barem tri neovisna ispitivanja.

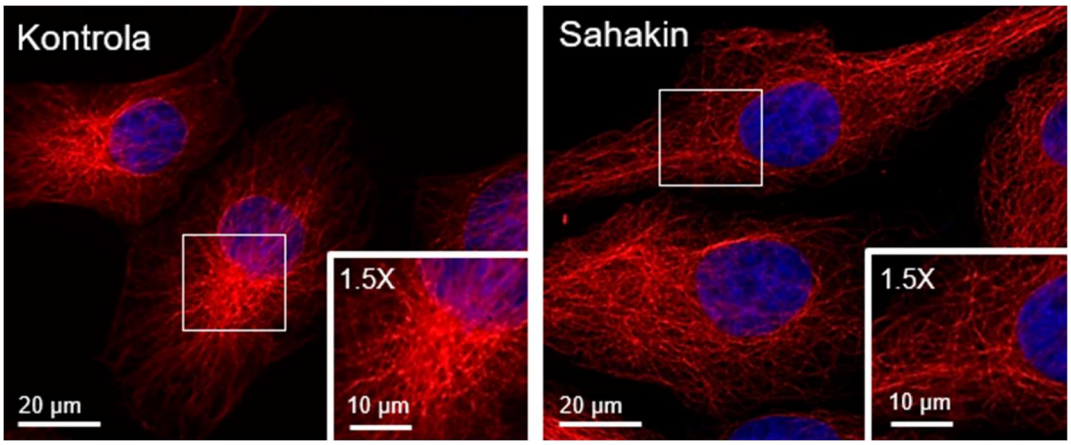

Slika S3. Reprezentativni fluorescentni mikrografi α-tubulina (obojen crveno) stanica glioblastoma koje su bile izložene djelovanju sahakina **17** u koncentraciji 10 µM kroz 24 h. Jezgre (obojene plavo) su obilježene Hoechst 33342. Inserti pokazuju organizacijski centar mikrotubula gdje se vidi reorganizacija α-tubulina.

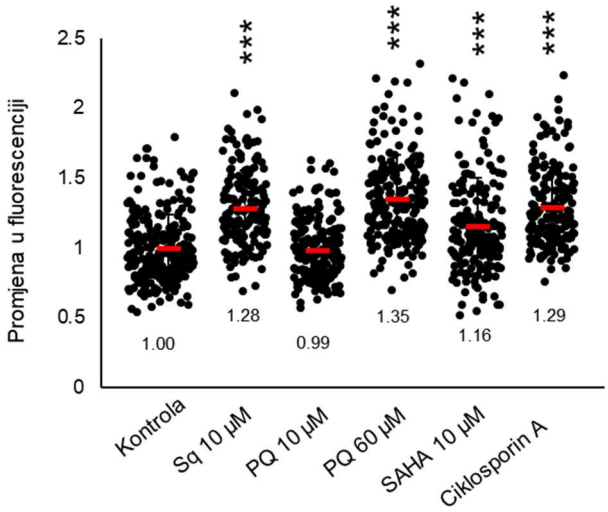

Slika S4. Unutarstanična akumulacija calceina-AM, supstrata P-glikoproteina. Stanice glioblastoma su tretirane sahakinom **17** (Sq, 10 µM, *n* = 176 stanica), primakinom (PQ, 10 µM *n* = 182 stanica, 60 µM *n* = 218 stanica) i SAHA-om (SAHA, 10 µM, *n* = 192 stanica) 24 h. Ciklosporin A (10 µM, 30 min, *n* = 172 stanica) služio je kao pozitivna kontrola. Stanice su snimane fluorescentim mikroskopom, a fluorescencija je analizirana programom ImageJ. Svaka točka predstavlja vrijednost koja je normalizirana prema kontroli (*n* = 310 stanica). Vertikalne linije predstavljaju aritmetičku sredinu (±SD) za kontrolu (1.00 ± 0.24), Sq (1.28 ± 0.27), PQ 10 µM (0.99 ± 0.22), PQ 60 µM (1.35 ± 0.29), SAHA (1.16 ± 0.33) i ciklosporin A (1.29 ± 0.28), iz tri neovisna ispitivanja (***$p < 0.001$, Welch's ANOVA s Games-Howell *post hoc* testom).

10. ŽIVOTOPIS

Maja Beus rođena je u Zagrebu, 11.11.1990. gdje je završila osnovnu i glazbenu školu, te VIII gimnaziju. Godine 2009. upisuje Farmaceutsko-biokemijski fakultet u Zagrebu, studij Farmacije. Godine 2014. dobila je Rektorovu nagradu za studentski rad „Sinteza pirazinskih analoga antitumorskog lijeka sorafeniba“ izrađen na Zavodu za farmaceutsku kemiju. Diplomski rad pod nazivom „Poništavanje hepatoprotektivnog djelovanja enkefalina opioidnim antagonistom naltreksonom“ izradila je na Zavodu za farmakologiju. Diplomirala je 2014. godine. Državni stručni ispit za magistre farmacije položila je 2015. godine. Od 1.9.2016. zaposlena je na Zavodu za farmaceutsku kemiju Farmaceutsko-biokemijskog fakulteta kao asistentica na zamjeni, a od 10.7.2018. u suradničkom zvanju doktorand-asistent na projektu „Dizajniranje, sinteza i evaluacija derivata primakina, vorinostata i sorafeniba kao potencijalnih citostatika“ (HRZZ-IP-09-2014-1501) Hrvatske zaklade za znanost. Godine 2016. upisala je na istom fakultetu poslijediplomski doktorski studij Farmaceutskih znanosti. Doktorski rad izrađuje pod vodstvom mentorice prof. dr. sc. Branke Zorc. Od 15.9. do 15.12. 2017. te od 1.4. do 1.7. 2018. izrađivala je biološki dio svog doktorata na Sveučilištu McGill u Montrealu pod vodstvom prof. dr. sc. Dusice Maysinger. Kroz stipendiju *British Scholarship Trust* boravila je na Sveučilištu Oxford kod prof. Paula Brennana od 1.4. do 30.6.2019. Sudjelovala je u sintezi potencijalnih TAOK inhibitora za koji je dobila *Voya Kondic Memorial Prize* koju dodjeljuje *British Scholarship Trust* za vrijedno istraživanje. Objavila je 6 znanstvenih i 3 stručna rada te sudjelovala na više kongresa s posterskim i oralnim priopćenjima. Godine 2019. dobila je *EFMC-YMCS Public's choice award* za oralnu prezentaciju održanu na EFMC kongresu u Ateni.

Znanstveni radovi:

1. **Beus M**, Rajić Z, Maysinger D, Mlinarić Z, Antunović M, Marijanović I, Fontinha D, Prudêncio M, Held J, Olgen S, Zorc B. SAHAquines, Novel Hybrids Based on SAHA and Primaquine Motifs, as Potential Cytostatic and Antiplasmodial Agents. *ChemistryOpen*, 2018, 7, 624–638.

2. Rajić Z, **Beus M**, Michnová H, Vlainić J, Persoons L, Kosalec I, Jampílek J, Schols D, Keser T, Zorc B. Asymmetric Primaquine and Halogenaniline Fumardiamides as Novel Biologically Active Michael Acceptors. *Molecules*, 2018, 23, 7.

3. Zhang I, **Beus M**, Stochaj U, Le PU, Zorc B, Rajić Z, Petrecca K, Maysinger D. Inhibition of glioblastoma cell proliferation, invasion, and mechanism of action of a novel hydroxamic acid hybrid molecule. *Cell Death Discov*, 2018, 5, 41.

4. **Beus M**, Fontinha D, Held J, Rajić Z, Prudêncio M, Zorc B. Synthesis and antiplasmodial evaluation of novel mefloquine-based fumardiamides. *Acta Pharm*, 2019, 69, 2, 233–248.

5. **Beus M**, Fontinha D, Held J, Rajić Z, Uzelac L, Kralj M, Prudêncio M, Zorc B. Primaquine and Chloroquine Fumardiamides as Promising Antiplasmodial Agents. *Molecules,* 2019, 24, 2812.

6. Zorc B, Perković I, Pavić K, Rajić Z, **Beus M**. Primaquine derivatives: Modifications of the terminal amino group. *Eur J Med Chem*, 2019, 182, 111640.

Temeljna dokumentacijska kartica

Sveučilište u Zagrebu **Doktorski rad**
Farmaceutsko-biokemijski fakultet
Zavod za farmaceutsku kemiju
A. Kovačića 1, 10000 Zagreb, Hrvatska

DIZAJNIRANJE, SINTEZA I CITOSTATSKO DJELOVANJE SAHAKINA

Maja Beus

SAŽETAK

U okviru ovog doktorskog rada dizajnirani su i sintetizirani sahakini, hibridni spojevi u kojima su spojeni dijelovi molekula antimalarika primakina, odnosno klorokina i citostatika SAHA-e (suberoilanilid hidroksamska kiselina). Sahakini sadrže tri ključna dijela: kinolinski prsten (dio molekule primakina ili klorokina), središnji dio (dikarboksilnu kiselinu: jantarnu, fumarnu, glutarnu, adipinsku, tereftalnu) te završni dio s dodatnom funkcionalnom skupinom (esterskom, karboksilnom, amidnom te *O*-benzil-, *O*-metil- ili nesupstituiranom hidroksamskom kiselinom). Sinteza sahakina polazila je od kinolinskog kraja. Primarna amino skupina primakina, odnosno analoga klorokina i monoester odgovarajućih dikarboksilnih kiselina povezani su amidnom vezom pomoću 1-[bis(dimetilamino)metilen]-1*H*-1,2,3-triazolo[4,5-*b*]piridinij 3-oksid heksafluorofosfata (HATU) u prisutnosti *N*,*N*-diizopropiletilamina (DIEA) ili preko kiselinskog klorida. Dobiveni su amido-esterski derivati koji su u sljedećem reakcijskom koraku hidrolizirani u amido-karboksilne kiseline te dalje amidirani s *O*-metil- ili *O*-benzilhidroksilaminima, odnosno halogenanilinima (s atomima fluora/klora ili trifluorometilnom skupinom u *meta* ili *para* položaju) uz HATU i DIEA. Sahakini sa slobodnom hidroksamskom skupinom dobiveni su katalitičkom hidrogenolizom *O*-benzilhidroksamskih derivata. Svi sahakini karakterizirani su uobičajenim analitičkim i spektroskopskim metodama (CHN, IR, ^{1}H NMR, ^{13}C NMR, MS). Antiproliferativno djelovanje sahakina ispitano je na humanim tumorskim stanicama: adenokarcinoma gušterače (Capan-1), akutne mijeloične leukemije (Hap1), karcinoma debelog crijeva (HCT-116), karcinoma pluća (NCI-H460), akutne limfoblastičke leukemije (DND-41), akutne promijelocitne leukemije (HL-60), kronične mijeloične leukemije (K-562), multiplog mijeloma (MM.1S), ne-Hodkinovog limfoma (Z-138), osteosarkoma (U2OS), hepatocelularnog karcinoma (HepG2), adenokarcinoma dojke (MCF-7), karcinoma pluća ne-malih stanica (H460) i glioblastoma (U251N). Najaktivniji derivati primakina bili su sahakini iz podskupine hidroksamskih kiselina te *meta*-supstituirani derivati halogenanilina s fumardiamidnom poveznicom. Sahakinu s najjačim citostatskim učinkom, N^1-hidroksi-N^5-(4-((6-metoksikinolin-8-il)amino)pentil)-glutaramidu, utvrđen je mehanizam djelovanja. Na staničnom modelu glioblastoma dokazano je da selektivno inhibira histon-deacetilazu 6, smanjuje ekspresiju matriks-metaloproteaze-2 i receptora za epidermalni faktor rasta.

Rad je pohranjen u Središnjoj knjižnici Sveučilišta u Zagrebu Farmaceutsko-biokemijskog fakulteta.

Rad sadrži: 174 stranica, 14 shema, 34 slike, 11 tablica i 186 literaturnih navoda. Izvornik je na hrvatskom jeziku.

Ključne riječi: primakin/klorokin/SAHA/hibridni spoj/hidroksamska kiselina/sinteza/citostatsko djelovanje/karcinom dojke/glioblastom

Mentor: **Dr. sc. Branka Zorc**, *redoviti profesor Sveučilišta u Zagrebu Farmaceutsko-biokemijskog fakulteta*

Ocjenjivači: **Dr. sc. Zrinka Rajić**, *izvanredna profesorica Sveučilišta u Zagrebu Farmaceutsko-biokemijskog fakulteta*
Dr. sc. Karmela Barišić, *redovita profesorica Sveučilišta u Zagrebu Farmaceutsko-biokemijskog fakulteta*
Dr. sc. Marko Anderluh, *redoviti profesor Univerza v Ljubljani Fakulteta za farmacijo*

Rad prihvaćen: travanj 2020.

Basic documentation card

University of Zagreb
Faculty of Pharmacy and Biochemistry
Department of Medicinal Chemistry
A. Kovačića 1, 10000 Zagreb, Croatia

PhD thesis

DESIGN, SYNTHESIS AND CYTOSTATIC ACTIVITY OF SAHAQUINES

Maja Beus

SUMMARY

This doctoral thesis describes the design and synthesis of sahaquines, hybrid molecules in which molecular parts of antimalarial drug primaquine/chloroquine and cytostatic drug SAHA (suberoylanilide hydroxamic acid) are merged. Sahaquines constitute of three key parts: quinoline ring (part of primaquine or chloroquine molecule), linker (dicarboxylic acid: succinic, fumaric, glutaric, adipic, terephthalic) and the terminal part with an additional functional group (ester, carboxylic, amide, *O*-benzyl-, *O*-methyl- or unsubstituted hydroxamic acid). Sahaquine synthesis starts from the quinoline end. The primary amino group of primaquine/chloroquine is linked with an appropriate dicarboxylic monoester through an amide bond achieved with 1-[bis(dimethylamino)methylene]-1*H*-1,2,3-triazolo[4,5-*b*]pyridinium 3-oxid hexafluorophosphate (HATU) in the presence of *N,N*-diisopropylethylamine (DIEA) or by previously activating carboxylic acid with thionyl chloride. Obtained amido-esters were hydrolysed to afford the corresponding amido-carboxylic acids, which were further coupled with *O*-benzyl- and *O*-methylhydroxylamine, or halogenanlines. HATU/DIEA was used again as the coupling system. Free hydroxamic acids were obtained by catalytic hydrogenation of *O*-benzyl derivatives. All new compounds were fully characterized by conventional spectroscopic and analytical methods (IR, ^{1}H and ^{13}C NMR, MS and elemental analyses). The cytostatic activity of sahaquines was tested on the following cancer cell lines: pancreatic adenocarcinoma (Capan-1), chronic myeloid leukemia (Hap1), colorectal carcinoma (HCT-116), lung carcinoma (NCI-H460), acute lymphoblastic leukemia (DND-41), acute myeloid leukemia (HL-60), chronic myeloid leukemia (K-562), multiple myeloma (MM.1S), non-Hodgkin lymphoma (Z-138), bone osteosarcoma (U2OS), hepatocellular carcinoma (HepG2), breast adenocarcinoma (MCF-7) and glioblastoma (U251N). The most active primaquine derivatives were sahaquines with free hydroxamic acid moiety and diamides with *meta*-substituted halogenanilines. The mechanism of action was determined for the most potent sahaquine, namely N^1-hydroxy-N^5-(4-((6-methoxyquinolin-8-yl)amino)pentyl)glutaramide. On the glioblastoma cell, it is shown that sahaquine selectively inhibits histone deacetylase 6, decreases the expression of matrix metalloproteinase-2 and the epidermal growth factor receptor.

The thesis is deposited in the Central Library of the University of Zagreb Faculty of Pharmacy and Biochemistry.

Thesis includes: 174 pages, 14 schemes, 34 figures, 11 tables and 186 references. Original is in Croatian language.

Keywords: primaquine/chloroquine/SAHA/hybrid compound/hydroxamic acid/synthesis/cytostatic activity/breast cancer/glioblastoma

Mentor: **Branka Zorc**, **Ph.D.** *Full Professor,* University of Zagreb Faculty of Pharmacy and Biochemistry

Reviewers: **Zrinka Rajić**, **Ph.D.** *Associate Professor,* University of Zagreb Faculty of Pharmacy and Biochemistry
Karmela Barišić, **Ph.D.** *Full Professor,* University of Zagreb Faculty of Pharmacy and Biochemistry
Marko Anderluh, **Ph.D.** *Full Professor,* University of Ljubljana Faculty of Pharmacy

The thesis was accepted: April 2020